

The Synthesis and Characterisation of Reactive MALDI Matrices for Mass Spectrometry Imaging of Steroids



Submitted to the Galway-Mayo Institute of Technology for the award of MSc. (By
Research)

By

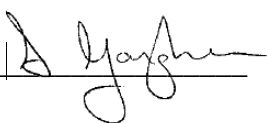
Sarah Gaughan BSc

Supervised by: Dr Philip White
 Dr Cormac Quigley
 Dr Diego Cobice

August 2019

Declaration

I (Sarah Gaughan), Declare that the work in this thesis is my own. All externally sourced materials and images have been cited and referenced according to the Harvard referencing system.

Signature: 

Date: 13/08/2019

Acknowledgements

I would firstly like to thank Galway-Mayo Institute of Technology for granting me the Research & Innovation Strategic Endowment (RISE) Scholarship and Allergan for their innovation award, both of which funded this research project.

I would like to sincerely thank the chemistry technicians for their assistance, for always pointing me in the right direction and for being so accommodating throughout the two years. To my supervisors, Cormac Quigley, thanks for joining the team, sharing your wealth of knowledge and giving me the direction I needed to see the project through; and to Philip White and Diego Cobice for their continued support and guidance during my research.

Special thanks goes to my fellow researchers in room 202, thank you all for your advice, assurance, reassurance and banter.

To my family for their encouragement, most notably my mum Eileen and sister Helena I am truly grateful for your constant support and encouragement. Finally, my deepest gratitude goes to my fiancé Liam, thank you so much for your love and support throughout this journey.

Table of Contents

1	Abstract.....	1
2	Introduction.....	3
2.1	Background to Mass Spectral Imaging.....	3
2.2	How Mass Spectral Images are Developed.....	5
2.2.1	Sample Preparation.....	5
2.2.2	Desorption and Ionisation.....	6
2.2.3	Mass Analyser.....	10
2.2.4	Image Registration.....	11
2.3	MALDI MSI of Endogenous Steroids in Therapeutic Research.....	12
2.4	MALDI Mass Spectrometry for Small Molecule Analysis.....	15
2.5	Comparing MALDI MSI with existing Autoradiography Techniques.....	17
2.6	Organic Synthesis.....	22
2.6.1	Knoevenagel Condensation.....	22
2.6.2	Knoevenagel Condensation with Cyanoacetic acid.....	24
2.6.3	Williamson Ether Synthesis.....	24
2.6.4	Friedel Crafts Acylation.....	25
2.6.5	Fries Rearrangement.....	27
2.6.6	Protection and Deprotection of Phenols.....	27
2.6.7	Baeyer Villiger Oxidation.....	28
2.6.8	Diels Alder Reaction.....	29
2.6.9	Urea formation.....	30
2.6.10	Dehydration.....	30
2.6.11	Hydrazone Formation.....	30
2.6.12	Purification.....	31
2.6.13	Characterisation Techniques.....	33

3	Designing Reactive Matrices	35
3.1	Role of a Matrix	35
3.2	Matrix Target Molecules	37
3.3	Matrix Development.....	39
3.4	Molecular Design – Laser Absorption Optimisation	43
3.5	Molecular design - Matrix Basicity Optimisation.....	45
3.6	Design of Matrix Reaction for structure B - Library.....	46
4	Synthesis and Characterisation Overview and Outcome.....	47
4.1	The Synthesis of Structure B Library	47
4.1.1	Matrix B2a	47
4.1.2	Matrix B2b	49
4.1.3	Matrix B2c	49
4.1.4	Matrix B2d and B2e.....	50
4.1.5	Matrix B2f and B2h	51
4.1.6	Matrix B2g	52
4.1.8	Matrix B3i.....	52
4.1.9	Matrix B2j and B2k.....	54
4.1.10	Matrix B2l.....	55
4.2	The Synthesis of Structure A.....	56
4.3	The synthesis of Structure C	59
4.4	Analysis by MALDI MS	63
4.4.1	Matrix Characterisation by MALDI MS.....	63
4.4.1	Matrix Reaction with Alcohol Analysed by MALDI-TOF MS.....	63
5	Results and Discussions.....	65
5.1	MALDI-TOF MS for Matrix Characterisation in Positive Ion Mode.....	65
5.1.1	Matrix B2a Molecular Weight 260 g/mol.....	66

5.1.2	Matrix B2b Molecular Weight 290 g/mol.....	67
5.1.3	Matrix B2d Molecular Weight 330 g/mol.....	68
5.1.4	Matrix B2f Molecular Weight 339 g/mol	69
5.1.5	Matrix B2g Molecular Weight 302 g/mol.....	70
5.1.6	Matrix B2h Molecular Weight 294.7 g/mol.....	71
5.1.7	Matrix B2j Molecular Weight 288 g/mol.....	72
5.1.8	Matrix B2k Molecular Weight 318 g/mol.....	73
5.1.9	Matrix C3 Molecular Weight 217 g/mol.....	74
5.2	Matrix Reaction with Alcohol Analysed by MALDI-TOF MS	75
5.2.1	Results for Matrix B2b Reaction with Alcohols	75
5.3	UV Absorption Results	79
5.4	Crystal Properties	81
5.5	Discussion of Results	82
6	Conclusion	85
7	Experimental Procedure.....	87
7.1	Experimental Procedure for Matrix Characterisation by MALDI	88
7.1.1	MALDI TOF MS General Procedure	88
7.1.2	MALDI -TOF/TOF General Procedure	89
7.2	Matrix Reaction with Alcohol analysed by MALDI MS	90
7.2.1	Sample Preparation for Reaction 1 and 2.....	90
7.2.2	Sample Preparation for Reaction 3.	90
7.3	UV Absorption	92
7.4	Experimental data for structure B library.....	93
7.4.1	Procedure A: General Procedure for the Addition of the Basic Moiety	93
7.4.2	4-[2-(Dimethylamino)ethoxy]benzaldehyde (B1a).....	94
7.4.3	4-(2-(dimethylamino)ethoxy)-3-methoxybenzaldehyde (B1b).....	94

7.4.4	5-bromo-4-(2-(dimethylamino)ethoxy)-3-methoxybenzaldehyde (B1c)	95
7.4.5	3-methoxy-4-(2-(piperidin-1-yl)ethoxy)benzaldehyde (B1d)	95
7.4.6	4-(2-(piperidin-1-yl)ethoxy)benzaldehyde (B1e)	95
7.4.7	3-bromo-4-(2-(dimethylamino)ethoxy)benzaldehyde (B1f)	96
7.4.8	4-(2-morpholinoethoxy)benzaldehyde (B1g)	96
7.4.9	3-chloro-4-(2-(dimethylamino)ethoxy)benzaldehyde (B1h)	97
7.4.10	4-formylphenyl 2-(2,2,2-trifluoroacetyl)hydrazinecarboxylate (B1i)	97
7.4.11	4-(2-(diethylamino)ethoxy)benzaldehyde (B1j)	98
7.4.12	4-(2-(diethylamino)ethoxy)-3-methoxybenzaldehyde (B1k)	98
7.4.13	S-(3-(4-formylphenoxy)propyl) ethanethioate (B1l)	98
7.5	Procedure B: General Procedure for the Knoevenagel Reaction with Cyanoacetic Acid	99
7.5.1	(Z)-2-cyano-3-(4-(2-(dimethylamino)ethoxy)phenyl)acrylic acid (B2a)	99
7.5.2	(Z)-2-cyano-3-(4-(2-(dimethylamino)ethoxy)-3-methoxyphenyl)acrylic acid (B2b)	100
7.5.3	(Z)-2-cyano-3-(3-methoxy-4-(2-(piperidin-1-yl)ethoxy)phenyl)acrylic acid (B2d)	101
7.5.4	(Z)-2-cyano-3-(4-(2-(piperidin-1-yl)ethoxy)phenyl)acrylic acid (B2e)	102
7.5.5	(Z)-2-cyano-3-(4-(2-(dimethylamino)ethoxy)-3-bromophenyl)acrylic acid (B2f)	102
7.5.6	(Z)-2-cyano-3-(4-(2-morpholineethoxy)phenyl)acrylic acid (B2g)	103
7.5.7	(Z)-3-(3-chloro-4-(2-(dimethylamino)ethoxy)phenyl)-2-cyanoacrylic acid (B2h)	104
7.5.8	(Z)-2-cyano-3-(4-(2-(2,2,2-trifluoroacetyl)hydrazinecarbonyl)oxy)phenyl)acrylic acid (B2i)	104
7.5.9	(Z)-2-cyano-3-(4-(2-(diethylamino)ethoxy)phenyl)acrylic acid (B2j)	105
7.6	Experimental procedures for Structure A	107
7.6.1	1,4-bis(benzyloxy)benzene (A1a)	107

7.6.2	1-(2,5-bis(benzyloxy)phenyl)ethenone (A3a).....	107
7.6.3	1,4-phenylene diacetate (A1b)	108
7.6.4	1-(2,5-dihydroxyphenyl)ethenone (A2b)	109
7.6.5	1-(2,5-bis(benzyloxy)phenyl)ethenone (A3).....	110
7.6.6	2,5-bis(benzyloxy)phenyl acetate (A4).....	111
7.6.7	2,5-bis(benzyloxy)phenol (A5)	111
7.7	Experimental Procedure for Structure C	112
7.7.1	Ethyl 2-((4-acetylphenyl)carbamoyl)hydrazinecarboxylate (C1).....	112
7.7.2	Ethyl 2-((4-acetylphenyl)carbamoyl)hydrazinecarboxylate (C1).....	112
7.7.3	4-(4-acetylphenyl)-1,2,4-triazolidine-3,5-dione (C2)	113
7.7.4	4-(4-acetylphenyl)-3H-1,2,4-triazole-3,5(4H)-dione (C3).....	113
7.7.5	4-(4-acetylphenyl)-3H-1,2,4-triazole-3,5(4H)-dione (C3).....	113
7.7.6	4-(4-acetylphenyl)-3H-1,2,4-triazole-3,5(4H)-dione (C3).....	114
8	References.....	115
9	Appendices.....	122
A.1	FTIR Spectra	122
A.2	NMR Spectra.....	130
A.3	MALDI spectra.....	142
A.4	UV spectra.....	157

Table of Figures

Figure 2. 1	Number of publications by year.....	3
Figure 2. 2	Principles of MSI.	5
Figure 2. 3	MALDI MS image.....	7
Figure 2. 4	Schematic of a MALDI-MSI experiment.	8
Figure 2. 5	Imaging MS experiments.....	11
Figure 2. 6	(A) Autoradiogram of AZD2820 in mouse kidney.....	19
Figure 2. 7	Knoevenagel Condensation.....	22
Figure 2. 8	Knoevenagel product reacting further in a Michael addition.....	23
Figure 2. 9	Knoevenagel condensation with aromatic aldehyde.....	24
Figure 2. 10	Williamson ether synthesis.....	25
Figure 2. 11	Friedel-Crafts acylation.....	26
Figure 2. 12	Baeyer Villiger oxidation.....	28
Figure 2. 13	Diels Alder Reaction.....	29
Figure 2. 14	Hydrazone formation.....	31
Figure 3. 1	Commercially available matrix α -cyano-4-hydroxycinnamic acid (CHCA).....	36
Figure 3. 2	Potential target groups for derivatising.....	37
Figure 3. 3	Novel matrix structure B.....	40
Figure 3. 4	Proposed matrix designs for Target A.....	40
Figure 3. 5	Proposed matrix structure C.....	41
Figure 5. 1	Matrix B2a mass spectrum.....	66
Figure 5. 2	Matrix B2b mass spectrum.....	67
Figure 5. 3	Matrix B2d mass spectra.....	68
Figure 5. 4	Matrix B2f mass spectra.....	69
Figure 5. 5	Matrix B2g mass spectra.....	70

Figure 5. 6	Matrix B2h mass spectra.....	71
Figure 5. 7	Matrix B2j mass spectra.....	72
Figure 5. 8	Matrix B2k mass spectrum	73
Figure 5. 9	Matrix C3 mass spectra.....	74
Figure 5. 10	Reaction 1: Matrix B2b with CORT	76
Figure 5. 11	Reaction 1: Matrix B2b with decanol.....	76
Figure 5. 12	Reaction 1: Matrix B2b with terpineol.....	76
Figure 5. 13	Reaction 2: Matrix B2b with CORT	77
Figure 5. 14	Reaction 2: B2b with decanol	77
Figure 5. 15	Reaction 2: Matrix B2b with terpineol.....	77
Figure 5. 16	Reaction 3: Matrix B2b with CORT and TFA.....	78
Figure 5. 17	Reaction 3: Matrix B2b with decanol and TFA	78
Figure 5. 18	Reaction 3: Matrix B2b with terpineol and TFA	78
Figure 5. 19	UV absorbance spectrum for matrix B2g.....	80
Figure 5. 20	UV absorbance spectrum for matrix B2h.....	80

Table of Tables

Table 2. 1	Comparison of MS imaging approaches	10
Table 3. 1	Target compounds for matrix design	38
Table 3. 2	Structure B	43
Table 5. 1	Molar absorptivity coefficient (ϵ) for structure B type matrices.....	79
Table 5. 2	Matrices crystal properties and visual appearance.....	81
Table 7. 1	Preparation of stock solutions for matrix characterisation by MALDI.....	88
Table 7. 2	Preparation of solid compound stock solutions for MALDI analysis.....	91
Table 7. 3	Preparation of liquid compound stock solutions for MALDI analysis	91

Table of Schemes

Scheme 4. 1	Synthesis of matrix B2a	47
Scheme 4. 2	Synthesis of matrix B2b	49
Scheme 4. 3	Synthesis of matrix B2c	49
Scheme 4. 4	Synthesis of matrix B2d and B2e	50
Scheme 4. 5	Synthesis of matrices B1f and B1h	51
Scheme 4. 6	Synthesis of matrix B2g	52
Scheme 4. 7	Synthesis of matrix B3i	52
Scheme 4. 8	Synthesis of matrices B2j and B2k.....	54
Scheme 4. 9	Synthesis of matrix B2l	55
Scheme 4. 10	Synthesis plan for matrix structure A (A8)	56
Scheme 4. 11	Original synthesis plan for matrix structure A to precursor A3	56
Scheme 4. 12	Synthesis plan for structure C matrix	59
Scheme 4. 13	Activation of carboxylic acid with alcohol	63

Abbreviations

3-MoSA	3-methoxysalicylamine
Å	Angstrom
ACN	Acetonitrile
CHCA	α -cyano-4-hydroxycinnamic acid
CORT	Corticosterone
DCM	Dichloromethane
DEM	Diethylmalonate
DESI	Desorption electrospray ionisation
DMNTH	4-Dimethylamino-6-(4-methoxy-1-naphthyl)-1,3,5-triazine-2-hydrazine
DMSO	Dimethylsulfoxide
DNPH	2,4-Dinitrophenylhydrazine
eq.	Equivalent
EtOAc	Ethylacetate
FTICR	Fourier transform ion cyclotron resonance FTIR Fourier transform infrared
GC-MS	Gas chromatography mass spectrometry
IR	Infrared
LC-MS	Liquid chromatography mass spectrometry
<i>m/z</i>	Mass/charge
MA	Micro autoradiography
MALDI	Matrix assisted laser desorption ionisation
MSI	Mass spectrometry imaging
MW	Molecular weight
NIST	National institute of standards and technology
NMR	Nuclear magnetic resonance
QWBA	Quantitative whole-body autoradiography
r.t	Room temperature
RDS	Rate determining step
RMA	Receptor micro-autoradiography
SIMS	Secondary ion mass spectrometry
TCDI	1,1-thiocarbonyldiimidazole
TFA	Trifluoroacetic acid

THF	Tetrahydrofuran
TLC	Thin layer chromatography
TOF	Time of flight
VDR	Vitamin D receptor
WBA	Whole-body autoradiography
α	<i>alpha</i>
β	<i>beta</i>
ϵ	Molar absorptivity coefficient
λ_{\max}	Wavelength of maximum absorption
σ_m	Hammett substituent constant, meta position
σ_p	Hammett substituent constant, para position

1 Abstract

Matrix assisted laser desorption ionisation (MALDI) mass spectrometry imaging (MSI) is an analytical technique for molecular spatial distribution imaging which presents unique advantages over existing 3D imaging techniques and offers novel perspectives for understanding the spatial distribution of biological processes. It is a well established technique in the analysis of large molecules however, small molecule analysis has been challenging due to matrix ion spectral interference (Chacon et al. 2011). Another obstacle for many endogenous steroid molecules is their poor ability to ionise. The purpose of this study was to design, synthesise and characterise novel matrices that would react with target functional groups on endogenous steroids. This study was limited to MALDI MS 2D analysis of the matrices to attain function and behaviour data, matrices were not tested directly on tissue samples.

The matrices designed in this project all have three essential components: 1) the reactive moiety, for steroids this is a carboxylic acid that can react with a hydroxyl or ketone on the target molecule, for vitamin D the reactive component was a triazolinedione which can react, in a Diels Alder reaction with the diene on the target molecule; 2) the absorbing core, a conjugated pi system that can absorb the laser energy and 3) a basic functional group for enhanced ionisation efficiency. A library of matrices targeting steroids was developed, this was aimed at optimising the molar absorption coefficient at the laser wavelength of 337 nm and enhancing ionisation efficiency.

Seven matrices designed to react with hydroxyl and ketone containing steroids were successfully synthesised and characterised, these matrices were involved in a simulation reaction in solution with an alcohol and a coupling agent in basic conditions. The reaction was directed at activating the carboxylic acid to form an ester in an addition reaction with the alcohol. However, the esterification did not take place. Investigations towards

synthesising a reactive matrix targeted to analyse vitamin D metabolites were undertaken. A variety of synthetic pathways were investigated and great strides in the groundwork towards finalising this matrix have been made. However further efforts to synthesise the stable matrix are required.

This thesis reports the design, synthesis and characterisation of a number of novel reactive MALDI matrices, optimisation analysis and activation reaction assays of the matrices. Although further work is required in developing the correct activation conditions for these matrices the development of a library of novel reactive matrices that can significantly enhance ionisation of small molecules in one application step is integral to overcoming adversities which hinder the use of MALDI MSI's for small molecule analysis.

2 Introduction

2.1 Background to Mass Spectral Imaging

MSI has become a fast-growing field within analytical chemistry which is demonstrated in *figure 2.1*. It was initially used 50 years ago to analyse semiconductor surfaces by secondary ion mass spectroscopy (Benninghoven and Sichtermann 1978). Caprioli, a pioneer of MSI was the first to introduce and expand MALDI with MSI. His work initiated great interest and the potential role MSI could play in molecular mapping of drug distribution, histology and proteomics was soon realised. This in turn triggered significant development and optimization of methodologies, instrumentation, and software for bioanalysis (Cobice et al. 2015)

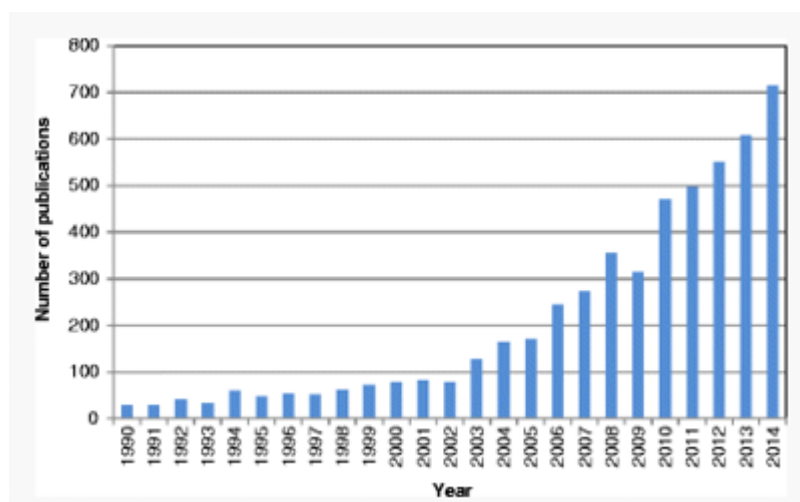


Figure 2.1 Number of publications by year data obtained from research with SciFinderScholar for imaging mass spectrometry (Caprioli 2015)

Imaging MS can produce a 3D molecular image of tissue sections and entire organs. The 3D image produced can identify thousands of molecules such as proteins, peptides, lipids and small molecules. It is becoming a very valuable tool in the analysis of biological and biomedical *ex vivo* distribution (Seeley and Caprioli 2012), which provides vast information of molecular spatial distribution within the sample tissue. Unlike other

recognised 3D imaging techniques such as fluorescence and radioimmunoassay, which require radiolabelling, MSI requires no specific labelling before analysis and can distinguish a drug molecule from a drug metabolite. It provides information about the distribution of the parent compound and its metabolites with high sensitivity and specificity (Karlsson and Hanrieder 2017).

Because of the major advancements in software and technology which include: developments in instrumentation, sample preparation and computational data analysis, this technique brings new and exciting possibilities to significantly enhance the understanding of health and disease. Examples of applications utilising MSI in an increasingly wider range of analysis are being researched (Addie et al. 2015). Applications for both exogenous and endogenous compounds show its effectiveness in determining complicated distribution patterns and the biological changes caused by drug target engagement or disease progression (Addie et al. 2015).

2.2 How Mass Spectral Images are Developed

MSI is a multi-step process as shown in *figure 2.2*, which involves sample preparation, analyte desorption and ionization, mass analysis and image registration.

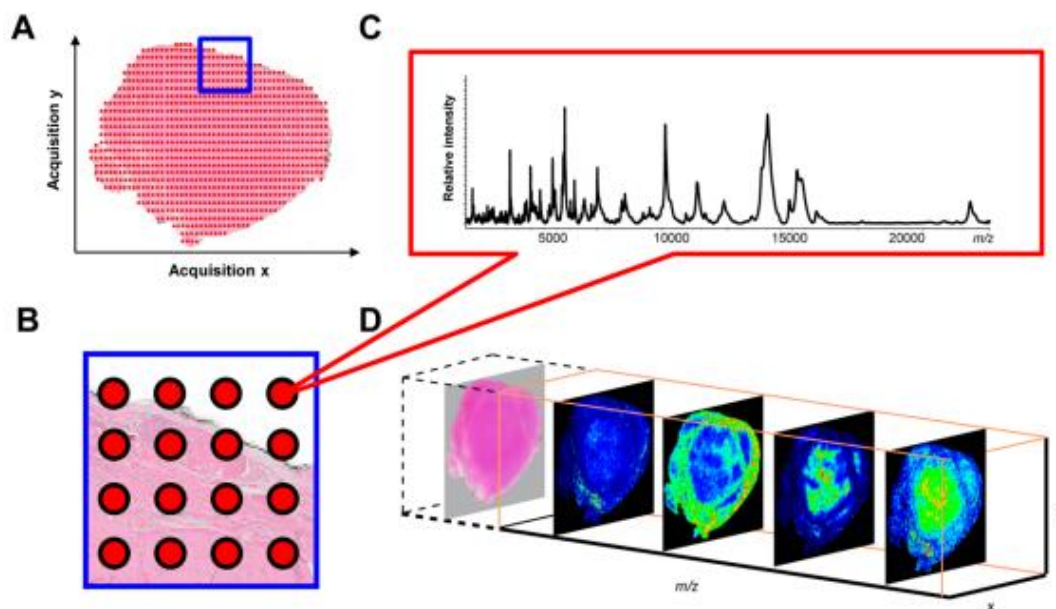


Figure 2.2 Principles of MSI. The surface of the tissue is analysed in a grid like manner. (B) Magnification of a measurement region of part A, producing a mass spectrum for each measurement spot. (C) The visualisation of mass signals. (D) Registration of the tissues histology with the imaging software (Addie et al. 2015)

2.2.1 Sample Preparation

Sample preparation is a crucial part of this technique the reproducibility and accuracy of the MSI can only be as good as the quality of the sample being analysed. Protocols for sample collection must ensure that histological integrity of tissue sections is retained so that spatial localisation of target molecules is uncorrupted by analyte degradation/diffusion (Caprioli 2015, Cobice et al. 2015). Rapid proteolytic activity has been reported in tissue sections (Goodwin, Pennington and Pitt 2008) and this highlights the fundamental importance of obtaining a well preserved sample. For consistency and reproducibility standardised sample preparation guidelines are crucial. These best

practice guidelines for sample preparation and software interpretation currently being developed and beginning to be utilised on a wider scale are vital in testing the capabilities of these highly cross-disciplinary tools against an array of diseases of concern today, both in terms of improved diagnosis and pharmacological development. Subsequent to this the European Cooperation in Science and Technology (COST) actions for mass spectral imaging was set up in 2011 initiated by Liam McDonnell and Garry Corthals. COST, an intergovernmental framework allows for the coordination of nationally-funded research on a European level. It enables European researchers to jointly develop their research ideas and new initiatives across all scientific disciplines through trans-European networking of nationally funded research activities (Stoeckli 2017).

MSI sample preparation is commonly conducted using snap-frozen cryosections cut from dissected organs rapidly frozen in liquid nitrogen. Consecutive tissue sections for traditional histology are commonly collected allowing MSI and histology images to be aligned. Tissue sections are usually cut at 10–20 μm , comparable with the thickness of a mammalian cell, so that the majority of cells are cut open (Cobice et al. 2015). Once sliced, tissue sections are then transferred and mounted onto a target plate or glass slide. When analysing peptides and proteins (high mass analytes), washing tissue sections with organic solvents is a recommended step to fix tissues, and remove ion-suppressing salts and lipids, that could interfere with the signal (Gemperline, Chen and Li 2014).

2.2.2 Desorption and Ionisation

Many different ionization modes have been used for imaging by MS, including MALDI, secondary ion mass spectrometry (SIMS), desorption electrospray ionisation (DESI), and a number of other electrospray ionisation variations, all have unique capabilities and limitations. In the biological and medical field, the most widely used technology for imaging biomolecules in tissues and cells is MALDI- MSI. The first use of this imaging

technique was published in 1997 by Caprioli. This work demonstrated that signals for peptides and proteins could be obtained directly from tissues (Caprioli, Farmer and Gile 1997). In this project the ionisation mode utilised was MALDI and this is discussed in more detail in *section 2.3*. Here a brief overview of the three ionisation methods mentioned is provided.

MALDI-MSI is currently the most popular and best developed technique in clinical MSI, this is due to its widespread commercial availability and its ability to analyse large molecules like peptides and proteins (which can then be validated using clinically well-established methods) (Addie et al. 2015). *Figure 2.3* shows an example of image quality.



Figure 2.3 MALDI MS image for one lipid in a transverse section of a mouse brain as an example of the image quality attainable today. (Left panel) – Partial microscopic image of a transverse section of stained mouse brain. (Right panel) – MALDI MS image of a partial brain section of the ion at m/z 885.5507 (Caprioli 2015)

MALDI utilises a matrix that usually consists of small acidic organic molecules with a conjugated pi system that absorb UV light. The steps involved in obtaining an analyte image can be seen in *figure 2.4*. The sample is evenly coated with the matrix. Following this application, solvent evaporation takes place and the molecules from the surface of the sample co-crystallise with the matrix. This surface is subsequently analysed by rastering (pixel scanning) across it with a MALDI laser irradiation (Fergusson et al. 2014a). The role of the MALDI matrix is to absorb laser energy in the MALDI source, leading to the explosive desorption of sample analytes held within matrix crystals. The analytes are then transported into the gas-phase with little degradation of the sample ions because the matrix is designed to absorb most of the incident laser energy, resulting in soft ionisation of the analyte (Fergusson et al. 2014b). Uniform matrix application plays a critical role in the quality of reproducible, high-resolution MSI data and the process must be controlled to enable homogenous co-crystallization of the analytes from the tissue within the matrix on the section surface, without causing diffusion or disruption of morphology (Cobice et al. 2015). The choice of matrix is important, as this affects the type of analytes that can be analysed. Many different matrices are available, allowing an array of molecular classes to be analysed using the same technique, these include metabolites, lipids, peptides, and proteins.

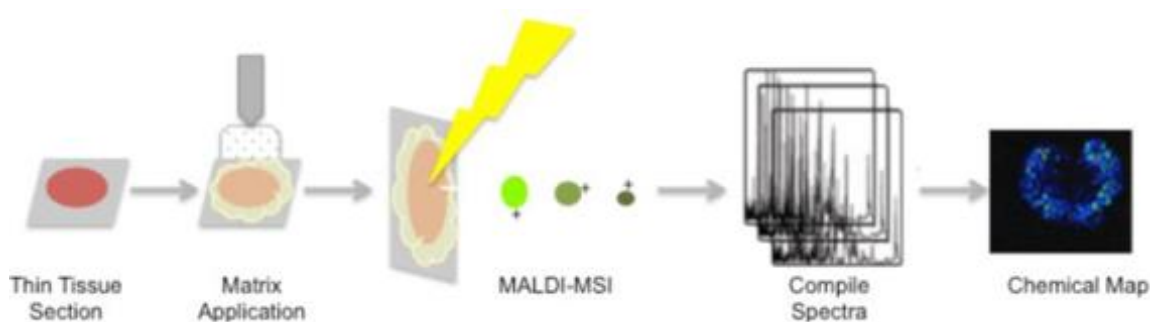


Figure 2. 4 Schematic of a MALDI-MSI experiment. At each point, or pixel, a mass spectrum is collected. These spectra are averaged, and individual masses are selected to create maps (Fergusson et al. 2014a)

DESI-MSI the youngest ionisation approach of the three, introduced in 2004 by the Cooks Group of researchers (Takats et al. 2004). DESI uses a combination of electrospray and desorption ionization. A beam of highly charged droplets, formed by an electrospray, is directed at the sample surface, where they create a thin liquid film, which dissolves the analytes. The analyte-containing charged droplets evaporate during their transition to the mass spectrometer. The advantage of this technique is that it is applicable to solid, liquid, frozen, and gaseous samples. DESI MSI allows the analysis of a wide range of organic and biological compounds without much sample preparation, at room temperature and under ambient conditions. DESI is considered a soft technique. The mass range of the analysis is usually limited to 2,000 Da, the mass range for MALDI is; 0-100,000 Da (Bodzón-Kulakowska and Suder 2016).

Recently, the development of dimethylformamide (DMF)-based solvent combinations has minimized the destructive nature of the technique and has enabled DESI-MSI to be performed with preservation of morphological features. By preserving morphological features DESI can be used adjacent to MALDI and histological staining analysis can be performed after MSI, thus providing an opportunity to correlate findings (Gemperline, Chen and Li 2014). This can generate a more complete evaluation and is expected to enhance diagnostic capabilities (Fergusson et al. 2014a).

SIMS-MSI is a long-established technique, developed in the 60's (Bodzón-Kulakowska and Suder 2016). The SIMS ionisation technique puts the sample under high vacuum and bombards it with high energy primary ions, which initiates a transfer of energy from primary ion beam to the surface molecules causing excitation and ionization of the analytes. The ionized analytes are referred to as secondary ions and are sputtered into microscopic particles, ejected from the sample surface and then drawn into the mass analyzer under vacuum for analysis. The highly focused ion beam in SIMS provides excellent spatial resolution. However, the primary ion source is fairly limited to small

molecules, under 2000 Da and due to its high energy it is prone to fragment large molecules in the ablation/ionization process (Bodzón-Kulakowska and Suder 2016). SIMS imaging does not require special preparation after sectioning and mounting the tissue, but there are some optional methods that improve the imaging results. The tissue can be coated with a thin layer of gold, silver or matrix to improve the ionization and reduce the fragmentation of larger molecules (Gemperline, Chen and Li 2014).

2.2.3 Mass Analyser

The ions generated by the techniques mentioned are detected by their mass/charge ratios (m/z) and a range of mass analysers are available, each with benefits and limitations, see *table 2.1*. One MSI experiment can produce multiple ion images within a narrow mass range of only a few hundred Da and therefore analysers with high mass accuracy and resolving power are desirable (Cobice et al. 2015). The majority of static SIMS and MALDI imaging measurements are performed using time of flight (TOF) mass analysers. TOF analysers provide high detection efficiency and high sensitivity. Modern TOF instruments combine this performance with excellent m/z resolution, accurate mass capabilities and can operate at high repetition rates (McDonnell et al. 2012).

Table 2.1 Comparison of MS imaging approaches (Gemperline, Chen and Li 2014)

Type of MSI	Ionization source	Common mass analyzer	Optimal analytes	Mass range (Da)	Spatial resolution (μm)
MALDI	UV/IR laser Soft ionization	TOF	Lipids, peptides, proteins, small molecules	0–50,000	30–50
SIMS	Ion gun Hard ionization	TOF Magnetic sector Orbitrap	Lipids, small peptides, small molecules	0–2000	0.5–1
DESI	Solvent spray Soft ionization	Orbitrap	Lipids, peptides, small molecules	0–2000	100

2.2.4 Image Registration

MALDI mass spectrometry can generate MS profiles that contain hundreds of biomolecules directly from tissue. Spatially correlated MSI reveals how each biomolecular ion varies across tissue samples. The data cube in *figure 2.5* of position-correlated spectra is aligned with an optical image of the stained tissue section (it is stained after the MALDI MSI experiment). Advanced data analysis tools allow the datasets to be correlated to reveal which molecules are found to have spatial distribution within specific histological features (Jones et al. 2012).

Data analysis is the one area where the experimentalist is less restrained. Commercially available and open source mathematics packages provide a broad array of statistical tools that can be applied to imaging mass spectrometry datasets (Jones et al. 2012).

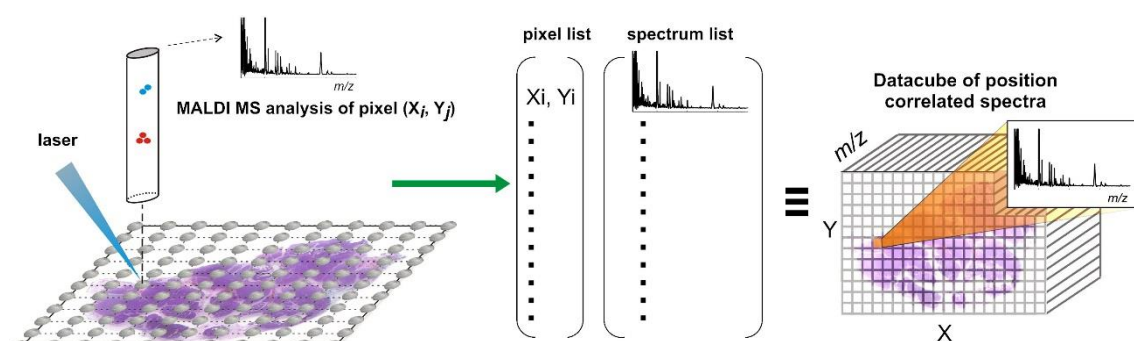


Figure 2.5 Imaging MS experiments typically record the data as a list of mass spectra, each of which corresponds to a specific pixel. The image of an MS peak is then created by displaying the peak's intensity in every pixel's mass spectrum at the pixel's coordinates. Such an approach enables the analyst to define measurement regions that trace the edges of irregular shaped tissue sections, thus minimizing measurement time and data load (Jones et al. 2012)

2.3 MALDI MSI of Endogenous Steroids in Therapeutic Research

In pharmaceutical research, distribution of drug metabolites plays an important role in drug development. Understanding the pharmacodynamics and pharmacokinetics of a drug help to determine the appropriate dosage levels to administer and the possible side effects that may occur (Cobice et al. 2015). Molecular imaging technology plays a key role in visualising anatomical structures and physiological activity both in preclinical research, development and in clinical practice. Wang defines molecular imaging technology as the “visualisation, characterisation and measurement of biological processes at the molecular and cellular levels in humans and other living systems” (Wang et al. 2013), *figure 2.3* supports this claim.

Steroids are low-molecular weight compounds that are lipophilic and derived from cholesterol. Steroid hormones are responsible for the coordination of physiological and behavioural responses for specific biological functions, e.g. reproduction (Levell 1980). Vitamin D is a collective name for a group of fat soluble secosteroids, D₃ being the most important. It is oxidised in the liver to become its most abundantly circulated metabolite – 25(OH)D₃ - which is further hydroxylated in the kidney to its active form – 25(OH)₂D₃. A good understanding of vitamin D distribution has been established by radiolabelling and histology, which are the methods that are used to date to provide drug localisation information at a cellular level in drug development (Solon et al. 2010). Radiolabelling techniques involve the integration of radioisotopes into the drug, typically ¹⁴C and ³H. The radiolabelled drug molecule’s behaviour *in-vivo* can then be traced to provide transport and metabolism information within a living system (Wang et al. 2013). This technique has been effective in contributing vast amounts of the intelligence available today regarding vitamin D interaction with the body. For example, Stumpf (1995) first reported that vitamin D deficiency in the body was linked to more diseases than previously understood by utilising receptor micro-autoradiography (RMA) imaging

technology to investigate their hypothesis. Stumpf was able to ascertain that vitamin D receptors were found all over the body. Prior to Stumpf's discovery it was strongly maintained that vitamin D's role was to regulate calcium through vitamin D receptors (VDR) in the intestine, bone, kidney and parathyroid gland only (Krishnan et al. 2010), while Stumpf's research in 1995 reported sixty different VDR locations around the body. Vitamin D deficiency is linked to many chronic diseases including prostate cancer. However, the inability to measure cell-specific metabolite concentrations currently prevents the understanding of tissue specific pharmacodynamics of VDR agonists on androgen metabolites (Qi, Muller and Volmer 2017). The pharmacokinetic analysis of small molecules in the later stages of drug development currently is typically done by quantitative whole-body autoradiography (QWBA). This is considered a sensitive method that has regulatory acceptance. However, it is unable to recover a spatial distribution image that distinguishes between parent drug and metabolite (Cobice et al. 2015). MALDI MSI is a molecular spatial distribution imaging analytical technique that is well established in analysis of large molecules. However, small molecule analysis has been challenging due to matrix ion spectral interference (Chacon et al. 2011). Another obstacle in analysis of many endogenous molecules is that they are not easily ionisable. Derivatisation reagents can be successfully used to limit this issue by increasing ionisation efficiently and by shifting the m/z range of compounds to higher values. Derivatisation can also decrease isobaric interference levels (Ding et al. 2010). Isobaric interference is a result of equal mass isotopes of different elements present in the sample solution. The drawback to this method of detection is the additional treatment step prior to desorption by MALDI, which is time consuming and may reduce recovery (Qi et al. 2018). Reactive MALDI matrices can simultaneously exhibit properties of both an efficient matrix and a derivatising reagent, minimising the sample preparation and show potential to enhance accuracy and understanding when analysing small molecules. It is

label free and has the ability to discriminate drug from metabolite while simultaneously reporting their distribution (Cobice et al. 2015).

Through advances in imaging technology, it is now accepted by pharmacologists that vitamin D performs a much more critical role than was previously in-grained. Vitamin D deficiency is now linked to a number of diseases including, cancer, diabetes, depression, neurodegenerative and cardiovascular diseases (Gueli et al. 2012). Vitamin D is a steroid prohormone that undergoes a two-step metabolism process that produces the biologically active metabolite known as calcitriol (Jeon and Shin 2018), which then binds to the VDR to express a number of metabolites. In cancer research vitamin D metabolites have been reported to have many anti-tumorigenic properties. There has also been some data published to indicate evidence of dysregulated behaviour (Tretli et al. 2009). Though an accurate understanding of the relationship between vitamin D metabolites and cancer cells is not obvious yet, it is clear that the unyielding connection is present. At present in the US and Canada it is reported that half the population are being diagnosed with deficiency in vitamin D and are being treated with supplements but the scientific evidence to support this treatment is based on observational studies and serum levels which are not adequate (Demer Linda, Hsu Jeffrey and Tintut 2018). Therefore understanding vitamin D metabolism, transport and function in disease is critical in the development of successful vitamin D based research (Jeon and Shin 2018). These findings also highlight the importance of method and technology development in imaging that is necessary to increase understanding of metabolite distribution for drug development and clinical research.

2.4 MALDI Mass Spectrometry for Small Molecule Analysis

In a study by Qi in 2018, standard matrices have been derivatised for direct analysis of 25(OH)D₃ in human serum. The researchers found that samples analysed by MALDI MS showed vitamin D quantification levels had no significant statistical difference to adjacent samples analysed by liquid chromatography tandem mass spectrometry (LC-MS/MS), which is a widely used method of quantification for vitamin D in fluids. The LC-MS/MS was found to be much more time consuming and requires a solvent mobile phase that MALDI does not (Qi et al. 2018). MALDI analysis in Qi's study did present inferior precision ability to LC-MS/MS, however Qi does reference examples where extensive signalling improved precision of MALDI MS albeit at the cost of longer analysis time (Qi et al. 2018).

Chacon in 2011 reports on the use of on-tissue derivatisation with MALDI /MSI for the analysis of 3-methoxysalicylamine (3-MoSA). 3-MoSA is not a steroid but it is a small organic molecule, therefore the same principle for steroid analysis can be applied. In Chacon's study the derivatising reagent used is 1,1-thiocarbonyldiimidazole (TCDI). The reagent attaches to 3-MoSA allowing it to be ionised by the MALDI process. The aim of Chacon's study was to develop a method for on tissue derivatisation that would improve sensitivity and limit matrix ion interference, Chacon also hoped to deliver a procedure that can be used for other small organic molecule analysis. In Chacon's experiment a mouse was dosed with 3-MoSA, sacrificed 30 min after dosing was completed, then dissected to prepare and treat liver samples with the derivatising reagent (Chacon et al. 2011). Derivatised and underderivatised samples were analysed by MALDI and cross-referenced with data obtained from LC-ESI MS/MS analysis. The key findings from this study were: a) without the TCDI treatment of tissue samples MALDI/MSI was not capable of detecting 3-MoSA due to its low sensitivity of detection (below noise level) for this molecule; b) images of liver sections showed good retention of spatial distribution

for 3-MoSA – TCDI molecules and c) the study demonstrated the possibilities of studying other small molecules like steroids, by using this process with adaptations to the chemical derivatisation reagents used (Chacon et al. 2011).

Flinders has utilised hydrazine based derivatising reagents for the analysis of compounds containing carbonyl functional groups to produce hydrazones. 2,4-Dinitrophenylhydrazine (DNPH) and 4-Dimethylamino-6-(4-methoxy-1-naphthyl)-1,3,5-triazine-2-hydrazine (DMNTH) were the derivatising reagents used. These are characterised as “reactive matrices” due to their derivatising abilities and ability to assist in desorption and ionisation with MALDI (Flinders et al. 2015). The corticosteroid analysed in his study was successfully derivatised to produce the expected mass detection by MALDI. Elements of note revealed from this research were: a) the crystallisation pattern of DNPH, which is a needle formation, did not cover the whole sample. This problem was resolved by using 1:1 molar equivalence mixture of DNPH with α -cyno-4-hydroxycinnamic acid (CHCA) matrix. The CHCA promoted an even crystal coverage while the DNPH maintains the reactive function; b) The analyte contained two carbonyl functional groups. However mono-derivatisation occurred due to steric hindrance, which highlights the importance of careful consideration when selecting derivatisation reagents (Flinders et al. 2015). Other factors to consider when selecting a reagent were, (1) the reagent must be pre-charged, (2) it must contain a suitable reactive group and (3) it should be commercially available or inexpensive and relatively straightforward to synthesise (Richardson et al. 2000).

2.5 Comparing MALDI MSI with existing Autoradiography Techniques

Several imaging techniques provide information in relation to drug distribution in tissue. Spectrometric methods include MALDI, DESI and SIMS. Radiography techniques include, whole body autoradiography (WBA), micro-autoradiography (MA) and RMA. These techniques use radiolabelling isotopes to identify drug distribution in a tissue section. Despite the method's many benefits, one fundamental limitation of this technology is the inability to distinguish the parent compound distribution from potential metabolite distributions (Solon et al. 2010). Radiolabelling techniques are often teamed with identification and quantification data obtained by LC-MS/MS from tissue extraction to enable metabolite recognition (Flinders et al. 2015). LC-MS/MS another drug tissue quantitative analysis method can provide results in nanograms of drug per gram of tissue. It discriminates between parent drug and metabolite and it is quantitative. However it provides no distribution information and interpretation and extrapolation of data is deemed to be dubious (Castellino, Groseclose and Wagner 2011).

To compare autoradiography methods of analysis with MALDI/MSI, WBMA is a low resolution, fast simple method approach but lacks sensitivity and metabolite recognition. It provides data that is similar to bioassays and is widely used for larger molecules or parent drugs. MA has high resolution but low specificity for metabolite binding sites and this lack of specificity can often cause false negatives deeming it unsuitable for metabolite analysis (Stumpf 2013). Autoradiography with radiolabelled compounds has provided valuable information with both low resolution WBMA and high-resolution MA. WBMA is a uniform and expedient single method approach providing convenient dose, time-related overviews and data similar to those obtained from conventional bioassays and is therefore widely used. However, WBMA, like common bioassays, has limitations. High specificity-low capacity sites of binding and deposition frequently remain unrecognized, while lack of cellular resolution can cause false negatives. Goodwin (2015) performed a

comparative analysis study of a therapeutic peptide, AZD2820 within a mouse kidney tissue section. The distribution of the drug obtained from MALDI TOF MSI was compared with corresponding data recovered using QWBA ^{14}C radiolabelled analogue of the same peptide. It is noted in the article the synthesis of the radiolabelled analogue took six months to synthesise. Imaging from QWBA found the compound predominantly at the injection site and in the kidney. Kidney tissue sections taken post dose and analysed by QWBA do not distinguish the parent drug from the metabolite. Neither does it distinguish whether the compounds are covalently bonded to the receptor or unattached. AZD2820 has two dominant metabolites -M1 and M2- that retain the radiolabel. MALDI-TOF MSI was employed to differentiate between AZD2820 and the two metabolites by mapping the relative abundance of their independent m/z ratio. *Figure 2.6* (A) shows the images obtained from the QWBA analysis and (B) images from MALDI-TOF MSI analysis at the time points shown. The ion distribution in (B) of AZD2820 $[\text{M}+\text{H}]^+$ at m/z 1045 was principally found along the outer medulla and cortex at T 30 min and at T 120 min it was found chiefly at the inner medulla and kidney pelvis. The M1 $[\text{M}+\text{H}]^+$ at m/z 878 ion distribution mapping at T 30 min showed predominant detection in the cortex with increased abundance of M1 at the cortex at T 120 min. The QWBA image showed a uniform distribution of the kidney section with a darker area at the pelvis indicating high deposits of radiolabelled molecules there.

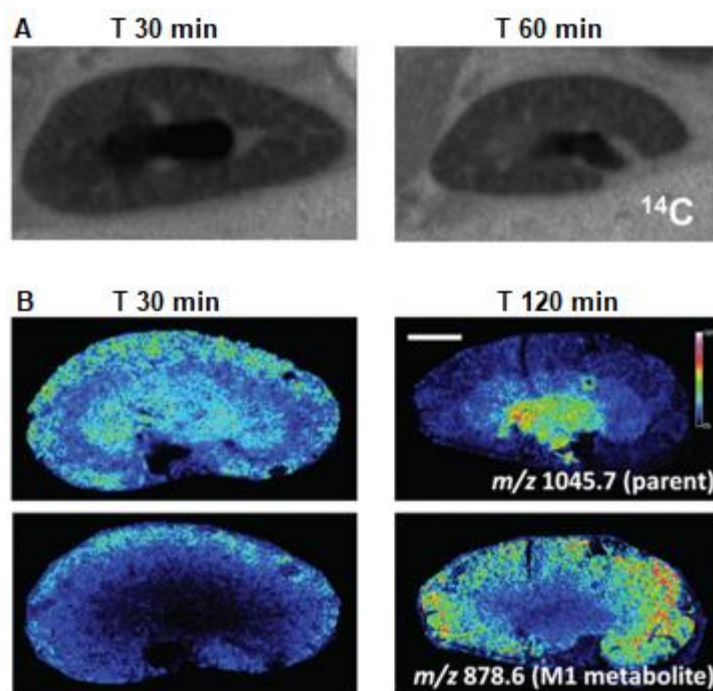


Figure 2. 6 (A) Autoradiogram of AZD2820 in mouse kidney. (B) MALDI MSI showing Relative abundance of AZD2820 $[M+H]^+$ at m/z 1045.7 and M1 metabolite $[M+H]^+$ at m/z 878. (Goodwin et al. 2016)

MALDI-TOF MSI of the second metabolite M2 $[M+H]^+$ at m/z 1046.53 was not as straightforward as M1. M2 has a very similar molecular mass to that of the parent compound AZD2820 which resulted in masking of the M2 peak. Typically, MSI can overcome this issue by performing fragmentation of the target and mapping the unique fragment masses. However, the composition of AZD2820 and M2 are very similar and were likely to generate further similar fragmentation masses. To get around the issue the analysis was carried out on a MALDI Fourier transform ion cyclotron resonance (FTICR) MS which has higher mass resolving power to the TOF mass analyser being using in the initial analysis. The FTICR possessed the required mass resolving power to differentiate AZD2820 from M2 (Goodwin et al. 2016). Although not performed in Goodwin's study the high-resolution MSI analysis of compounds can simultaneously identify endogenous metabolites. That data could be used as pharmacodynamic or toxicity marker data (Goodwin et al. 2016).

A study carried out by Manuel et al, in 2015, was aimed at the evaluation of receptor autoradiography in pharmacodynamics drug discovery studies teamed with MSI as a complementary method of analysis. Focusing on the anatomical distribution of radio ligand binding sites resulted in the activation of neuro transmitter receptors and G protein coupled receptors, which is one of the principle drug-targeting site. The study highlights the key role receptor autoradiography has played over forty years in the identification and mapping of small molecules and their receptor sites. It is capable of high-resolution imaging, is a very sensitive technique and has been, and continues to be an essential validated analytical method of analysis in drug discovery. The study goes on to mention limitations concerning the use of radioactive materials and the health and safety implications that it has and the inability to distinguish original binding sites to a signal from a metabolite and the often time-consuming effort in synthesising the radiolabelled molecule. These limitations have led to an increased interest in the development of label free techniques. Manuel's review claims "...the future of autoradiography probably lies in MSI and drug discovery departments should begin to take this into account" (Manuel et al. 2015). Professor Walter Stumpf, who revealed undiscovered properties of vitamin D through analysis with receptor autoradiography is an avid supporter of the technique. Stumpf states no alternative technique can successfully match RMA's sensitivity but does recognise the shift towards label free imaging and predicts RMA and MSI will coexist (Stumpf 2013).

MALDI MSI is a much faster technique to existing imaging methods and its ability to identify multiple compounds simultaneously just by their molecular mass and ionisation makes it an attractive new method of analysis for small molecules. MALDI-MSI is a relatively new technique in small molecule analysis and is already influencing drug development. It is being utilised as an investigational tool in areas such as compound toxicity and to support new drug regulatory applications (Cobice et al. 2015). With

radiolabelling techniques, detection is based on the quantification of radioisotopes present in a tissue sample, but it cannot distinguish the parent drug from a metabolite retaining the label and can produce inaccurate distribution intensity images. Since drug metabolites are often the cause of drug toxicity and side effects, an unclear distinction using labelling limits its ability to determine pharmacological and toxicological responses in drug development (Solon et al. 2010). Notwithstanding these restraints, labelling techniques have good specificity for drug related material, are quantitative, sensitive, have a large dynamic range and are the regulatory accepted industrial standard method in use today (Castellino, Groseclose and Wagner 2011).

MALDI MSI has novel attributes that provide an opportunity to deliver prudent tissue distribution for metabolites and parent drug that may surpass autoradiography methods that are used today as standard. Recent advances in technology, instrumentation and software at an ever increasing pace are facilitating more research in this approach that may lead to the standardisation and utilisation of this method beyond the laboratories of the pioneers in this area (Castellino, Groseclose and Wagner 2011).

2.6 Organic Synthesis

The organic synthesis of reactive MALDI matrices involves the application of several different chemical reactions. The Knoevenagel condensation and the Williamson Ether synthesis were some of the more heavily employed reactions. This section gives an overview of the types of reactions used, how they work, the conditions they require and the types of products they produce.

2.6.1 Knoevenagel Condensation

In 1894 Emil Knoevenagel discovered the condensation reaction which involves a nucleophilic addition of an active hydrogen compound to a carbonyl group followed by a dehydration reaction, it is a classic carbon – carbon double bond forming reaction (Jones 2011). The reaction is regularly used in organic synthesis and produces intermediates for the synthesis of natural and therapeutic drugs, polymer, cosmetic and perfumes (Kwak and Fujiki 2004). It requires relatively mild reaction conditions, short reaction time and provides good yields (Patel 2014).

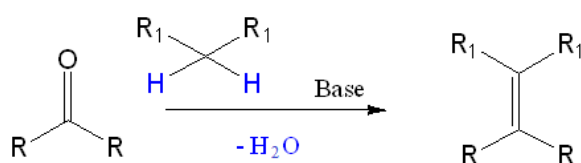


Figure 2.7 Knoevenagel Condensation

Knoevenagel reaction is a base catalysed reaction that generally occurs between an aldehyde (or ketone) and any compound with an active methylene group, the general scheme is shown in *figure 2.7*. The organic solvent is a weak base, this deprotonates the methylene group forming a carbanion. The activation of the methylene is a result of a directly attached electron withdrawing, acyl, cyano or nitro group, often two of such

groups are present. The carbanion then attaches to the aldehyde (or ketone) carbon to form a new carbon – carbon double bond that is an α , β unsaturated compound (Jones 2011). The aldehyde in the reaction can be of a wide range of aliphatic or aromatic aldehydes. Ketones are less reactive and therefore their scope is more limited. Aromatic aldehydes can condense at room temperature while aliphatic require the use of moderate temperature. In a 1:1 molar ratio aliphatic aldehydes produce the Knoevenagel product, for a 1:2 molar ratio reaction the Knoevenagel product will react further forming a second adduct in what is known as a Michael Addition reaction with the second methylene compound (Jones 2011), *figure 2.8* depicts this with diethylmalonate (DEM) as the methylene group.

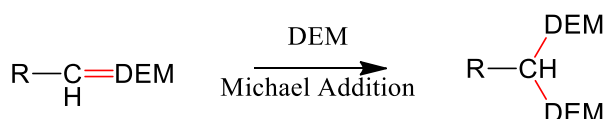


Figure 2. 8 Knoevenagel product reacting further in a Michael addition reaction in a 1 : 2 molar ratio

Choosing the appropriate catalyst is critical in achieving the expected results. Primary, secondary or tertiary amines or their corresponding ammonium salts are commonly used, but many others can be applied (Tietze 1991). The reaction is solvent dependant as the first step; the formation of the carbanion and its addition to the carbonyl of the aldehyde (or ketone) is promoted in polar solvent. The second elimination step is inhibited by excess protic solvent, for this reason the water produced in the reaction is ordinarily removed either azeotropically using a dean stark apparatus or by the introduction of molecular sieves (Tietze 1991).

In more recent years an awareness of environmental issues in chemical research and industry has led to a move towards cleaner organic synthesis. For example in 2002 Ren

reported the successful condensation reaction of aromatic aldehydes and malononitrile by grinding at room temperature in a solvent and catalyst free synthesis which was simple and environmentally benign (Ren, Cao and Tong 2002).

2.6.2 Knoevenagel Condensation with Cyanoacetic acid

Cyanoacetic acids are sufficiently reactive to undergo condensation with a range of aldehydes or ketones. Cyanoacetic acid condensation with aldehydes produces only the Knoevenagel product with no Michael adducts formed typically (Tietze 1991). The reaction follows the scheme shown in *figure 2.9*. Where aromatic aldehydes condense to form a new carbon – carbon double bond with cyanoacetic acid in the base catalysed reaction.

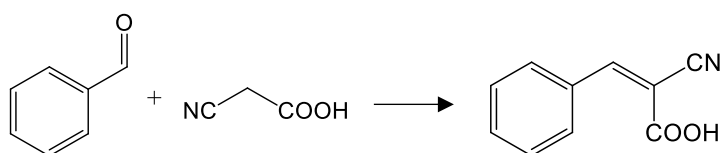


Figure 2. 9 Knoevenagel condensation with aromatic aldehyde and cyanoacetic acid

2.6.3 Williamson Ether Synthesis

Alexander Williamson developed the Williamson ether synthesis in 1850 (Williamson 1850). It remains today the simplest and most popular method of preparing ethers. It is a S_N2 reaction. It involves a nucleophile that is an alkoxide or a phenoxide ion, with an alkyl halide compound (Ouellette and Rawn 2015). Because the reaction occurs by S_N2 displacement, the best yields are obtained by using primary alkyl halides (as the halogen ion is the leaving group). Secondary halides give poorer yields as they also react in a competing elimination reaction with the alkoxide. Tertiary alkyl halides are unsuitable in the Williamson ether synthesis because they do not participate in the S_N2 reaction but instead undergo an elimination reaction (Ouellette and Rawn 2015).

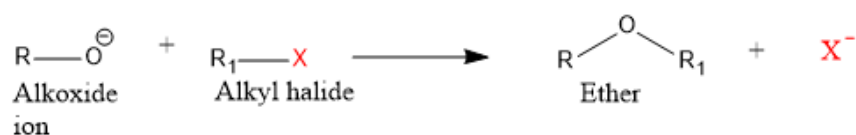


Figure 2. 10 Williamson ether synthesis of alkoxide with primary alkyl halide to produce an ether

The alcohol that supplies the electron rich alkoxide is formed by treating the alcohol with a strong base, such as sodium hydride which deprotonates the alcohol leaving a highly reactive alkoxide that can immediately react with the alkyl halide to form the desired ether compound (Gunawardena 2017), as shown above in *figure 2.10*. In the case of phenol, a weaker base like potassium carbonate is sufficiently strong enough to deprotonate phenol, as it is a more acidic alcohol.

2.6.4 Friedel Crafts Acylation

In 1877 Charles Friedel and James Crafts developed a set of reactions that involved the attachment of a substituent to an aromatic ring. Friedel Crafts alkylation involves the attachment of an alkyl group, while Friedel Crafts acylation involves the attaching of an acyl group to the ring forming aromatic ketone products. Both reactions proceed by electrophilic aromatic substitution. Friedel-Crafts Acylation is an important conversion reaction that produces compounds that constitute fundamental intermediates in the pharmaceutical, fragrance, flavour, dye, and agrochemical industries (Sartori and Maggi 2006).

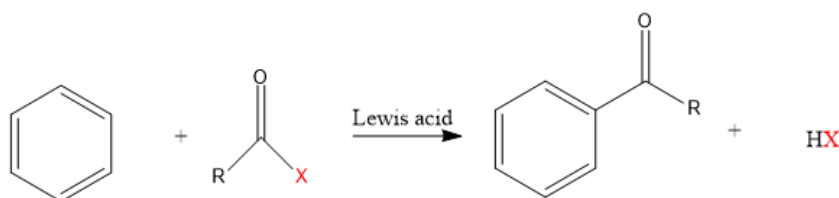


Figure 2. 11 Friedel-Crafts acylation of an aromatic ring with acyl halide and a Lewis acid

Friedel-Crafts acylation involves an acyl halide component typically acylchloride which reacts with an aromatic substrate in the presence of a catalyst usually aluminium chloride (a Lewis acid) to produce an aromatic ketone (Sartori and Maggi 2006). Initially the acylchloride converts to an acylium ion by losing a chloride ion to the Lewis acid. The nucleophilic benzene ring then attacks the electrophilic acylium ion forming one complex as shown in *figure 2.11*. This is followed by proton elimination, where the conjugate base removes the proton from the carbon bearing the acyl group to form hydrogen chloride and regenerates the original Lewis acid for reuse. The ketone produced is nucleophilic and forms a complex with the Lewis acid which needs to be treated with water to liberate the acylated aromatic ring plus aluminium salts (Hollis et al. 2006).

Friedel-Crafts acylation is considered superior and more reliable to alkylation (Clayden, Greeves and Warren 2001). The R group of the acylchloride has no limitations and can be almost any functional group, whereas the alkyl group in alkylation must be capable of forming a cation or the reaction will not work reliably. The acylation reaction also stops cleanly after a single substitution, while the alkylation reaction often goes on to give a mixture of products (Clayden, Greeves and Warren 2001). However, the Friedel-Craft acylation does have a major drawback in terms of environmental chemistry. The complex that forms between the aromatic ketone and the Lewis acid (metal halide) proves problematic as it induces the necessary use of stoichiometric Lewis acid to complete the

reaction. The complex formed also requires hydrolysis during work up to liberate the product, this leads to the loss of the catalyst and produces corrosive waste. Due to these disadvantages an increased amount of research is being done in developing more efficient catalyst that can provide a more environmentally friendly Friedel-Craft acylation (Sartori and Maggi 2006).

2.6.5 Fries Rearrangement

The Fries rearrangement is named after the German chemist Karl Theophil Fries. It is typically a Lewis acid catalysed conversion of phenolic esters to hydroxyaryl ketones. The rearrangement is *ortho para* selective, low temperatures generally favour *para* products and higher temperatures for *ortho* products (Smith and March 2007). Solvent and the amount of catalyst used can also be contributing factors.

2.6.6 Protection and Deprotection of Phenols

In organic synthesis, protective groups are necessary to render a functional group on a molecule temporarily inert allowing chemo selectivity in modifying another functional group on the same molecule during a chemical reaction. The protecting group chosen for a particular functional group should fulfil the following criteria. It should be relatively easy to introduce, inexpensive, easily characterised, stable to chromatography, stable to a wide range of reaction conditions and removed selectively with by-products easily separated from substrate (Kocienski 2006).

There are a large number of protecting groups available for phenols, the largest branch being the ether branch of protecting groups, consisting of silyl ethers, alkyl ether and alkoxyethyl ethers. Here we focus on alkyl ethers and specifically from that group, benzyl ethers. Preparation of benzyl ethers commonly involves the alkylation, via Williamson ether synthesis of the metal alkoxide with benzyl bromide or chloride to form the benzyl ether. Cleavage is typically done by catalytic hydrogenolysis, which is the

mildest approach in removing benzyl ethers (Kocienski 2006). Benzyl ethers are robust, and stable in acid, base and aqueous conditions, they are not readily attacked by metal halides or mild oxidising agents. Benzyl bromide and chloride are both strong lachrymators and also intensely irritating to skin and mucous membranes, extra care should be taken when handling these compounds (*Benzyl bromide MSDS* 2016).

Another large branch of hydroxyl protecting groups are esters and specifically within that group acetate esters. The ester is typically introduced by acylation with anhydrides or acyl chlorides in the presence of tertiary amine bases or a Lewis acid (Lugemwa, Shaikh and Hochstedt 2013). Cleavage is achieved generally under mildly basic conditions it can also be cleaved by acid catalysed solvolysis. Esters are a cheap and efficient means of protecting hydroxyl groups and are stable enough to endure a broad range of reaction conditions. However they can be attacked by stronger nucleophiles such as Grignard reagents (Kocienski 2006).

2.6.7 Baeyer Villiger Oxidation

The Baeyer – Villiger oxidation reaction was named after chemists Adolf von Baeyer and Victor Villiger who first reported the reaction in 1899. The reaction is comprised of ketones that are converted into esters or cyclic ketones into lactones using peroxy-acids as the oxidising agents (Renz and Meunier 1999).

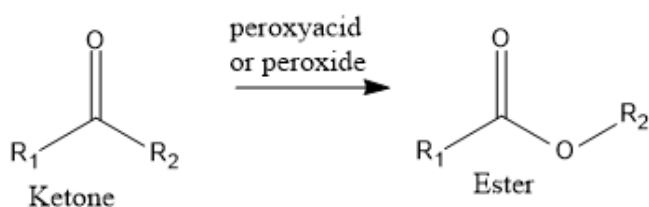


Figure 2. 12 Baeyer Villiger oxidation of a ketone to an ester

The peroxyacid first protonates the ketone carbonyl group, the carbonyl carbon is then attacked to form an intermediate with an electron deficient oxygen. Simultaneously the more nucleophilic group attached to the original ketone carbon migrates to the electron deficient peroxy oxygen group while the carboxylic acid leaves. The deprotonation in the final step forms the ester (Clayden, Greeves and Warren 2001). The migrating R group is the one that is a stronger electron donor (Clayden, Greeves and Warren 2001).

2.6.8 Diels Alder Reaction

The [4+2] cycloaddition Diels Alder reaction is named after Professor Otto Diels and his student Kurt Alder for their critical publication in 1928. Among the plethora of organic synthesis reactions, the Diels Alder reactions is one of the most well understood and useful. It provides the ability to rapidly generate molecular complexity through the simultaneous formation of carbon-carbon bonds (Nawrat and Moody 2014).

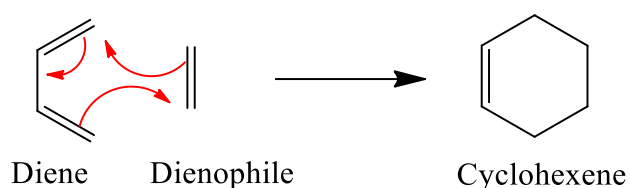


Figure 2. 13 Diels Alder Reaction

The Diels Alder reaction is a pericyclic reaction which, in a concerted mechanism, forms a substituted cyclohexene from a conjugated diene and a substituted alkene (dienophile) (Nawrat and Moody 2014). The diene can be cyclic or open chain and can have many different kinds of substituents. The dienophile typically will have an electron withdrawing group conjugated to the alkene (Clayden, Greeves and Warren 2001).

2.6.9 Urea formation

Wöhler has been described as the person responsible for bridging the gap between organic and inorganic synthesis when he first synthesised urea, the first organic compound made from inorganic substances (Ramberg 2000). In urea synthesis, an isocyanate like potassium isocyanate reacts with ammonia to form the intermediate ammonium cyanate. The intermediate decomposes to cyanic acid and ammonia which further reacts in a nucleophilic addition preceded by a tautomerisation to form urea (Ramberg 2000).

2.6.10 Dehydration

Dehydration reactions are often referred to as a subset of condensation reactions. Condensation occurs when two reactants combine to form a product and in doing so release a low molecular weight by-product. Examples of the by-products released are water, methanol, hydrogen chloride and acetic acid. When a water molecule is produced, the reaction is termed a dehydration reaction. When the water molecule leaves the product formed is often an unsaturated compound. Dehydration reactions are generally acid catalysed reactions. The reverse reaction, where the water molecule recombines with the reactant(s) is a hydrolysis reaction (Lougee 2018). Intermolecular dehydration occurs when a hydrogen ion from one reactant and a hydroxyl ion from the other reactant are released to produce a water molecule. Intramolecular dehydration is a result of one substrate releasing a water molecule.

2.6.11 Hydrazone Formation

Hydrazone formation is a condensation reaction, the reaction involves a ketone or aldehyde, which reacts with a hydrazine under dehydration conditions, see *figure 2.14* for scheme. Hydrazones fall under the more general term imines or Schiff base, imines are the nitrogen analogue of carbonyl compounds (Clayden, Greeves and Warren 2001).

Mechanistically in a two-step reaction, the amines nucleophilic nitrogen attacks the electrophilic carbon atom of the aldehyde or ketone's carbonyl group. This nucleophilic addition step is followed by the removal of a water molecule, replacing the carbon oxygen double bond with a carbon nitrogen double bond. The rate-determining step (RDS) depends on the pH, under acidic conditions the initial nucleophilic addition step is the RDS, whereas the dehydration step is under basic conditions (Soberberg 2013).

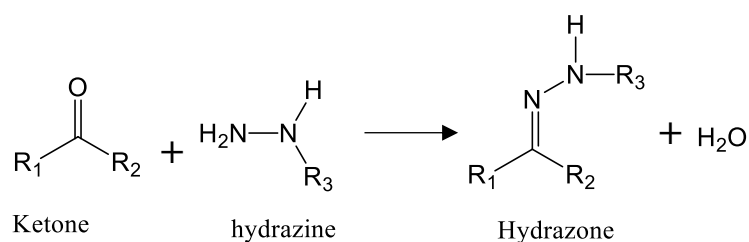


Figure 2. 14 Hydrazone formation from ketone and hydrazine

Imines are generally unstable and easily hydrolysed back to the primary amine and the carbonyl compound. However, hydrazones are produced from hydrazines and are considered a stable imine, this is due to the lone pairs on the nitrogen group attached to the amine, which increases the nucleophilicity of the amine in what's called the α -effect (Clayden, Greeves and Warren 2001). Like all unsymmetrically substituted double bonds, when synthesising these compounds the stereochemistry of the product must be considered (Sayer et al. 1974).

2.6.12 Purification

In organic synthesis, the literature focus is predominantly based on the reaction itself, the design and progress of going from starting material to product by chemical reaction, but there is more to synthesis than reactions. Each step in a synthetic sequence can typically be subdivided into three stages: reaction, purification and identification/analysis (Curran 1998). In the purification stage the reaction product is separated from by-products, solvent

and unreacted starting material. It is often the most expensive and time-consuming stage of the synthesis. The purification of an organic substance is generally achieved in two phases. The first workup stage may utilise simple phase separation techniques such as, filtration, evaporation and extraction to yield a crude product. The second phase is implemented to accomplish a higher level of purity, often involving purification techniques such as chromatography, distillation, recrystallisation and sublimation.

Here is a brief overview of the aforementioned purification techniques.

Evaporation: This method is suitable to separate a soluble solid from a volatile liquid. Heat is applied to the solution, which liberates the volatiles from the solution leaving the non-volatile solids behind.

Filtration: partitions a mixture into a solid and liquid phase, the mixture is passed through a porous membrane, which collects the solid and allows the liquid pass through.

Extraction: a liquid-liquid extraction separates compounds based on their relative solubility between two immiscible phases, usually an aqueous (polar) phase and an organic (non-polar) phase (Paterson 2018).

Chromatography: is both a purification and analytical technique, there are a number of different types of chromatographic techniques, the focus here is on purification by column chromatography, the most efficient form of purification. Column chromatography separates a mixture of chemical substances into its individual compounds. The principles of this technique involves, a stationary phase which is typically a glass column packed with silica gel and a mobile phase (solvent), the mobile phase transports the mixture through the stationary phase. The compounds are separated by their different levels of affinity to adhere to the stationary phase. The stationary phase is polar and the mobile phase is non-polar, therefore the nonpolar compounds in the mixture will elute first while

the polar compounds will adhere to the stationary phase for longer (Calvin Giddings 2017).

Distillation: separates a mixture of compounds based on differing boiling points.

Recrystallisation: this is the purification of an impure solute in a suitable solvent. The mixture is heated, which promotes the formation of a solution containing compound, impurities and solvent. The solution is then cooled slowly, which reduces the solubility of the substance, the substance then crystallises in a purer form. This is followed by filtration, the process can be repeated several times.

Sublimation: is the purification of a solid, that phase transitions from solid to gas phase without passing through the intermediate liquid phase. The success of sublimation depends on the compound having a higher vapour pressure than melting point. Once vaporised it is then cooled on a cold finger and transitions to a pure solid (Johnson 1948).

2.6.13 Characterisation Techniques

Nuclear Magnetic Resonance (NMR) spectroscopy uses nuclear magnetic spin to analyse the molecular structure of a sample. An NMR instrument consists of a superconducting magnet that generates a powerful magnetic field. Samples with nucleus such as ^1H or ^{13}C , that possess magnetic moment are placed within this magnetic field and exposed to radio waves of the same frequency and an NMR spectrum can then be obtained. NMR can determine content, purity and molecular structure of a sample (Breitmaier 2002).

Gas Chromatography Mass Spectroscopy (GC/MS) is a separating technique, most suitable to smaller, volatile molecules. The sample is first vaporised in the gas phase then transported by an inert carrier gas through the packed capillary column (stationary phase). It is then separated into its component parts, once the compounds elute from the column they are ionised by the MS, transported through the mass analyser where the ions are then

separated based on their m/z ratio. Compound peaks on a mass spectrum can be identified using the national institute of standards and technology (NIST) Library (Gere et al. 1993). ***Fourier Transform Infrared*** (FTIR) spectroscopy passes an IR beam through a sample, which can be solid liquid or gas to provide an IR spectrum of absorption. The spectrum generated at the detector represents a molecular fingerprint unique to the analyte. It is used to determine the structure of molecules by the molecules characteristic absorption of infrared radiation. The region for IR absorption is typically $4000 - 400 \text{ cm}^{-1}$ (Doyle 2017)

3 Designing Reactive Matrices

3.1 Role of a Matrix

Twenty years ago, the imaging of steroids by MALDI MSI was considered an unattainable method of analysis for these poorly ionisable, small molecules. MSI is now an established method of analysis for large molecules like proteins and peptides and with major technical advancements that have been made in all aspects of technology involved, the analysis and imaging of small molecules by MALDI MSI is now becoming available. Development in matrix technology plays a key role in this progression, derivatising reagents teamed with MALDI matrices have been utilised to overcome the poor ionisation issue and target specific reactive matrices have bridged the gap further. The MALDI matrix has several key functions which comprise of the following:

- It must rapidly and efficiently absorb the energy from the laser at the emission wavelength which is usually 337 or 355 nm for UV. For organic matrices this is achieved by a planer aromatic π system that absorbs the laser irradiation (Schulz et al. 2006).
- It serves as a solvent for the analyte, so that the intermolecular forces are reduced, and cluster formation of the analyte molecules is inhibited. After spotting the mixture containing the matrix, analyte and solvent on the target plate, the solvent evaporates leaving a co-crystallised matrix now with analyte molecules embedded (Leopold et al. 2018).
- The MALDI ionisation process takes place post desorption under high vacuum, therefore the matrix must remain stable under high vacuum conditions.
- The matrix must ensure the ion formation of the analyte. Typically, the matrix reactive moiety is benzoic acid or cinnamic acid derivatives, See *figure 3.1* for the commercially available matrix CHCA. The carboxylic group is both polar and

acidic, it ensures solubility of the matrix in polar solvent and is a proton source that encourages ionisation of the analyte (Leopold et al. 2018).

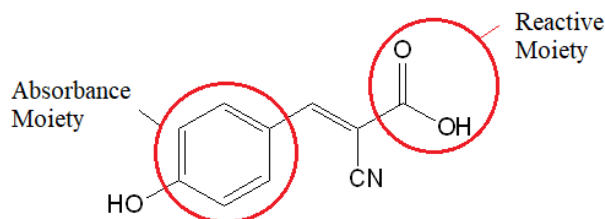


Figure 3.1 Commercially available matrix α -cyano-4-hydroxycinnamic acid (CHCA)

It is yet to be confirmed how the sample molecules become ionised, but it is the widely accepted view that once desorption has taken place the then neutral sample molecules are transported while surrounded by the matrix as a gas cloud into the vacuum chamber. There the neutral sample molecules are ionised by acid-base transfer reactions with the protonated matrix ions (Leopold et al. 2018).

When designing a matrix, the key functions of the matrix are fundamental to its design as well as that there are a number of other factors that need to be taken into consideration. It should have a fairly low molecular weight to ensure easy evaporation whilst at the same time large enough not to evaporate during sample preparation. The matrix should be relatively straightforward to synthesise from commercially available starting materials that are not expensive. The co-crystallisation of the matrix and analyte should be homogenous which is very important in terms of reproducibility of the acquired MALDI mass spectrum (Leopold et al. 2018). Another important aspect to consider when designing a matrix is the level of fragmentation attained. Although MALDI TOF is considered a soft ionisation process fragmentation does still occur. A level of fragmentation can be useful in terms of structure elucidation, but it can be problematic in

terms of quantitative analysis. Fragmentation is heavily associated with the nature of the matrix (Gidden et al. 2007).

3.2 Matrix Target Molecules

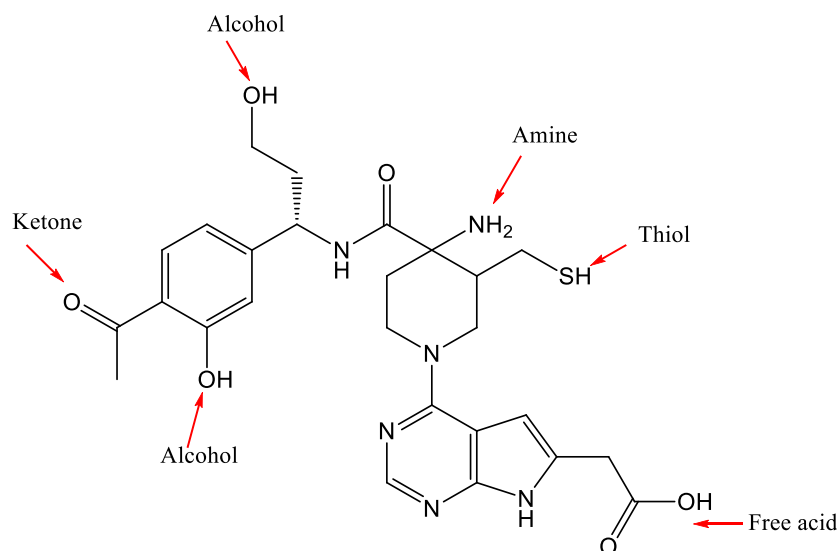
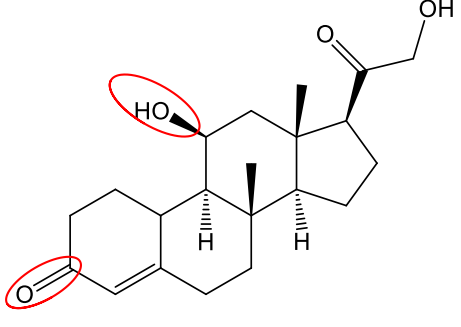
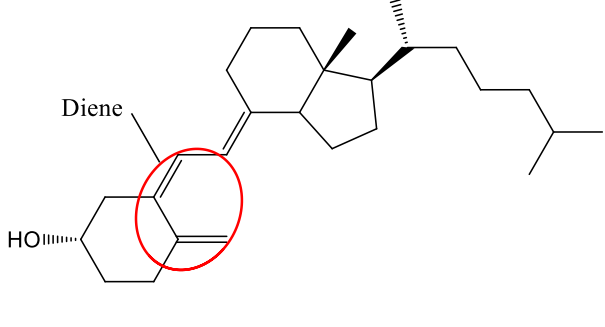


Figure 3.2 Potential target groups for derivatising

In biomolecules, there are several functional groups that can be targeted for derivatisation, ionisation and reaction with a target specific matrix as illustrated in *figure 3.2*. In this study the matrices are designed to target two groups of analytes as represented in *table 3.1 Target A*, consists of carbonyl and alcohol containing endogenous steroids for example cortisol, testosterone, aldosterone, progesterone and many more. Using solution analysis of corticosterone as a model reactive compound to analyse the matrices. *Target B*: Vitamin D₃, and its metabolites. Using a simple diene comprising molecule as a model reactive compound to verify the presence of a dienophile matrix in a Diels Alder reaction.

Table 3.1 Target compounds for matrix design

Target A: Ketone / hydroxyl containing steroids	Target B: Vitamin D₃
	

These target compounds need special attention in order to be analysed by MALDI MS. The obstacles these molecules incur are firstly associated with their size, small molecules often suffer matrix interference and have a poor signal to noise ratio. This is due to background matrix peaks in the low mass region (MW < 500 Da) from matrix fragmentation and cluster formation which are inevitably introduced following combined desorption and ionisation of matrix molecules during analyte detection (Guo 2007). A number of approaches have been reported that are aimed at circumventing this issue. High resolution mass analysers is one option, but it is an expensive one. Most research efforts instead have been directed at reducing the matrix background interference. In 1996 Knochenmuss et al. report the suppression of matrix background by optimising the analyte to matrix molar ratio, although this is not so straightforward in biological samples as the concentrations are unknown (Knochenmuss et al. 1996). Matrix additives have been used to compete for protons and subdue matrix ionisation. Guo reported in 2017 the use of a combined 1:1 matrix mixture containing CHCA, an acidic matrix and 9-aminoacridine (9-AA) a basic matrix. The study found that thermodynamic competition for protons resulted in the prevailing formation of [CHCA-H]⁻ and [9AA+H]⁺ and overall

reduction of other matrix clusters. This removal of the matrix background peaks simplified the detection of low mass analyte peaks (Guo 2007).

A second issue when analysing these molecules is their poor ionisability, the ketone and hydroxyl groups found in steroid molecules are low proton affinity functional groups. To boost the ionisation capacity by protonation or deprotonation of the steroid molecule, chemical addition to these functional groups in the steroid ring via a suitable reactive matrix can increase ionisability for MS analysis (de Kock et al. 2018). The vitamin D molecule target B is also a poorly ionisable compound with low proton affinity hydroxyl group, but the vitamin D molecules contains a diene moiety which can be utilised to react with a dienophile from a reactive matrix in a Diels Alder reaction.

3.3 Matrix Development

Bearing all of these factors in mind when developing suitable matrices: key functions of a matrix, the target analytes and their impediments, health and safety, cost of the matrix, it should be inexpensive and produced from commercially available starting material and relatively straightforward to synthesise. Based on these factors and *in silico* design, potential matrices see *Figure 3.3* and *3.4*, were proposed for target molecule A. These matrices were designed to have three integral component parts:

1. The absorbing core: for laser ablation and desorption for MALDI at the absorption wavelength.
2. The reactive moiety: Hydrazine for ketones, terminal COOH for OH via condensation with coupling reagents *N,N'*-Dicyclohexylcarbodiimide (DCC) / 4-Dimethylaminopyridine (DMAP).
3. The basic enhancer spacer: For ionisation efficiency tertiary or quaternary amines for positive ion mode.

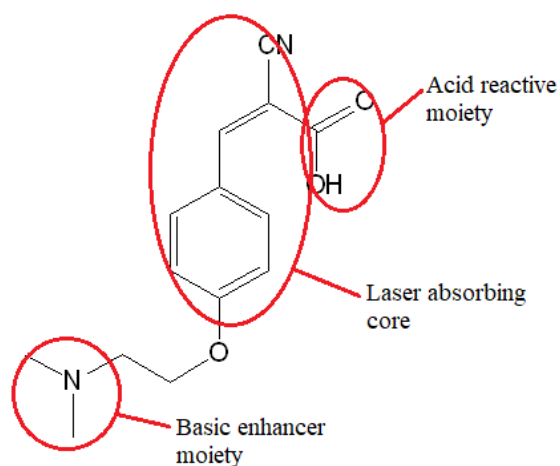


Figure 3.3 Novel matrix structure B highlighting the three integral components

Structure B and E were devised from a modified CHCA-based matrix; which is used to improve the detection of a low concentration protein and peptide digest on MALDI-TOF. Structure B is consisting of a strong UV absorbing core with the cyano group contributing to the level of conjugation. The acid reactive moiety is present to ionise the analyte and increase solubility in polar solvent. The novel attribute to this matrix is the additional tertiary amine moiety, which is intended to increase ionisability and reduce matrix fragmentation.

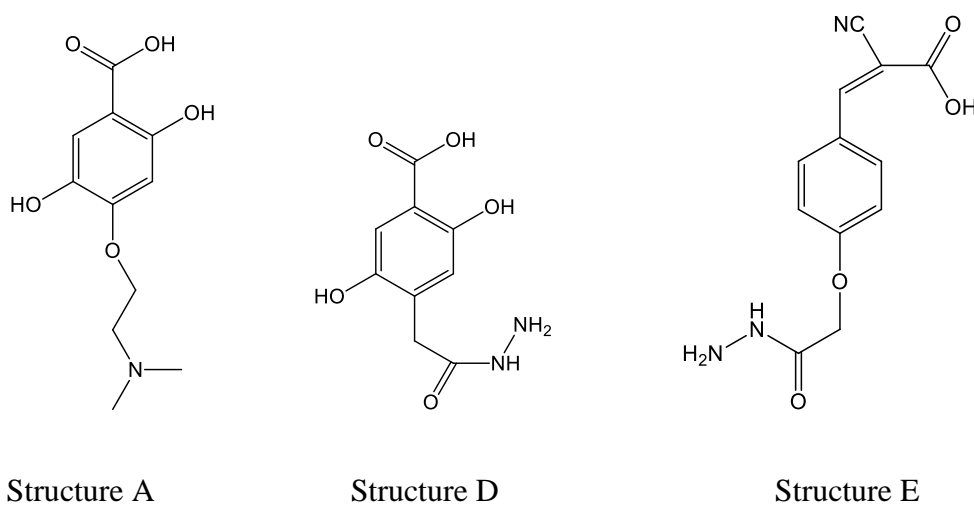


Figure 3.4 Proposed matrix designs for Target A

Structures A and D's design were derived from the already commercially available matrix, 2,5 dihydroxybenzoic acid (DHB), which is reported to contribute less pronounced background than the cinnamic acid derivatives that tend to produce undesirable matrix ion clusters (Leopold et al. 2018). These structures maintain the carboxylic acid for interaction with biomolecules and can bind closely through ion pairing thus facilitating better ionisation. The 2,5 hydroxyl groups on the benzene make the molecule a dihydroquinone and will allow it to act as a mild oxidising agent. The hydroxyls also effect the absorption by UV light.

At this point in the project, synthetic pathways were formulated initially for structure B and structure A as these were deemed to be the simplest to synthesise. Structures E and D were hypothesised to have similar synthetic routes to B and A respectively. Following successful synthesis of structures B and A it was postulated that the latter two structures could take a similar synthetic approach, using the acquired knowledge of structural behaviour and reaction modus operandi from the synthesis of the first two synthetic pathways to assist and guide in the synthesis of the latter two.

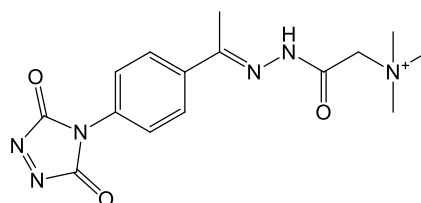


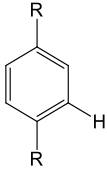
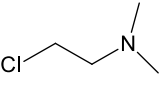
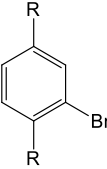
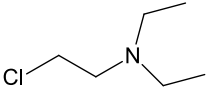
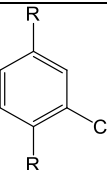
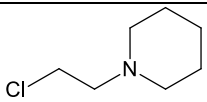
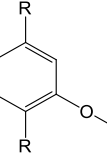
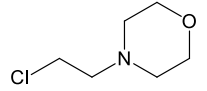
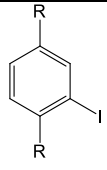
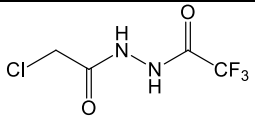
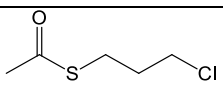
Figure 3.5 Proposed matrix structure C designed for Target B

Structure C as per *figure 3.5* was designed to target vitamin D₃ molecules and its metabolites. A structurally similar derivatising agent 4-phenyl-1,2,4-triazoline-3,5-dione (PTAD) was reported by Qi to successfully derivatise 25(OH)D₃ from human serum samples. The dienophile reacts in a Diels Alder reaction with the *cis* diene from the analyte which decreases interference levels by shifting the *m/z* range of the derivatised

species to a higher range than possible matrix background clusters, allowing for ease of detection (Qi et al. 2018). It also limits isobaric interference from similar metabolites. This reactive matrix is designed to derivatise target molecules on tissue and simultaneously react via the pre-charged quaternary amine moiety that ensures ionisation of the analyte. Because of the structural limitations in terms of ionisability of vitamin D type analytes the charged quaternary amine is necessary for MALDI analysis of these molecules. The conjugated absorbing core is also present to absorb the laser energy. In most vitamin D metabolite published assays, the work has been done on serum or plasma using ESI, other biological sources have rarely been used (Kattner and Volmer 2017). This on-tissue reactive matrix would allow for a new approach to vitamin D analysis by MALDI MSI. Spatially resolving these metabolites would provide invaluable tissue distribution information.

The synthetic pathways for the matrices developed in this section are discussed in detail in chapter four. Structure B involved a Williamson ether reaction followed by a Knoevenagel reaction with cyanoacetic acid. The chemistry for this structure worked very well. This led to an option to continue to develop structurally different matrices for target A, which would require ordering more starting material and developing a new synthetic pathway for the alternative matrices. Another option, the chosen route, was to alter the components of structure B to develop a library of structure B type matrices but using the same synthetic pathways. Alterations included changing the substituents on the benzene ring to optimise the laser irradiation absorption and by modifying the basicity of the enhancer moiety to optimise ionisation and limit fragmentation. See *table 3.2* for proposed substituent and basic enhancer moiety alterations.

Table 3.2 Structure B proposed meta substituents and basic enhancers

Meta Sub't Name	Meta Sub't Structure	C ₄ Basic Enhancer Name	C ₄ Basic Enhancer Structure
Hydrogen		2-chloro- <i>N,N</i> -dimethylethanamine	
Bromine		2-chloro- <i>N,N</i> -diethylethanamine	
Chlorine		1-(2-chloroethyl) piperidine	
Methoxy		4-(2-chloroethyl) morpholine	
Iodine		<i>N</i> ' – (2-chloroacetyl)-2,2,2-trifluoroacetohydrazide	
		3-Chloropropyl thiolacetate	

3.4 Molecular Design – Laser Absorption Optimisation

A MALDI matrix is designed to absorb the energy of the laser irradiation to create ions from molecules with minimum fragmentation (it is reported as a “soft” ionisation technique). In order for this to be achieved it is crucial that the matrix absorbs strongly at the emission wavelength of the laser, which is typically at the UV range of 337 nm or more recently 355 nm (Leopold et al. 2018). The absorbance wavelength target for this

project was 337 nm. Examples of classic organic MALDI matrices include benzoic acid and cinnamic acid derivatives, these and all established matrices possess an aromatic ring system with delocalised electrons which increase the absorption coefficient of the matrix and in turn the ionization efficiency and ion yield (Leopold et al. 2018).

In organic synthesis optimisation of the photochemical properties of an aromatic compound can be done by incorporating substituent groups on the conjugated pi system to efficiently tune the photophysical properties and procure the most favourable absorption characteristics. Substituent factors which effect the aromatic systems absorbance include, the electron withdrawing / donating attributes, the position (ortho, meta or para), inductive and resonance effect of the functional group (Abou-Hatab, Spata and Matsika 2017). The Hammett substituent constants – σ_x - are a measure of the total polar effect exerted by a substituent. Hammett constant σ_m provides a measure of the electron withdrawing or donating, inductive effect. σ_p Hammett constant describes the movement of electrons (inductive and resonance effect). The substituent constant for each individual functional group does not vary from reaction to reaction and therefore is often used to correlate data from spectroscopic methods to rationalise findings. In a recent study of benzene substituent effects on UV absorption, good correlation was observed between absorbance and substituent constants which led the author to conclude that “the shifting of spectral lines toward lower and/or higher wavelengths is influenced by both the inductive and resonance effects depending on the nature of the substituents” (Sarmah, Bhattacharyya and Bania 2014).

3.5 Molecular design - Matrix Basicity Optimisation

The basic enhancer component of these matrices increases ionisation because as a base it will readily accept a proton (H^+). This leads to a heightened ionic environment, which boosts primary ion formation of the matrix and successively an enhancement of secondary ion formation of the analyte ions. Having both a basic moiety and acid group on the matrix reduces the quantity of matrix adducts that can form, leaving the analyte more identifiable and easier to detected. The quality of crystallisation is also an integral aspect as to how well a matrix will work. It is difficult to predict the character of crystals each matrix will produce but the basic enhancer does affect the resulting matrices crystallisation. Some of the basic enhancers in table 3.2 were chosen due to differences in inter and intra-molecular bonding, with the view to optimise matrix crystal formation. In order to analyse this accurately, the matrix crystal and the co crystallisation of sprayed tissue samples need to be viewed and measured microscopically. In this project the matrices were not sprayed directly on tissue samples therefore a co crystallisation of analyte and matrix analysis was not possible. Despite this limitation, the crystal formation is an essential element in the development of a successful matrix and cannot be neglected. For this project a visual crystallisation analysis was to be carried out for each matrix.

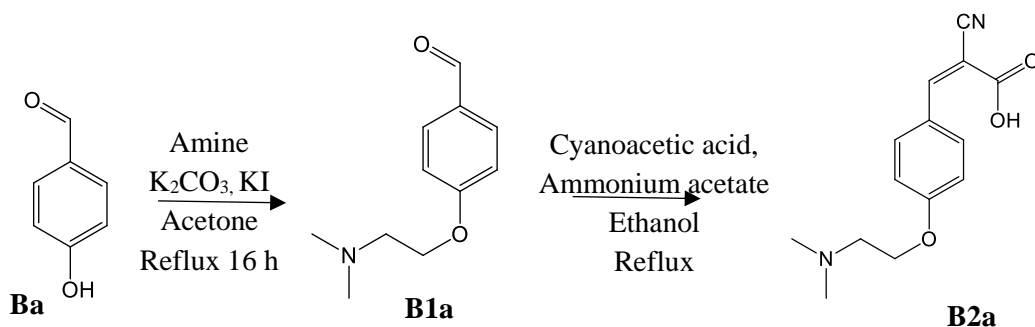
3.6 Design of Matrix Reaction for structure B - Library

In order to establish if the matrix can react with the target molecules they were first characterised by MALDI MS to identify the matrix peak and to ensure the ions travel to the mass analyser. Secondly for structure B type molecules, they were designed to react with the hydroxyl groups present in steroid molecules. A reaction was designed to test the matrices by performing an activation reaction in solution by reacting the matrices with alcohol to activate the carboxylic acid and generate the ester. The reaction also comprised of an activator, coupling reagent and a base in excess. The three alcohols chosen for the reactions were: 1) decanol, a primary alcohol; 2) terpineol, a tertiary alcohol and 3) corticosterone (CORT), which contains two hydroxyl groups. The reaction was designed to perform an efficient convergent synthesis that forms the ester and the free acid in mild conditions using a coupling reagent (Twibanire and Grindley 2011).

4 Synthesis and Characterisation Overview and Outcome

This chapter provides an overview of the matrices synthesised, outlining the reactions employed, difficulties encountered and successful results obtained. For a more detailed account of the experimental procedure for each matrix, see *Chapter 7*.

4.1 The Synthesis of Structure B Library



Scheme 4.1 Synthesis of matrix B2a

The first B type molecule, **B2a** was successfully synthesised in a two-step reaction and at a low cost. This is a most favoured outcome in the synthesis of a matrix and for any novel compound. Considering this outcome, the steps mentioned in section 4.1.1 to optimise the synthetic pathway and yield obtained were implemented and aimed at reducing time, consumables and effort when developing a library of B type matrices [see procedure A and B in *chapter 7* for general experimental detail of all B type matrices produced].

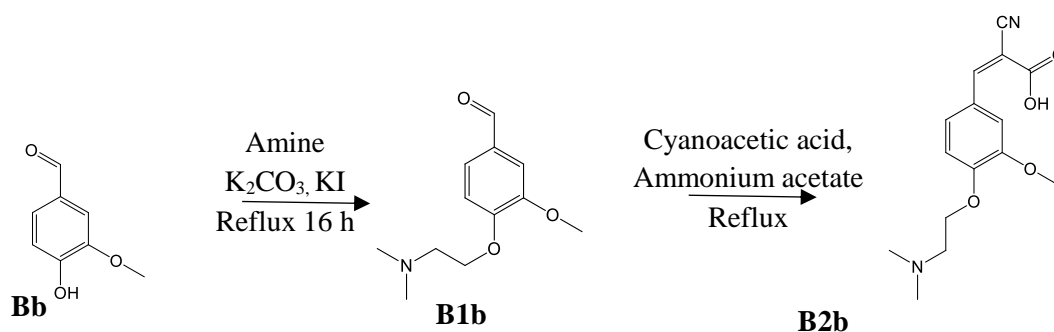
4.1.1 Matrix B2a

The first matrix undertaken was structure **B2a**, following a procedure carried out by Liew et al in 2015 for step one comprising of the addition of the basic enhancer, 2-chloro-*N,N*-dimethylethylamine, to 4-Hydroxybenzaldehyde in a Williamson ether synthesis (Liew, Chan and Lee 2015). The reaction proceeded appropriately but the yield was quite poor, < 20 %. Adjustments were made to the procedure to maximise the yield and reduce waste. Liew et al. had isolated the product by filtering off the inorganic salts, the solvent was

evaporated off and this was followed by purification by column chromatography. That process leads to an excessive loss of product, most likely due to it sticking to the inorganic salts and was unrecovered following filtration despite several acetone washes of the salts. To get around this a separation was carried out. A number of partitioning solvents were experimented with including, 5% NaOH with chloroform, water and DCM, the best results and highest yield > 50 % were accomplished using water and ethyl acetate, followed by solvent evaporation. No further purification was necessary to continue to step two. Isolation by separation also reduced the number of phases involved in step one while greatly reducing the amount of solvent required by eliminating column chromatography.

The second step, the Knoevenagel condensation to produce the final product applied a similar reaction procedure reported in 2014 by Monopoli et al. Their starting material was [(E)-4-(2-cyano-2-carboxyvinyl) phenyl]boronic acid 1 (CCPBA), but the same standard Knoevenagel mechanism was applicable for the synthesis of **B2a** (Monopoli et al. 2014). Monopoli et al. used toluene as solvent in their experiment, **B1a** was insoluble in toluene. A number of other solvents were tested finally settling on ethanol as the most suitable. The dean stark apparatus used in Monopoli's procedure was replaced by a molecular sieve, glass wool trap which worked well and was more convenient. The white crystals that formed as the final product with 68 % yield had poor solubility in most solvents, including DMSO, acetone, heptane, DCM and acetonitrile. They were found to be soluble in acidic or basic water. Water as a solvent is unsuitable for several spectrometry analysis such as GC-MS and MALDI MS which was problematic going forward. However, NMR characterisation analysis was successful in D₂O basified with Na₂CO₃.

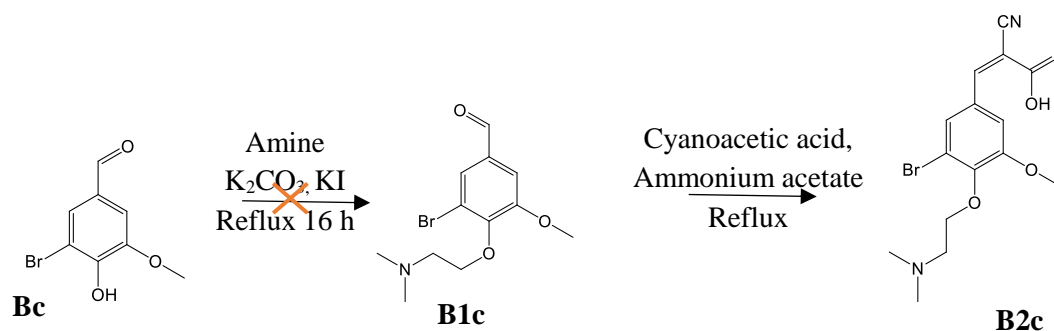
4.1.2 Matrix B2b



Scheme 4.2 Synthesis of matrix B2b

Matrix **B2b** used the same basic enhancer as in matrix **B2a**, the difference with this matrix was the methoxy group on the *meta* position of the benzene ring, thus using a different starting material (4-Hydroxy-3-methoxybenzaldehyde) for this matrix. **Procedure A** and **B** proceeded smoothly to give the desired compound in 56 % yield in the form of yellow crystals.

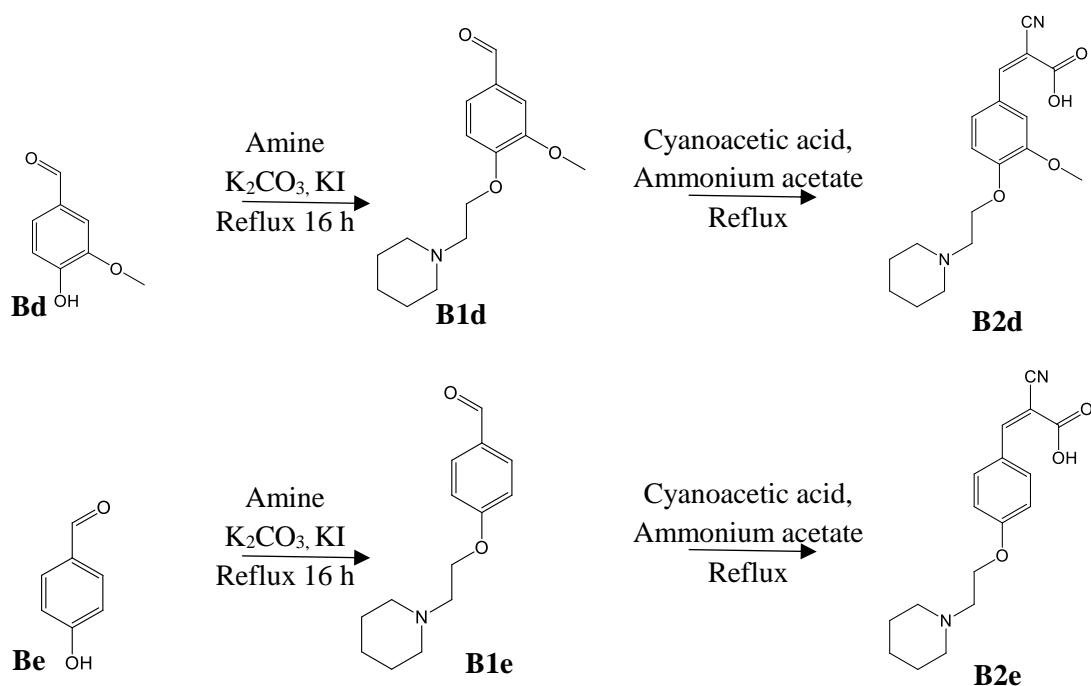
4.1.3 Matrix B2c



Scheme 4.3 Synthesis of matrix B2c

Matrix **B2c** starting material was **Bc** as the benzaldehyde. This molecule proved incapable of undergoing the Williamson ether reaction, failing to produce the desired **B1c** in step one. A second attempt was made this time using 1 eq. of sodium iodide in the reaction but again the ether synthesis was ineffective. No further action was taken with this matrix and it was noted that 2,6 disubstituted phenols were unsuitable in this context.

4.1.4 Matrix B2d and B2e

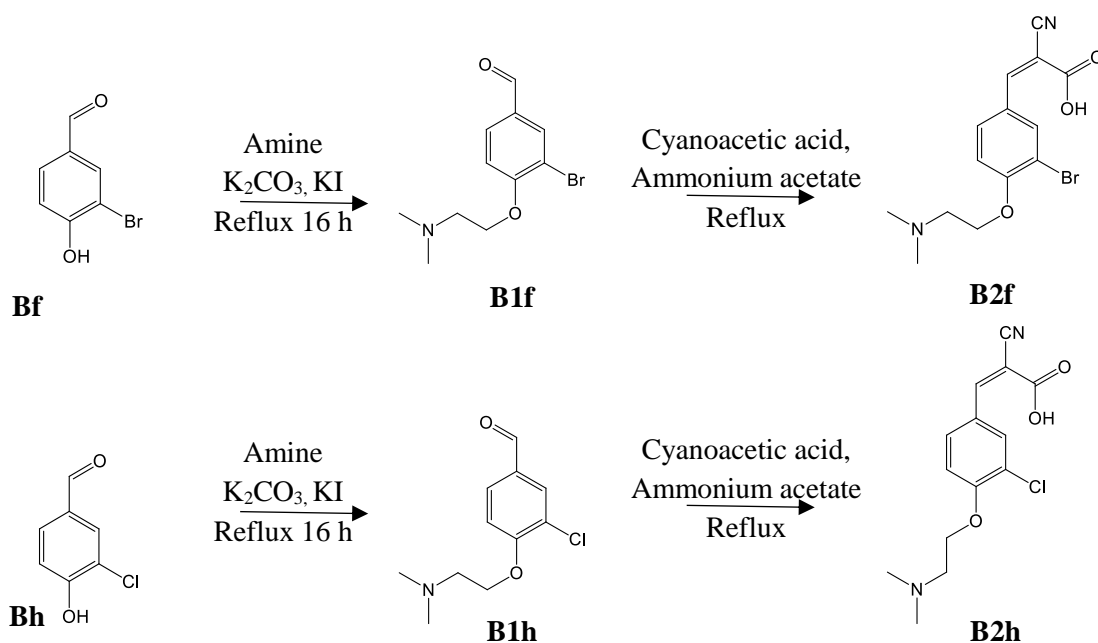


Scheme 4.4 Synthesis of matrix B2d and B2e

Matrix **B2d** retained the same absorbing core as **B2b** and provided a 95 % crude yield for step one using vanillin as the absorbing core and 1-(2-chloroethyl) piperidine as the basic enhancer in the ether synthesis to give **B1d** as a brown oil. Step 2 was not so straightforward, unlike in the previous successful synthesis, after a 3 h reflux no precipitation occurred. The TLC plate did show both starting material and another compound on the baseline assumed to be the product **B2d**. Step two was attempted using different solvents, toluene then acetone, which were both deemed unsuitable due to poor solubility and no product formation visible on TLC respectively. Before embarking on the addition of an extra phase to step two. Step two, was carried out again with extreme care taken to ensure there was no water carried over from the first step. The results were the same for step two (no precipitation) at this point it was decided to remove all solvent and perform column chromatography to isolate and purify the compound that remained on the baseline of the TLC. The column chromatography was executed using DCM and

10 % methanol which was increased to 20 % to flush out any unwanted material, then 1 % triethylamine was introduced to recover the product **B2d**. The product, an orange solid was recovered in 21 % yield. Matrix **B2e** was synthesised simultaneously with **B2d**, like **B2d** the precursor ether synthesis **B1e** delivered a good yield, but the product was not recovered by column chromatography in step two. No further development was carried out on **B2e**.

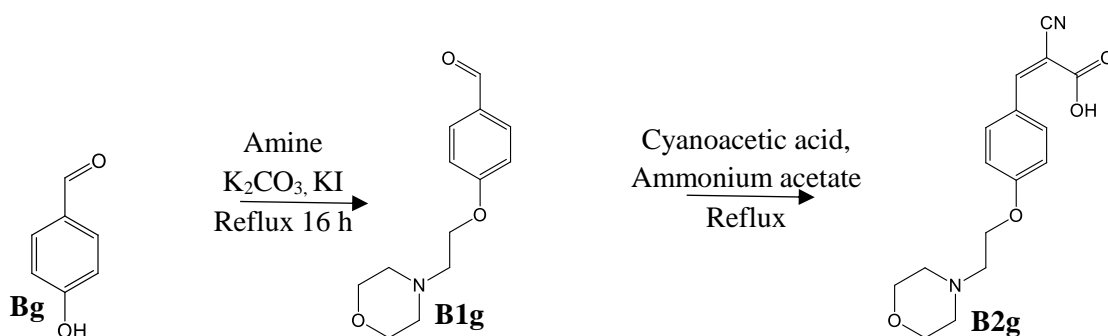
4.1.5 Matrix **B2f** and **B2h**



Scheme 4.5 Synthesis of matrices **B1f** and **B1h**

Matrix **B2f** and **B2h** applied the same basic enhancer moiety, 2-chloro-*N,N*-dimethylethanamine. The compounds differing only be the halogen on C₃, bromine for **B2f** and chlorine for **B2h**. The chemistry for procedure A and B proceeded expectedly with good yields for both compounds. Though recrystallisation was executed, the products recovered were both white and of a fine powder consistency with yields of 65 % and 54 % respectively.

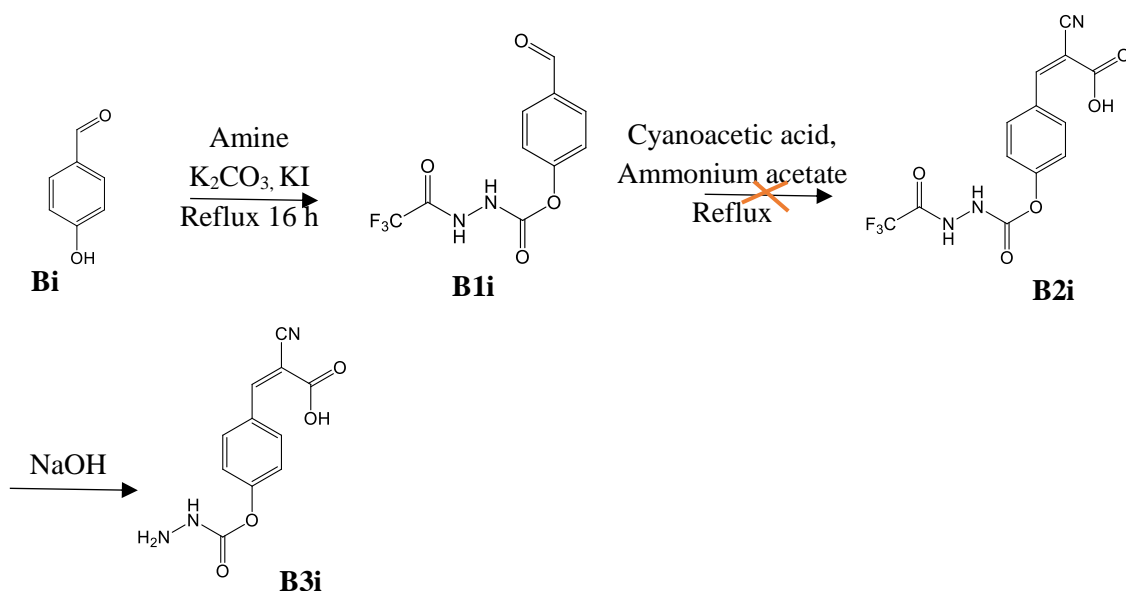
4.1.6 Matrix B2g



Scheme 4.6 Synthesis of matrix B2g

The 4-hydroxybenzaldehyde absorbing core was reacted with 4-(2-chloroethyl) Morpholine to give the ester in a 61 % yield. Following this the Knoevenagel reaction was performed with no precipitation formed. Column chromatography was carried out to isolate the product to afford a yield of 19 % as a white powder.

4.1.8 Matrix B3i

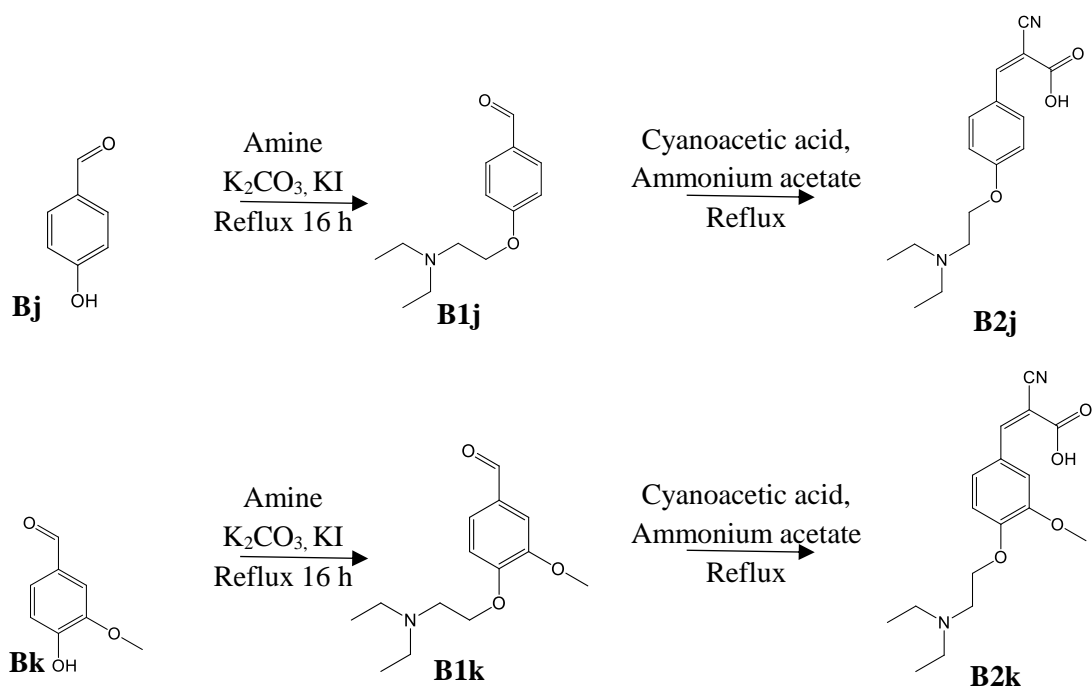


Scheme 4.7 Synthesis of matrix B3i

This matrix was a modified version of the originally designed matrix, structure **E**. It was anticipated that the same approach used for all of the B type matrices would bring to bear the desired product. **Procedure A** was applied to form the precursor **B1i** using 4-hydroxybenzaldehyde and the hydrazine basic moiety, TLC monitoring of the separation indicated the product was in the aqueous phase, with some difficulty water was removed. No further purification was carried out at this stage and **B1i** was advanced to step two. Ethanol was not efficacious in dissolving **B1i**, procedure B was carried out using other solvents i.e. methanol and THF again with poor solubility. The reactions were allowed to run with what did make it into solution but IR analysis of **B1i** and the recovered material appeared to reveal it was the same compound, indicating one of the procedures was not successful. It was postulated at this stage the compound **B1i** was reacting with itself and polymerising.

The hydrazine compound used for this matrix, *N'* – (2-chloroacetyl)-2,2,2-trifluoroacetohydrazide, was much more expensive than other basic enhancers used [€100 for 1 g] therefore supplies were minimal which limited repeat experimental opportunities. However, one final endeavour was undertaken, this time eliminating the separation phase in **procedure A** by reverting to Liew's original isolation method that avoided the addition of water to isolate the product. What was deemed to be **B1i** by TLC and IR analysis was isolated in low yields and **procedure B** was initiated. Precipitation did occur after 1 h, however the compound retrieved was not UV active. This led to the conclusion that the compound was polymerising. **B1i** is a novel compound therefore could not be positively identified by comparison with the literature. No further action was taken on this matrix [as no more *N'* – (2-chloroacetyl)-2,2,2-trifluoroacetohydrazide was available].

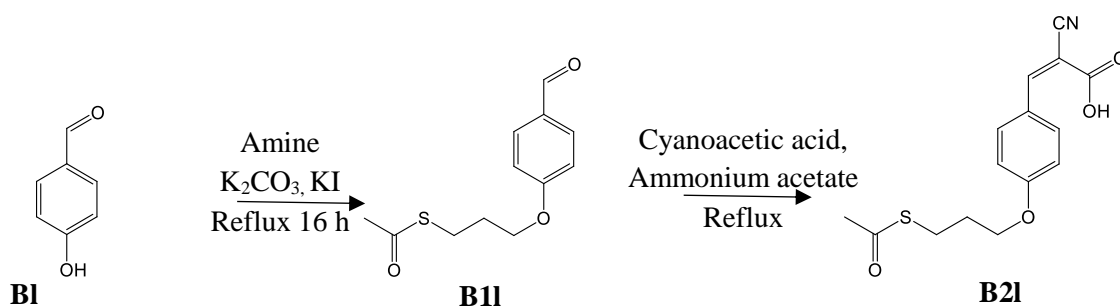
4.1.9 Matrix B2j and B2k



Scheme 4. 8 Synthesis of matrices B2j and B2k

Both of the title matrices availed of 2-chloro-*N,N*-diethylethanamine as the base and 4-hydroxybenzaldehyde and Vanillin respectively as the absorbing core. Procedure **A** and **B** were both carried out successfully with no deviation to give yellow crystals in both cases and yields of 63 % and 51 % accordingly.

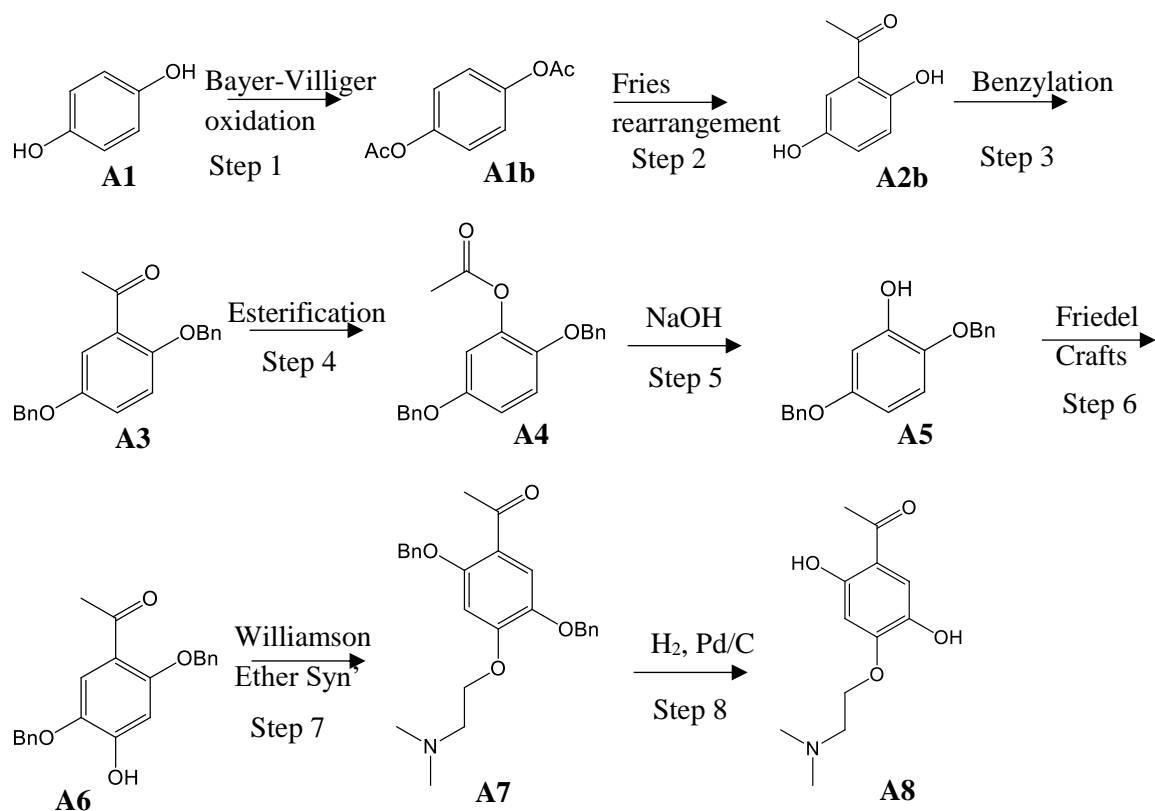
4.1.10 Matrix B21



Scheme 4. 9 Synthesis of matrix B21

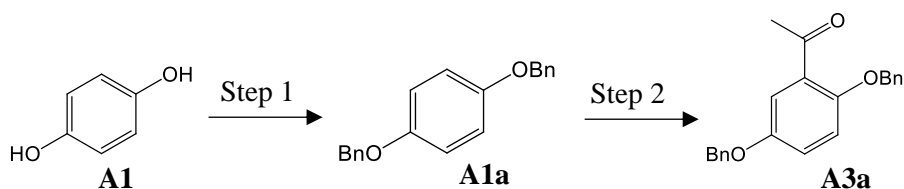
Matrix **B11** utilised 3-Chloropropyl thiolacetate at the basic enhancer, this compound is quite pungent and extra care was required when handling it and any glassware it came into contact with. Domestic bleach in water was used to soak all glassware in before removal from the fume hood. The rotary evaporator was not used for odour containment reasons. After reflux, the reaction was filtered, and solvent was removed by distillation. TLC analysis indicated some starting material understood to be **B11** close to the base line. Column chromatography was proposed as the product isolation technique. However, on reassessment of the odour problem, notwithstanding the measures taken to contain it, it was decided to take no further action with this matrix.

4.2 The Synthesis of Structure A



Scheme 4.10 Synthesis plan for matrix structure A (A8)

The synthetic plan for structure A involved a number of steps as shown in *scheme 4.10*. Typically, this is not preferable when synthesising a matrix however the materials proposed for use were inexpensive and commercially available. Initially an alternative route to **A3** was undertaken as seen in *scheme 4.11*.



Scheme 4.11 Original synthesis plan for matrix structure A to precursor A3

Benzyl bromide was used as the protection group for the hydroxyl groups on the benzene. Benzyl bromide is a category two eye and skin irritant and extra care was taken during

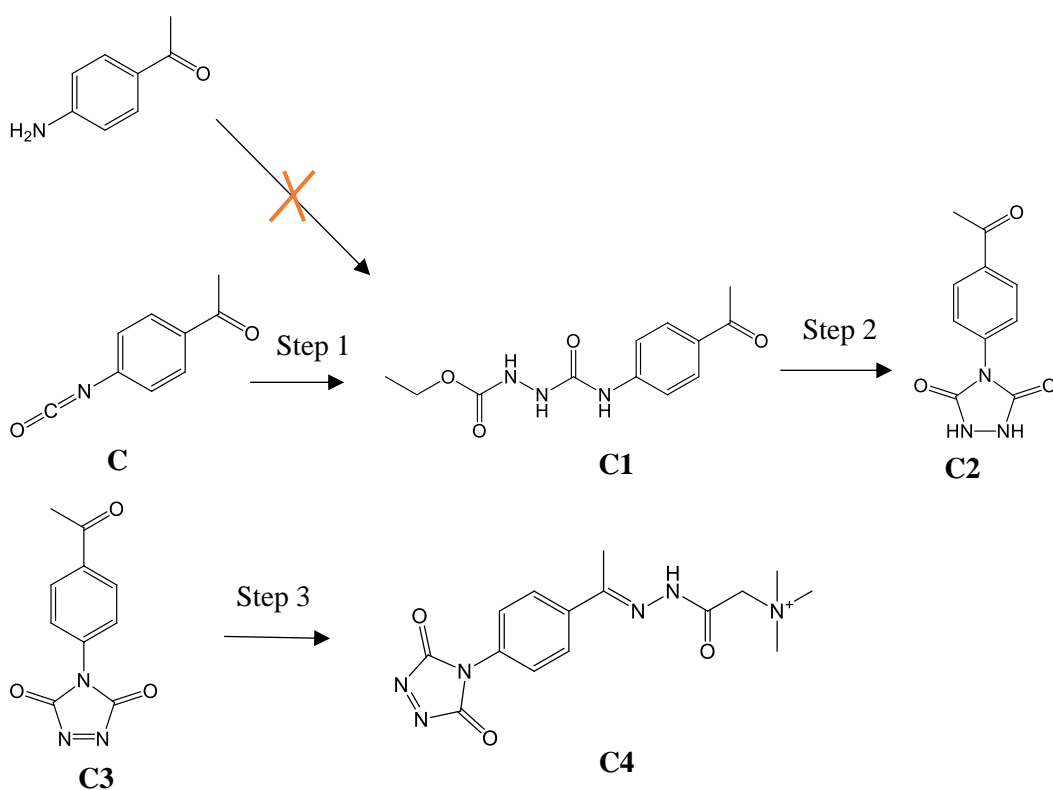
handling. All glassware that came into contact with it was soaked in 1 M NaOH overnight before leaving the fume hood. Protecting groups were successfully added according to the procedure (see experimental section for details). This was followed by the acylation of **A1a**, but this reaction was not successful as the starting material was never fully in solution. An alternative approach was then initiated see *scheme 4.10*. It is worth noting, 2,5 Dihydroxyacephenone (**A2b**) is a relatively low-cost, commercially available compound, but a large in-house stock of hydroquinone was available to use therefore the first 2 steps were included in the synthetic plan. If the matrix was successful and optimisation and reduction of materials used was to be considered at a later stage these steps could be removed.

Proceeding with *scheme 4.10*, step one and two were effectively accomplished on first trial and were scaled up on repeat to ensure adequate quantities of starting material was readily available as the subsequent steps were attempted. Step one involved the sulphuric acid catalysed reaction of hydroquinone with acetic acid to form the ester (**A1b**) in a Baeyer Villager oxidation reaction. Step two involved the gentle heating of hydroquinone diacetate with anhydrous aluminium chloride in a Fries rearrangement to give 2,5-dihydroxyacetophenone (**A2b**). In order to take this compound further it was necessary at this stage to protect the two hydroxyl groups on the benzene ring. This was done using benzyl bromide which is commonly used to install benzyl protecting groups on alcohols. Some difficulties were encountered during extraction in step three due to the formation of an emulsion, several partitioning solvents were assayed; water / chloroform, water /DCM and the appointed NaOH (5 %) / EtOAc as the most suitable aqueous and organic solvents that generated the least emulsion. Post partitioning, some benzyl bromide remained in the organic solution. In order to remove this and purify (**A3**) column chromatography with hexane and ethyl acetate in low concentration initially was used to remove the remaining benzyl bromide. Once removed the concentration of ethyl acetate

was increased to intensify the polarity and encourage the elution of (**A3**). The deprotection of the alcohols would take place in the final step performed as a palladium-catalysed hydrogenation.

Step four, the esterification of the acyl group using glacial acetic acid in a Baeyer Villager reaction with hydrogen peroxide as the oxidising agent and *p*-toluenesulfonic acid as the catalyst. The first attempt at this reaction proceeded by heating the aforementioned compounds followed by an endeavour to remove the glacial acetic acid by vacuum prior to separation, which was unsuccessful due to its high boiling point (118.1 °C). Second attempt involved the addition of excess sodium bicarbonate wash post separation to remove glacial acetic acid with cautious measures taken to ensure the safe release of excess gas produced from NaHCO₃. A test run of step five the transesterification of (**A4**) was performed but at that stage the progress of this matrix was reassessed and due to the time consuming number of steps involved, the difficulties encountered in purification, the toxicity of the materials in use and the distance to go to obtain the pursued final product (**A8**) it was decided to suspend further development of this matrix and divert efforts to more attainable alternative matrices such as the library of structure B type matrices and the development of structure C matrix targeted at vitamin D analysis.

4.3 The synthesis of Structure C



Scheme 4.12 Synthesis plan for structure C matrix

Structure C, step one, the synthesis of the unsymmetrical phenylurea formation of (**C1**), which involved the addition elimination reaction between 4-nitrophenyl chloroformate and the aromatic amine, 4-aminoacetophenone) in the presence of a base, triethyl amine, to form the intermediate carbamate. This was then followed by the addition of more triethyl amine along with the hydrazine molecule which initiated a subsequent addition elimination reaction between the carbamate and the hydrazine to form **C1**. Typically, the formation of urea is in the presence of a catalyst (Pd, Ru, Rh and Al). In this instance no catalyst was used to limit side reactions. However, during this reaction, a precipitate continued to form. It was first speculated that the precipitate forming was diphenylurea, but this was dismissed upon analysis as diphenylurea is highly conjugated and the precipitate was displaying no UV activity. Knowing it was not the product it was filtered off. Numerous attempts were made following this general procedure, with minor

adjustments each time, but to no avail. Spectroscopic analysis of products obtained showed the presence of all starting material and some 4-acetylphenyl isocyanate but none of the sought-after compound **C1**. In one instance the product obtained from the efforts of this experiment was brought forward to observe how it behaved in step two of the synthesis, it was instantly clear **C1** was not present. Having exhausted this procedure with fruitless results an alternative approach was researched, and a much more uncomplicated method was discovered (Alakurtti et al. 2010). By starting the reaction with the commercially available 4-acetylphenyl isocyanate in toluene to react with ethyl carbazate the formation of the unsymmetrical urea proceeded smoothly to give **C1** an open chain amide.

Step two, the strong base catalysed hydrolysis of the **C1** ester to form ethanol and the carboxylate salt which was acidified to produce the cyclised 4-substituted urazole **C2**. This reaction proceeded efficiently and as expected resulting in a yellow solid. The next stage, step three, oxidation of the urazole to form the corresponding 4-substituted 1,2,4-triazoline-3,5-dione (NH-NH to N=N) was first undertaken with SiO₂-HNO₃ as the oxidising agent. An advantage to this reaction is there is an expected strong colour change from yellow to bright red once oxidation occurs, providing early visual results as to how the reaction is proceeding which is unavailable in most reactions. The unfavourable elements to this reaction are the sensitivity of **C3**, these compounds are reported as being temperature, light and solvent sensitive, as well as that they are very difficult to isolate. Compounds similar to **C3** were reported back in 1912 by Stolle but they were unable to isolate them (Mallakpour 1992). This was the case with our first attempt using SiO₂-HNO₃ as the oxidising agent. The oxidation was apparent almost immediately by the red quality of the solution obtained. However, like Stolle, the difficulty lay in recovery of the product, removal of solvent by rotary evaporation caused decomposition of the remaining product. It was speculated that by-products were destroying the highly sensitive

triazolinedione. The subsequent reaction was aimed at reducing the amount of possible by-products by creating a more inert environment for the reaction to take place by pumping the flask with inert nitrogen first followed by the passing of NO₂ gas through a slurry of **C2** and anhydrous sodium sulphate in ethyl acetate. The sodium sulphate role was to act as a drying agent for the nitrogen dioxide. As the gas was pumped through, the slurry changed from yellow to bright red and the urazole dissolved, oxidation had occurred. Removal of solvent was done *in vacuo* at < 40 °C to give a red oil but within a few minutes it violently decomposed, leaving behind charred material. Again, this approach was repeated with alterations each time to a) solvent used, or b) means of isolating the oxidised product but the same decomposition of the red oil occurred each time. At this stage it was hypothesised the oxidation reaction was successfully taking place and the product was in solution, to test this theory a quick Diels Alder reaction was performed. Due to the *cis* conformation of **C3** type compounds they are considered to have powerful dienophilic properties and react rapidly in a Diels Alder reaction. The concerted reaction undergoes a rapid colour change that is easily observed. Therefore, a high concentration solution of **C3** was added to solution of 1,3-butadiene, which should react instantly with a dienophile (**C3**) in a Diels Alder reaction. Indeed a colour change from red to yellow was observed, which indicated **C3** was present. There was confirmed confidence the urazole oxidation reaction was taking place, producing the desired product. However, the isolation and by-product issue remained.

N-bromosuccinamide was next to be tested as an oxidising agent. It was reported in the literature to produce less by-products and positive results with good yields have been obtained using it for similar urazoles (Bausch and David 1992). This reaction did proceed smoothly, and a stable red solid was obtained which indicated the reduction of by-products being produced in the reaction. Again, a Diels Alder reaction was performed with a 1: 1 eq. of **C3** and 1,3-butadiene, resulting in an immediate colour change,

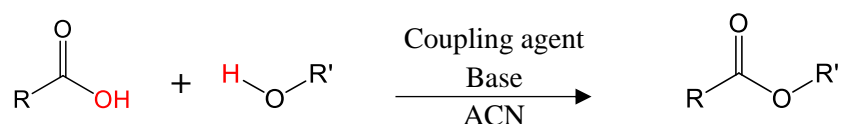
confirming the presence of the dienophile. **C3** structure is not the final desired structure for targeting vitamin D metabolites. However, it is a matrix in itself and was sent to Ulster University for characterisation and analysis. **C3** was then reacted with Girard's reagent for the synthesis of **C4** but TLC monitoring of the reaction indicated no product had formed. For future research, a new approach in synthesising the final product **C4** would be necessary.

4.4 Analysis by MALDI MS

4.4.1 Matrix Characterisation by MALDI MS

Matrix sample solutions were prepared as 1 mg/ml solutions of matrix in 80 % acetonitrile, 20 % water with 0.1 % trifluoroacetic acid, which works as a proton enrichment media in positive ion mode. The matrix analysed were B2a, B2b, B2d, B2f, B2g, B2h, B2j, B2k and C3. They were tested on the MALDI-TOF MS and the MALDI-TOF-TOF with the intension of identifying the structures by their M+1 ions and identifying dimers and sodium and potassium clusters.

4.4.1 Matrix Reaction with Alcohol Analysed by MALDI-TOF MS



Scheme 4. 13 Activation of carboxylic acid with alcohol

To activate the matrix carboxylic acid, it was reacted with an alcohol in a 1 eq. reaction. There were three alcohols (decanol, terpineol and CORT) analysed with each structure B matrix and there were three sets of reaction conditions. Each reaction contained an alcohol (0.1 eq.), the coupling agent (0.1 eq.), the base (0.2 eq.) and the matrix (1 eq.). 0.1 eq. of the matrix is involved in the esterification reaction and the remainder 0.9 eq. is there in excess to absorb a large degree of the energy from the laser. In the reactions containing CORT which has two hydroxyl groups, 0.2 eq. of CORT and 0.4 eq. of base were added. There were three reaction conditions: Reaction 1) consisted of the above reaction mixture with an additional 10 % water. It was allowed to react for 2 h at 40 °C; Reaction 2) differing from one by the amount of time allowed to react which was 5 h and this was at room temperature; Reaction 3) Contained the same reaction components but instead of

water had a 1 % TFA solution added, which was introduced to neutralise the base. This was also allowed to react for 5 h at r.t. There were eighteen samples for each reaction, providing a total of 54 samples that were analysed by MALDI-TOF MS and the acquired spectra were evaluated to determine if the esterification occurred.

5 Results and Discussions

5.1 MALDI-TOF MS for Matrix Characterisation in Positive Ion Mode

The matrices were analysed on the MADLI-TOF MS and the MALDI-TOF-TOF. The mass accuracy for MALDI MS is +/- 1 Da. The spectral range for matrix **B2a** was 150-1000 Da and for the remaining matrices 150 – 600 Da. The spectra were evaluated to identify the molecular ion, dimers, molecular fragmentation and water, sodium and potassium ion clusters.

5.1.1 Matrix B2a Molecular Weight 260 g/mol

In *figure 5.1* the ions identified included the molecular ion plus hydrogen visible at m/z 261, A dimer ion $[2M+H]^+$ is detected at m/z 532, a molecular ion plus potassium, water and hydrogen at m/z 318. The strongest, most abundant peak at m/z 332 could be the molecular ion plus hydrogen and four water molecules $[M+H+(H_2O)_4]^+$, or it could potentially be the amine spacer of the molecular ion fragmenting and reforming/ attaching as $[M+H+(CH_2CH_2-N-(CH_3)_2)]^+$.

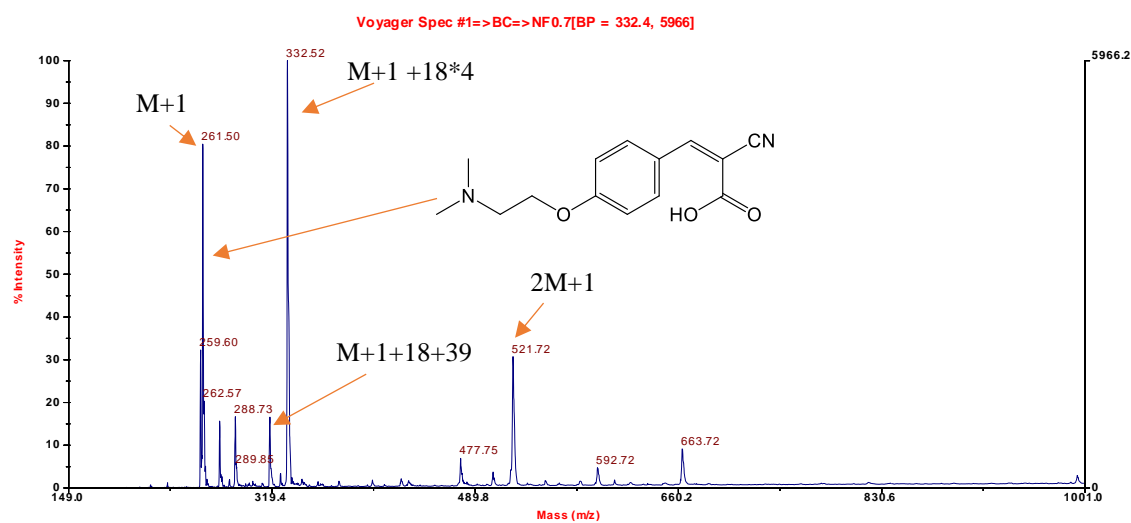


Figure 5.1 Matrix B2a mass spectrum featuring positive identification of the M+1 ion acquired from MALDI-TOF MS

5.1.2 Matrix B2b Molecular Weight 290 g/mol

In *figure 5.2* the ions detected consist of the molecular ion plus hydrogen visible at m/z 291 and a dimer ion $[2M+H]^+$ with an m/z of 581. The fragment ion at m/z 246 is understood to be the molecular ion plus hydrogen minus $(N-(CH_3)_2)$, another possibility is the fragmentation of the carboxylic acid group $COOH$. A sodium ion cluster $[M+H+Na]^+$ is visible in low abundance at m/z 314. The ion at m/z 361 $[M+H+71]^+$, similar to matrix **B2a** the +71 ion could be the addition of four water molecules $[M+H+(H_2O)_4]^+$ or the amine spacer of the molecular ion fragmenting and reforming/attaching at the double bond as $[M+H+(CH_2CH_2-N-(CH_3)_2)]^+$. From both spectra.

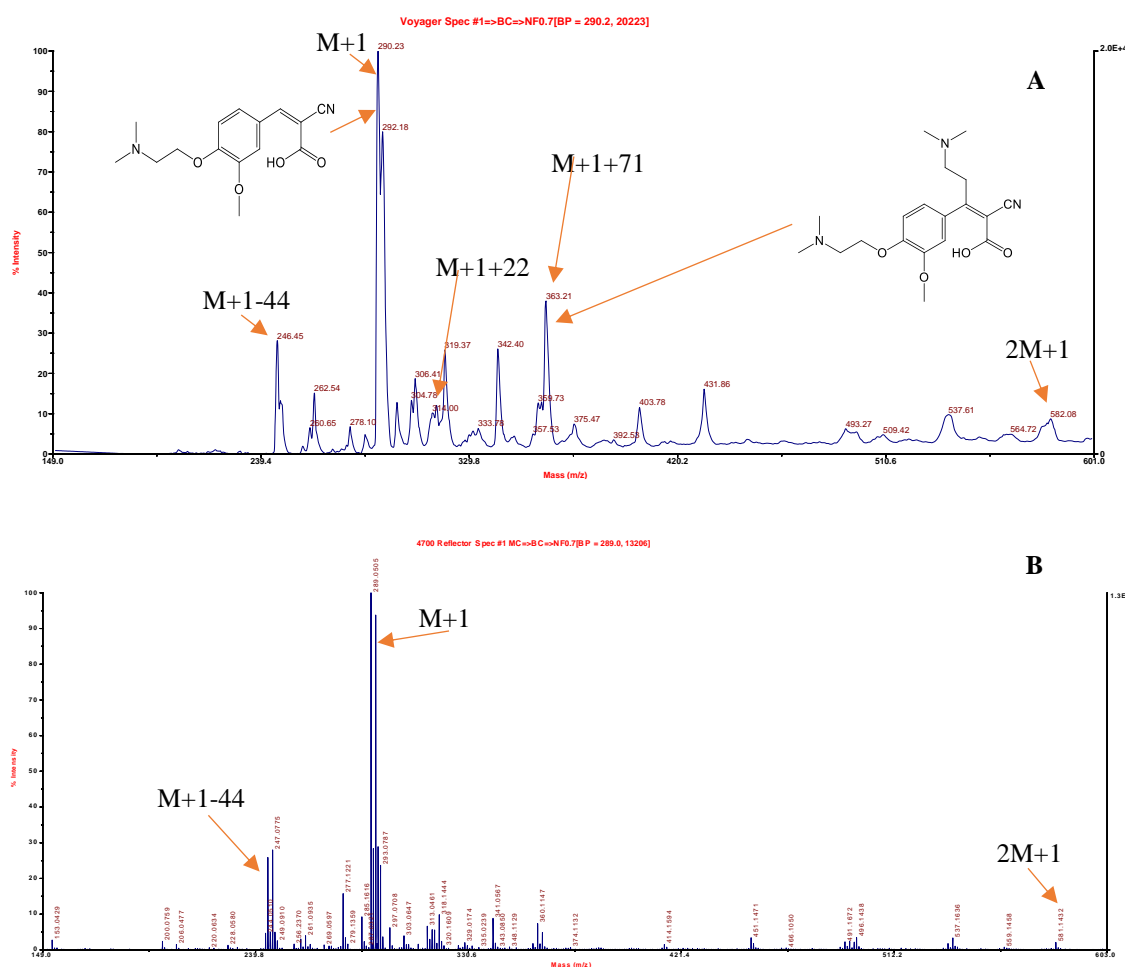
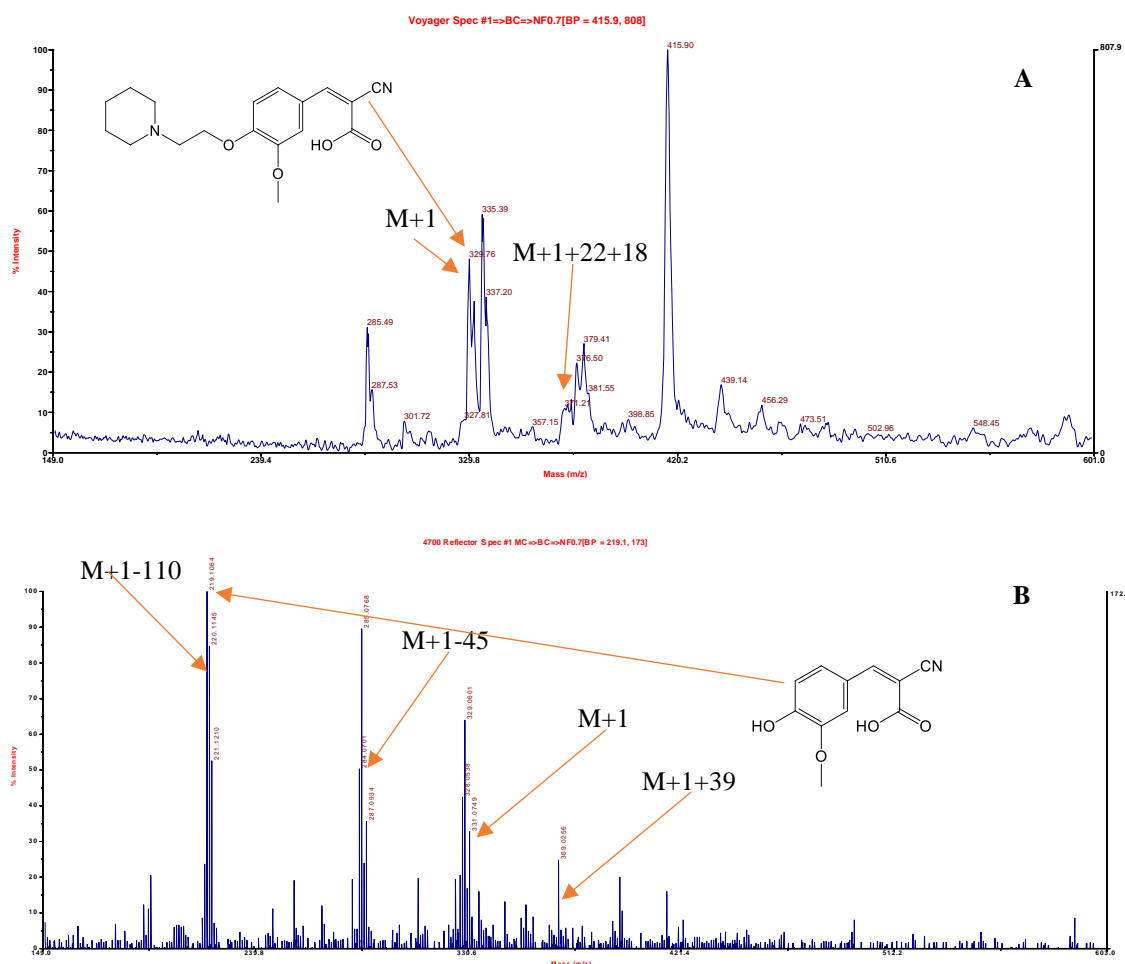


Figure 5.2 Matrix B2b mass spectrum featuring positive identification of the M+1 ion acquired from A) MALDI-TOF MS and B) MALDI-TOF-TOF

5.1.3 Matrix B2d Molecular Weight 330 g/mol

Both spectra obtained for Matrix **B2d** are shown in *figure 5.3*, evident from both spectra is the $[M+H]^+$ ion at m/z 331. Also apparent in both spectra is a fragment cluster at m/z 283 – 287, which holds some ambiguity but is most likely due to the loss of the acid group COOH . From spectrum A, a low abundance sodium ion cluster is apparent at m/z 371 $[M+H+(\text{H}_2\text{O})+\text{Na}]^+$. The base peak from the spectrum B corresponds to the fragmentation of the amine spacer as identified in *figure 5.3*. A potassium ion cluster was also found on the same spectrum at m/z 369.



5.1.4 Matrix B2f Molecular Weight 339 g/mol

The molecular ion peak cluster is also the most abundant base peak cluster in both spectra acquired for matrix **B2f** at m/z 340. Clearly apparent from *figure 5.4* is the fragmented peak which corresponds to the loss of a bromine ion at m/z 259, $[M+H-(Br)]^+$, this ion further fragments with the loss of $(N-(CH_3)_2)$ which equates to the ion at m/z 215. There is a sodium ion cluster apparent from spectrum B at m/z 362.

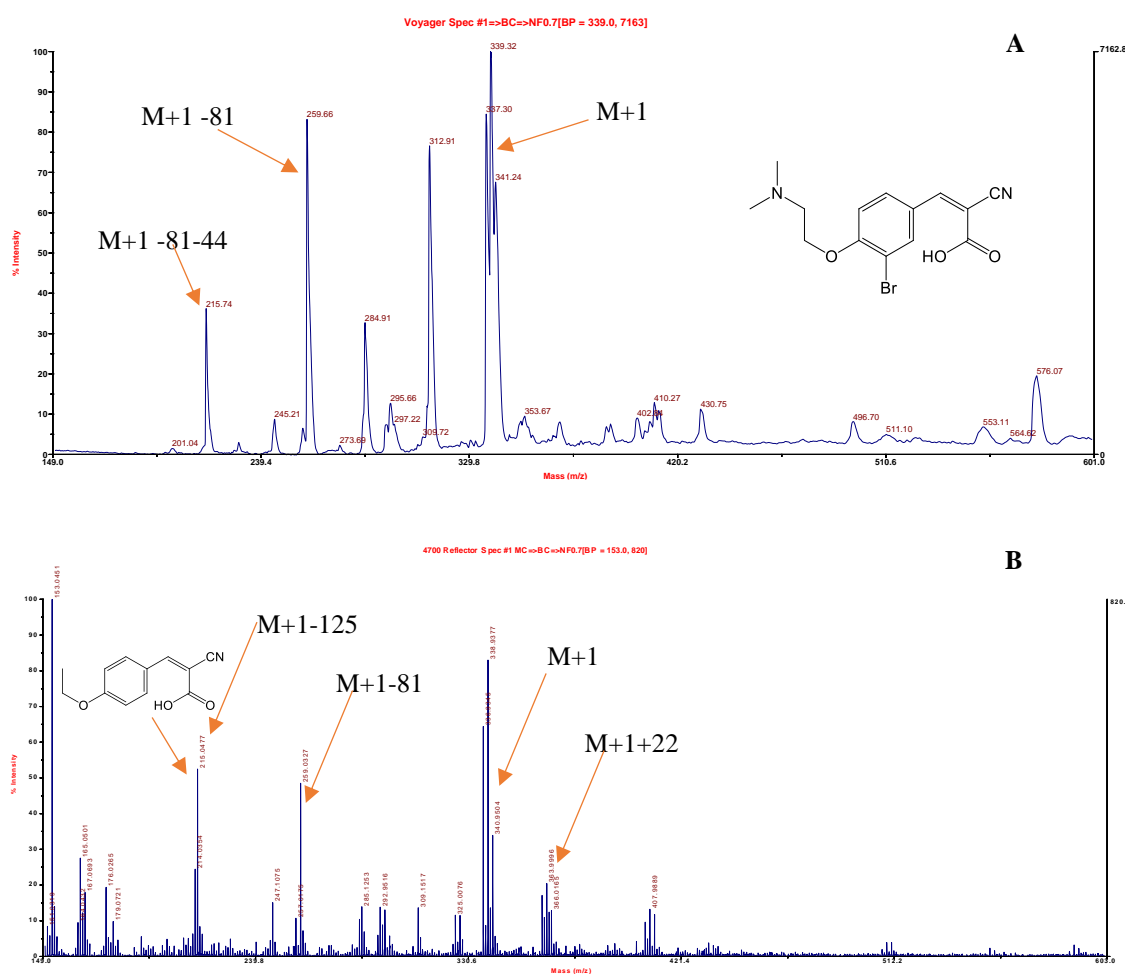


Figure 5.4 Matrix B2f mass spectra featuring positive identification of the M+1 ion acquired from A) MALDI-TOF MS and B) MALDI-TOF-TOF

5.1.5 Matrix B2g Molecular Weight 302 g/mol

The spectra acquired from the MALDI-TOF MS and the MALDI-TOF-TOF show little difference in ion peaks. The prominent base peak, also the molecular ion is visible as m/z 303. The peak found in both spectra at m/z 416 could potentially be, as with matrix **B2b**, the fragmentation and reformation of the molecular ion's amine spacer as indicated in spectrum A *figure 5.5*. A fragmentation ion is present at m/z 257, which would correspond to the loss of an acid group (COOH).

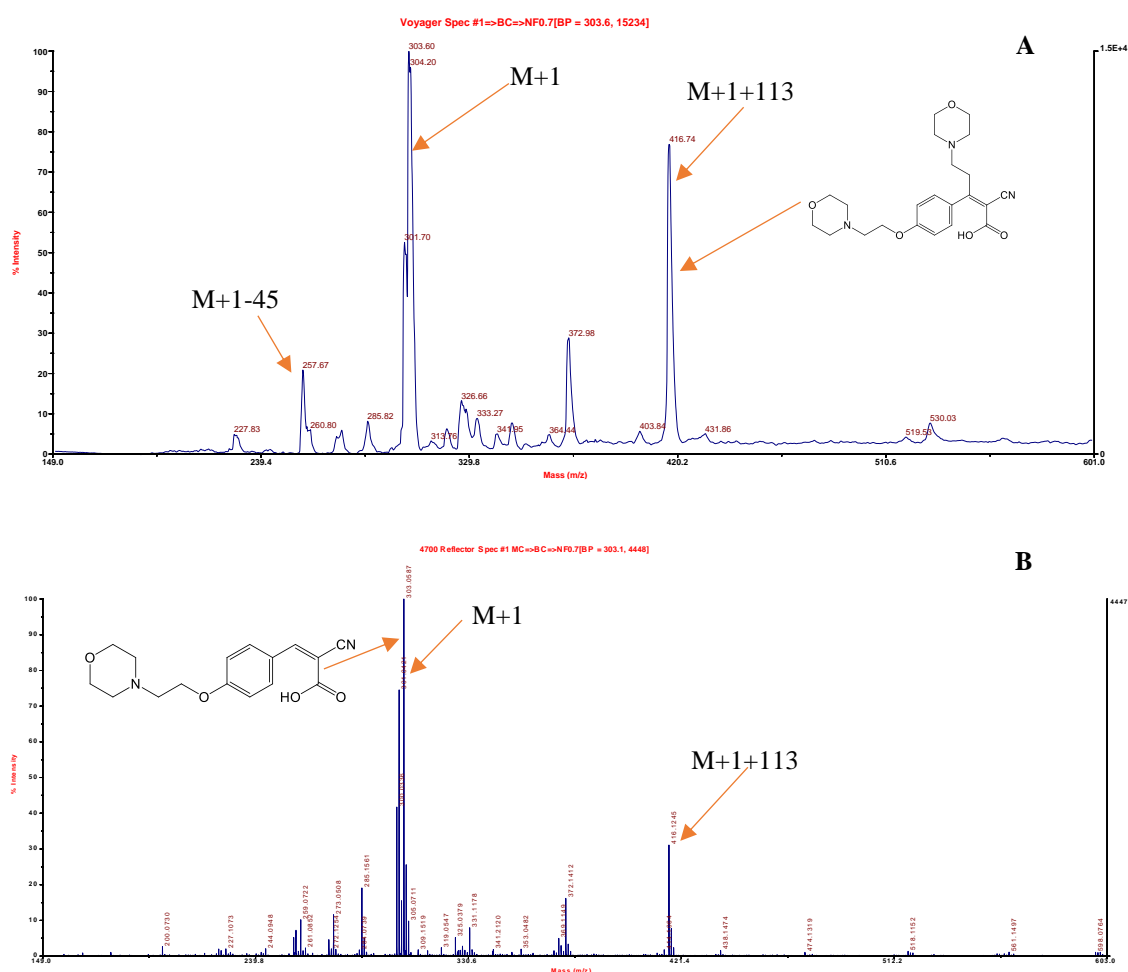


Figure 5.5 Matrix B2g mass spectra featuring positive identification of the M+1 ion acquired from A) MALDI-TOF MS and B) MALDI-TOF-TOF

5.1.6 Matrix B2h Molecular Weight 294.7 g/mol

The spectral data collected for matrix **B2h** identifies the matrix from its molecular mass plus hydrogen ion peak detected at m/z 259. The fragmentation peaks that coincides with the loss of a chlorine atom are apparent at m/z 259, and the fragment peak that indicates the loss of chlorine and an acid group $[M+H-(ClCOOH)]^+$ has been detected at m/z 215. Both spectra provide harmonized fragmentation results. The peak attained at m/z 366, correlates to the $[M+H+71]^+$ which is in considerable abundance and is postulated to be the attachment of a fragment ion to the molecular ion $[M+H+(CH_2CH_2-N-(CH_3)_2)]^+$ as indicated in *figure 5.6* spectrum A.

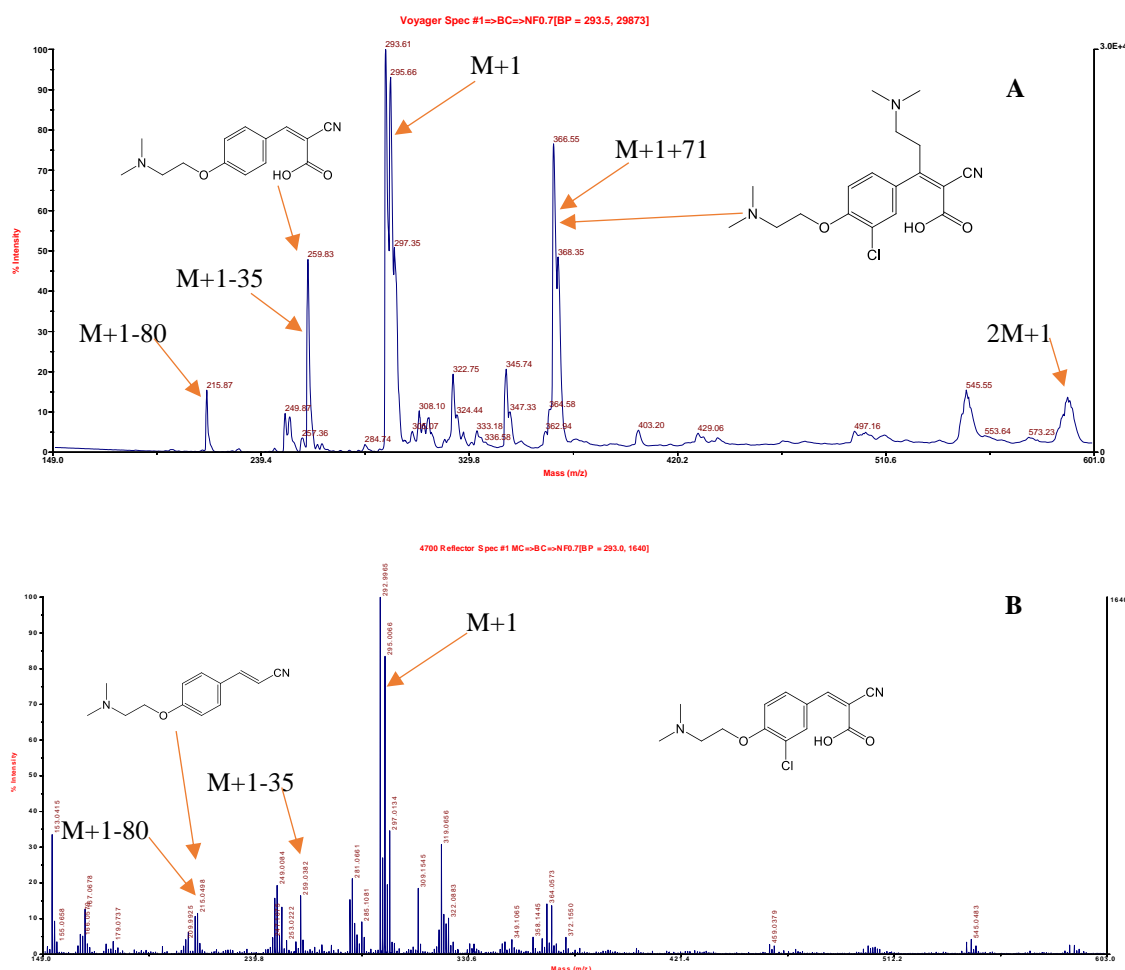


Figure 5.6 Matrix B2h mass spectra featuring positive identification of the M+1 ion acquired from A) MALDI-TOF MS and B) MALDI-TOF-TOF

5.1.7 Matrix B2j Molecular Weight 288 g/mol

The < 300 g/mol molecular mass of **B2j** allow for the spectrum range to detect a dimer ion at m/z 578, which was detected by both means of data acquisition. The ion at m/z 389 is hypothesised to be $[M+H+(CH_2CH_2-N-(CH_3)_2)]^+$. The molecular ion also the base peak for both spectra is discernible at m/z 289. The low abundance ion at m/z 345 is considered to be $[M+H+(H_2O)+K]^+$, representing a potassium cluster. Finally, the fragment ion at m/z 244 present in both spectra is most likely due to decarboxylation.

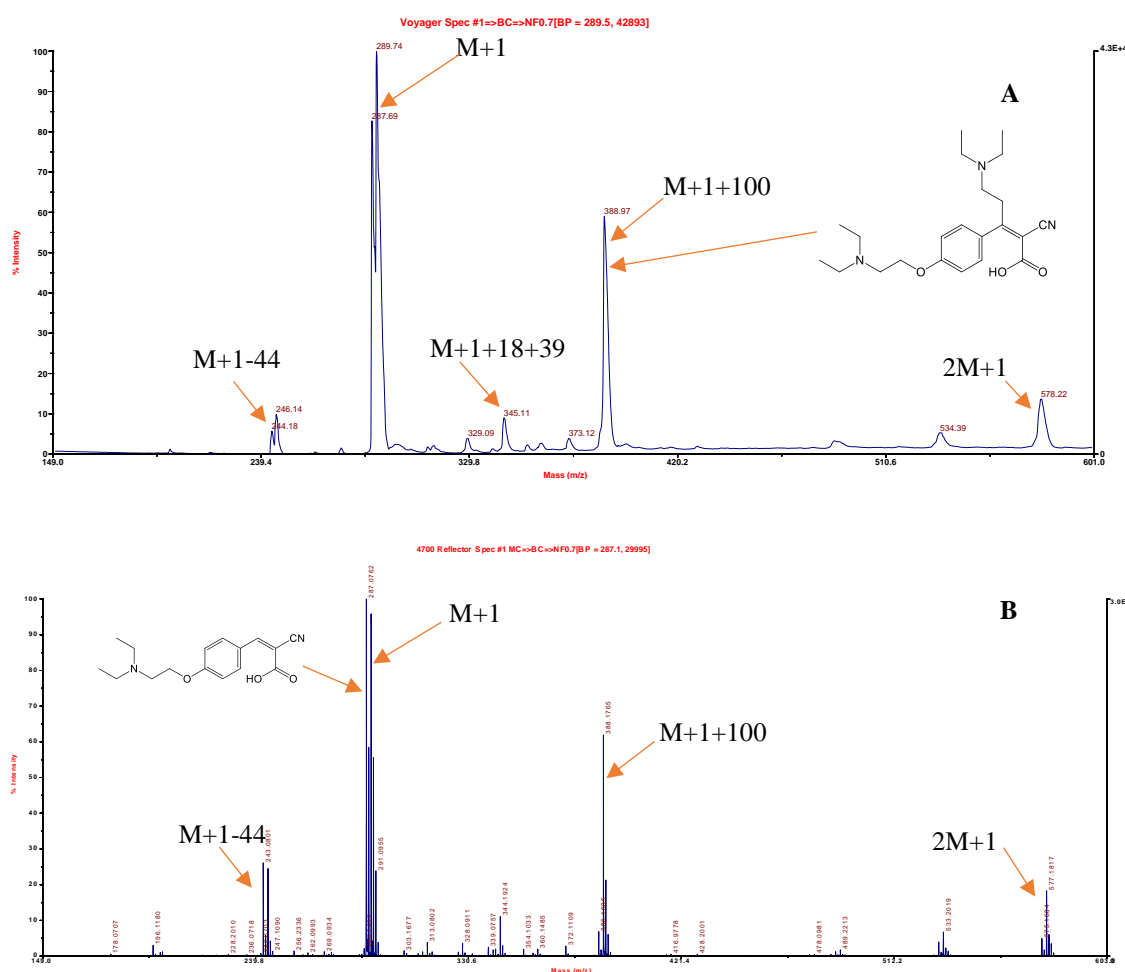


Figure 5.7 Matrix B2j mass spectra featuring positive identification of the M+1 ion in both spectra acquired from A) MALDI-TOF MS and B) MALDI-TOF-TOF

5.1.8 Matrix B2k Molecular Weight 318 g/mol

The mass spectrum for matrix **B2k** was generated using ESI TOF MS and was collected at a later date to the other structure B matrices.

It is clear from this spectrum the $[M+H]^+$ molecular ion is prominent at m/z 319, which positively identifies matrix **B2k**.

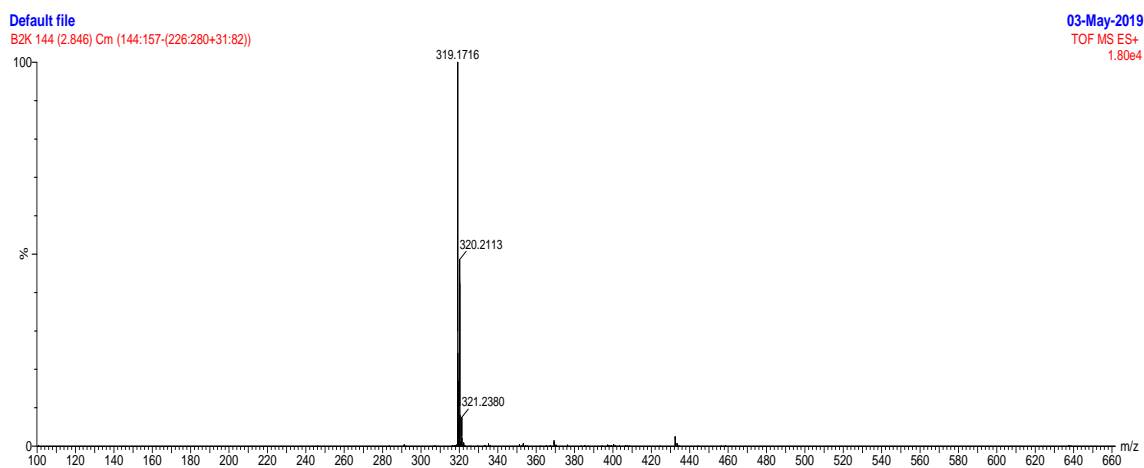


Figure 5.8 Matrix B2k mass spectrum acquired from ESI-TOF MS displaying positive identification of the M+1 ion

5.1.9 Matrix C3 Molecular Weight 217 g/mol

Matrix C3 was analysed by ESI-TOF MS a number of times with varying concentrations. Spectra obtained are shown below in *figure 5.9*. The molecular ion was not detected. No sodium or potassium clusters were identified either. Due to the sensitive nature of this compound it was speculated that the matrix was disintegrating prior to analysis. On the bottom spectrum in *figure 5.9* there is a peak at m/z 220, which would correspond to the molecular ion of the precursor to C3, compound C2. However, this is considered unlikely as the Diels Alder reaction carried out confirmed that C3 was present.

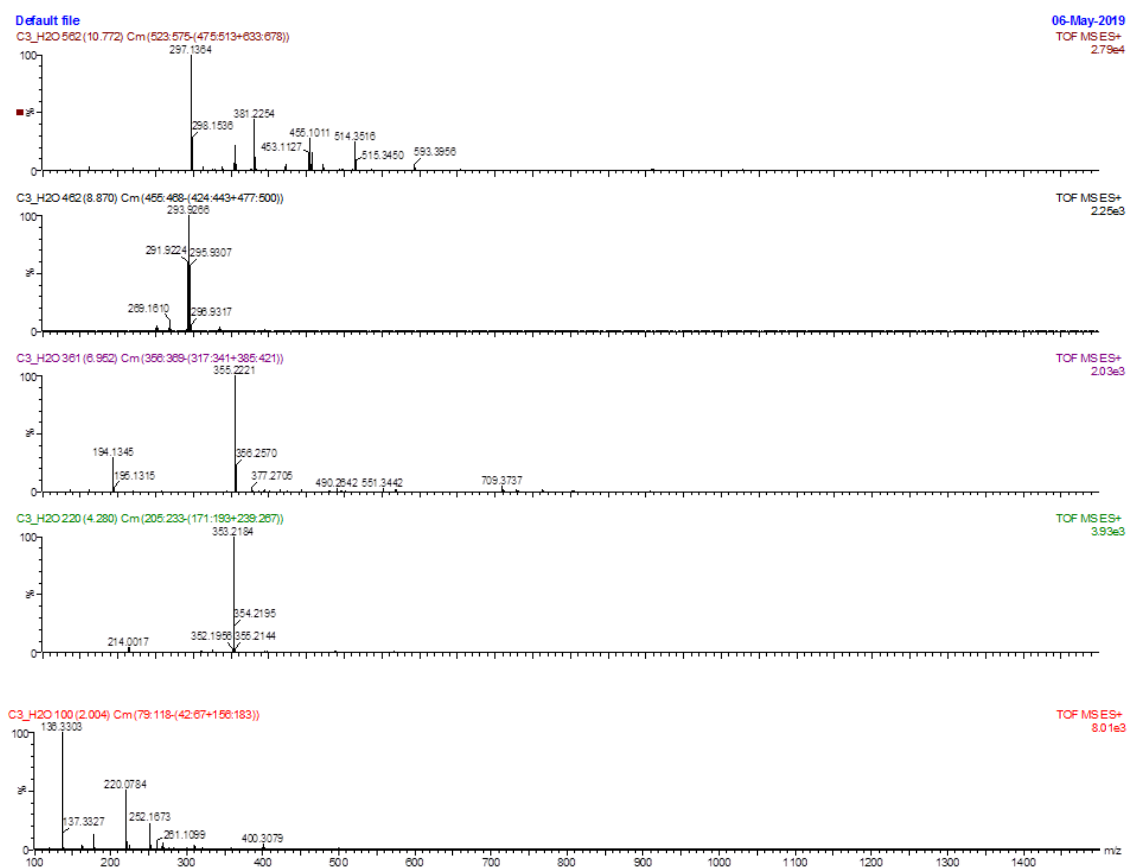


Figure 5.9 Matrix C3 mass spectra with increasing concentration of C3 from top to bottom. Acquired from ESI TOF MS. No positive identification of the M+1 ion detected

5.2 Matrix Reaction with Alcohol Analysed by MALDI-TOF MS

The matrices were reacted with three different alcohols: corticosterone, decanol and terpineol, in three different reaction conditions: reaction 1) with 10 % water at 40 °C for 2 h; reaction 2) with 10 % water at r.t for 4 h; reaction 3) with 10 % of a 1% TFA solution at r.t for 4 h. The matrices involved in these reactions: **B2b**, **B2d**, **B2f**, **B2g**, **B2h** and **B2j** all behaved analogously to one another in the varying reaction conditions. In this section we take a look at the reaction results of matrix **B2b** as a representative of all matrices that underwent a reaction with an alcohol. The reaction was designed to activate the matrices carboxylic acid to form the corresponding ester. The reactions were analysed by MALDI-TOF MS in positive ion mode and were examined to identify the ester ion peak, sodium and potassium clusters and dimers. The spectral data obtained for the remaining matrix reactions with alcohol are available to view in chapter 9 *Appendices*.

5.2.1 Results for Matrix **B2b** Reaction with Alcohols

In Reaction 1, the spectra obtained from all three alcohol reactions show the recognisable $[2M+H]^+$ Dimer ion peak at m/z 581. With reference back to the **B2b** characterisation spectra in *section 5.1.2*, both spectra also possess the dimer ion at m/z 581, confirming the identity of this peak. An ion visible in Reaction 1 with CORT having an m/z of 618.87, was first calculated to be the ester ion $[M+H+347-18]^+$ and beside it at m/z 641 a sodium cluster of the ester ion $[M+H+347-18+39]^+$. However, upon further inspection these same two peaks occur for matrix **B2b** with decanol and terpineol and therefore are most probably not as a result of the ester ion in the CORT reaction with **B2b**. After overlay analysis of spectra, it is clear that the peaks obtained in Reaction 1 for one of the alcohols are the same peaks obtained in all reactions for all of the alcohols. This exposes the most plausible reality, which is the esterification did not take place for any of the reaction conditions for matrix **B2b** and that the alcohols did not interact with the matrix.

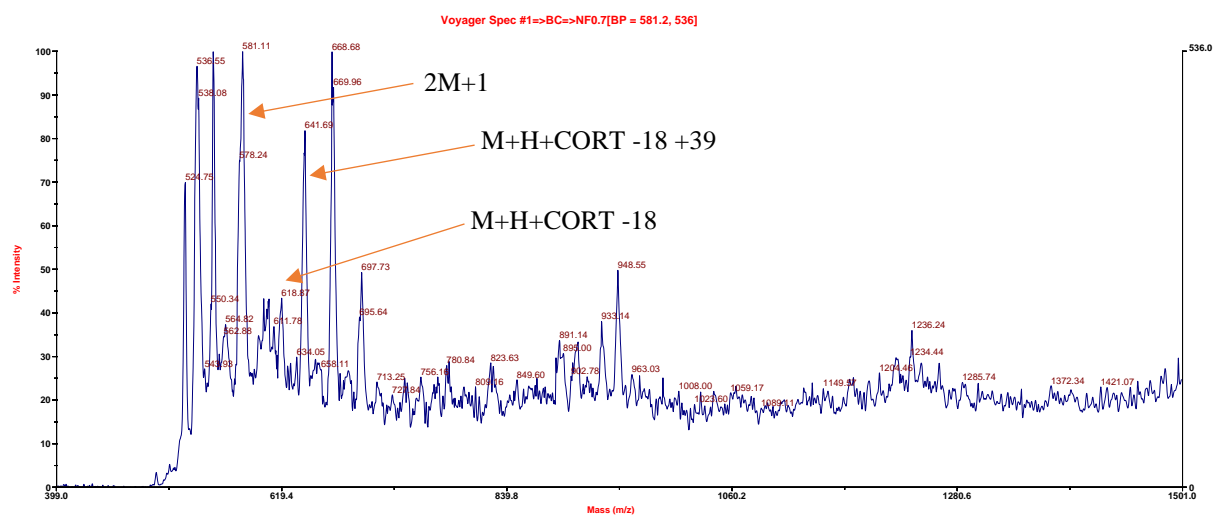


Figure 5. 10 Reaction 1: Matrix B2b with CORT, MALDI-TOF MS spectrum

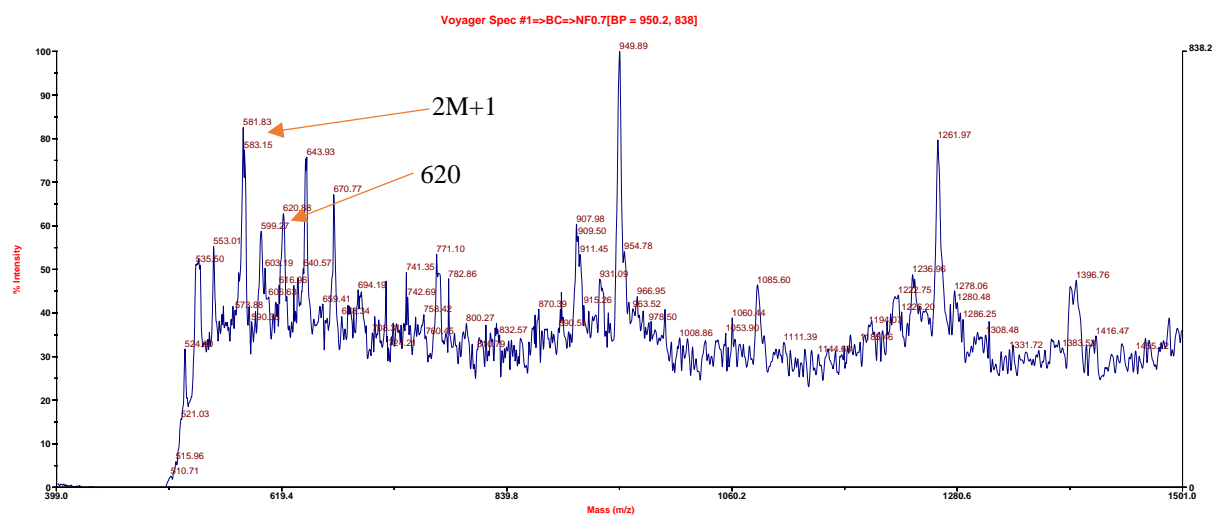


Figure 5. 11 Reaction 1: Matrix B2b with decanol, MALDI-TOF MS spectrum

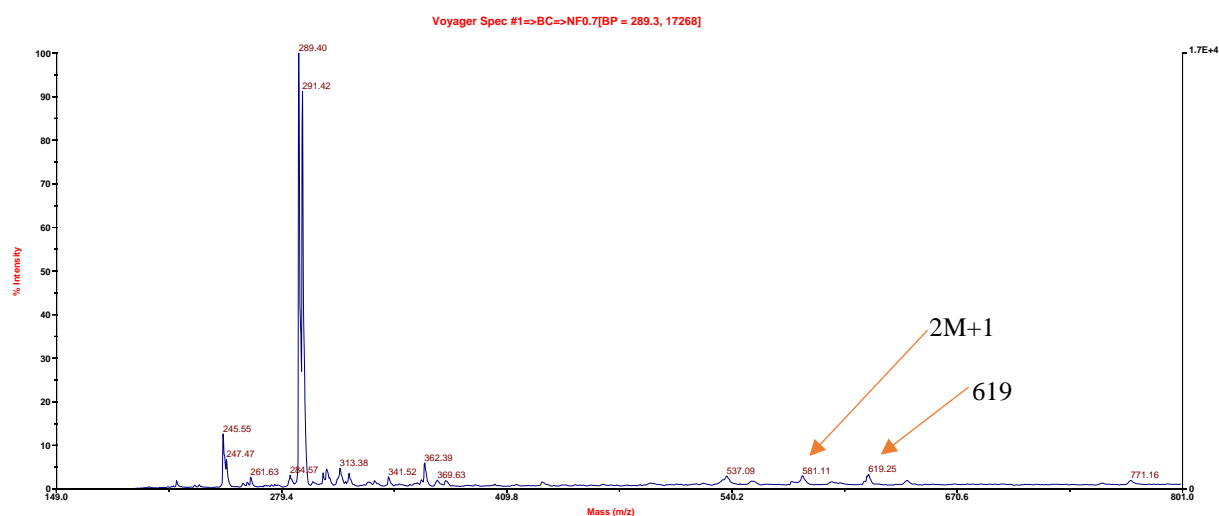


Figure 5. 12 Reaction 1: Matrix B2b with terpineol, MALDI-TOF MS spectrum

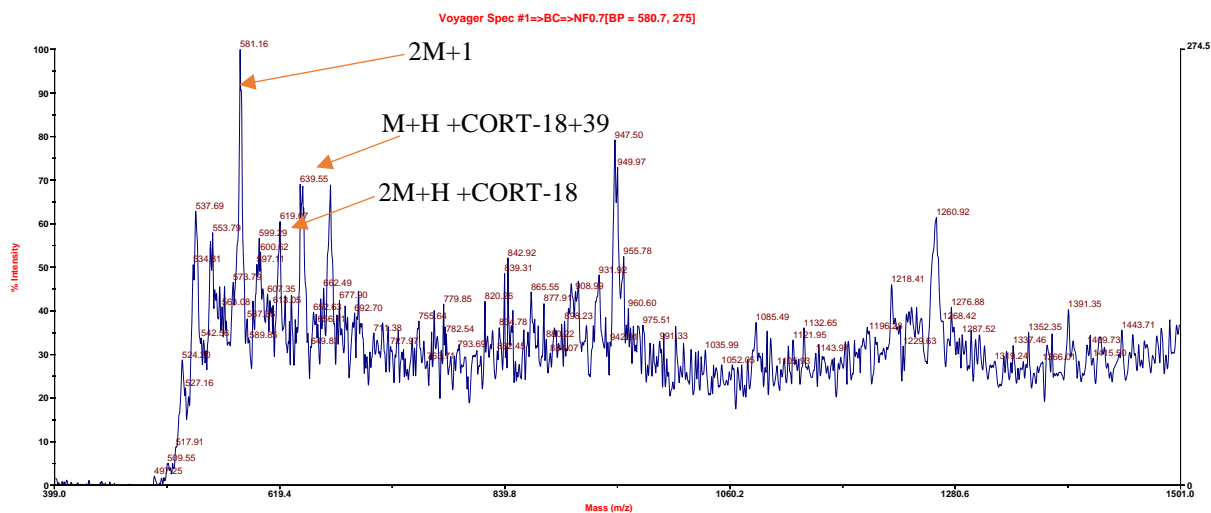


Figure 5. 13 Reaction 2: Matrix B2b with CORT, MALDI-TOF MS spectrum

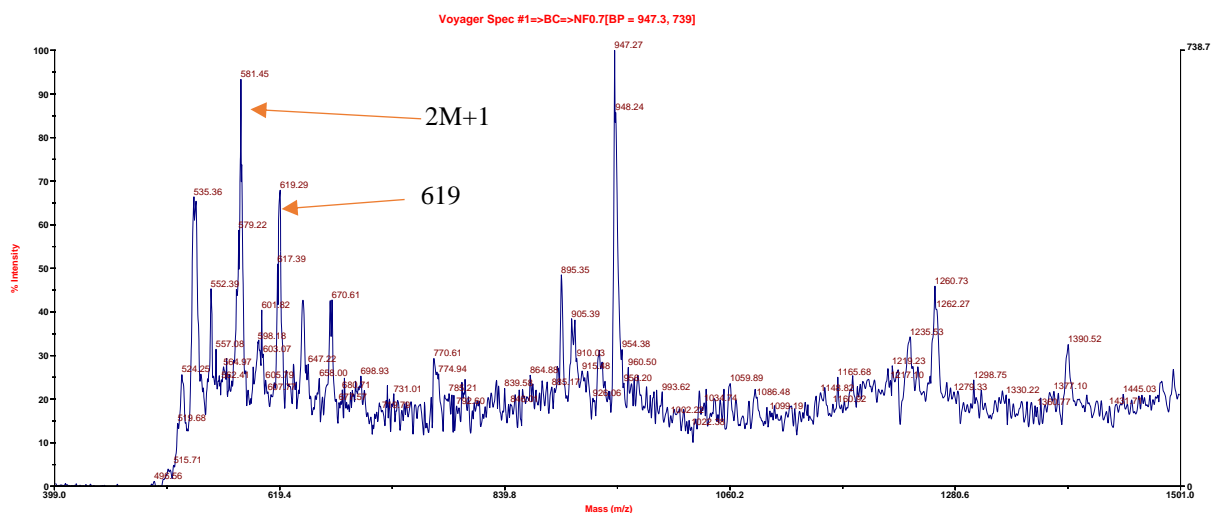


Figure 5. 14 Reaction 2: B2b with decanol, MALDI-TOF MS spectrum

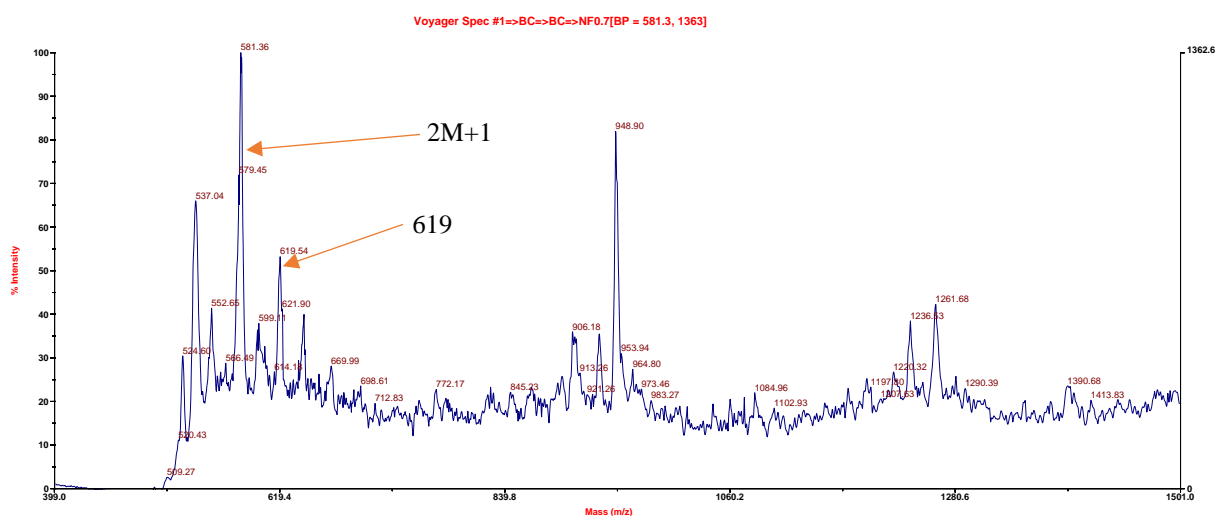


Figure 5. 15 Reaction 2: Matrix B2b with terpineol, MALDI-TOF MS spectrum

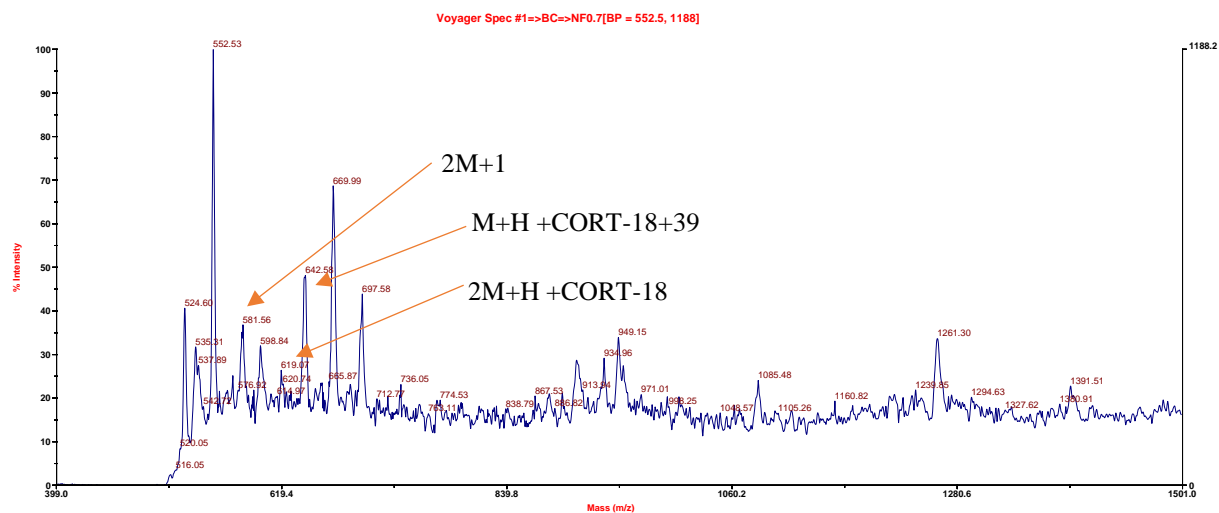


Figure 5. 16 Reaction 3: Matrix B2b with CORT and TFA, MALDI-TOF MS spectrum

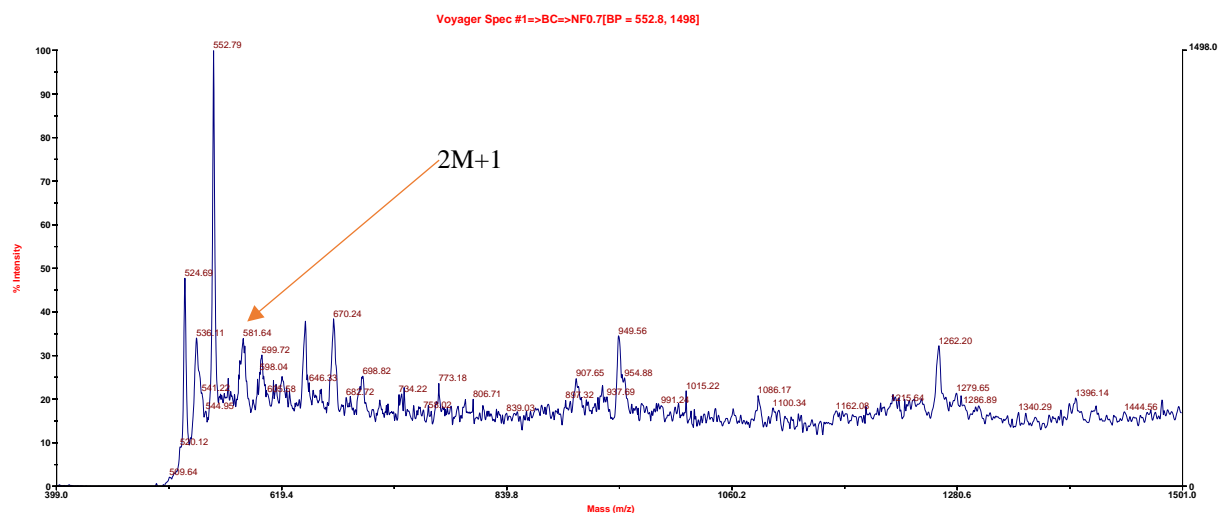


Figure 5. 17 Reaction 3: Matrix B2b with decanol and TFA, MALDI-TOF MS spectrum

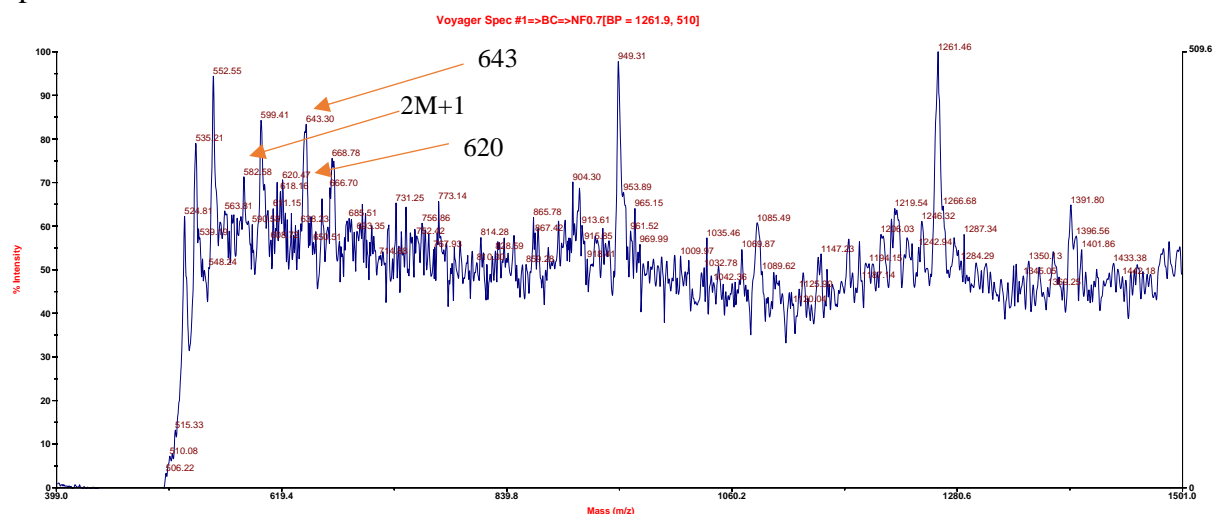


Figure 5. 18 Reaction 3: Matrix B2b with terpineol and TFA, MALDI-TOF MS spectrum

5.3 UV Absorption Results

Table 5.1 Molar absorptivity coefficient (ϵ) for structure B type matrices

Matrix	λ_{\max} (nm)	Conc' (g/L)	Mm (g/mol)	Conc' (mol/L)	Path length (cm)	Abs'	ϵ (L/ mol cm)
B2a	320.1	0.01	260	3.85E-05	1	0.789	20514
B2b	350.1	0.01	290	3.45E-05	1	0.651	18879
B2d	350.1	0.01	330	3.03E-05	1	0.294	9702
B2f	330.0	0.01	339	2.95E-05	1	0.625	21188
B2g	335.0	0.01	302	3.31E-05	1	0.699	21110
B2h	330.0	0.01	295	3.39E-05	1	0.777	22922
B2j	330.0	0.01	288	3.47E-05	1	0.737	21226

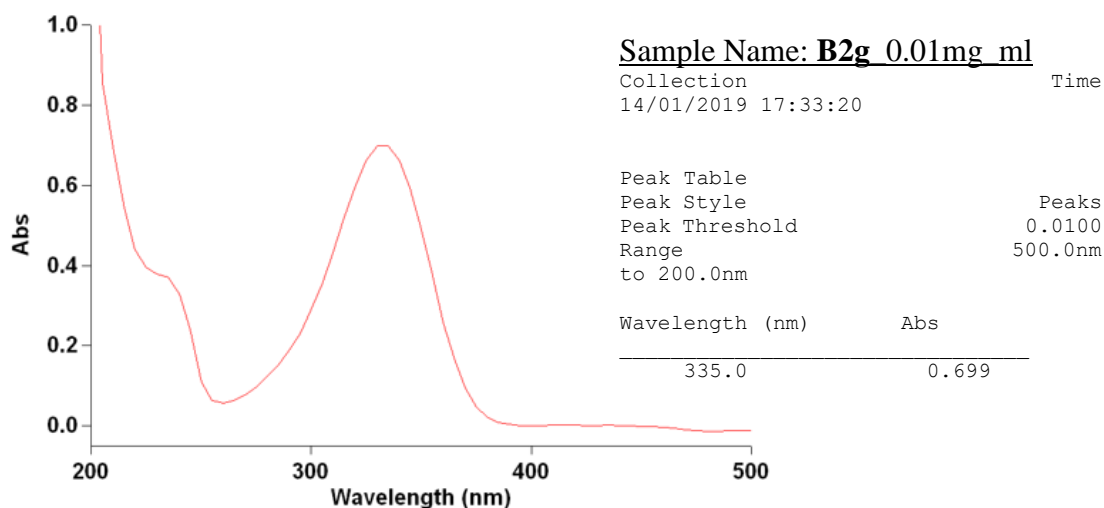


Figure 5.19 UV absorbance spectrum for matrix B2g

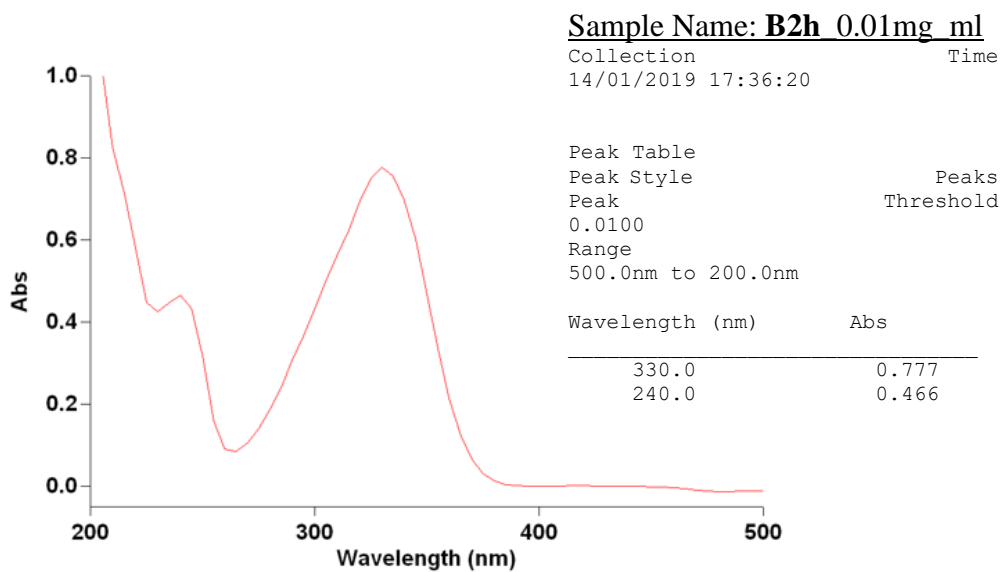


Figure 5.20 UV absorbance spectrum for matrix B2h

5.4 Crystal Properties

Table 5.2 Matrices crystal properties and visual appearance

Matrix	Colour	Form
B2a	White	Fine crystal needles
B2b	Yellow	Crystals
B2d	Orange	Solid
B2f	White	Powder
B2g	Faintly yellow	Powder
B2h	White	Powder
B2j	Yellow	Crystals
B2k	Yellow	Crystals
C3	Red	Solid

5.5 Discussion of Results

The characterisation analysis of the structure B library of matrices assayed on both MALDI TOF MS Voyager and MALDI TOF/TOF 4800, displayed good comparable results. The molecular ion was positively identified in all B type matrices by both means of analysis and in most cases was the most abundant peak. The mass range analysed was 150 – 600 Da. For many of the matrices with molecular mass > 300 g/mol, their dimer ion $[2M+H]^+$ falls out of this range. But for the matrices with lower molecular mass, **B2a**, **B2b**, **B2h** and **B2j** their dimer ion is within the mass range and was positively identified for all these matrices. There were some common reoccurring fragmentation patterns identified such as $[M+H-45]^+$, which is most likely as a result of a fragmented acid group (COOH). In some cases, it is a loss of m/z 44, which is within the tolerance range of +/- 1 Da to also be the loss of an acid group. Another possibility, for matrices that contain the dimethylethylamine spacer, **B2a**, **B2b**, **B2f** and **B2h**, it may equate to the loss of (N-(CH₃)₂). Matrix **B2f** and **B2h** which both encompass a *meta* halogen substituent. Both have fragmentation ions that correspond to the loss of the halogen atom. Some potassium and sodium ion clusters were identified for matrix **B2a**, **B2b**, **B2d**, **B2f** and **B2h**. An interesting occurrence was observed in matrices **B2a**, **B2b**, **B2g**, **B2h** and **B2j** where a prominent peak arises with a higher m/z value than the molecular ion. For matrix **B2a**, **B2b** and **B2h** which all have the same dimethylethylamine spacer, it appears at $[M+1+71]^+$. It was first thought it could be $[M+H+(H_2O)_4]^+$. Alternatively to this theory it could be the fragmentation of the amine spacer and reformation to the molecular ion in the form of $[M+H+(CH_2CH_2-N-(CH_3)_2)]^+$. Matrix **B2g** has an ethylmorpholine spacer. The higher mass conspicuous peak appears for **B2g** at $[M+H+113]^+$, which does correlate to the fragmentation and reformation of the ethylmorpholine spacer to form $[M+H+(C_6H_{12}NO)]^+$. Similarly, for matrix **B2j** which possess a diethylethylamine spacer, the fragmentation and reformation theory prevails, where the higher mass peak appears

at $[M+H+100]^+$ and is quite possibly the result of $[M+H+(CH_2CH_2-N-(CH_2CH_3)_2)]^+$ ion. Because it is not just a once off and the arrangement pattern recurs for matrices with different amine spacers, it suggests that there is some molecular ion pairing occurring that is producing this fragmentation pattern when evaporated.

The MALDI spectra obtained for matrix **C3** fails to resolve any identifiable peaks regardless of the numerous runs carried out with varying concentration levels. The ion observed in the bottom spectra of *figure 5.9* at m/z 220, has been considered to be the precursor to **C3**, compound **C2**. However, this is considered unlikely as the Diels Alder reaction carried out on **C3** confirmed that it was the dienophile that was present and the NMR obtained does correspond to the structure. Due to the sensitive nature of **C3** the theory put forward to rationalise the inconclusive MALDI spectra is that the matrix is decomposing with the addition of solvent.

As with matrix **B2b**, all of the other matrices that were involved in the reactions with alcohols, revealed the same trends in data obtained by MALDI TOF MS. The Dimer ion $[2M+H]^+$ was present for all matrices. All corticosterone reactions identified a peak that equated to the ester ion $[M+H+347-18]^+$ and in many cases a sodium ion cluster next to this $[M+1+347-18+22]^+$. However for each matrix the peaks that appeared in the CORT reaction that equate to the ester and a sodium ion cluster were reappearing with the same m/z value in the matrix reaction spectra for the other alcohols (decanol and terpeneol), and the overlays were almost identical. It was therefore deduced from this evidence that the esterification did not take place and that the alcohols were not ionising or interacting with the matrices, it also implies the alcohols were not responsible for the peaks presenting in the spectra. Further research into the activation of the carboxylic acid in solution is necessary to develop these matrices before they can be tested directly on tissue samples. Some future adjustments to the reaction conditions that could be considered include: the use of an alternative coupling agent; adjustments to the time and/or temperature; using

alcohols with more activated hydroxyl groups or increasing the concentration of TFA in the reaction. Failing that an alternative approach could be researched.

Matrix UV absorption analysis of structure B type matrices to determine the molar absorptivity coefficient (ϵ) revealed the matrix with the best ϵ value was **B2h** at 22922 L mol⁻¹ cm⁻¹ and a λ_{max} value 330 nm. Matrix **B2a**, **B2h** and **B2f** differ only by their C₃ substituents which are, hydrogen, chlorine and bromine respectively and can therefore be comparatively examined with respect to their UV absorption. The halogen substituents can donate their lone pairs in a mesomeric effect and resonate around the ring while simultaneously, due to their *meta* position, inductively withdraw electrons from the whole conjugated system. A possible reason for the chloro matrix bearing a higher ϵ value is because chlorine is more electronegative than bromine and it will inductively withdraw more strongly than bromine, effecting the nature of the conjugated system more. However, there are a lot of possible contributing factors as to why some of the matrices gave a higher ϵ value than others. It is important to note, the substituents do influence the ϵ value, which is evident when comparing **B2a** (no *meta* substituent) with **B2h** and **B2f**. **B2a** has a lower ϵ value and a lower λ_{max} value of 320 nm. Matrix **B2g** and **B2j** also have high ϵ values. These matrices have no substituents but have different amine spacers. It is difficult to say why one matrix has a higher absorption coefficient to another as there are a number of components to consider like how the matrix interacts with the solvent etc. But for future research the information obtained can be used as a guide to optimise a structure B type matrix and influence the design of more matrices. For example, it would be worthwhile trying matrices with C₂ substituents and observe the effect they might have on the ϵ values.

Many of the NMR spectra obtained are of poor quality, this is due to poor solubility of the matrices analysed. Going forward repeat NMR analysis would be required.

6 Conclusion

The successful generation of a library of novel reactive MALDI matrices to target endogenous steroid molecules on biological tissue samples has been described. Furthermore, it has been made possible, through systemic modifications, to identify features in the matrix that enhance absorptivity at the laser wavelength through UV analysis. The addition of C₃ substituents increased the ϵ value of the matrix.

Structure B library of matrices all ionise and travel to the mass analyser as anticipated when analysed by MALDI TOF MS. They were all positively identified according to their molecular ion and fragmentation pattern and this analysis also revealed some interesting fragmentation and reformation patterns for these matrices that may be as a result of ion pairing. Matrix B2h which possesses a chloro substituent gave the best ϵ value and matrix B2b, B2j and B2k the best crystal structure. These findings demonstrate the benefits of synthesising a library of similar structures that can help optimise the efficiency of the leading matrix. Future research for this project could include the synthesis of structure B2h's absorbing core with structure B2j's basic enhancer moiety to further optimise absorptivity and ionisation efficiency of the resulting matrix. *Ortho* substituted cores could also be pursued. In spite of considerable efforts to successfully synthesise the vitamin D targeted matrix, due to the sensitive nature of the matrix, decomposition issues hindered completion of the final product. A new approach to the addition of a charged tertiary amine to C₃ would need to be researched in future development of this matrix.

Additional research is required into advancing the conditions required to activate the carboxylic acid of the matrices prior to on-tissue analysis. Reaction alterations in temperature, time, solvent and coupling agent are all avenues worth pursuing in the future to initiate the esterification reaction.

The library of reactive matrices, successfully synthesised from commercially available, inexpensive material which possess the novel enhancer spacer can potentially play a key role in MALDI MSI analysis of endogenous steroids and provide a greater insight into the biological distribution of these molecules.

7 Experimental Procedure

MALDI-TOF MS was performed using: a), A PerSeptive Biosystems Voyager-DE Biospectrometer (Hertfordshire, UK) equipped with a 1m time-of-flight tube and nitrogen laser set at 337nm; b), An Applied Biosystems / MDS Sciex 4800 MALDI TOF/TOF mass spectrometer (Foster City, California, USA) equipped with a Nd:YAG laser operating at 355 nm (200 Hz repetition rate). UV spectra were acquired on a Cary 50 Bio UV-Visible Spectrophotometer, scanning between 200 – 500nm. Quartz cuvettes, path length 10 mm. Instrument zeroed using sample diluent.

The GC/MS analysis was performed using a GC/MS system consisting of a 5977E MSD single-quadrupole mass spectrometer with a 7820A GC by Agilent Technologies.

Proton Nuclear Magnetic resonance spectra were recorded on a Varian 500 MHz Spectrometer, running on Vnmrj software Version 4.2 in DMSO-d₆, CDCl₃ and D₂O. Chemical shifts were referenced relative to residual solvent chemical shifts and are reported in ppm and coupling constant in Hertz. All proton NMR were acquired using 64 scans. All Carbon NMRs were run using 512 scans. Samples B1a, B1b, A1b, A2b and A3 Proton and carbon NMR spectra were recorded on a 500 MHz Agilent VnmrS console spectrometer, equipped with a OneNMR probe. All samples were run at 25 °C.

Infrared spectra were obtained on a Perkin Elmer UATR Two spectrophotometer. Column chromatography was carried out using silica gel, pore size 60 Å 70-230 mesh, 63-200 µm. TLC analysis was performed on precoated 60F254 slides and visualised by UV irradiation using UVGL-58 handheld UV lamp. All melting points are uncorrected. Acetone, methanol and ethanol were stored with molecular sieves (3 Å). For all known compounds the spectral characteristics were in agreement with those reported in the literature. MALDI and almost all NMR data obtained was for final products only. All reagents were purchased from Sigma Aldrich and used as received.

7.1 Experimental Procedure for Matrix Characterisation by MALDI

Solution of each matrix was prepared as shown in *table 7.1*. to provide sample solutions of 1 mg/ml. The samples were analysed for characterisation according to the following two procedures first on the MALDI-TOF MS and secondly on the MALDI TOF/TOF.

Table 7. 1 Preparation of stock solutions for matrix characterisation by MALDI

Sample	Mass (mg)	vol (μ l)	Conc' Stock mg/ml	Vol sample (μ l)	Vol Solvent (μ l)	Final Conc' mg/ml
B2b	10.3	1030	10	100	900	1
b2d	5.3	1060	5	200	800	1
B2f	4.7	940	5	200	800	1
B2g	4.9	980	5	200	800	1
B2h	4.6	920	5	200	800	1
B2j	4.8	960	5	200	800	1

7.1.1 MALDI TOF MS General Procedure

A 1 mg/ml solution of sample matrix was prepared in 80 % acetonitrile, 20 % water with 0.1 % trifluoroacetic acid. The matrix was vortexed thoroughly to mix. A 1.5 μ l aliquot of the sample matrix was pipetted onto a predefined well of a 100-well stainless steel plate. Once the spots were dried on the plate, the plate was inserted into the MALDI-TOF. An internal mass calibration of the instrument was performed prior to sample analysis using Peptide Calibration Mix 2 (LaserBio Labs, Spohia-Antipolis, Cedex, France) containing four individual peptides; Neurotensin, ACTH fragment 18-39, Insulin bovine β -chain oxidised and Insulin bovine with monoisotopic masses of 1672.9176, 2465.1989, 3494.6514 and 5730.6087 respectively. All sample measurements were collected in linear positive ionisation mode using 100 laser shots/spectrum. The accelerating voltage was

maintained at 20,000 V, the grid voltage and guide wire voltages were set at 91 % and 0.05 % respectively of the accelerating voltage. The nitrogen laser set at 337 nm was directed toward the densest area of the sample / matrix spot and the laser intensity adjusted to obtain the best spectral response. The m/z ratio was plotted against relative abundance.

7.1.2 MALDI -TOF/TOF General Procedure

A 1 mg/ml solution of sample matrix was prepared in 80 % acetonitrile, 20 % water with 0.1 % trifluoroacetic acid. The matrix was vortexed thoroughly to mix. A 0.5 μ l aliquot of the sample matrix was pipetted onto a predefined well of a 384-well stainless-steel plate. Once the spots were dried on the plate, the plate was inserted into the MALDI-TOF/TOF analyser. An internal mass calibration of the instrument was performed prior to sample analysis using TOF/TOF Calibration Mixture (Sciex, Framingham, Massachusetts, USA) containing des-Arg¹-Bradykinin, Angiotensin I, Glu¹-Fibrinopeptide B, ACTH (1-17 clip), ACTH (18-39 clip) and ACTH (7-38 clip) with monoisotopic masses of 904.4681, 1296.6853, 1570.6774, 2093.0867, 2465.1989 and 3657.9294 respectively. All sample measurements were acquired in reflector positive ion mode using 100 laser shots/spectrum. The laser intensity was adjusted to obtain the best spectral response. The m/z ratio was plotted against relative abundance.

7.2 Matrix Reaction with Alcohol analysed by MALDI MS

The following reaction mixtures were prepared for each matrix (B2b, B2d, B2f, B2g, B2h and B2j) with each alcohol (Decanol, Terpeneol and CORT) giving 18 samples for each reaction and a total of 54 samples for all three reactions.

7.2.1 Sample Preparation for Reaction 1 and 2

Matrix, alcohol, base and coupling reagent solutions were prepared according to *tables 7.2 and 7.3* in anhydrous ACN. To an eppendorf tube was added matrix solution (0.3 mg/ml, 100 μ l), alcohol solution (10 μ l), 0.3 mg/ml TBTU solution (10 μ l) and DIEA solution (1.74 μ l/ml, 20 μ l). This was mixed thoroughly. Water was then added (15.5 μ l), mixed and the solution was allowed to react for 2 h at 40 °C (reaction 1) and for 5 h at r.t (reaction 2). The reaction mixture was analysed by MADLI-TOF MS following the general procedure outlined in *section 7.6.1*.

7.2.2 Sample Preparation for Reaction 3.

Matrix, alcohol, base and coupling reagent solutions were prepared according to *tables 7.2 and 7.3* in anhydrous ACN. To an eppendorf tube was added matrix solution (0.3 mg/ml, 100 μ l), alcohol solution (10 μ l), 0.3 mg/ml TBTU solution (10 μ l) and DIEA solution (1.74 μ l/ml, 20 μ l). This was mixed thoroughly. TFA solution (1%, 15.5 μ l) was then added, mixed and the solution was allowed to react for 5 h at r.t. The reaction mixture was analysed by MADLI-TOF MS.

Table 7.2 Preparation of solid compound stock solutions for MALDI analysis

Sample	Mm (g/mol)	Mass weighed (mg)	vol ACN (μl)	Conc' (mg/ml)	Dilution factor	Conc' (mg/ml)
B2b	290	3.6	1240	2.9	10	0.3
b2d	330	3.8	1150	3.3	10	0.3
B2f	339	3.1	912	3.4	10	0.3
B2g	302	3.8	1260	3.0	10	0.3
B2h	295	2.7	915	3.0	10	0.3
B2j	288	2.9	1000	2.9	10	0.3
CORT	347	3.8	1090	3.4	10	0.3
TBTU	321	3.1	968	3.2	10	0.3

Table 7.3 Preparation of liquid compound stock solutions for MALDI analysis

Sample	Mm (g/mol)	Density (g/cm³)	Mass (g)	Vol (cm³)	Conc' (μl/ml)
Decanol	158	0.83	0.00158	0.00190	1.90
Terpineol	154	0.93	0.00154	0.00166	1.66
DIEA	129	0.74	0.00129	0.00174	1.74

7.3 UV Absorption

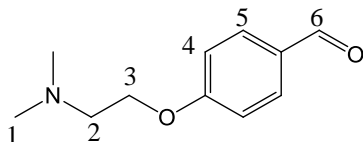
Matrix samples were prepared as 0.01 mg/ml solutions in ACN (80 %) : Water (20 %) : TFA (0.1 %). UV absorption spectra obtained were analysed to determine ϵ , the molar absorption coefficient.

7.4 Experimental data for structure B library

7.4.1 Procedure A: General Procedure for the Addition of the Basic Moiety

To a dry round bottom flask, the appropriately substituted 4-hydroxybenzaldehyde (1.0 eq.), potassium carbonate (3.0 eq.) and dry acetone (0.2 M) were added and the contents stirred and heated at reflux for 2 h. The reaction mixture was allowed cool to room temperature and potassium iodide (0.2 eq.), the appointed alkyl halide (1.5 eq.) mixed in dry acetone were added and the reaction mixture was heated to reflux and protected by a CaCl₂ trap to exclude water. The progress of the reaction was monitored by TLC (10 percent methanol/dichloromethane). After 16 h reflux volatiles were removed *in vacuo* and the resulting residue was partitioned between water and ethyl acetate. The aqueous layer was removed and extracted once more with ethyl acetate. The organic washings were combined and washed with brine, dried over magnesium sulphate, filtered and concentrated *in vacuo* to yield **B1x**. In some cases further purification was necessary and carried out by column chromatography using gradient elution (0-10% methanol in DCM).

7.4.2 4-[2-(Dimethylamino)ethoxy]benzaldehyde (**B1a**)



Procedure A was followed using 4-hydroxybenzaldehyde (**Ba**, 4.88 g, 40 mmol), potassium carbonate (16.58 g, 120 mmol), potassium iodide (1.32 g, 8 mmol), 2-chloro-*N,N*-dimethylethylamine hydrochloride (8.64 g, 60 mmol and dry acetone (200 ml) to give 4-[2-(Dimethylamino)ethoxy]benzaldehyde (**B1a**, 6.03 g, 78 %) as a yellow oil (Yadav et al. 2011).

^1H NMR (500 MHz, Chloroform-*d*): δ 9.89 (s, 1H, H-6), 7.83 (d, 2H, H-5), 7.03 (d, 2H, H-4), 4.15 (t, 2H, H-3), 2.77 (t, 2H, H-2), 2.35 (s, 6H, H-1).

^{13}C NMR (126 MHz, CDCl_3): δ 190.79, 163.85 (q), 131.94, 129.97 (q), 114.82, 66.39, 58.04, 45.90.

GCMS M^+ ion (194) found.

ν_{max} (neat) cm^{-1} : 2945, 2823, 2773, 1683, 1599, 1509, 1461, 1250, 1158, 1027, 961, 910, 832, 752, 618, 514, 415.

7.4.3 4-(2-(dimethylamino)ethoxy)-3-methoxybenzaldehyde (**B1b**)

Procedure A was followed using 4-hydroxy-3-methoxybenzaldehyde (**Bb**, 3.04 g, 20 mmol), potassium carbonate (8.29 g, 60 mmol), potassium iodide (0.66 g, 4 mmol), 2-chloro-*N,N*-dimethylethylamine hydrochloride (4.32 g, 30 mmol and dry acetone (100 ml), to give 4-[2-(Dimethylamino)ethoxy]-3-methoxybenzaldehyde (**B1b**, 2.77 g, 62 %) as a brown oil (Velema, Kietrys and Kool 2018).

GCMS M^+ ion (224) found.

ν_{max} (neat) cm^{-1} : 2942, 2823, 2773, 1680, 1585, 1509, 1340, 1264, 1135, 1026, 962, 865, 781, 731, 655, 592, 464, 413.

7.4.4 5-bromo-4-(2-(dimethylamino)ethoxy)-3-methoxybenzaldehyde (**B1c**)

Procedure A was followed using 5-bromo-4-hydroxy-3-methoxybenzaldehyde (**Bc**, 4.62 g, 20 mmol), potassium carbonate (8.29 g, 60 mmol), potassium iodide (0.66 g, 4 mmol), 2-chloro-*N,N*-dimethylethylamine hydrochloride (4.32 g, 30 mmol) and dry acetone (100 ml). No product was obtained.

7.4.5 3-methoxy-4-(2-(piperidin-1-yl)ethoxy)benzaldehyde (**B1d**)

Procedure A was followed using 4-hydroxy-3-methoxybenzaldehyde (**Bd**, 3.04 g, 20 mmol), potassium carbonate (8.29 g, 60 mmol), potassium iodide (0.66 g, 4 mmol), 1-(2-chloroethyl) piperidine (4.43 g, 30 mmol) and dry acetone (100 ml). To give 3-methoxy-4-(2-(piperidin-1-yl)ethoxy)benzaldehyde (**B1b**, 5.00 g, 95 %) as a brown oil (Nagarapu et al. 2009).

GCMS M^+ ion (264) found.

V_{\max} (neat) cm^{-1} : 2935, 2854, 2794, 1680, 1586, 1509, 1340, 1263, 1134, 1027, 944, 865, 781, 730, 656, 590, 458.

7.4.6 4-(2-(piperidin-1-yl)ethoxy)benzaldehyde (**B1e**)

Procedure A was followed using 4-hydroxybenzaldehyde (**Be**, 1.22 g, 10 mmol), potassium carbonate (4.15 g, 30 mmol), potassium iodide (0.33 g, 2 mmol), 4-(2-(piperidin-1-yl)ethoxy)benzaldehyde (2.76 g, 15 mmol) and dry acetone 60 ml. To give 4-(2-(piperidin-1-yl)ethoxy)benzaldehyde (**B1e**, 2.03 g, 87 %) as a brown oil (Duplantier et al. 2009).

GCMS M^+ ion (234) found.

V_{\max} (neat) cm^{-1} : 2934, 2853, 2788, 1689, 1599, 1509, 1428, 1372, 1250, 1157, 1043, 948, 832, 619, 514, 425.

7.4.7 3-bromo-4-(2-dimethylamino)ethoxybenzaldehyde (**B1f**)

Procedure A was followed using 3-bromo-4-hydroxybenzaldehyde (**Bf**, 1.00 g, 5 mmol), potassium carbonate (2.07 g, 15 mmol), potassium iodide (0.17 g, 1 mmol), 2-chloro-*N,N*-dimethylethylamine hydrochloride (1.08 g, 7.5 mmol) and dry acetone (50 ml), to give 3-bromo-4-(2-dimethylamino)ethoxybenzaldehyde (**B1f**, 1.07 g, 79 %) as a light brown oil (Chen et al. 2015).

GCMS M⁺ ion (273) found.

V_{\max} (neat) cm⁻¹: 2944, 2823, 2773, 1692, 1592, 1493, 1371, 1254, 1189, 1043, 898, 812, 666, 556, 437.

7.4.8 4-(2-morpholinoethoxy)benzaldehyde (**B1g**)

Procedure A was followed using 4-hydroxybenzaldehyde (**Bg**, 1.22 g, 10 mmol), potassium carbonate (4.15 g, 30 mmol), potassium iodide (0.33 g, 2 mmol), 4-(2-chloroethyl)morpholine (2.24 g, 15 mmol) and dry acetone 60 ml. To give 4-(2-morpholinoethoxy)benzaldehyde (**B1e**, 1.43 g, 61 %) as a dark brown oil (Bisht et al. 2010).

V_{\max} (neat) cm⁻¹: 2957, 2807, 1683, 1599, 1509, 1454, 1252, 1159, 1114, 1009, 915, 833, 607, 515.

7.4.9 3-chloro-4-(2-dimethylamino)ethoxybenzaldehyde (**B1h**)

Procedure A was followed using 3-chloro-4-hydroxybenzaldehyde (**Bh**, 1.00 g, 6.39 mmol), potassium carbonate (2.65 g, 19.17 mmol), potassium iodide (0.21 g, 1.28 mmol), 2-chloro-*N,N*-dimethylethylamine hydrochloride (1.38 g, 9.59 mmol) and dry acetone (50 ml), to give 3-chloro-4-(2-dimethylamino)ethoxybenzaldehyde (**B1h**, 1.45 g, 68 %) as a light brown oil.

GCMS M⁺ ion (229) found.

V_{\max} (neat) cm⁻¹: 2945, 2823, 2773, 1690, 1593, 1497, 1376, 1271, 1191, 1054, 922, 813, 685, 561, 428.

7.4.10 4-formylphenyl 2-(2,2,2-trifluoroacetyl)hydrazinecarboxylate (**B1i**)

Procedure A was followed using 4-hydroxybenzaldehyde (**Bi**, 0.40 g, 3.26 mmol), potassium carbonate (1.35 g, 9.78 mmol), potassium iodide (0.11 g, 0.65 mmol), *N'*-(2-chloroacetyl)-2,2,2-trifluoroacetohydrazide (1.00g, 4.89 mmol) and dry acetone (50 ml), to give 4-formylphenyl 2-(2,2,2-trifluoroacetyl)hydrazinecarboxylate (**B1i**, 0.39 g, 44 %) as a light yellow solid. M.p. 158.7-159.5 °C.

V_{\max} (neat) cm⁻¹: 3348, 2920, 1682, 1599, 1509, 1410, 1307, 1240, 1171, 1114, 830, 731, 578, 514.

7.4.11 4-(2-(diethylamino)ethoxy)benzaldehyde (B1j)

Procedure A was followed using 4-hydroxybenzaldehyde (**Bg**, 1.22 g, 10 mmol), potassium carbonate (4.15 g, 30 mmol), potassium iodide (0.33 g, 2 mmol), 2-chloro-N,N-diethylethanamine (2.24 g, 15 mmol) and dry acetone 60 ml. To give 4-(2-(diethylamino)ethoxy)benzaldehyde (**B1j**, 1.51 g, 68 %) as a brown oil (Yadav et al. 2011).

GCMS M⁺ ion (222) found.

V_{max} (neat) cm⁻¹: 2945, 2823, 2773, 1683, 1599, 1509, 1461, 1250, 1158, 1027, 961, 910, 832, 752, 618, 514, 415.

7.4.12 4-(2-(diethylamino)ethoxy)-3-methoxybenzaldehyde (B1k)

Procedure A was followed using 4-hydroxy-3-methoxybenzaldehyde (**Bk**, 1.52 g, 10 mmol), potassium carbonate (4.15 g, 30 mmol), potassium iodide (0.33 g, 2 mmol), 2-chloro-N,N-diethylethanamine (2.24 g, 15 mmol) and dry acetone 60 ml. To give 4-(2-(diethylamino)ethoxy)-3-methoxybenzaldehyde (**B1k**, 1.63 g, 65 %) as a brown oil (Amombo et al. 2012).

V_{max} (neat) cm⁻¹: 2970, 2816, 1736, 1682, 1586, 1509, 1372, 1241, 1135, 1031, 936, 868, 781, 730.

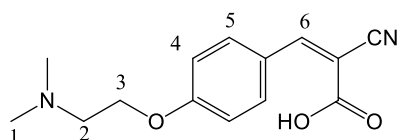
7.4.13 S-(3-(4-formylphenoxy)propyl) ethanethioate (B1l)

Procedure A was followed using 4-hydroxybenzaldehyde (**B1**, 1.22 g, 10 mmol), potassium carbonate (4.15 g, 30 mmol), potassium iodide (0.33 g, 2 mmol), 3-Chloropropyl thiolacetate (2.24 g, 15 mmol) and dry acetone 60 ml. No product was obtained.

7.5 Procedure B: General Procedure for the Knoevenagel Reaction with Cyanoacetic Acid

To a solution of cyanoacetic acid (1.0 eq.) in dry ethanol **B1x** (0.9 eq.) was added and heated under reflux for 3 h, using ammonium acetate (0.15 eq.) as the catalyst. The reaction water was separated using a glass wool, molecular sieves (3 Å) trap. The reaction mixture was allowed to cool and precipitate was filtered, the crude product was washed with sufficient amounts of acetone and recrystallised from 70 % acetonitrile / 30 % water. The crystals that formed were filtered and dried in vacuum desiccator overnight to yield **B2x** final product.

7.5.1 (Z)-2-cyano-3-(4-(2-(dimethylamino)ethoxy)phenyl)acrylic acid (**B2a**)



Procedure B was followed using, cyanoacetic acid (1.00 g, 12 mmol), was added to a solution of **B1a** (2.08 g, 10.8 mmol), ammonium acetate (0.14 g, 1.80 mmol) in dry ethanol (60 ml). To give (Z)-2-cyano-3-(4-(2-(dimethylamino)ethoxy)phenyl)acrylic acid (**B2a**, 1.4 g, 50 %) as white needle like crystals. M.p. 210-212 °C.

¹H NMR (500 MHz, Deuterium Oxide with Na₂CO₃): δ 8.01 (s, 1H, H-6), 7.92 (d, 2H, H-5), 7.10 (d, 2H, H-4), 4.24 (t, 2H, H-3), 2.85 (t, 2H, H-2), 2.33 (s, 6H, H-1).

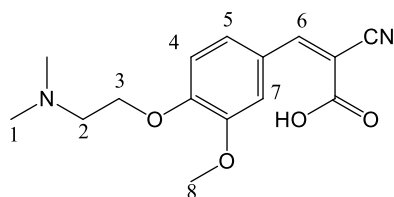
¹³C NMR (126 MHz, D₂O): δ 168.99 (q), 161.23 (q), 152.03, 132.47, 125.08 (q), 118.96 (q), 115.00, 105.39 (q), 65.15, 56.63, 43.96.

V_{max} (solid) cm⁻¹: 3541, 2204, 1603, 1509, 1427, 1325, 1251, 1159, 1030, 935, 819, 752, 611, 507.

MALDI-TOF MS: M⁺ ion (*m/z* 261) found.

7.5.2 (Z)-2-cyano-3-(4-(2-(dimethylamino)ethoxy)-3-methoxyphenyl)acrylic acid

(B2b)



Procedure B was followed using, cyanoacetic acid (1.00 g, 12 mmol), was added to a solution of **B1b** (2.41 g, 10.8 mmol), ammonium acetate (0.14 g, 1.80 mmol) in dry ethanol (60 ml). To give (Z)-2-cyano-3-(4-(2-(dimethylamino)ethoxy)-3-methoxyphenyl)acrylic acid (**B2b**, 1.76 g, 56 %) as orange solid. M.p. 197 – 200 °C.

^1H NMR (500 MHz, Deuterium Oxide) δ 7.05 (s, 1H, H-6), 6.77 – 6.69 (m, 2H, H-5,7), 6.60 (s, 1H, H-4), 4.14 (t, 2H, H-3), 3.43 (s, 3H, H-8), 2.88 (s, 6H, H-1), 2.87 (t, 2H, H-2).

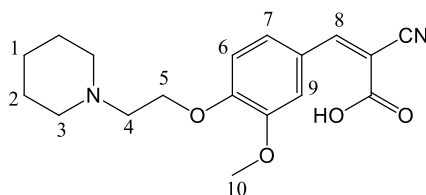
^{13}C NMR (126 MHz, D_2O) δ 167.70 (q), 150.54 (q) 149.52 (q), 147.39, 127.41 (q), 125.35, 118.45, 111.85, 110.03 (q), 103.99, 62.15 (q), 56.29, 55.02, 43.19, 43.11.

V_{max} (solid) cm^{-1} : 3456, 3363, 2207, 1640, 1580, 1510, 1468, 1325, 1272, 1147, 1025, 930, 852, 801, 721, 634, 532.

MALDI-TOF MS: M^+ ion (m/z 291) found.

7.5.3 (Z)-2-cyano-3-(3-methoxy-4-(2-(piperidin-1-yl)ethoxy)phenyl)acrylic acid

(B2d)



Procedure B was followed using, cyanoacetic acid (1.00 g, 12 mmol), was added to a solution of **B1d** (2.84 g, 10.8 mmol), ammonium acetate (0.14 g, 1.80 mmol) in dry ethanol (60 ml). To give (Z)-2-cyano-3-(3-methoxy-4-(2-(piperidin-1-yl)ethoxy)phenyl)acrylic acid (**B2d**, 0.75 g, 21 %) as yellow crystals. M.p. 189 – 192 °C.

¹H NMR and ¹³C NMR: Poor quality – inconclusive.

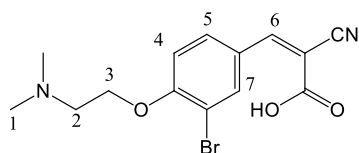
V_{\max} (solid) cm^{-1} : 3394, 2949, 2211, 1620, 1513, 1456, 1336, 1264, 1144, 1029, 954, 788, 720, 487.

MALDI-TOF MS: M^+ ion (m/z 331) found.

7.5.4 (Z)-2-cyano-3-(4(2-(piperidin-1yl)ethoxy)phenyl)acrylic acid (B2e)

Procedure B was followed using, cyanoacetic acid (0.25 g, 2.92 mmol), was added to a solution of **B1e** (0.61 g, 2.63 mmol), ammonium acetate (0.03 g, 0.44 mmol) in dry ethanol (15 ml). No product recovered.

7.3.5 (Z)-2-cyano-3-(4-(2-(dimethylamino)ethoxy)-3-bromophenyl)acrylic acid (B2f)



Procedure B was followed using, cyanoacetic acid (210 mg, 2.43 mmol), was added to a solution of **B1f** (600 mg, 2.21 mmol), ammonium acetate (30 mg, 0.365 mmol) in dry ethanol (10 ml). To give (Z)-2-cyano-3-(4-(2-(dimethylamino)ethoxy)-3-bromophenyl)acrylic acid (**B2f**, 0.49 g, 65 %) as white powder. M.p. 204 – 206 °C.

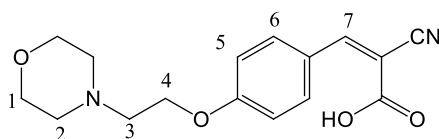
^1H NMR (500 MHz, DMSO- d_6) δ 8.17 (s, 1H, H-7), 7.93 – 7.82 (m, 3H, H-6+5), 7.27 (d, $J = 8.7$ Hz, 1H, H-4), 4.38 (t, $J = 5.3$ Hz, 2H, H-3), 2.61 (m, 8H, H-1+2).

^{13}C NMR: Poor quality (inconclusive)

V_{max} (solid) cm^{-1} : 3636, 3454, 2199, 1592, 1499, 1323, 1267, 1190, 1060, 1000, 807, 753, 666, 595, 530, 442.

MALDI-TOF MS: M^{+1} ion (m/z 340) found.

7.5.6 (Z)-2-cyano-3-(4-(2-morpholineethoxy)phenyl)acrylic acid (**B2g**)



Procedure B was followed using, cyanoacetic acid (100 mg, 12 mmol), was added to a solution of **B1g** (600 mg, 10.8 mmol), ammonium acetate (140 mg, 1.80 mmol) in dry ethanol (60 ml). To give (Z)-2-cyano-3-(4-(2-morpholineethoxy)phenyl)acrylic acid (**B2g**, 1.99 g, 61 %) as white powder. M.p. 204 – 207 °C.

^1H NMR (500 MHz, DMSO- d_6) δ 8.20 (s, 1H, H-7), 8.02 (d, $J = 9.0$ Hz, 2H, H-6), 7.14 (d, $J = 8.9$ Hz, 2H, H-5), 4.22 (t, $J = 5.5$ Hz, 2H, H-4), 3.58 (t, $J = 4.6$ Hz, 4H, H-1), 2.76 (t, 2H, H-3), 2.51 (t, $J = 4.2$ Hz, 4H, H-2).

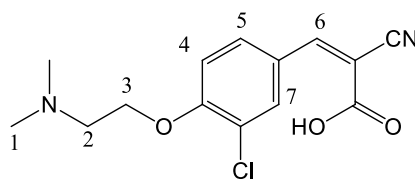
^{13}C NMR: Poor quality (inconclusive)

V_{max} (solid) cm^{-1} : 2965, 2869, 2215, 1599, 1511, 1426, 1322, 1257, 1188, 1111, 1032, 819, 749, 578, 519.

MALDI-TOF MS: M^{+1} ion (m/z 303) found.

7.5.7 (Z)-3-(3-chloro-4-(2-(dimethylamino)ethoxy)phenyl)-2-cyanoacrylic acid

(B2h)



Procedure B was followed using, cyanoacetic acid (0.25 g, 2.90 mmol), was added to a solution of **B1h** (0.60 g, 2.64 mmol), ammonium acetate (34 mg, 0.435 mmol) in dry ethanol (10 ml). To give (Z)-3-(3-chloro-4-(2-(dimethylamino)ethoxy)phenyl)-2-cyanoacrylic acid (**B2h**, 0.42 g, 54 %) as white powder. M.p. 203 – 205 °C.

¹H NMR (500 MHz, DMSO-*d*₆) δ 8.03 (s, 1H, H-6), 7.93 – 7.83 (m, 2H, H-4 + H-7), 7.31 (d, *J* = 8.7 Hz, 1H, H-5), 4.38 (t, *J* = 5.9 Hz, 2H, H-4), 3.15 (t, 2H, H-3), 2.59 (s, 6H, H-1).

¹³C NMR: Poor quality (inconclusive).

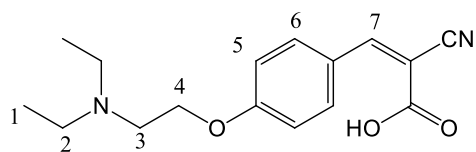
ν_{\max} (solid) cm^{-1} : 2211, 1597, 1505, 1418, 1318, 1265, 1210, 1162, 1063, 997, 880, 807, 754, 682, 597, 523, 452.

MALDI-TOF MS: M^{+1} ion (*m/z* 296) found.

7.5.8 (Z)-2-cyano-3-(4-((2-(2,2,2-trifluoroacetyl)hydrazinecarbonyl)oxy)phenyl)acrylic acid (B2i)

Procedure B was followed using, cyanoacetic acid (34 mg, 0.398 mmol), was added to a solution of **B1i** (100 mg, 0.362 mmol), ammonium acetate (4.6 mg, 0.06 mmol) in dry ethanol (5 ml). No product recovered.

7.5.9 (Z)-2-cyano-3-(4-(2-(diethylamino)ethoxy)phenyl)acrylic acid (B2j)



Procedure B was followed using, cyanoacetic acid (0.43 g, 4.97 mmol), was added to a solution of **B1j** (1.00 g, 4.52 mmol), ammonium acetate (57 mg, 0.74 mmol) in dry ethanol (30 ml). To give (Z)-2-cyano-3-(4-(2-(diethylamino)ethoxy)phenyl)acrylic acid (**B2j**, 0.82 g, 63 %) as yellow crystals. M.p. 207 – 209 °C.

^1H NMR (500 MHz, DMSO- d_6) δ 7.97 (s, 1H, H-7), 7.93 (d, $J = 8.6$ Hz, 2H, H-6), 7.11 (d, $J = 8.4$ Hz, 2H, H-5), 4.40 (t, 2H, H-4), 3.45 (t, 2H, H-3), 3.16 (q, $J = 7.1$ Hz, 4H, H-2), 1.22 (t, $J = 7.1$ Hz, 6H, H-1).

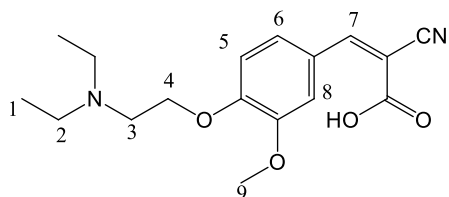
^{13}C NMR (126 MHz, DMSO) δ 164.42, 161.20, 151.48, 132.86, 125.72, 118.13, 115.74, 63.72, 50.79, 47.71, 9.29.

V_{max} (solid) cm^{-1} : 3541, 2204, 1603, 1509, 1427, 1325, 1251, 1159, 1030, 935, 819, 752, 611, 507.

MALDI-TOF MS: M^{+1} ion (m/z 289) found.

7.5.10 (Z)-2-cyano-3-(4-(2-(diethylamino)ethoxy)-3-methoxyphenyl)acrylic acid

(B2k)



Procedure B was followed using, cyanoacetic acid (1.00 g, 12 mmol), was added to a solution of **B1k** (2.71 g, 10.8 mmol), ammonium acetate (0.14 g, 1.80 mmol) in dry ethanol (60 ml). To give (Z)-2-cyano-3-(4-(2-(diethylamino)ethoxy)-3-methoxyphenyl)acrylic acid (**B2k**, 1.75 g, 51 %) as yellow crystals. M.p. 201 – 204 °C.

^1H NMR (500 MHz, Deuterium Oxide) δ 7.21 (s, 1H, H-7), 6.90 (s, 1H, H-8), 6.82 (d, 1H, H-6), 6.67 (d, 1H, H-5), 4.66 (s, 3H, H-9), 4.17 (t, $J = 7.5$ Hz, 2H, H-4), 3.48 (t, 2H, H-3), 3.21 (q, 4H, H-2), 1.23 (t, $J = 7.1$ Hz, 6H, H-1).

^{13}C NMR (126 MHz, D_2O) δ 167.75, 149.61, 147.49 (q), 127.30 (q), 125.43, 118.50 (q), 111.86, 110.54 (q), 104.30, 62.18, 60.46 (q), 55.11, 50.81, 47.43, 7.85.

V_{max} (solid) cm^{-1} : 2207, 1593, 1514, 1464, 1333, 1264, 1150, 1030, 805, 755.

MALDI-TOF MS: M^{+1} ion (m/z 289) found.

7.6 Experimental procedures for Structure A

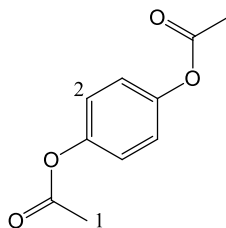
7.6.1 1,4-bis(benzyloxy)benzene (A1a)

Benzyl bromide (19.8 g, 0.116 mol) was slowly added to a solution of p-hydroquinone (5.55 g, 0.050 mol) and potassium hydroxide (6.80 g, 0.121 mol) in ethanol (100 ml), to form a precipitate right away. The suspension was rotated over night (12 h,) at room temperature, then poured into water (100 ml), the precipitate was filtered and recrystallised with ethanol to yield 1,4-bis(benzyloxy)benzene (**A1a**, 10.45 g, 72 %) in the form of white crystals. M.p. 125 – 128 °C.

7.6.2 1-(2,5-bis(benzyloxy)phenyl)ethenone (A3a)

A mixture of anhydrous aluminium chloride (7.33 g, 0.055 mol, 1.1 eq.) and dichloromethane (15 ml) were placed in a 3 neck round bottom flask that was fitted with a septum capped reflux condenser, a dropping syringe and a septum. The mixture was stirred and cooled to 0 °C on an ice bath. A solution of acetyl chloride (4.32, 0.055 mol, 1.1 eq.) in DCM (10 ml) was added through the dropping syringe over 10 min. **A1a** in DCM (10 ml) was then added in the same manner, adjusting the addition rate accordingly to ensure the solution did not boil excessively. The reaction was allowed to come to room temperature and stirred for an additional 15 min. The solution was then poured onto 25 g of ice and concentrated HCl, (15 ml). The resulting reaction was then partitioned with water, the organic layer was removed and the aqueous layer extracted with DCM (2 x 20 ml). The combined organic layers were washed with saturated NaHCO₃, dried over anhydrous MgSO₄, filtered and concentrated *in vacuo*.

7.6.3 1,4-phenylene diacetate (**A1b**)



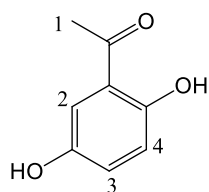
To a mixture of hydroquinone (22.00 g, 0.200 mol) and acetic anhydride (41.20 g, 38 ml, 0.404 mol) in a conical flask, concentrated sulfuric acid (1 drop) was added and stirred gently by hand. After 5 min the clear solution is poured onto approx. 150 ml of crushed ice. At room temperature the precipitate was filtered and washed with water. The crude product was recrystallised from ethanol (50 %). The white crystals that formed were filtered and dried to constant weight in vacuum desiccator to yield 30.00g (77 %) of 1,4-phenylene diacetate (**A1b**). M.p. 121 – 122 °C (Melero, van Grieken and Morales 2006).

$^1\text{H NMR}$ (500 MHz, Chloroform- d) δ 7.10 (s, 4H, H-1), 2.29 (s, 6H, H-2).

$^{13}\text{C NMR}$ (126 MHz, CDCl_3) δ 169.30, 148.02 (q), 122.39, 21.07.

V_{max} (solid) cm^{-1} : 1823, 1747, 1504, 1366, 1210, 1170, 1041, 1010, 919, 851, 764, 607, 522.

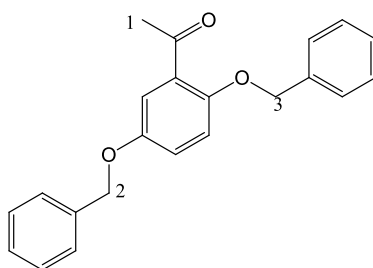
7.6.4 1-(2,5-dihydroxyphenyl)ethenone (**A2b**)



To a three necked round bottom flask fitted with a reflux condenser topped with a CaCl₂ guard tube and connected to a gas absorption trap was added, a finely powdered mixture of **A1b** (25 g, 0.129 mol) and anhydrous aluminium chloride (58 g, 0.44 mol). It was placed in an oil bath and slowly heated to 100 – 110 °C for 30 min, upon which the evolution of HCl gas begins. The temperature was then slowly raised to 160 °C and maintained at that point for 3 h. The reaction was allowed cool to r.t. The reaction mixture was then added to approx. 180 g of crushed ice, followed by the addition of concentrated hydrochloric acid. The solid was filtered and washed with adequate amounts of water. The crude product was recrystallised with 95 % ethanol to give 1-(2,5-dihydroxyphenyl)ethenone (**Ab2**, 14.72 g 75 %) as green crystals M.p. 200 – 203 °C (Melero, van Grieken and Morales 2006).

V_{\max} (solid) cm⁻¹: 3078, 1753, 1623, 1583, 1479, 1368, 1207, 1014, 945, 903, 786, 636, 535, 497

7.6.5 1-(2,5-bis(benzyloxy)phenyl)ethenone (A3)



A round bottom flask was charged with **Ab2** (4.9 g, 0.032 mol), K_2CO_3 (8.85 g, 0.064 mol), benzyl bromide (13.77 g, 9.56 ml, 0.081 mol) and acetone (80 ml). This was heated under reflux overnight, protected by a $CaCl_2$ guard tube to exclude moisture. The mixture was cooled and partitioned between NaOH (5 %) and DCM. The aqueous layer was extracted with a second portion of CH_2Cl_2 , the organic washings were combined and the solvent was removed *in vacuo*. The resulting product was purified by flash chromatography using gradient elution (EtOAc (10 %) and hexane) to give 1-(2,5-bis(benzyloxy)phenyl)ethenone (**A3**, 6.49 g, 61 %), M.p. 60-62 °C.

1H NMR (500 MHz, Chloroform-*d*) δ 7.45 – 6.94 (m, 13H), 5.12 (s, 2H, H-3), 5.04 (s, 2H, H-2), 2.60 (s, 3H, H-1).

^{13}C NMR (126 MHz, $CDCl_3$) δ 199.38 (q), 152.76 (q), 152.71 (q), 136.82 (q), 136.42 (q), 128.98 (q), 128.67, 128.57, 128.19, 128.00, 127.54, 121.10, 115.16, 114.56, 77.25, 77.00, 76.74, 71.33, 70.64, 32.09.

V_{max} (solid) cm^{-1} : 3033, 2927, 1659, 1489, 1408, 1279, 1194, 1011, 896, 802, 694, 592,

537

7.6.6 2,5-bis(benzyloxy)phenyl acetate (A4)

A3 (0.6 g, 2 mol) was dissolved in glacial acetic acid (7 ml, 0.122 mmol) followed by the addition of p-toluenesulfonic acid monohydrate (76 mg, 0.4 mmol) and hydrogen peroxide (30 %, 1.1 ml, 10 mmol). The reaction mixture was then heated at 80 °C for 1 h under stirring. The solution was then poured into 50 ml water containing sodium bicarbonate (20 mg) and extracted with EtOAc (4 x 50 ml). The organic extracts were combined, dried under Na₂SO₄, filtered and the solvent was removed *in vacuo*, to give the crude 2,5-bis(benzyloxy)phenyl acetate (**A4**, 0.02 g, 42 %) as a brown solid.

7.6.7 2,5-bis(benzyloxy)phenol (A5)

To a round bottom flask was added **A4** (0.28 g, 0.8 mmol), followed by HCl (37 %, 1 ml) in MeOH (4 ml). The mixture was heated to 70 °C with stirring for 30 min. The reaction mixture was cooled to room temperature, solvent evaporated and the residue was diluted in ethyl acetate (60 ml) and washed with water (60 ml). The organic layer was dried over Na₂SO₄, filtered and the solvent was removed *in vacuo*, to give a brown oil.

7.7 Experimental Procedure for Structure C

7.7.1 Ethyl 2-((4-acetylphenyl)carbamoyl)hydrazinecarboxylate (C1)

To a solution of 4-aminoacetophenone (676 mg, 5.0 mmol) in THF (25 ml) cooled to 0 °C was added triethylamine (1.4 ml, 10 mmol) and 4-nitrophenyl chloroformate (1512 mg, 7.5 mmol). After stirring for 2 h at room temperature, ethyl carbazate (1565 mg, 15.0 mmol) and additional triethylamine (2.1 ml, 15.0 mmol), the mixture was stirred for 2 h at 55 °C. The reaction mixture was then partitioned with water (50 ml) and DCM (2 x 50 ml), the organic layers were combined and washed with saturated sodium bicarbonate, dried over MgSO₄, filtered and concentrated *in vacuo*. The residue was triturated in ethyl acetate, filtered (yellow solid) and concentrated *in vacuo* to give a yellow oil. This was not identified as the product.

7.7.2 Ethyl 2-((4-acetylphenyl)carbamoyl)hydrazinecarboxylate (C1)

A solution of ethyl carbazate (3.32 g, 31.03 mmol) in toluene (50 ml) was added to a single neck round bottom flask, followed by the slow addition of a solution of 4-acetylphenyl isocyanate (5.00 g, 31.03 mmol) in toluene (125 ml). The reaction mixture was stirred at room temperature for 2 h and at 80 °C for a further 2 h. The precipitation formed was filtered and dried in vacuum desiccator overnight to give Ethyl 2-((4-acetylphenyl)carbamoyl)hydrazinecarboxylate (C1, 7.38 g, 90 %) as a white solid. This was used without further purification in the next step. M.p. 145-148 °C.

V_{\max} (solid) cm⁻¹: 3290, 1677, 1600, 1410, 1236, 1178, 1019, 960, 844, 718, 592, 502.

7.7.3 4-(4-acetylphenyl)-1,2,4-triazolidine-3,5-dione (C2)

A mixture of **C1** (7.03 g, 26.5 mmol) and 4 M KOH solution were heated at 70 °C for 2 h. Using a sintered glass crucible the remaining undissolved solids were filtered off. The filtrate was allowed to cool to room temperature and acidified with concentrated HCl. The yellow precipitate that formed was filtered and dried in vacuum desiccator to give 4-(4-acetylphenyl)-1,2,4-triazolidine-3,5-dione (**C2**, 5.00 g, 86 %) as a yellow solid. M.p. 240-243 °C.

V_{\max} (solid) cm^{-1} : 3048, 2825, 1782, 1704, 1605, 1415, 1284, 1214, 1098, 977, 835, 659, 522, 480, 417.

7.7.4 4-(4-acetylphenyl)-3H-1,2,4-triazole-3,5(4H)-dione (C3)

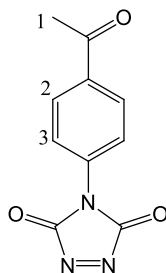
A mixture of $\text{SiO}_2\text{-HNO}_3$ was first prepared by adding silica 5 g to HNO_3 (8 ml) and evenly mixed with glass rod for 10 min. $\text{SiO}_2\text{-HNO}_3$ (5 g) was added to a **C2** (1.91 g, 8.72 mmol) in DCM (50 ml). The red mixture was stirred at room temperature for 30 min. filtered and concentrated in vacuo. No product was isolated.

7.7.5 4-(4-acetylphenyl)-3H-1,2,4-triazole-3,5(4H)-dione (C3)

A three-necked RBF containing zinc pellets was fitted with a hand-held pump, a dropping funnel holding nitric acid (60 %) and a gas dispersion tube. The gas tube was connected to a second three-necked RBF placed on an ice bath that contained a stirred slurry of **C2** (0.400 g, 3.7 mmol) in ethyl acetate (25 ml) and anhydrous sodium sulphate (3.0 g, 21.12 mmol) was added to remove any water present in NO_2 . The nitric acid from the dropping funnel was slowly added to the first RBF and the gas produced was pumped from RBF-1 to RBF-2 for 20 min, until the urazole was fully dissolved and the reaction mixture had

become a bright red colour. The mixture was allowed to stir for another 30 min. The sodium sulfate was removed by filtration and the solvent removed by rotary evaporation at $< 40\text{ }^{\circ}\text{C}$ to give a red oil, which disintegrated shortly after.

7.7.6 4-(4-acetylphenyl)-3H-1,2,4-triazole-3,5(4H)-dione (C3)



To an ice-cold suspension of **C2** (1.00 g, 4.60 mmol) in DCM (50 ml), *N*, bromosuccinimide (NBS, 1.63 g, 9.16 mmol) was added and stirred for 20 min to generate a red solution, which was extracted 3 times with water. The organic layer was dried over MgSO_4 , filtered and concentrated in vacuo at $< 35\text{ }^{\circ}\text{C}$ to give the title compound (**C3**, 0.60 g, 60 %) as a red solid. Further purification was attempted by sublimation of 0.10 g of product, it did not sublime. M.p. $87\text{-}89\text{ }^{\circ}\text{C}$.

^1H NMR (500 MHz, Acetonitrile- d_3) δ 8.19 (d, $J = 8.5$ Hz, 2H, H-3), 7.64 (d, $J = 8.5$ Hz, 2H, H-2), 2.17 (s, 3H, H-1).

^{13}C NMR (126 MHz, CD_3CN) δ 130.63 (q), 130.51 (q), 126.43 (q), 125.59 (q), 120.15, 118.82, 118.26, 27.09.

ν_{max} (solid) cm^{-1} : 1753, 1683, 1586, 1509, 1387, 1271, 1168, 1014, 958, 900, 834, 742, 670, 590, 489.

8 References

ABOU-HATAB, S., SPATA, V.A. & MATSIKA, S., 2017. 'Substituent Effects on the Absorption and Fluorescence Properties of Anthracene'. *The Journal of Physical Chemistry A*, 121 (6), pp. 1213-1222.

ADDIE, R.D., BALLUFF, B., BOVÉE, J.V.M.G., MORREAU, H. & MCDONNELL, L.A., 2015. 'Current State and Future Challenges of Mass Spectrometry Imaging for Clinical Research'. *Analytical Chemistry*, 87 (13), pp. 6426-6433.

ALAKURTTI, S., HEISKA, T., KIRIAZIS, A., SACERDOTI-SIERRA, N., JAFFE, C.L. & YLI-KAUHALUOMA, J., 2010. 'Synthesis and anti-leishmanial activity of heterocyclic betulin derivatives'. *Bioorganic Medicinal Chemistry*, 18 (4), Feb 15, pp. 1573-82.

AMOMBO, G.M., KRAMER, T., LO MONTE, F., GORING, S., FACH, M., SMITH, S., KOLB, S., SCHUBENEL, R., BAUMANN, K. & SCHMIDT, B., 2012. 'Modification of a promiscuous inhibitor shifts the inhibition from gamma-secretase to FLT-3'. *Bioorganic Medicinal Chemistry Letter*, 22 (24), Dec 15, pp. 7634-40.

BAUSCH, M.J. & DAVID, B., 1992. 'Proton, electron, and hydrogen atom transfers from ions, radicals, and radical ions derived from substituted urazoles and triazolinediones'. *The Journal of Organic Chemistry*, 57 (4), pp. 1118-1124.

BENNINGHOVEN, A. & SICHTERMANN, W.K., 1978. 'Detection, identification, and structural investigation of biologically important compounds by secondary ion mass spectrometry'. *Analytical Chemistry*, 50 (8), pp. 1180-1184.

Benzyl bromide MSDS [Online], 2016. Sigma Aldrich. Available from: <https://www.sigmaaldrich.com/MSDS/MSDS/DisplayMSDSPage.do?country=GB&language=en&productNumber=B17905&brand=ALDRICH&PageToGoToURL=https%3A%2F%2Fwww.sigmaaldrich.com%2Fcatalog%2Fproduct%2Faldrich%2Fb17905%3Flang%3Den> [Viewed 2019-02-21].

BISHT, S.S., DWIVEDI, N., CHATURVEDI, V., ANAND, N., MISRA, M., SHARMA, R., KUMAR, B., DWIVEDI, R., SINGH, S., SINHA, S.K., GUPTA, V., MISHRA, P.R., DWIVEDI, A.K. & TRIPATHI, R.P., 2010. 'Synthesis and optimization of antitubercular activities in a series of 4-(aryloxy)phenyl cyclopropyl methanols'. *European Journal of Medicinal Chem*, 45 (12), Dec, pp. 5965-78.

BODZON-KULAKOWSKA, A. & SUDER, P., 2016. 'Imaging mass spectrometry: Instrumentation, applications, and combination with other visualization techniques'. *Mass Spectrometry Reviews*, 35 (1), 2019/05/03, pp. 147-169.

BREITMAIER, E., 2002. *Structure elucidation by NMR in organic chemistry*. Third ed. Germany: Wiley.

CALVIN GIDDINGS, J., 2017. *Dynamics of Chromatography : Principles and Theory* [Online]. CRC Press. Available from: <https://content.taylorfrancis.com/books/download?dac=C2006-0-15997-7&isbn=9781315275871&format=googlePreviewPdf> [Viewed].

CAPRIOLI, R.M., 2015. 'Imaging mass spectrometry: enabling a new age of discovery in biology and medicine through molecular microscopy'. *Journal of the American Society of Mass Spectrometry*, 26 (6), Jun, pp. 850-2.

CAPRIOLI, R.M., FARMER, T.B. & GILE, J., 1997. 'Molecular imaging of biological samples: localization of peptides and proteins using MALDI-TOF MS'. *Analytical Chemistry*, 69 (23), Dec 1, pp. 4751-60.

CASTELLINO, S., GROSECLOSE, M.R. & WAGNER, D., 2011. 'MALDI imaging mass spectrometry: bridging biology and chemistry in drug development'. *Bioanalysis*, 3 (21), Nov, pp. 2427-41.

CHACON, A., ZAGOL-IKAPITTE, I., AMARNATH, V., REYZER, M.L., OATES, J.A., CAPRIOLI, R.M. & BOUTAUD, O., 2011. 'On-tissue chemical derivatization of 3-methoxysalicylamine for MALDI-imaging mass spectrometry'. *Journal of Mass Spectrometry*, 46 (8), 2019/02/13, pp. 840-846.

CHEN, S., ZHANG, T., WANG, J., WANG, F., NIU, H., WU, C. & WANG, S., 2015. 'Synthesis and evaluation of 1-hydroxy/methoxy-4-methyl-2-phenyl-1H-imidazole-5-carboxylic acid derivatives as non-purine xanthine oxidase inhibitors'. *European Journal of Medicinal Chemistry*, 103, pp. 343-353.

CLAYDEN, J., GREEVES, N. & WARREN, S., 2001. *Organic chemistry*. Second ed.: [Oxford ; New York] : Oxford University Press, [2001].

COBICE, D.F., GOODWIN, R.J.A., ANDREN, P.E., NILSSON, A., MACKAY, C.L. & ANDREW, R., 2015. 'Future technology insight: mass spectrometry imaging as a tool in drug research and development'. *British Journal of Pharmacology*, 172 (13), pp. 3266-3283.

CURRAN, D.P., 1998. 'Strategy-Level Separations in Organic Synthesis: From Planning to Practice'. *Angewandte Chemie International Edition*, 37 (9), 2019/04/30, pp. 1174-1196.

DE KOCK, N., ACHARYA, S.R., UBHAYASEKERA, S. & BERGQUIST, J., 2018. 'A Novel Targeted Analysis of Peripheral Steroids by Ultra-Performance Supercritical Fluid Chromatography Hyphenated to Tandem Mass Spectrometry'. In: *Sci Rep*.

DEMER LINDA, L., HSU JEFFREY, J. & TINTUT, Y., 2018. 'Steroid Hormone Vitamin D'. *Circulation Research*, 122 (11), 2019/03/25, pp. 1576-1585.

DING, S., SCHOENMAKERS, I., JONES, K., KOULMAN, A., PRENTICE, A. & VOLMER, D.A., 2010. 'Quantitative determination of vitamin D metabolites in plasma using UHPLC-MS/MS'. *Analytical & Bioanalytical Chemistry*, 398 (2), Sep, pp. 779-89.

DOYLE, W.M. 'Principles and Applications of Fourier Transform Infra-red (FTIR) Process Analysis'. [Online]. @allenai_org. Available from: <https://pdfs.semanticscholar.org/8b91/08726fe76043badeecd1c75ed6e72352b8a1.pdf>.

DUPLANTIER, A.J., EFREMOV, I., CANDLER, J., DORAN, A.C., GANONG, A.H., HAAS, J.A., HANKS, A.N., KRAUS, K.G., LAZZARO, J.T., JR., LU, J., MAKLAD, N., MCCARTHY, S.A., O'SULLIVAN, T.J., ROGERS, B.N., SIUCIAK, J.A.,

SPRACKLIN, D.K. & ZHANG, L., 2009. '3-Benzyl-1,3-oxazolidin-2-ones as mGluR2 positive allosteric modulators: Hit-to lead and lead optimization'. *Bioorganic Medicinal Chemistry Letters*, 19 (9), May 1, pp. 2524-9.

FERGUSON, C.N., FOWLER, J.W.M., WAXER, J.F., GATTI, R.A. & LOO, J.A., 2014a. 'Mass Spectrometry Based Tissue Imaging of Small Molecules'. In: WOODS, A.G. & DARIE, C.C. (eds.), *Advancements of Mass Spectrometry in Biomedical Research*. Switzerland: Springer, pp. 283-299.

FERGUSON, C.N., FOWLER, J.W.M., WAXER, J.F., GATTI, R.A. & LOO, J.A., 2014b. 'Mass Spectrometry Based Tissue Imaging of Small Molecules'. In: WOODS, A.G. & DARIE, C.C. (eds.), *Advancements of Mass Spectrometry in Biomedical Research*. Switzerland: Springer, pp. 283-299.

FLINDERS, B., MORRELL, J., MARSHALL, P.S., RANSHAW, L.E. & CLENCH, M.R., 2015. 'The use of hydrazine-based derivatization reagents for improved sensitivity and detection of carbonyl containing compounds using MALDI-MSI'. - 407 (- 8), pp. - 2094.

GEMPERLINE, E., CHEN, B. & LI, L., 2014. 'Challenges and recent advances in mass spectrometric imaging of neurotransmitters'. *Bioanalysis*, 6 (4), Feb, pp. 525-40.

GERE, D.R., KNIPE, C.R., CASTELLI, P., HEDRICK, J. & FRANK, L.G.R., 1993. 'Bridging the Automation Gap Between Sample Preparation and Analysis: An Overview of SFE, GC, GC-MS, and HPLC Applied to Environmental Samples'. *Journal of Chromatographic Science*, 31 (7), pp. 246-258.

GIDDEN, J., LIYANAGE, R., DURHAM, B. & LAY, J.O., JR., 2007. 'Reducing fragmentation observed in the matrix-assisted laser desorption/ionization time-of-flight mass spectrometric analysis of triacylglycerols in vegetable oils'. *Rapid Communications in Mass Spectrometry*, 21 (13), pp. 1951-7.

GOODWIN, R.J., NILSSON, A., MACKAY, C.L., SWALES, J.G., JOHANSSON, M.K., BILLGER, M., ANDREN, P.E. & IVERSON, S.L., 2016. 'Exemplifying the Screening Power of Mass Spectrometry Imaging over Label-Based Technologies for Simultaneous Monitoring of Drug and Metabolite Distributions in Tissue Sections'. *Journal of Biomolecular Screening*, 21 (2), Feb, pp. 187-93.

GOODWIN, R.J., PENNINGTON, S.R. & PITT, A.R., 2008. 'Protein and peptides in pictures: imaging with MALDI mass spectrometry'. *Proteomics*, 8 (18), Sep, pp. 3785-800.

GUELI, N., VERRUSIO, W., LINGUANTI, A., DI MAIO, F., MARTINEZ, A., MARIGLIANO, B. & CACCIAFESTA, M., 2012. 'Vitamin D: drug of the future. A new therapeutic approach'. *Archives Gerontology Geriatrics*, 54 (1), Jan-Feb, pp. 222-7.

GUNAWARDENA, G., 2017. *Williamson Ether Synthesis* [Online]. Libre Texts Libraries: Mind touch. Available from: https://chem.libretexts.org/Ancillary_Materials/Reference/Organic_Chemistry_Glossary/Williamson_Ether_Synthesis [Viewed 2019-02-18].

GUO, Z.A.G.Z.A.H.L., 2007. 'A binary matrix for background suppression in MALDI-MS of small molecules'. *Analytical and bioanalytical chemistry*, v. 387 (no. 5), pp. pp. 1939-1944-2007 v.387 no.5.

HOLLIS, G., DAVIES, D.R., JOHNSON, T.M. & WADE, L.G., 2006. *Organic chemistry, sixth edition, L.G. Wade Jr. : test item file*. Upper Saddle River, N.J.: Pearson Prentice Hall.

JEON, S.-M. & SHIN, E.-A., 2018. 'Exploring vitamin D metabolism and function in cancer'. *Experimental & Molecular Medicine*, 50 (4), p. 20.

JOHNSON, A.W. 1948. *A Text-Book of Practical Organic Chemistry* Arthur I. Vogel. Edward Arnold & Co.

JONES, E.A., DEININGER, S.O., HOGENDOORN, P.C.W., DEELDER, A.M. & MCDONNELL, L.A., 2012. 'Imaging mass spectrometry statistical analysis'. *Journal of Proteomics*, 75 (16), Aug 30, pp. 4962-4989.

JONES, G., 2011. 'The Knoevenagel Condensation'. *Organic Reactions*, 2019/02/17.

KARLSSON, O. & HANRIEDER, J., 2017. 'Imaging mass spectrometry in drug development and toxicology'. In: *Archives of Toxicology*. pp. 2283-94.

KATTNER, L. & VOLMER, D.A., 2017. 'Synthesis of Low Abundant Vitamin D Metabolites and Assaying Their Distribution in Human Serum by Liquid Chromatography-Tandem Mass Spectrometry (LC-MS/MS) as a New Tool for Diagnosis and Risk Prediction of Vitamin D Related Diseases'. In: GOWDER, T.J.S. (ed.) *A Critical Evaluation of Vitamin D - basic Overview* London: InTechOpen Limited.

KNOCHENMUSS, R., DUBOIS, F., DALE, M.J. & ZENOBI, R., 1996. 'The Matrix Suppression Effect and Ionization Mechanisms in Matrix-assisted Laser Desorption/Ionization'. *Rapid Communications in Mass Spectrometry*, 10 (8), 2019/05/13, pp. 871-877.

KOCIENSKI, V.P.J., 2006. 'Protecting Groups'. *Chemie in unserer Zeit*, 40 (4), pp. 268-268.

KRISHNAN, A.V., TRUMP, D.L., JOHNSON, C.S. & FELDMAN, D., 2010. 'The role of vitamin D in cancer prevention and treatment'. *Endocrinology & Metabolism Clinics of North America*, 39 (2), Jun, pp. 401-18, table of contents.

KWAK, G. & FUJIKI, M., 2004. 'Colored and Luminous Aliphatic Polyester via One-Pot Intra- and Intermolecular Knoevenagel Reactions'. *Macromolecules*, 37 (6), pp. 2021-2025.

LEOPOLD, J., POPKOVA, Y., ENGEL, M.K. & SCHILLER, J., 2018. 'Recent Developments of Useful MALDI Matrices for the Mass Spectrometric Characterization of Lipids'. *Biomolecules*, 8 (4).

LEVELL, M.J., 1980. 'Steroid hormones: By D B Gower. pp 115. Croom Helm, London. 1979. £7.95 (hardback), £2.95 (paperback). ISBN 0-85664-838-8 (hardback) and 0-85664-8 (paperback)'. *Biochemical Education*, 8 (4), 2019/05/08, pp. 125-125.

LIEW, K.-F., CHAN, K.-L. & LEE, C.-Y., 2015. 'Blood–brain barrier permeable anticholinesterase auronones: Synthesis, structure–activity relationship, and drug-like properties'. *European Journal of Medicinal Chemistry*, 94, pp. 195-210.

LOUGEE, M., 2018. *What is a Dehydration Reaction?* [Online]. @RealSciencing. Available from: <https://sciencing.com/what-is-a-dehydration-reaction-13712138.html> [Viewed 2019/04/07].

LUGEMWA, N.F., SHAIKH, K. & HOCHSTEDT, E., 2013. 'Facile and Efficient Acetylation of Primary Alcohols and Phenols with Acetic Anhydride Catalyzed by Dried Sodium Bicarbonate'. *Catalysts*, 3 (4).

MALLAKPOUR, S.E., 1992. 'A new method for the oxidation of 4-phenylurazole to 4-phenyltriazolinedione'. *Journal of Chemical Education*, 69 (3), p. 238.

MANUEL, I., BARREDA-GÓMEZ, G., GONZÁLEZ DE SAN ROMÁN, E., VELOSO, A., FERNÁNDEZ, J.A., GIRALT, M.T. & RODRÍGUEZ-PUERTAS, R., 2015. 'Neurotransmitter Receptor Localization: From Autoradiography to Imaging Mass Spectrometry'. *ACS Chemical Neuroscience*, 6 (3), pp. 362-373.

MCDONNELL, L.A., HERREN, R.M.A., ANDREN, P.E., STOECKLI, M. & CORTHALS, G.L., 2012. 'Going forward: Increasing the accessibility of imaging mass spectrometry - ScienceDirect'. *Journal of Proteomics*, 75 (16), pp. 5113-5121.

MELERO, J.A., VAN GRIEKEN, R. & MORALES, G., 2006. 'Advances in the Synthesis and Catalytic Applications of Organosulfonic-Functionalized Mesoporous Materials'. *Chemical Reviews*, 106 (9), pp. 3790-3812.

MONOPOLI, A., CALVANO, C.D., NACCI, A. & PALMISANO, F., 2014. 'Boronic acid chemistry in MALDI MS: a step forward in designing a reactive matrix with molecular recognition capabilities'. *Chemical Communications*, 50 (33), pp. 4322-4324.

NAGARAPU, L., ANEESA, SATYENDER, A., CHANDANA, G. & BANTU, R., 2009. 'Synthesis and antimicrobial activity of novel analogs of trifenagrel'. *Journal of Heterocyclic Chemistry*, 46 (2), 2019/06/16, pp. 195-200.

NAWRAT, C.C. & MOODY, C.J., 2014. 'Quinones as Dienophiles in the Diels–Alder Reaction: History and Applications in Total Synthesis'. *Angewandte Chemie International Edition*, 53 (8), 2019/05/30, pp. 2056-2077.

OUELLETTE, R.J. & RAWN, J.D., 2015. '16 - Ethers and Epoxides'. In: *Organic Chemistry Study Guide*. Boston: Elsevier, pp. 277-297.

PATEL, H.D., 2014. 'Recent Advances in the Synthesis of Coumarin Derivatives via Knoevenagel Condensation: A Review AU - Vekariya, Rajesh H'. *Synthetic Communications*, 44 (19), pp. 2756-2788.

PATERSON, D., 2018. *Evaporation, filtration and crystallisation* [Online]. Royal Society of Chemistry. Available from: <https://eic.rsc.org/cpd/evaporation-filtration-and-crystallisation/3009017.article> [Viewed 2019/04/30].

QI, Y., MULLER, M., STOKES, C.S. & VOLMER, D.A., 2018. 'Rapid Quantification of 25-Hydroxyvitamin D₃ in Human Serum by Matrix-Assisted Laser Desorption/Ionization Mass Spectrometry'. *Journal of the American Society of Mass Spectrometry*, 29 (7), Jul, pp. 1456-1462.

QI, Y., MULLER, M.J. & VOLMER, D.A., 2017. 'Activation of Reactive MALDI Adduct Ions Enables Differentiation of Dihydroxylated Vitamin D Isomers'. *Journal of the American Society of Mass Spectrometry*, 28 (12), Dec, pp. 2532-2537.

RAMBERG, P.J., 2000. 'The Death of Vitalism and The Birth of Organic Chemistry: Wohler's Urea Synthesis and the Disciplinary Identity of Organic Chemistry'. *Ambix*, 47 (3), pp. 170-195.

REN, Z., CAO, W. & TONG, W., 2002. 'THE KNOEVENAGEL CONDENSATION REACTION OF AROMATIC ALDEHYDES WITH MALONONITRILE BY GRINDING IN THE ABSENCE OF SOLVENTS AND CATALYSTS'. *Synthetic Communications*, 32 (22), pp. 3475-3479.

RENZ, M. & MEUNIER, B., 1999. '100 Years of Baeyer–Villiger Oxidations'. *European Journal of Organic Chemistry*, 1999 (4), 2019/02/20, pp. 737-750.

RICHARDSON, S.D., CAUGHRAN, T.V., POIGER, T., GUO, Y. & CRUMLEY, F.G., 2000. 'Application of DNPH Derivatization with LC/MS to the Identification of Polar Carbonyl Disinfection Byproducts in Drinking Water'. *Ozone: Science & Engineering*, 22 (6), pp. 653-675.

SARMAH, N., BHATTACHARYYA, P.K. & BANIA, K.K., 2014. 'Substituent and Solvent Effects on the Absorption Spectra of Cation- π Complexes of Benzene and Borazine: A Theoretical Study'. *Journal of Physical Chemistry A*, 118 (21), May 29, pp. 3760-3774.

SARTORI, G. & MAGGI, R., 2006. 'Use of Solid Catalysts in Friedel–Crafts Acylation Reactions'. *Chemical Reviews*, 106 (3), pp. 1077-1104.

SAYER, J.M., PINSKY, B., SCHONBRUNN, A. & WASHTIEN, W., 1974. 'Mechanism of carbinolamine formation'. *Journal of the American Chemical Society*, 96 (26), pp. 7998-8009.

SCHULZ, E., KARAS, M., ROSU, F. & GABELICA, V., 2006. 'Influence of the Matrix on Analyte Fragmentation in Atmospheric Pressure MALDI'. *Journal of the American Society for Mass Spectrometry*, 17 (7), pp. 1005-1013.

SEELEY, E., H. & CAPRIOLI, R., M., 2012. '3D Imaging by Mass Spectrometry: A new Frontier'. *Analytical Chemistry*, 84 (5), 2012/03/16 pp. 2105-2110.

SMITH, M.B. & MARCH, J., 2007. *March's Advanced Organic Chemistry: Reactions, Mechanisms, and Structure*. Canada: Wiley.

SOBERBERG, T., 2013. '11.6: Imine (Schiff base) formation'. In: *Organic Chemistry With a Biological Emphasis*. University of Minnesota.

SOLON, E.G., SCHWEITZER, A., STOECKLI, M. & PRIDEAUX, B., 2010. 'Autoradiography, MALDI-MS, and SIMS-MS imaging in pharmaceutical discovery and development'. *The AAPS journal*, 12 (1), Mar, pp. 11-26.

STOECKLI, M., 2017. *What is COST?* [Online]. Available from: <https://ms-imaging.org/wp/what-is-cost/> [Viewed 2019/04/29].

STUMPF, W.E., 2013. 'Whole-body and microscopic autoradiography to determine tissue distribution of biopharmaceuticals — Target discoveries with receptor micro-autoradiography engendered new concepts and therapies for vitamin D'. *Advanced Drug Delivery Reviews*, 65 (8), pp. 1086-1097.

TAKATS, Z., WISEMAN, J.M., GOLOGAN, B. & COOKS, R.G., 2004. 'Mass spectrometry sampling under ambient conditions with desorption electrospray ionization'. *Science*, 306 (5695), Oct 15, pp. 471-3.

TIETZE, L.F.B., UWE, 1991. *Comprehensive Organic Synthesis*. Elsevier.

TRETLI, S., HERNES, E., BERG, J.P., HESTVIK, U.E. & ROBSAHM, T.E., 2009. 'Association between serum 25(OH)D and death from prostate cancer'. In: *British Journal of Cancer*. pp. 450-4.

TWIBANIRE, J.-D.A.K. & GRINDLEY, T.B., 2011. 'Efficient and Controllably Selective Preparation of Esters Using Uronium-Based Coupling Agents'. *Organic Letters*, 13 (12), pp. 2988-2991.

VELEMA, W.A., KIETRYS, A.M. & KOOL, E.T., 2018. 'RNA Control by Photoreversible Acylation'. *Journal of the American Chemical Society*, 140 (10), Mar 14, pp. 3491-3495.

WANG, Z.J., CHANG, T.-T.A., SLAUTER, R. & FAQI, A.S., 2013. 'Chapter 32 - Use of Imaging for Preclinical Evaluation'. In: *A Comprehensive Guide to Toxicology in Preclinical Drug Development*. Academic Press, pp. 759-775.

WILLIAMSON, A., 1850. 'XLV. Theory of ætherification'. *The London, Edinburgh, and Dublin Philosophical Magazine and Journal of Science*, 37 (251), pp. 350-356.

YADAV, Y., MACLEAN, E.D., BHATTACHARYYA, A., PARMAR, V.S., BALZARINI, J., BARDEN, C.J., TOO, C.K. & JHA, A., 2011. 'Design, synthesis and bioevaluation of novel candidate selective estrogen receptor modulators'. *European Journal of Medicinal Chemistry*, 46 (9), Sep, pp. 3858-66.

9 Appendices

A.1 FTIR Spectra

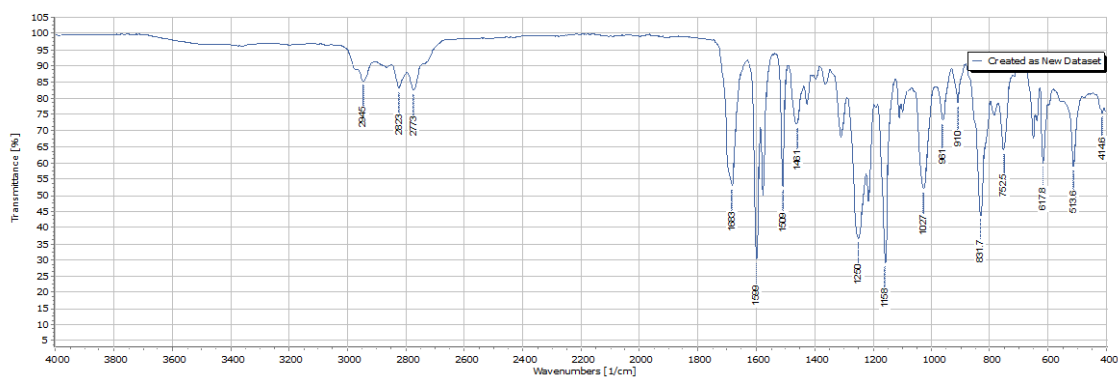


Figure A 1.1 B1a

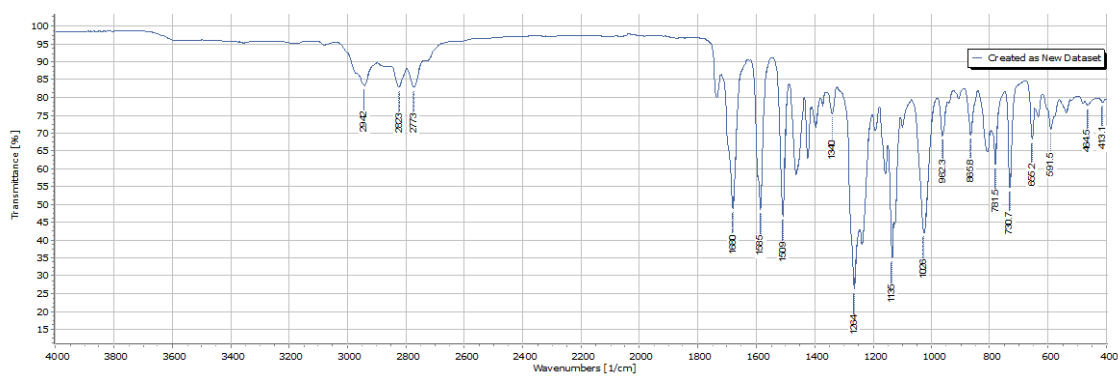


Figure A 2.2 B1b

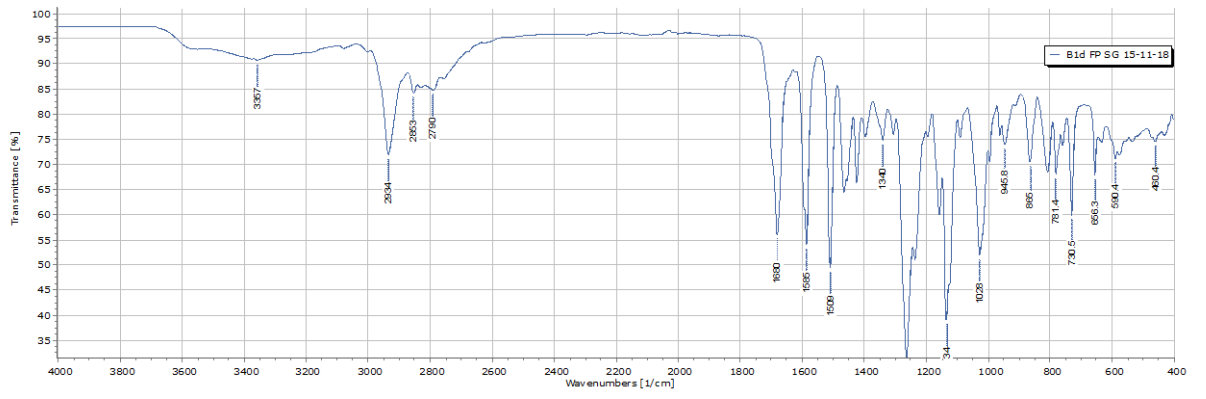


Figure A 3.3 B1d

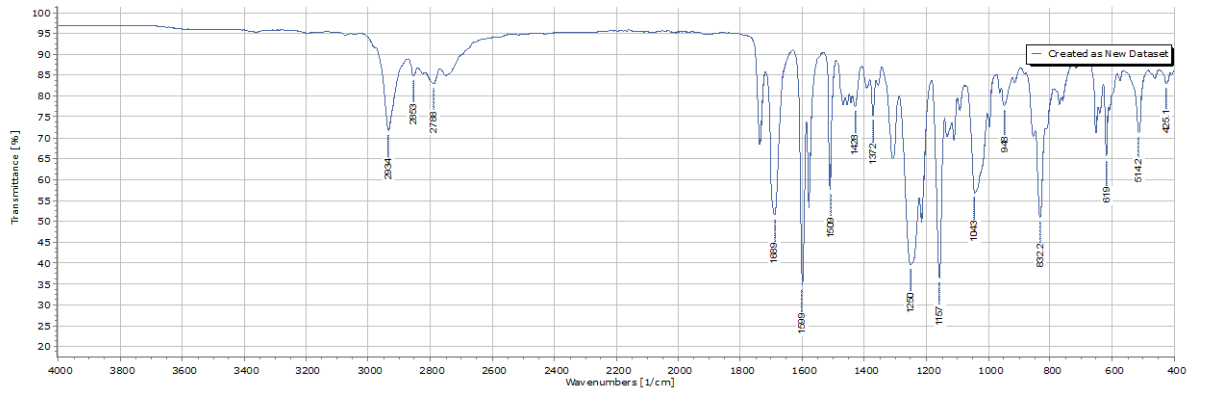


Figure A 4.4 B1e

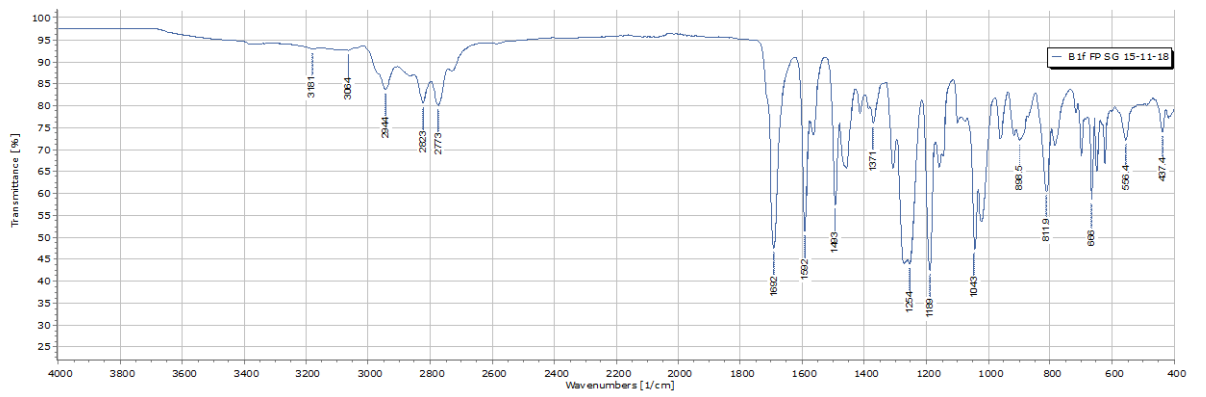


Figure A 5.5 B1f

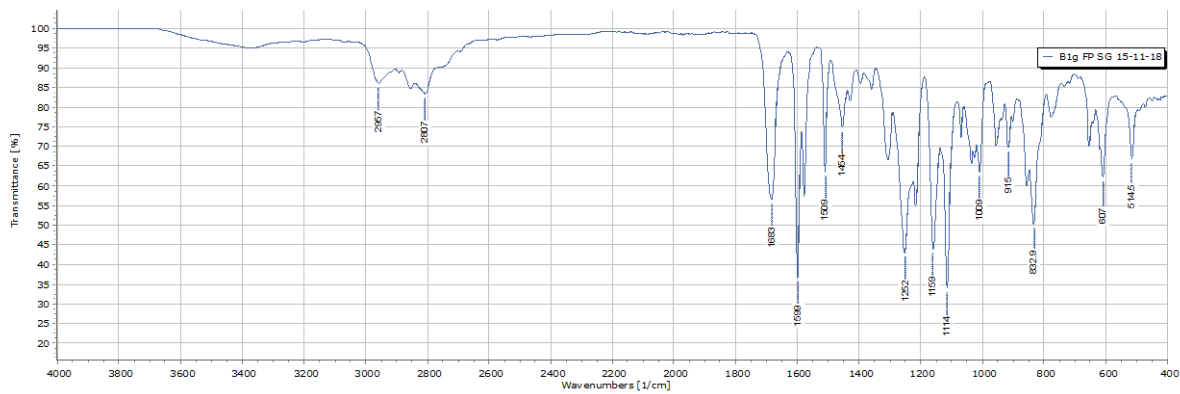


Figure A 6.6 B1g

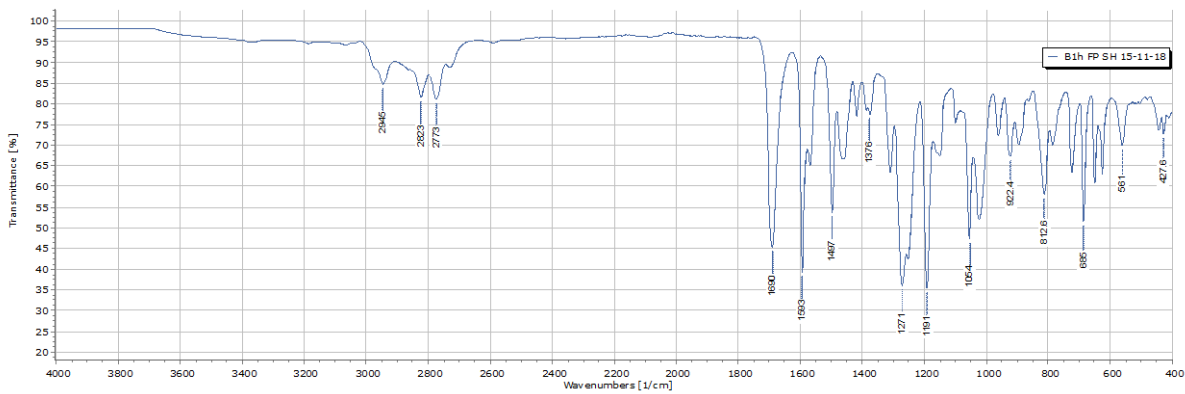


Figure A 7.7 B1h

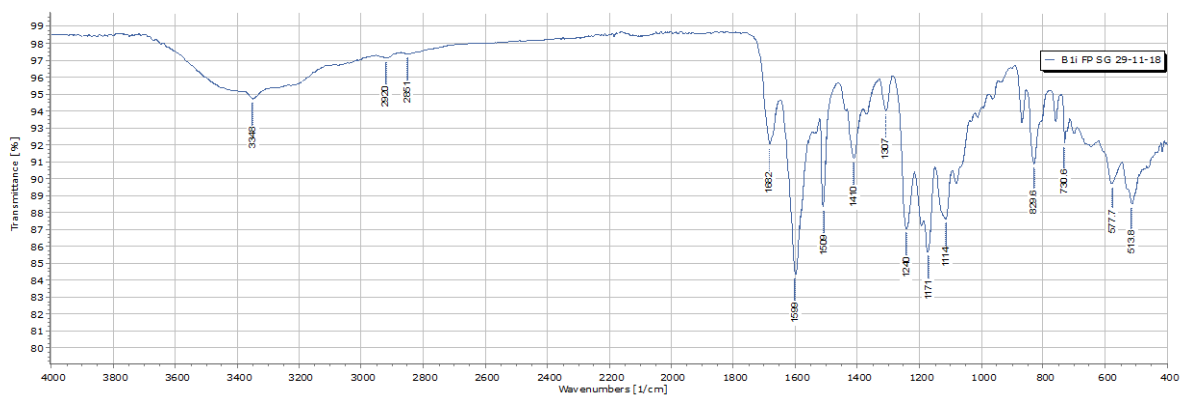


Figure A 8.8 B1i

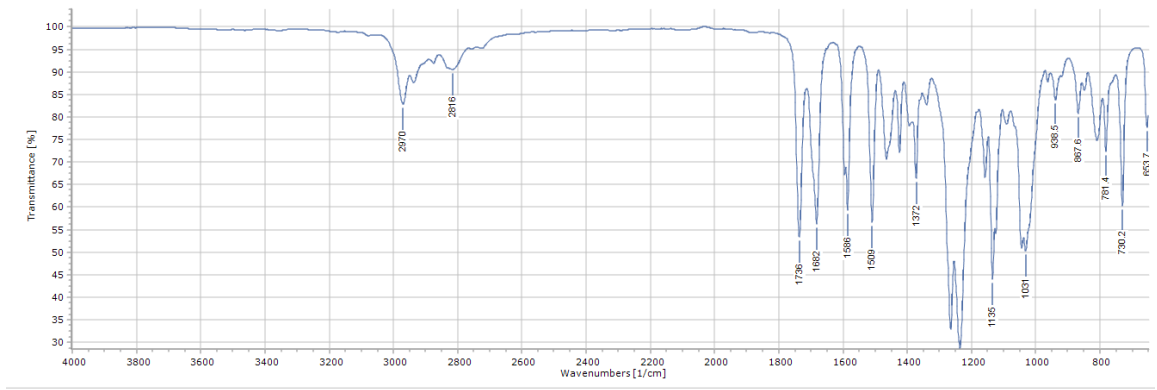


Figure A 9.9 B1k

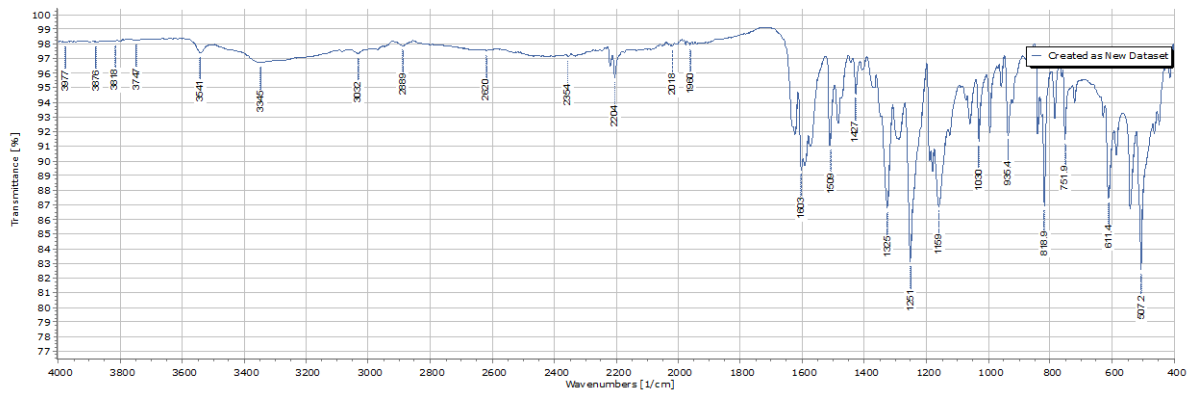


Figure A 10.10 B2a

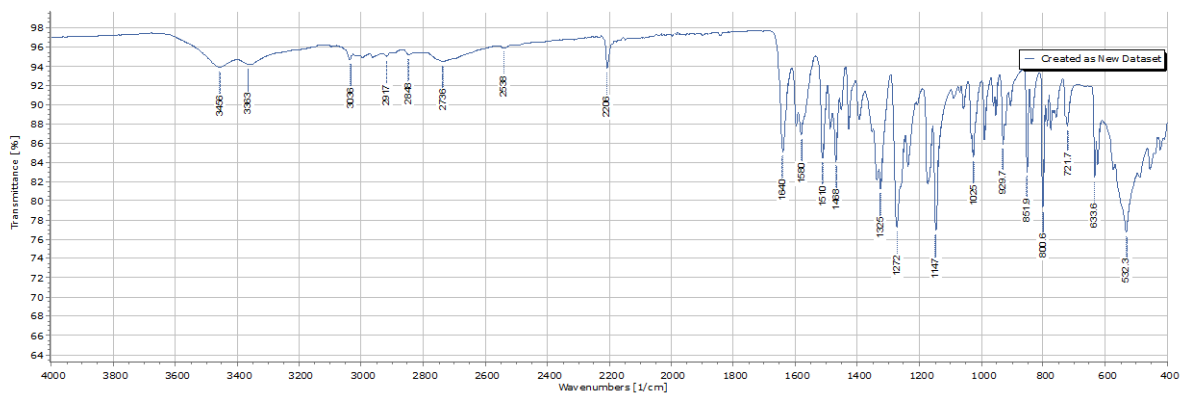


Figure A 11.11 B2b

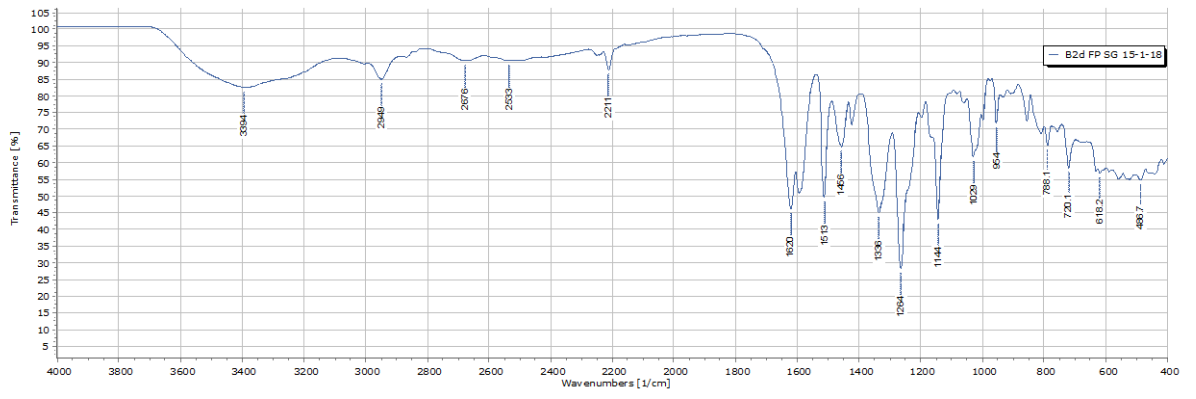


Figure A 12.12 B2d

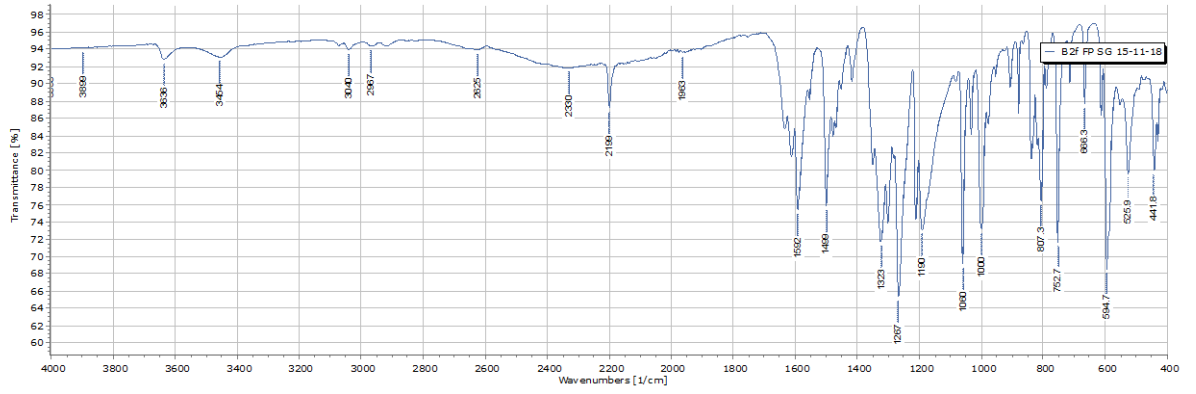


Figure A 13.13 B2f

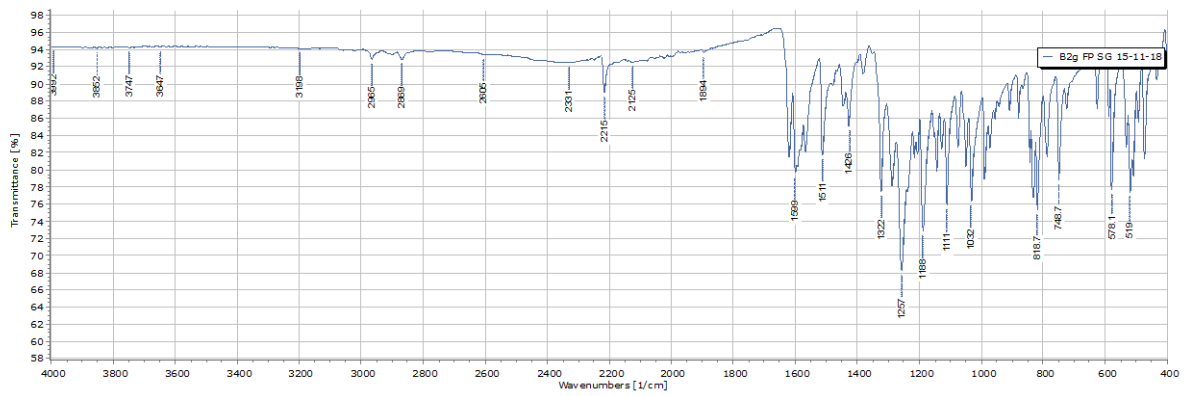


Figure A 14.14 B2g

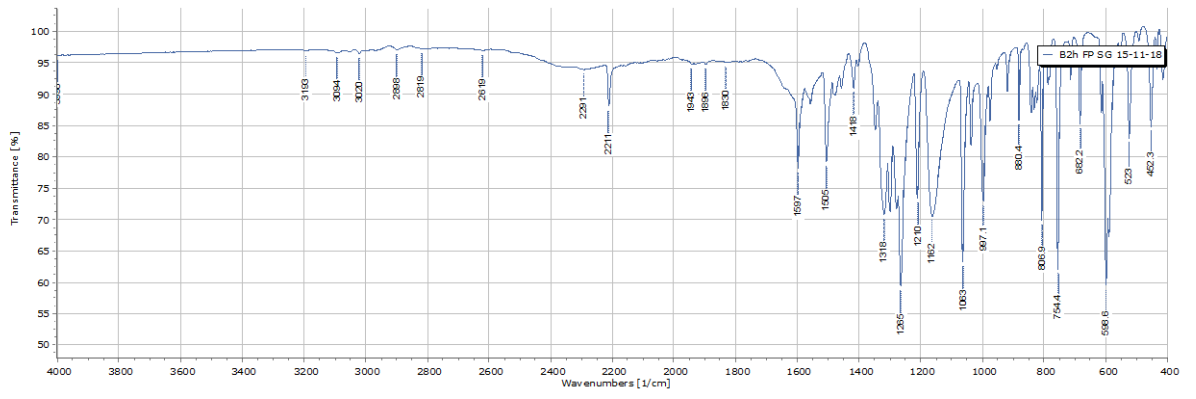


Figure A 15.15 B2h

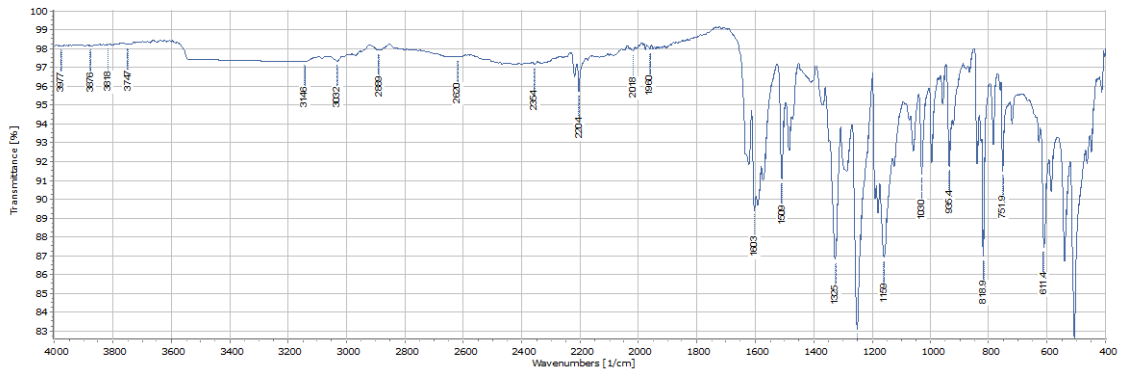


Figure A 16.16 B2j

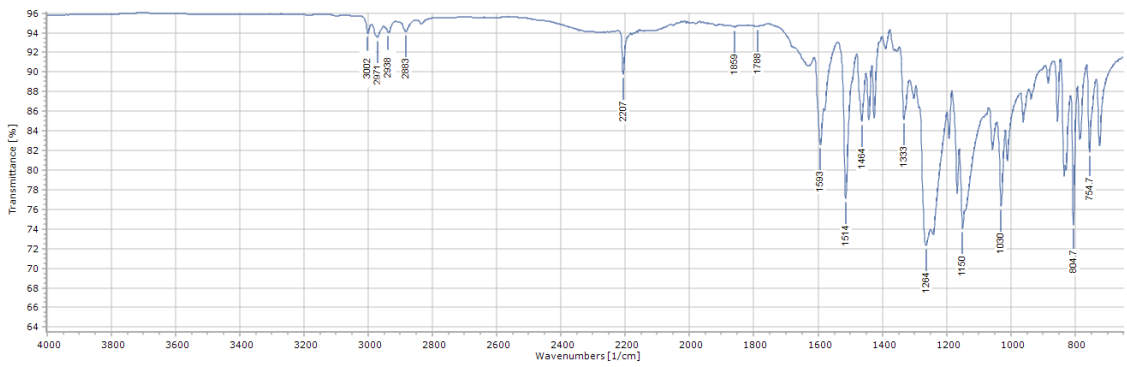


Figure A 17.17 B2k

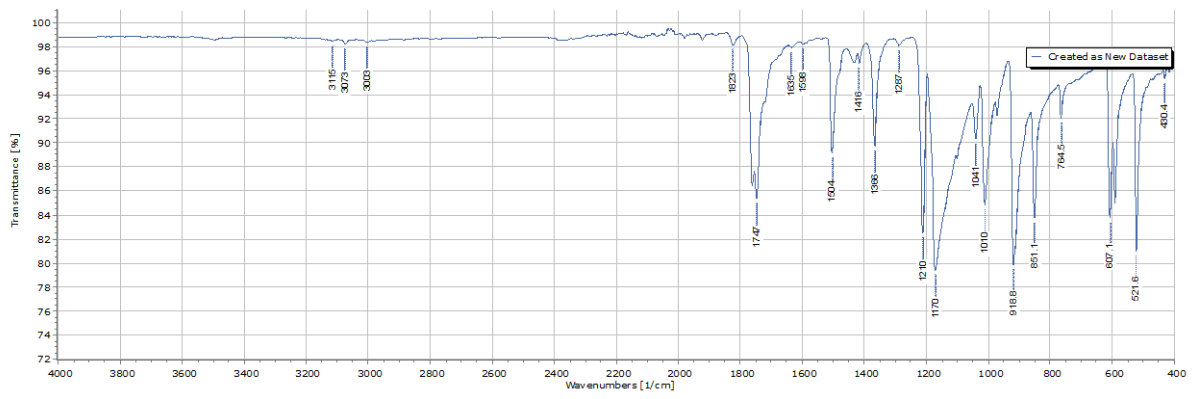


Figure A 18.18 A1b

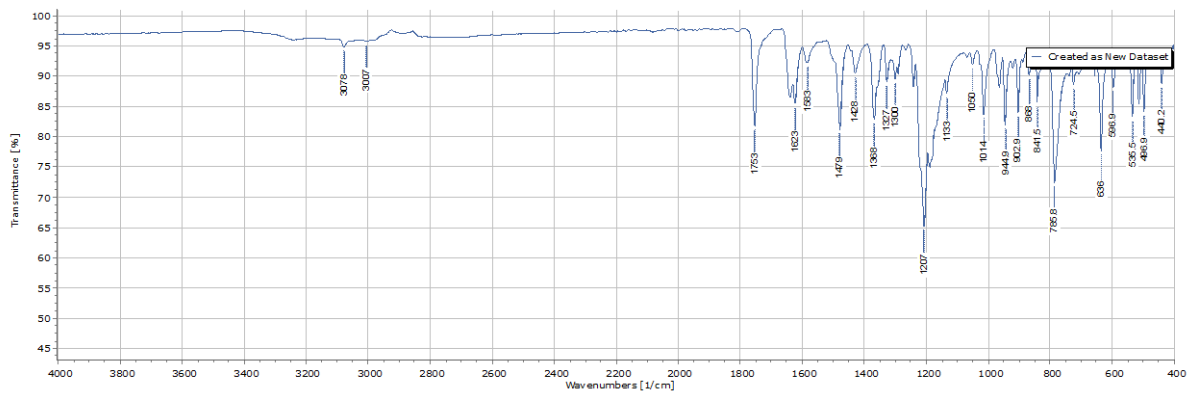


Figure A 19.19 A2b

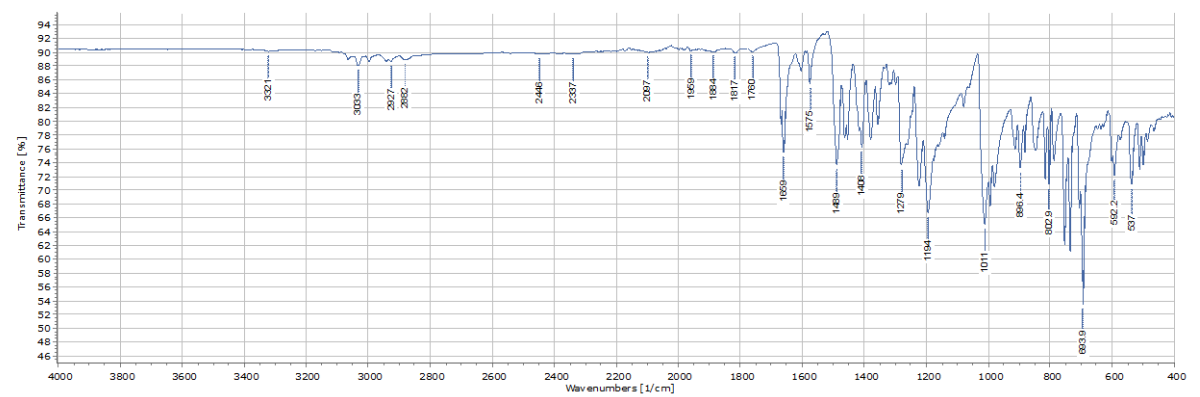


Figure A 20.20 A3

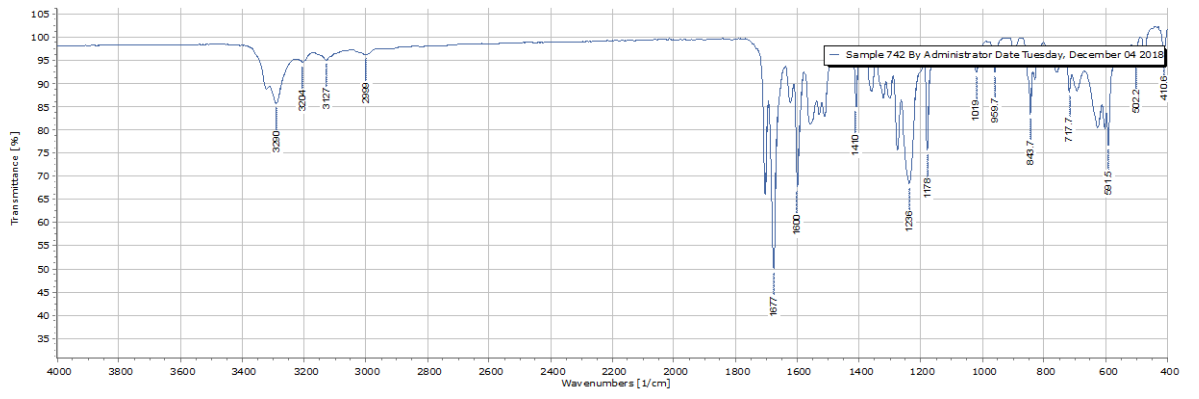


Figure A 21.21 C1

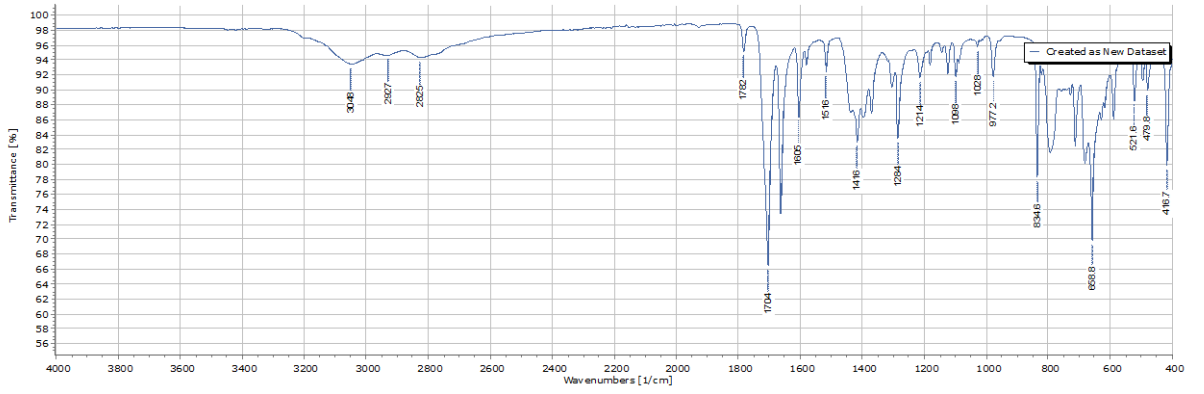


Figure A 22.22 C2

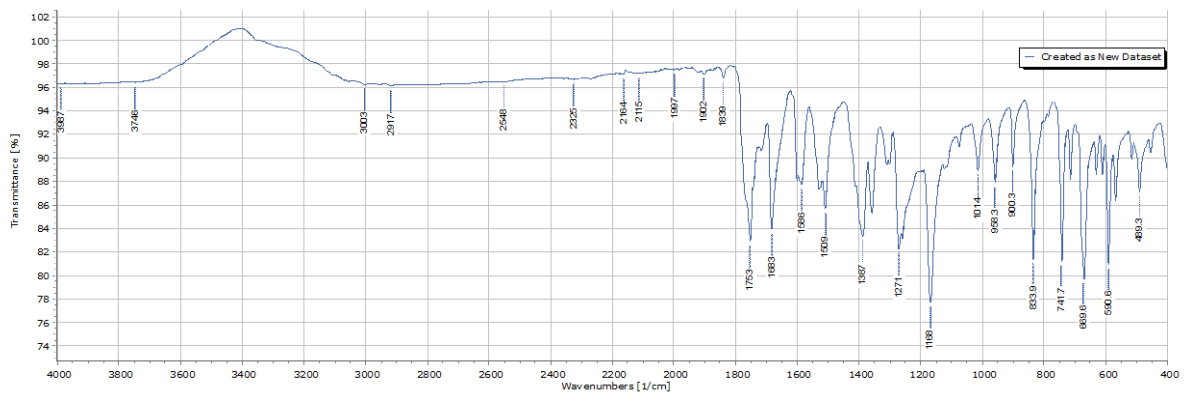


Figure A 23.23 C3

A.2 NMR Spectra

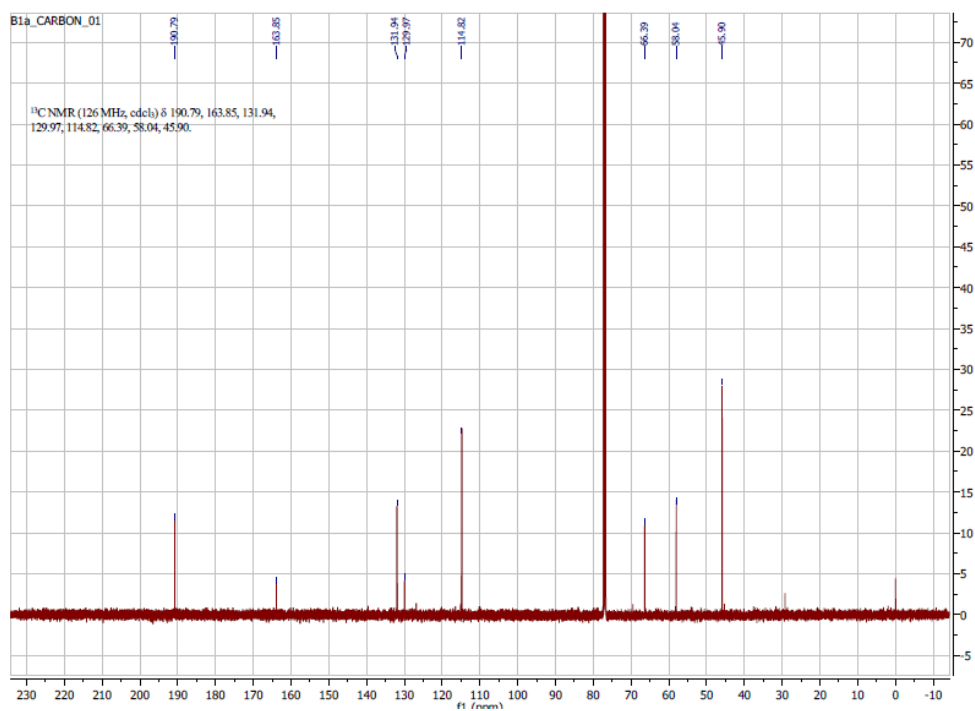


Figure A 2.1 B1a ^{13}C NMR

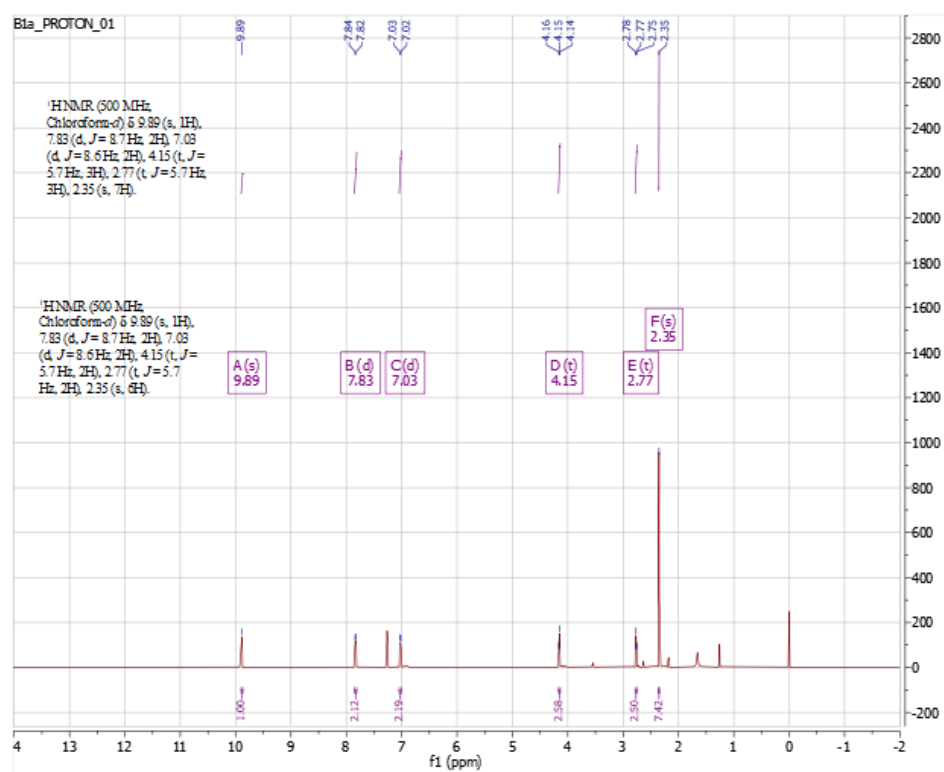


Figure A 2.2 B1a ^1H NMR

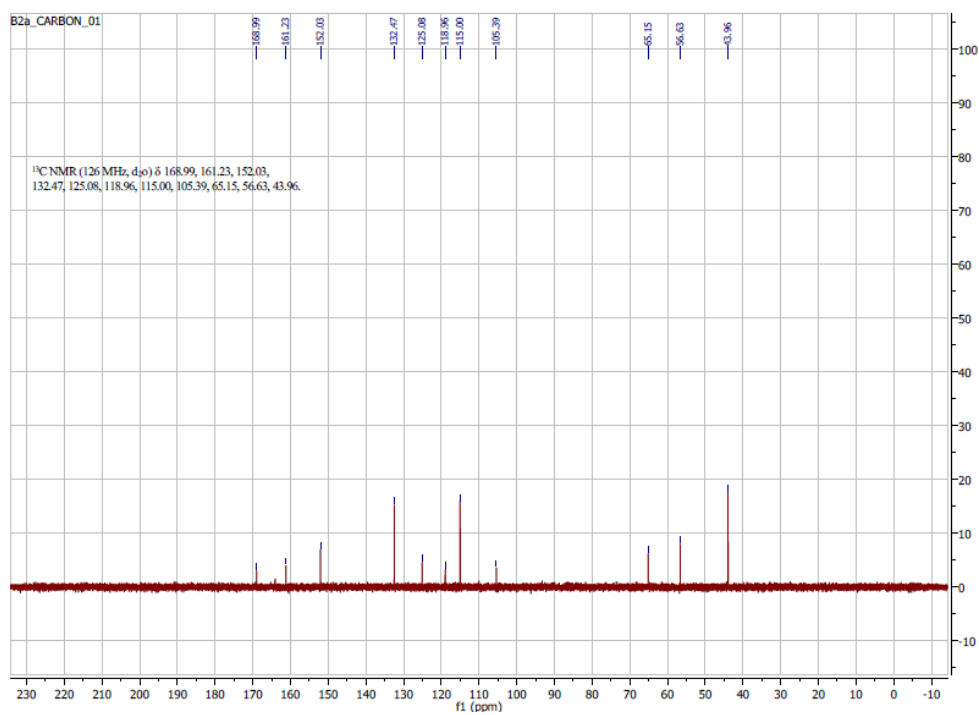


Figure A 2.3 B2a ^{13}C NMR

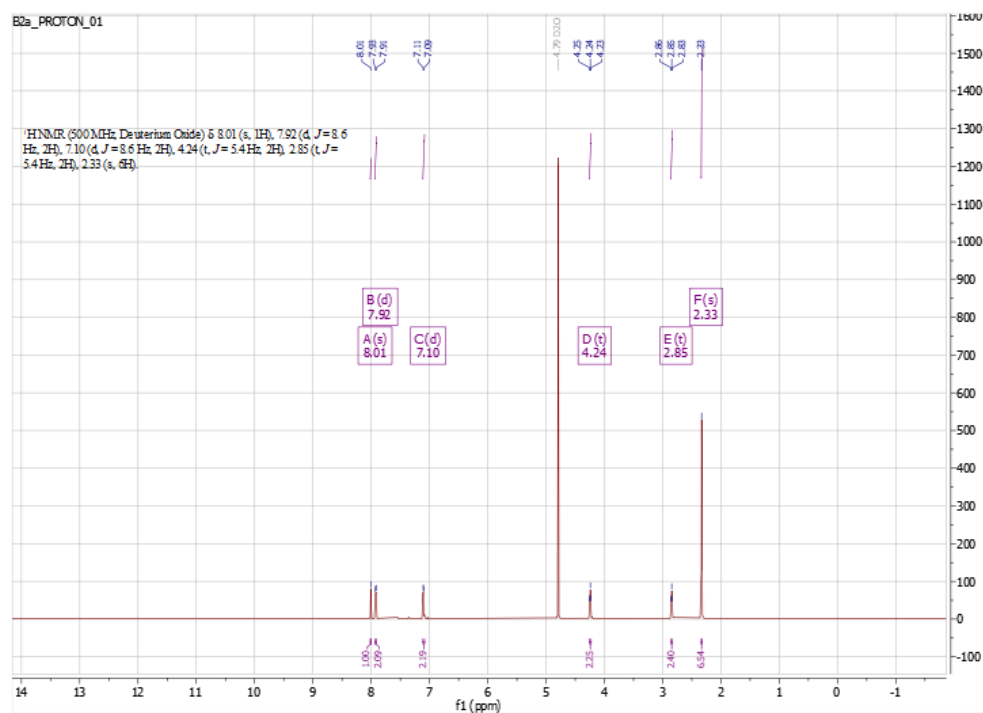


Figure A 2.4 B2a ^1H NMR

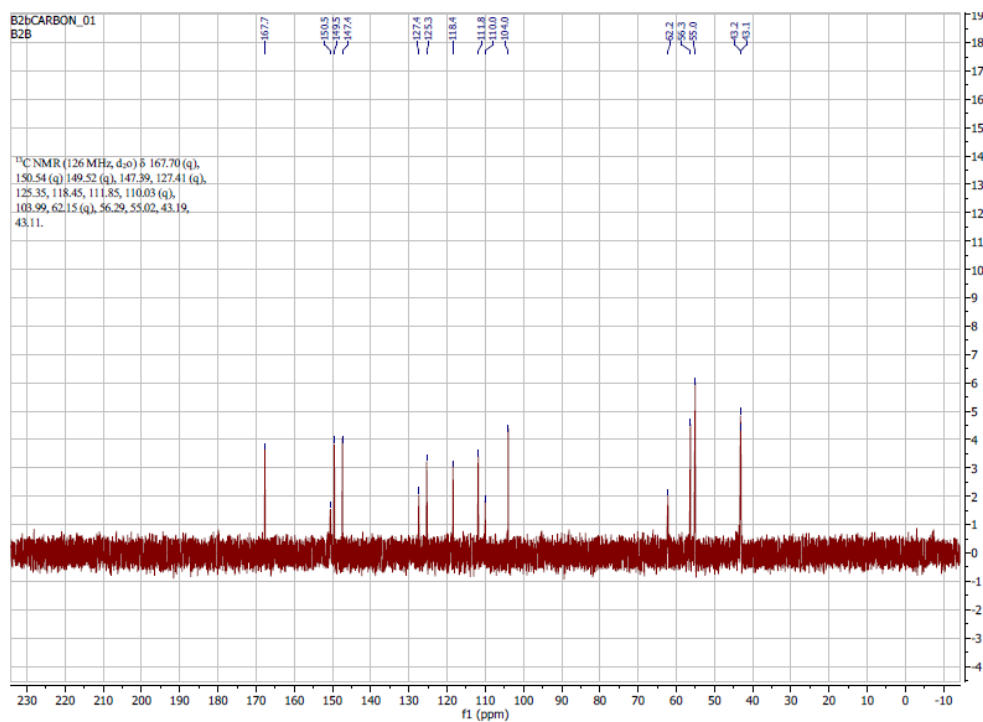


Figure A 2.5 B2b ^{13}C NMR

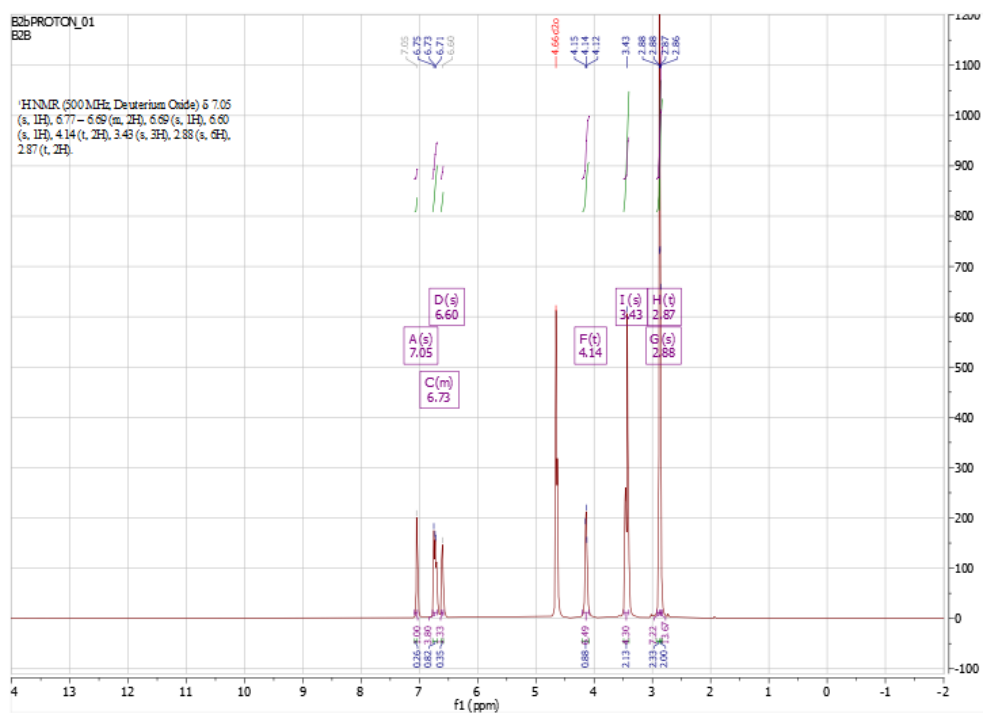


Figure A 2.6 B2b ^1H NMR

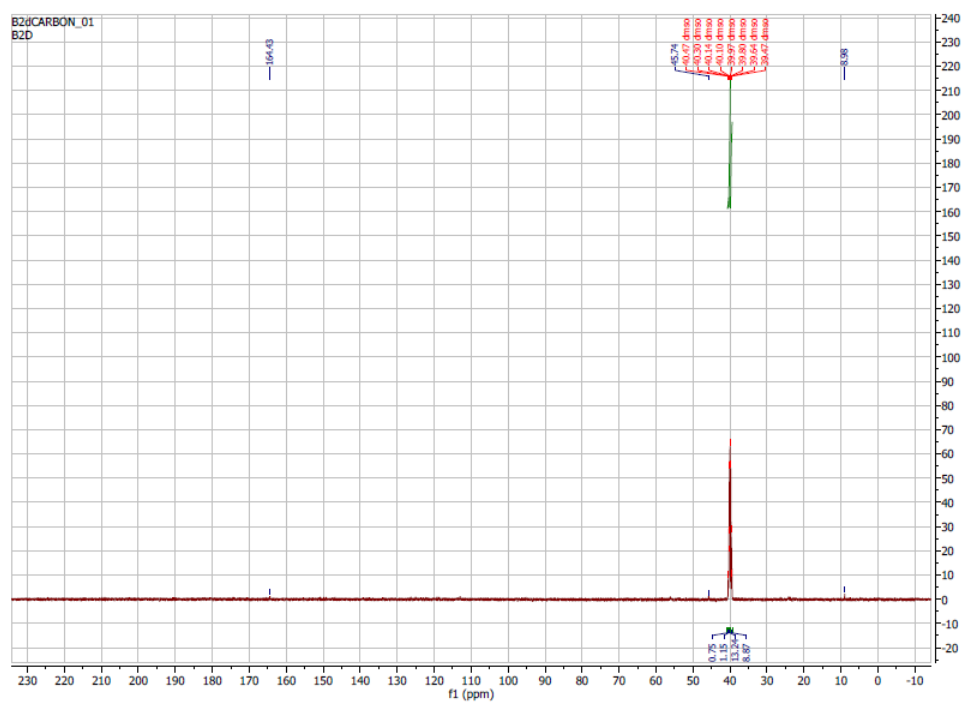


Figure A 2.7 B2d ^{13}C NMR

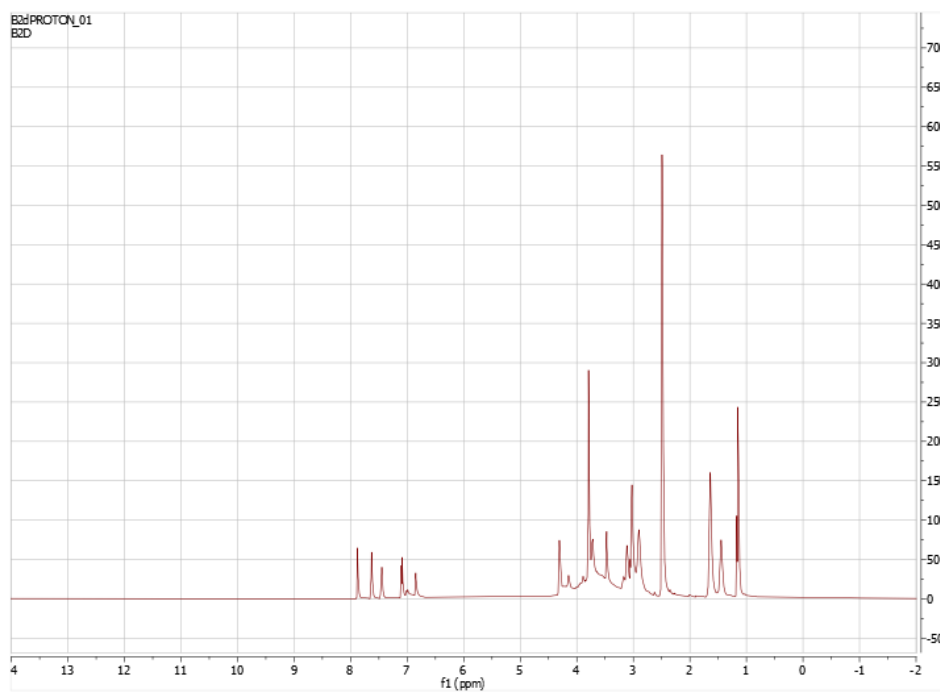


Figure A 2.8 B2d ^1H NMR

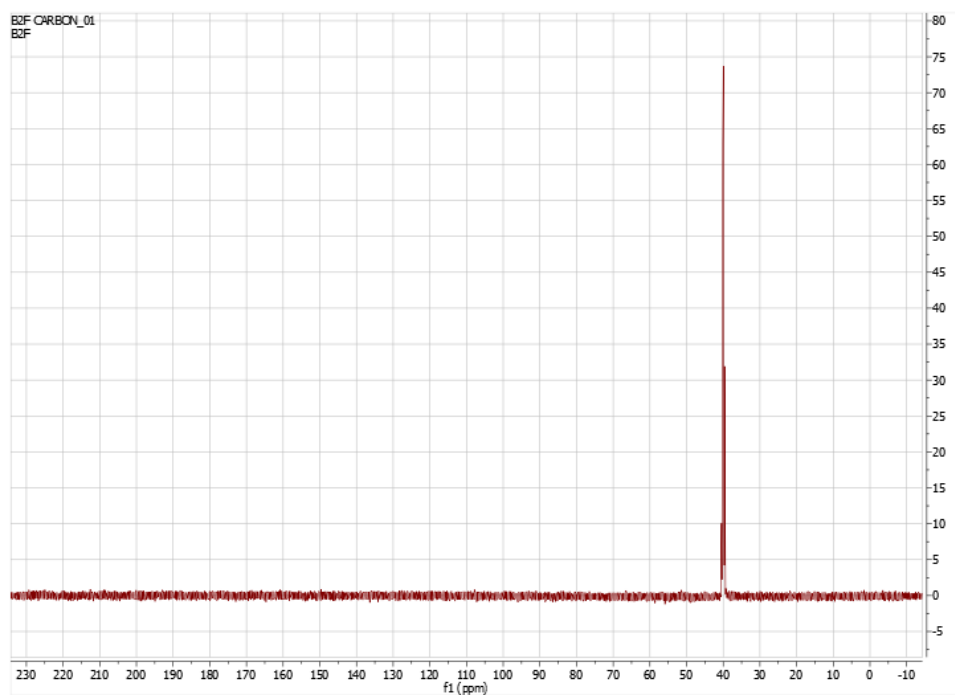


Figure A 2.9 B2f ^{13}C NMR

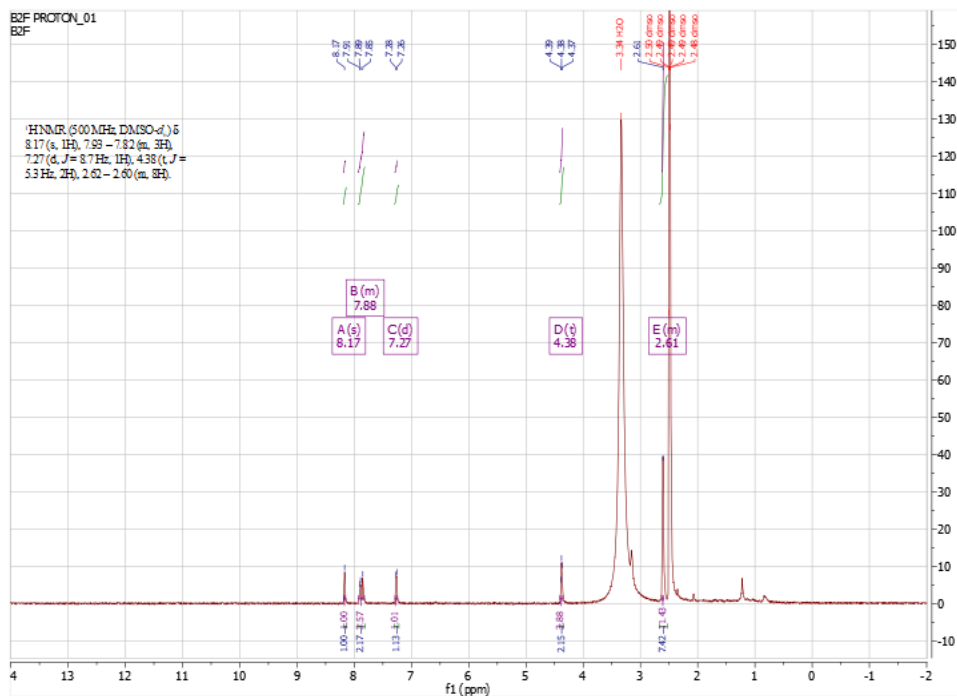


Figure A 2.10 B2f ^1H NMR

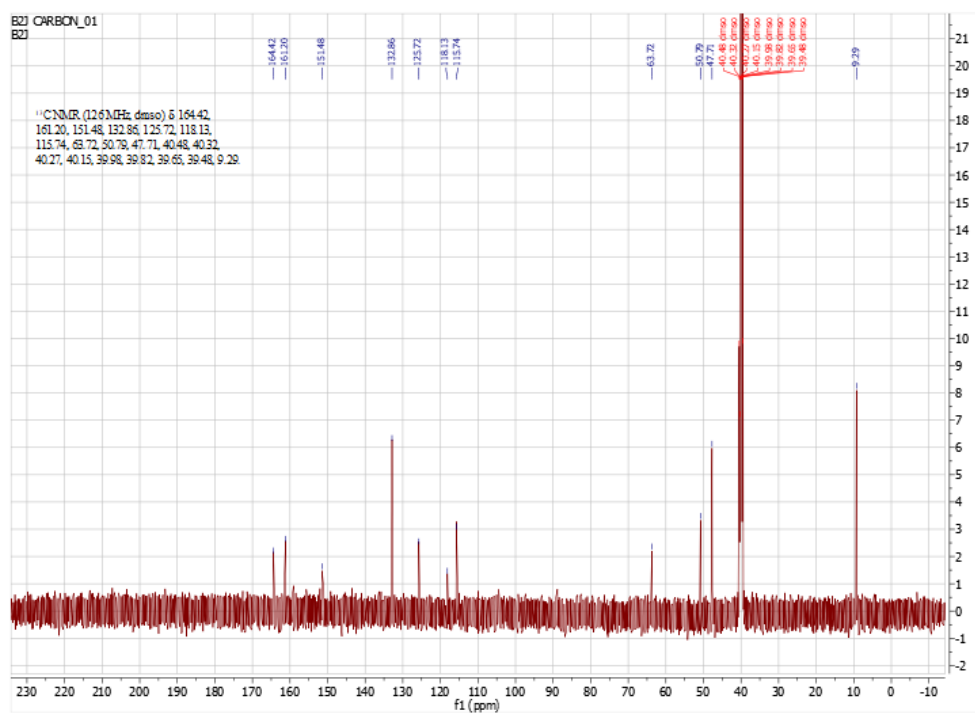


Figure A 2.15 B2j ¹³C NMR

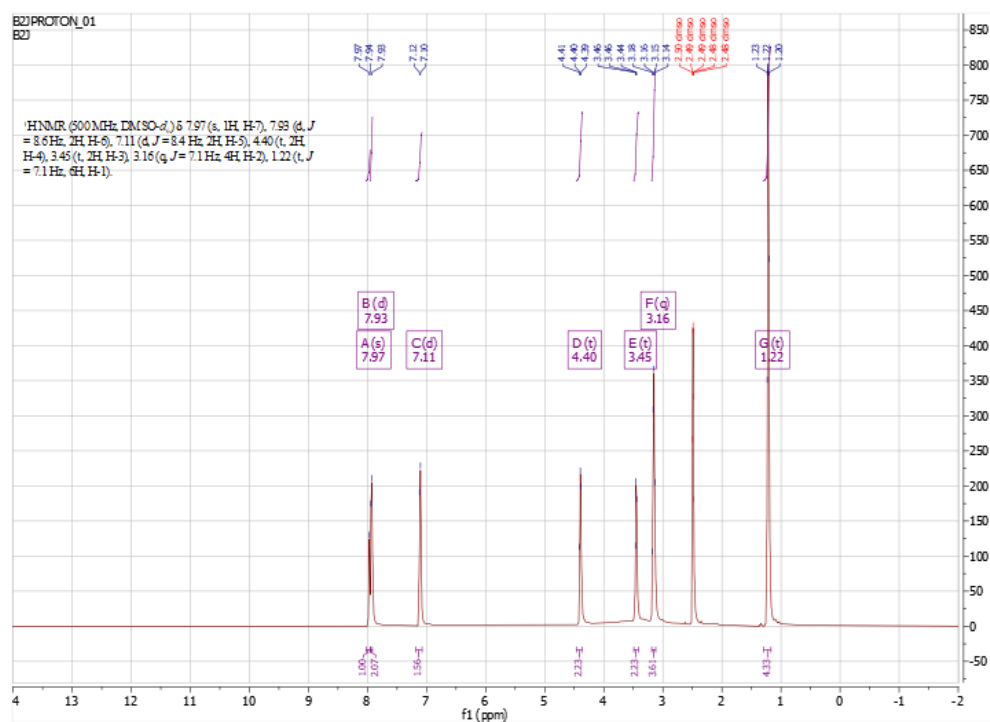


Figure A 2.16 B2j ¹H NMR

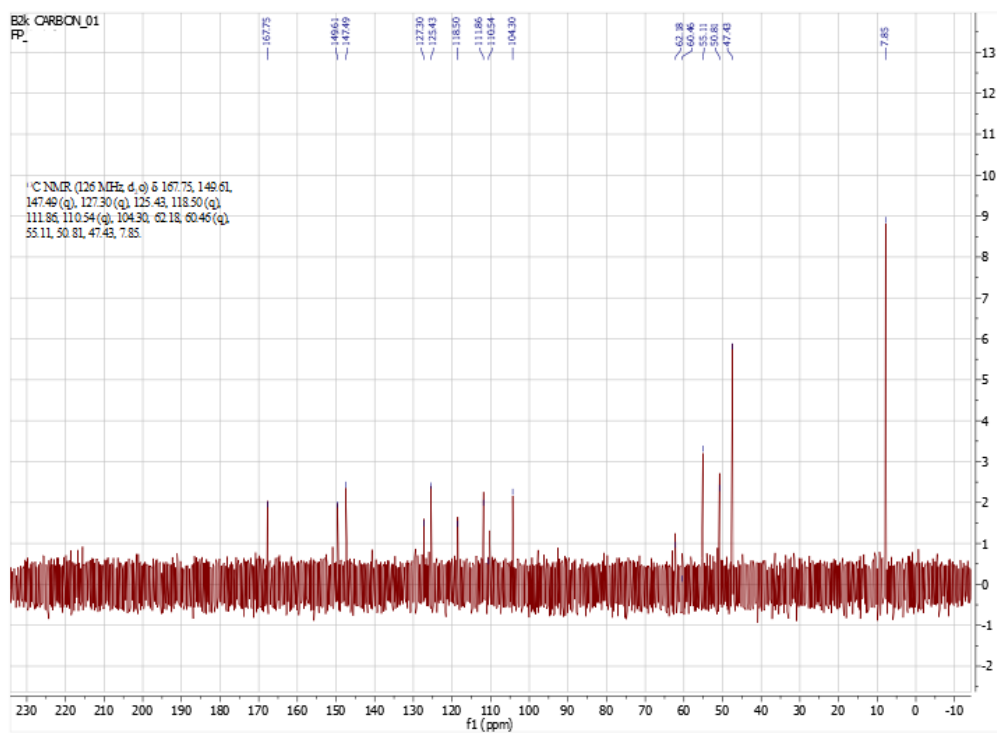


Figure A 2.17 B2k ^{13}C NMR

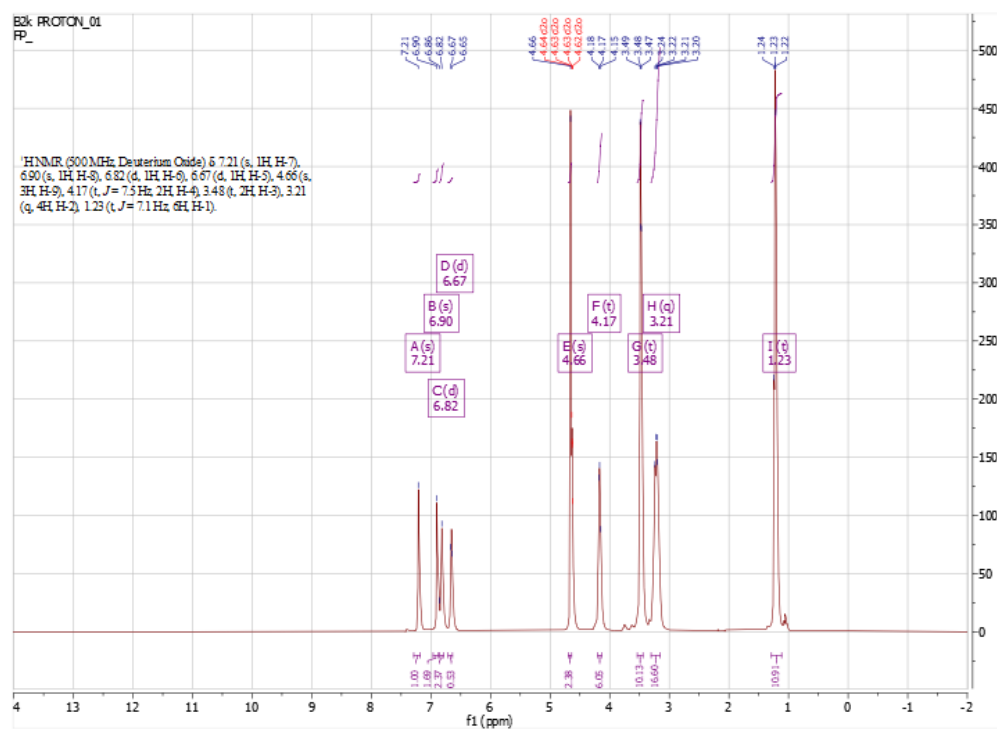


Figure A 2.18 B2k ^1H NMR

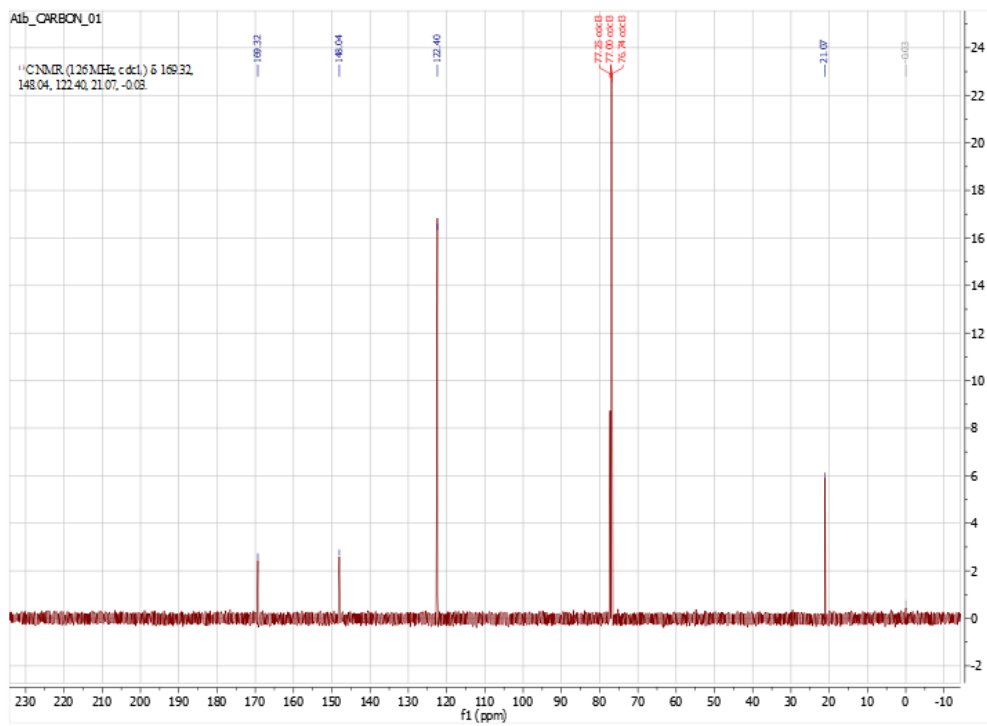


Figure A 2.19 A1b ^{13}C NMR

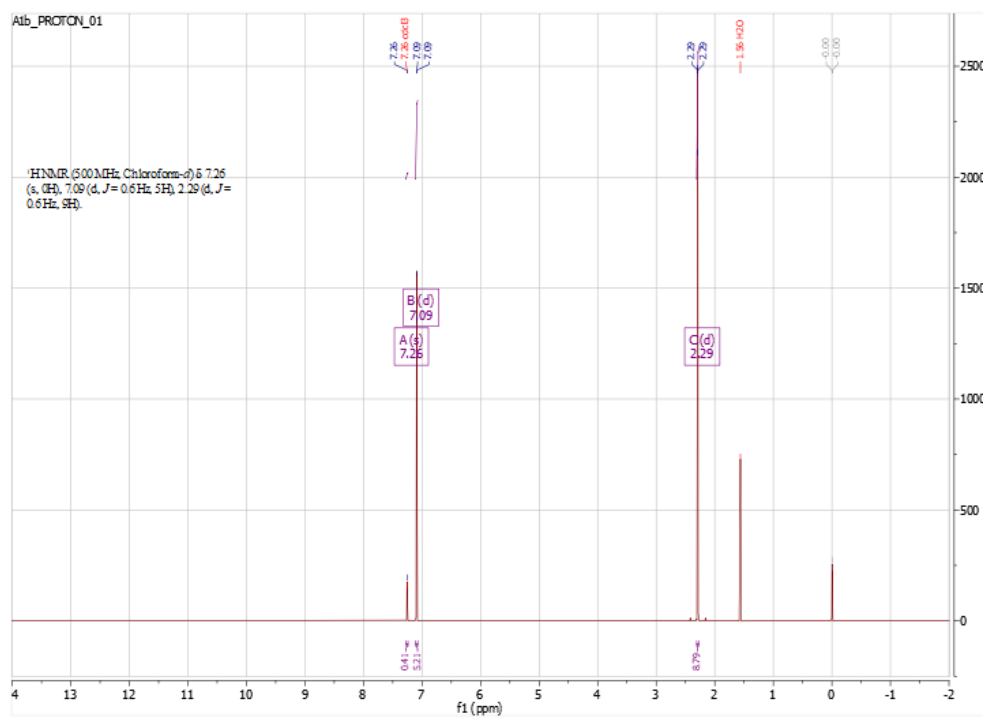


Figure A 2.20 A1b ^1H NMR

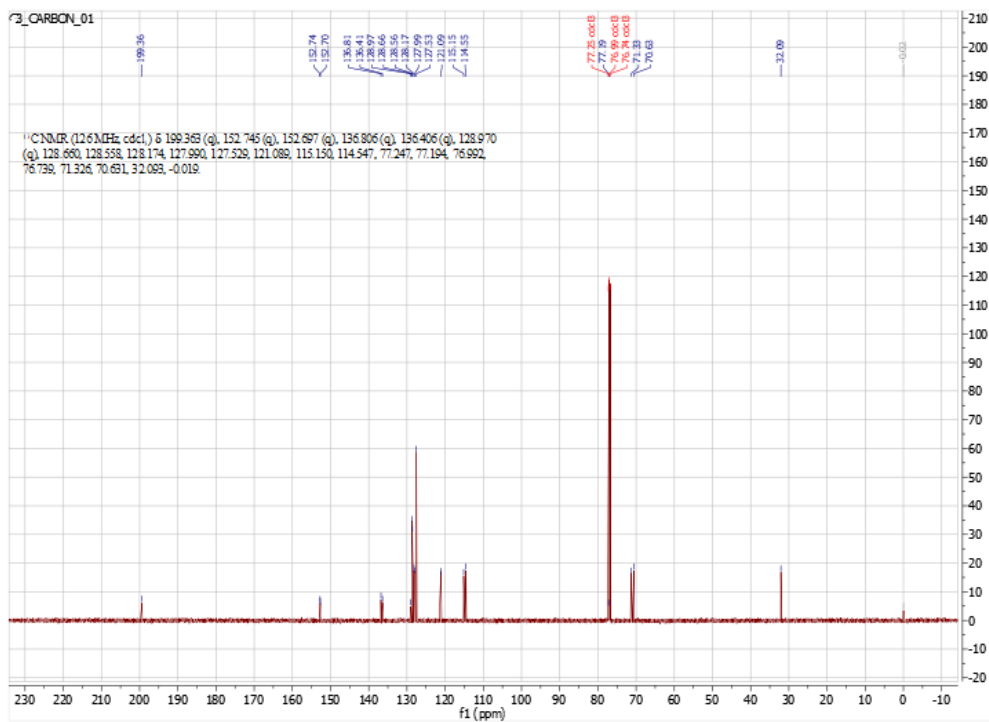


Figure A 2.21 A3 ¹³C NMR

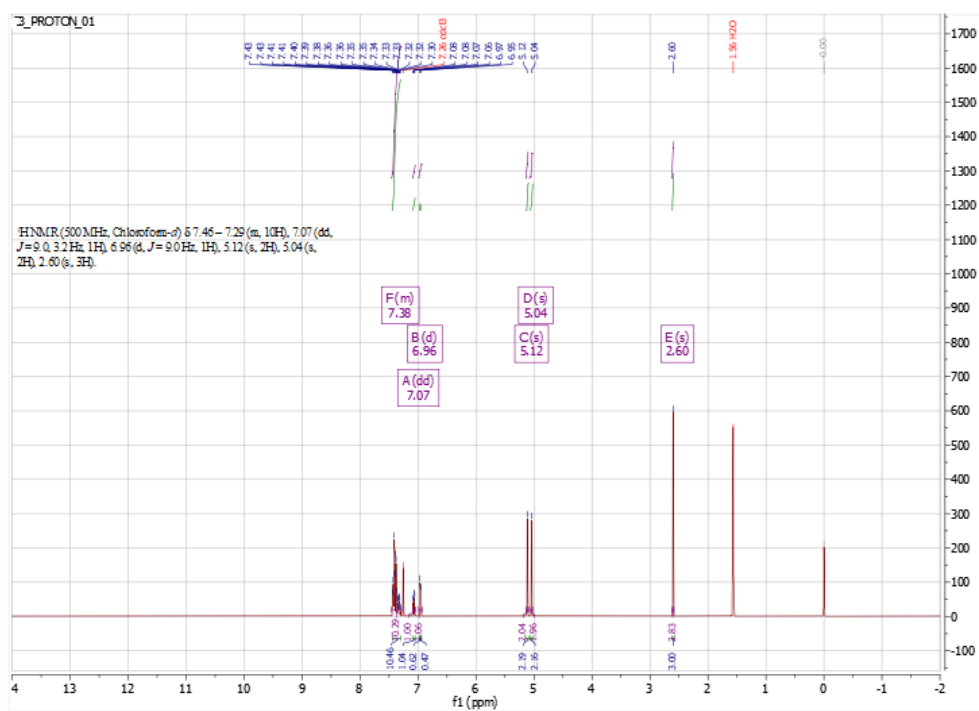


Figure A 2.22 A3 ¹H NMR

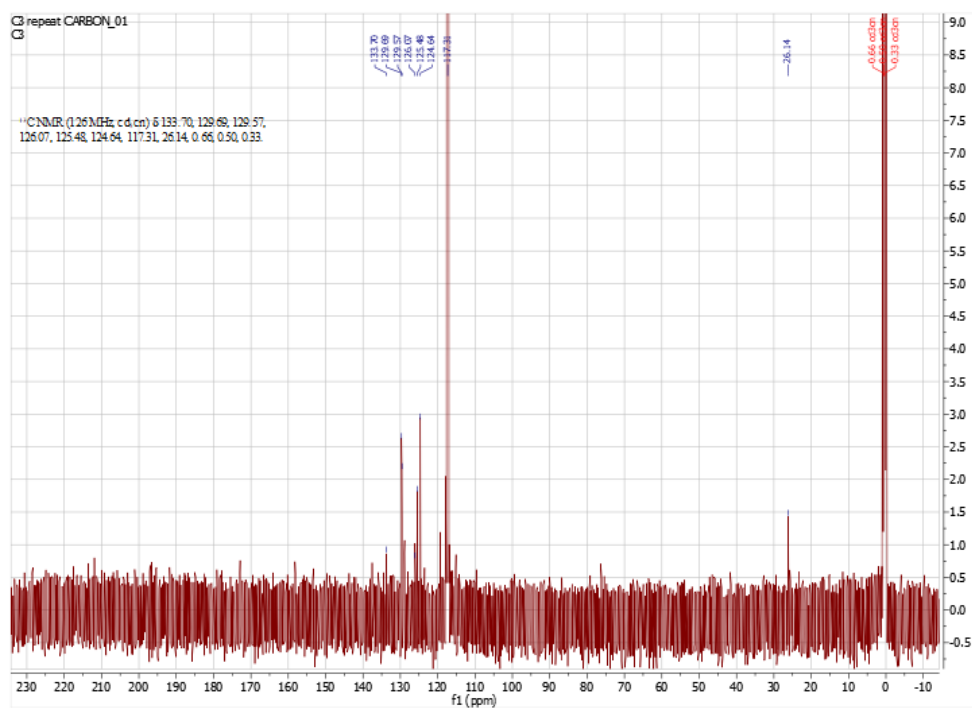


Figure A 2.23 C3 ^{13}C NMR

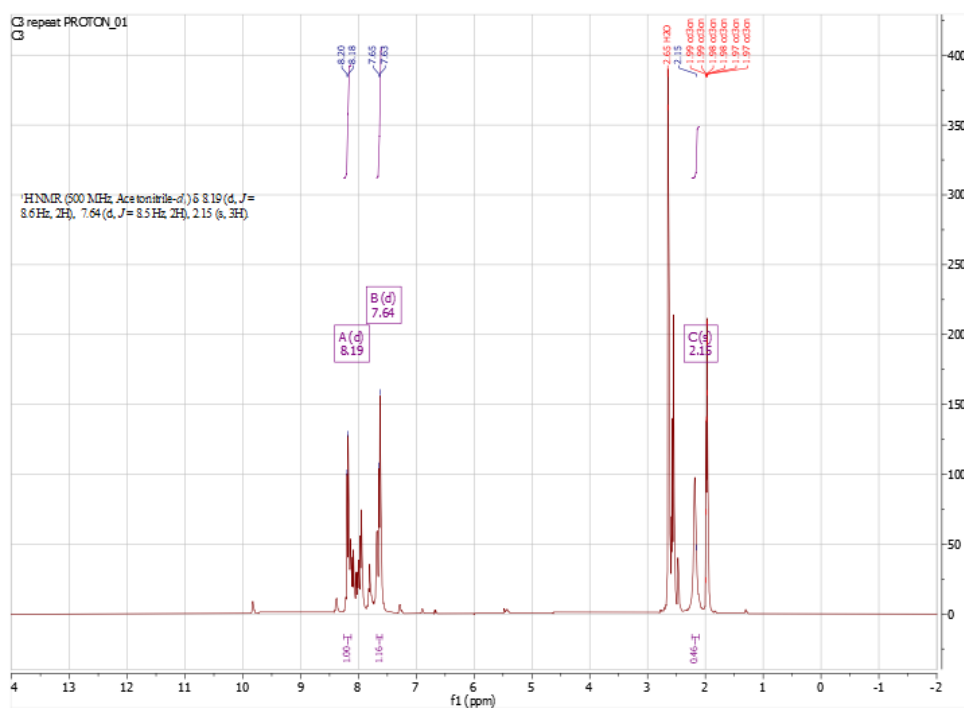


Figure A 2.24 C3 ^1H NMR

A.3 MALDI spectra

B2d

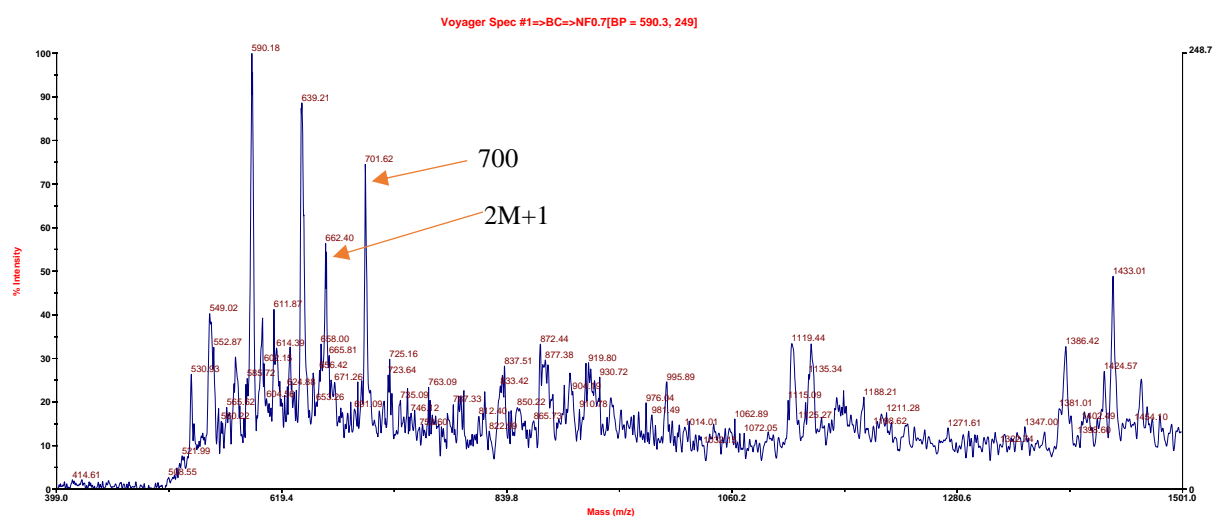


Figure A.3.1 Reaction 1 B2d_Cort

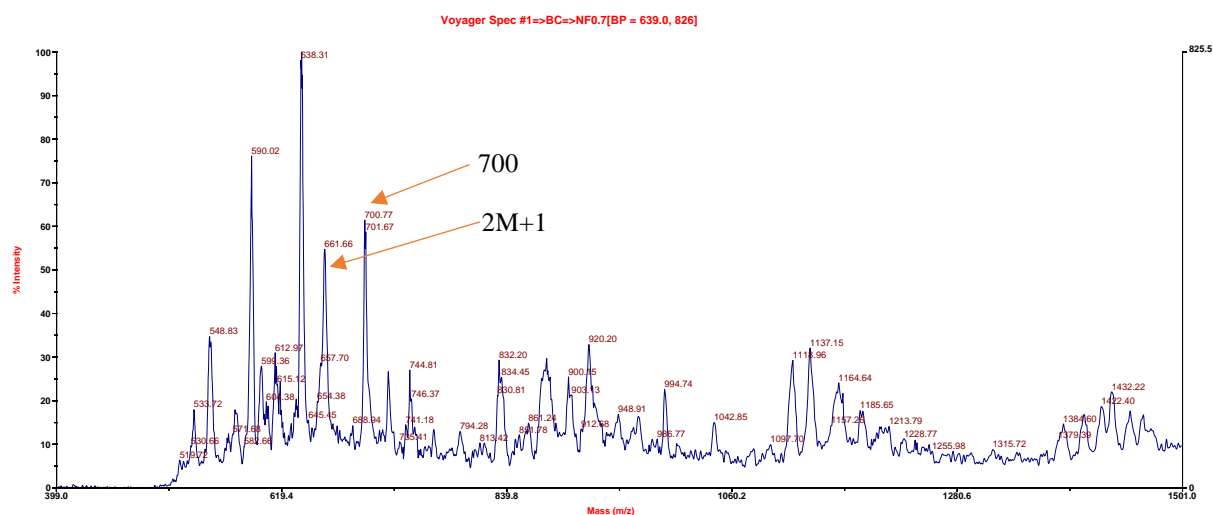


Figure A.3.2 Reaction 1 B2d_Decanol

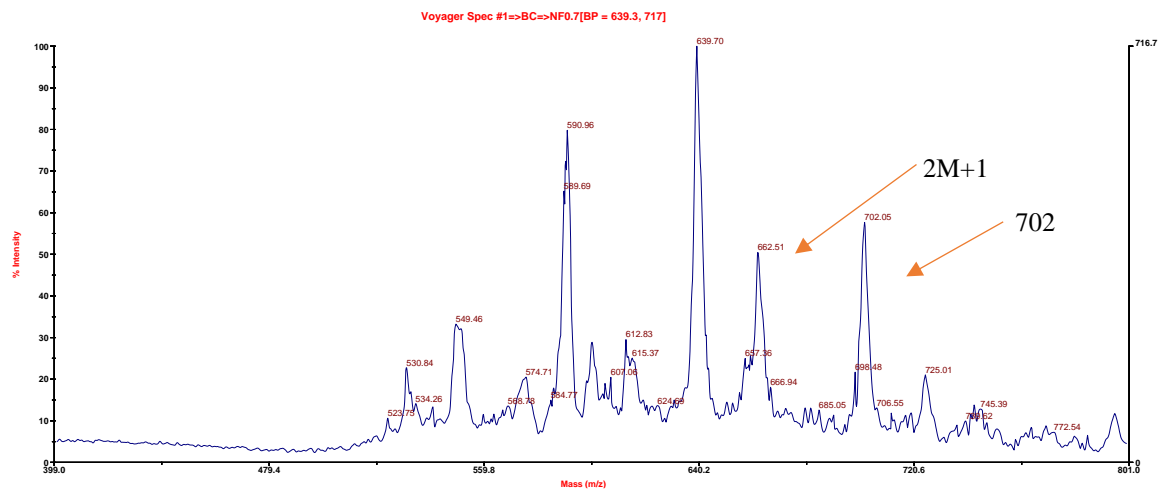


Figure A.3.3 Reaction 1 B2d_Terp

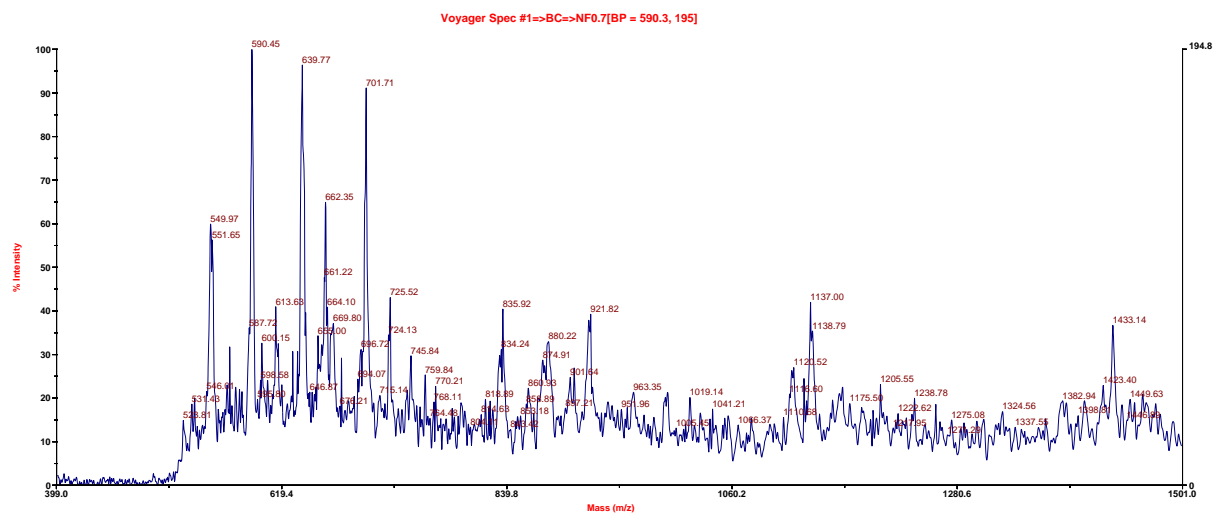


Figure A.3.7 Reaction 3 B2d_Cort

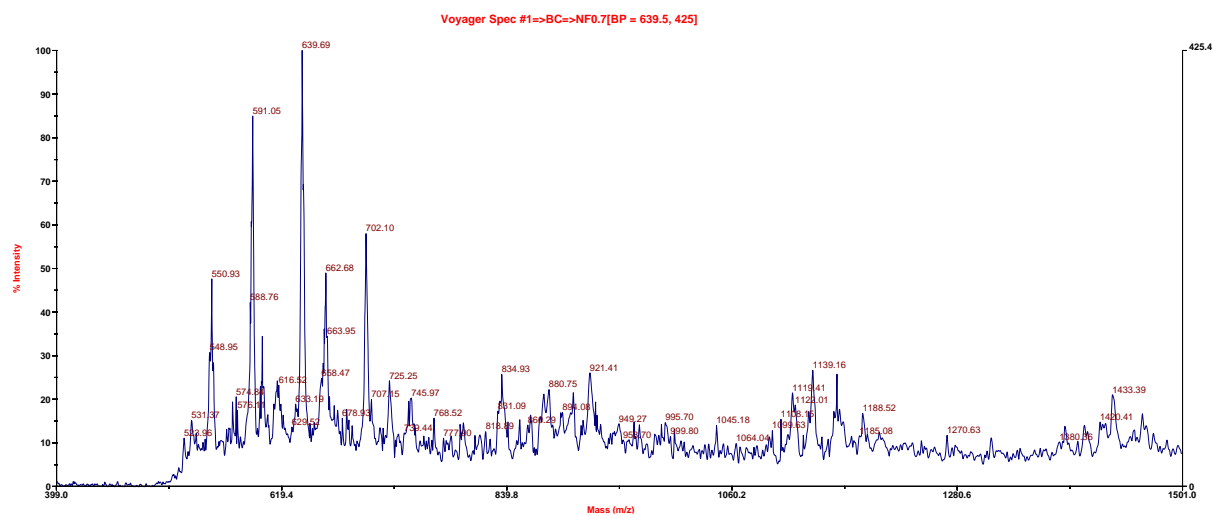


Figure A.3.8 Reaction 3 B2d_Decanol

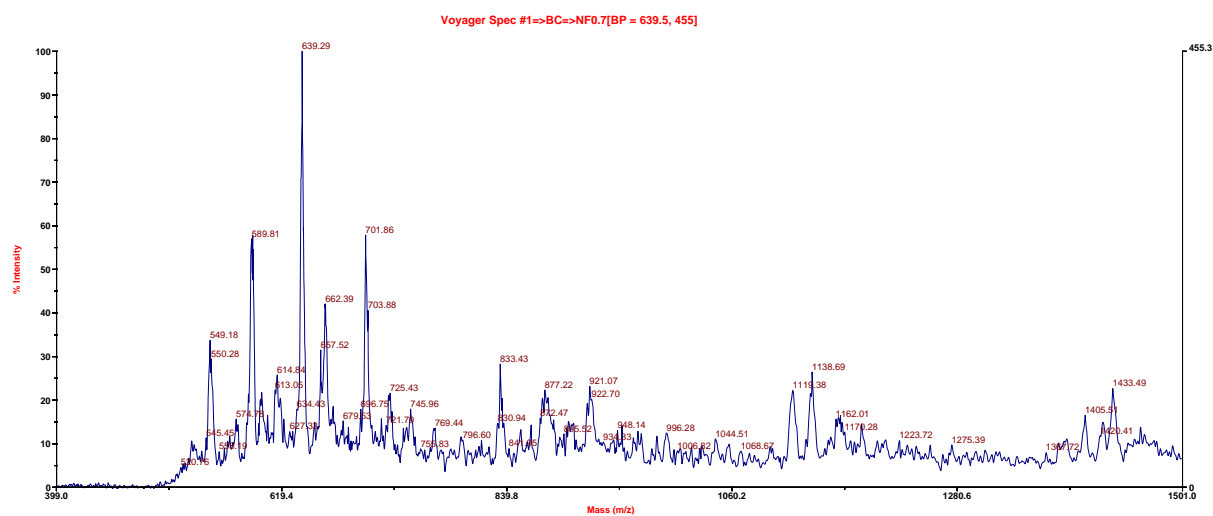


Figure A.3.9 Reaction 3 B2d_Terp

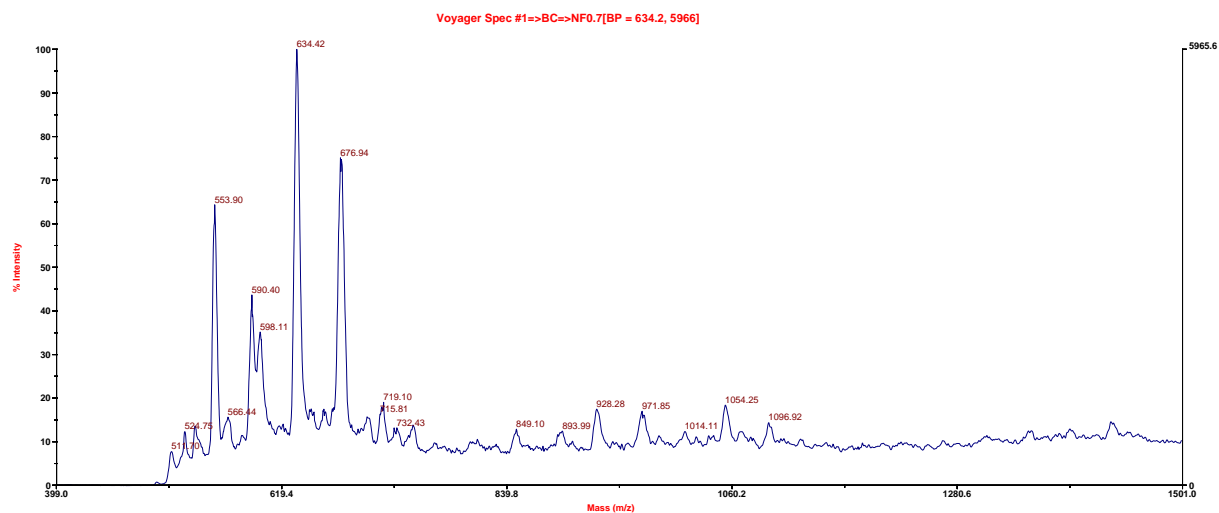


Figure A.3.10 Reaction 1 B2f_Cort

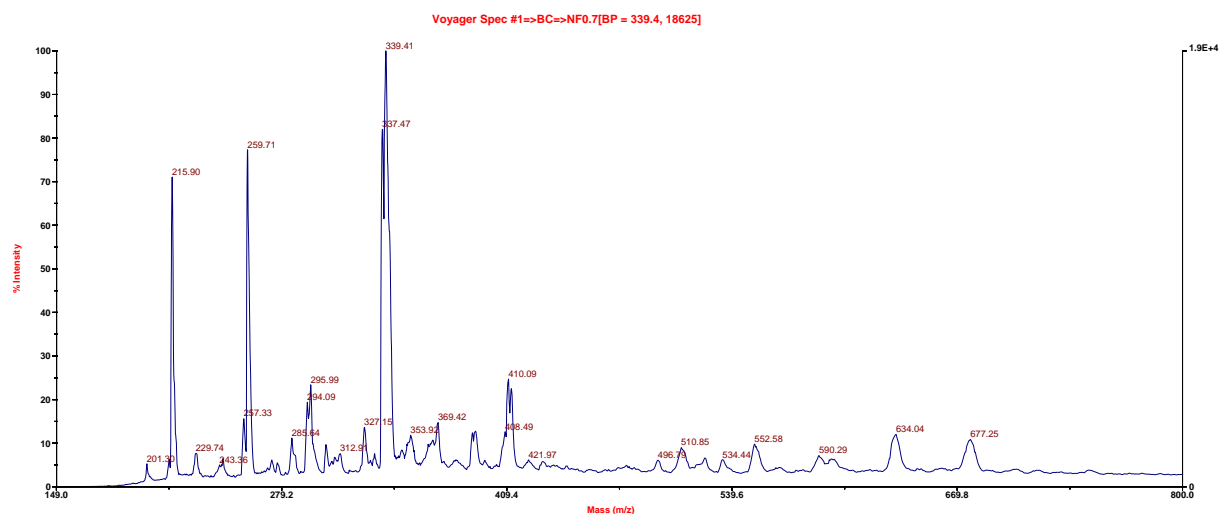


Figure A.3.11 Reaction 1 B2f_Decanol

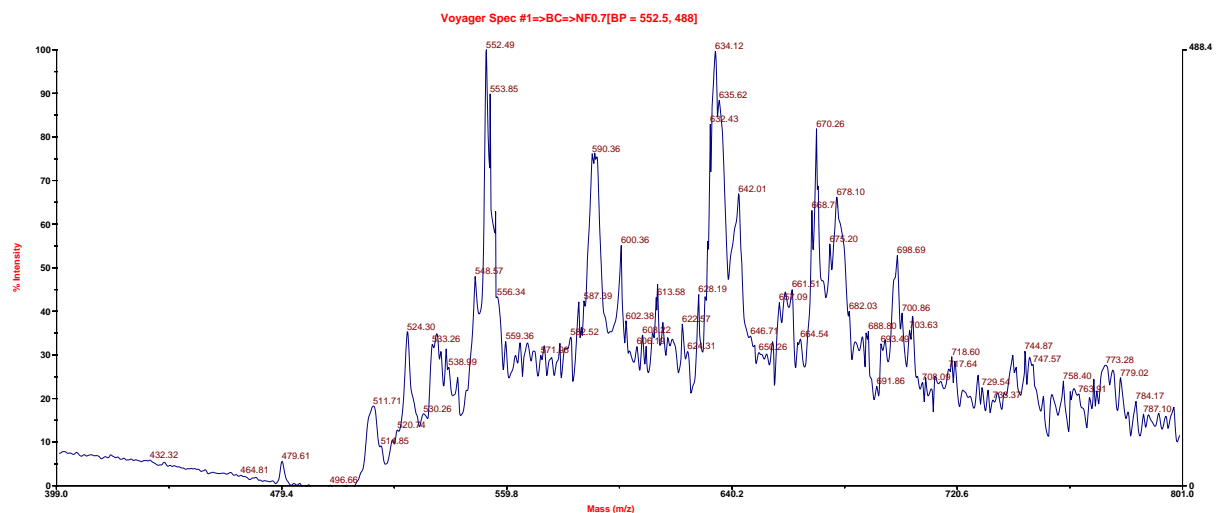


Figure A.3.12 Reaction 1 B2f_Terp

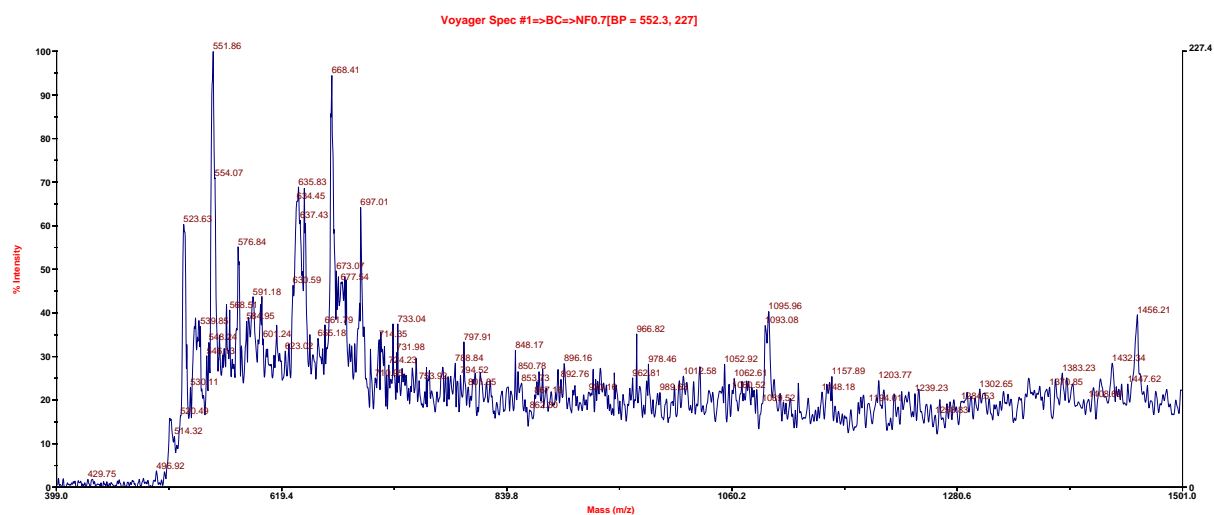


Figure A.3.13 Reaction 2 B2f_Cort

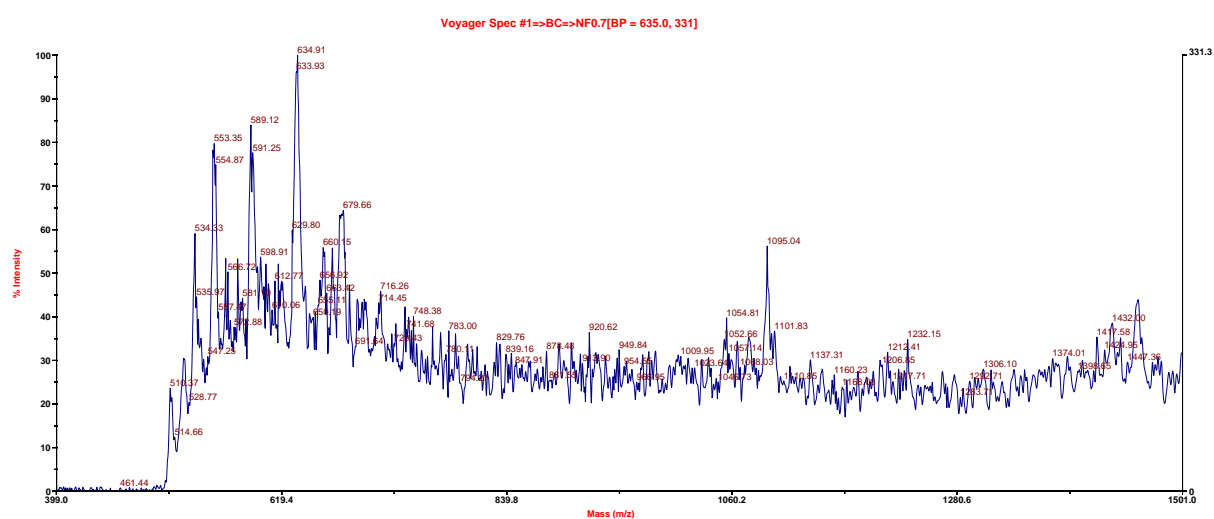


Figure A.3.14 Reaction 2 B2f_Decanol

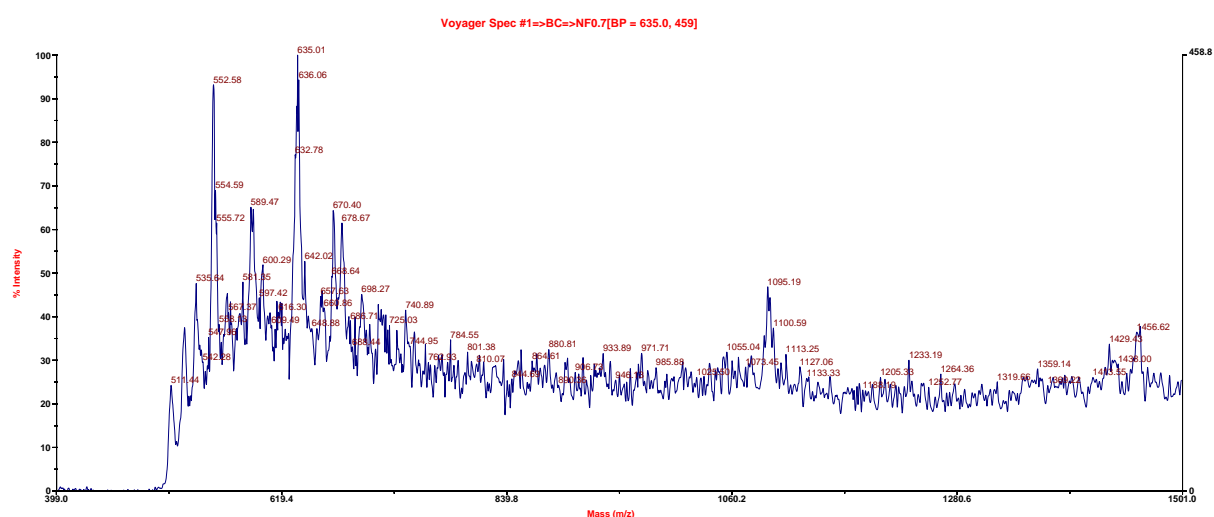


Figure A.3.15 Reaction 2 B2f_Terp

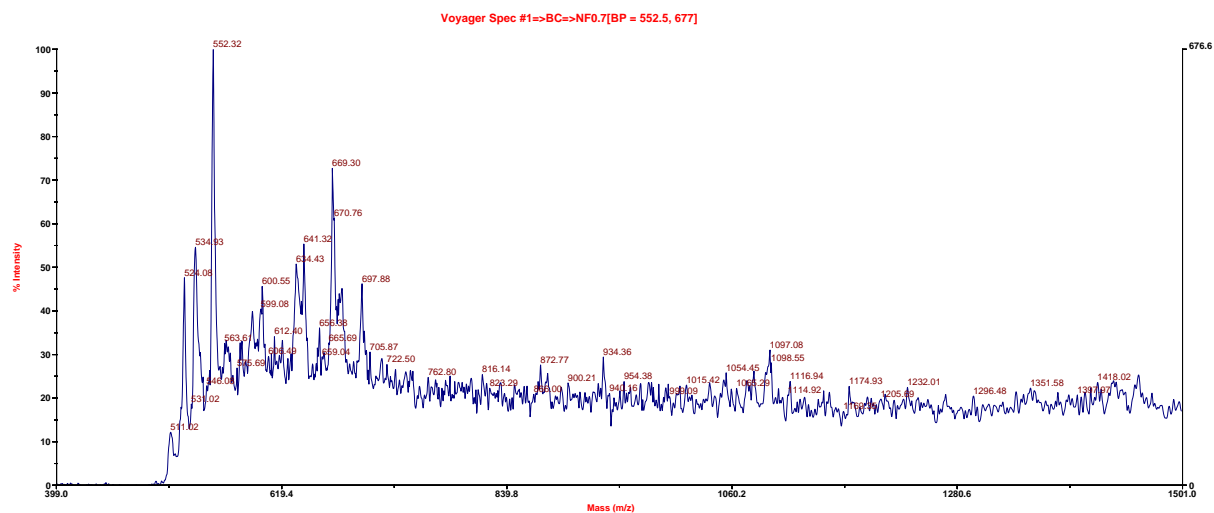


Figure A.3.16 Reaction 3 B2f_Cort

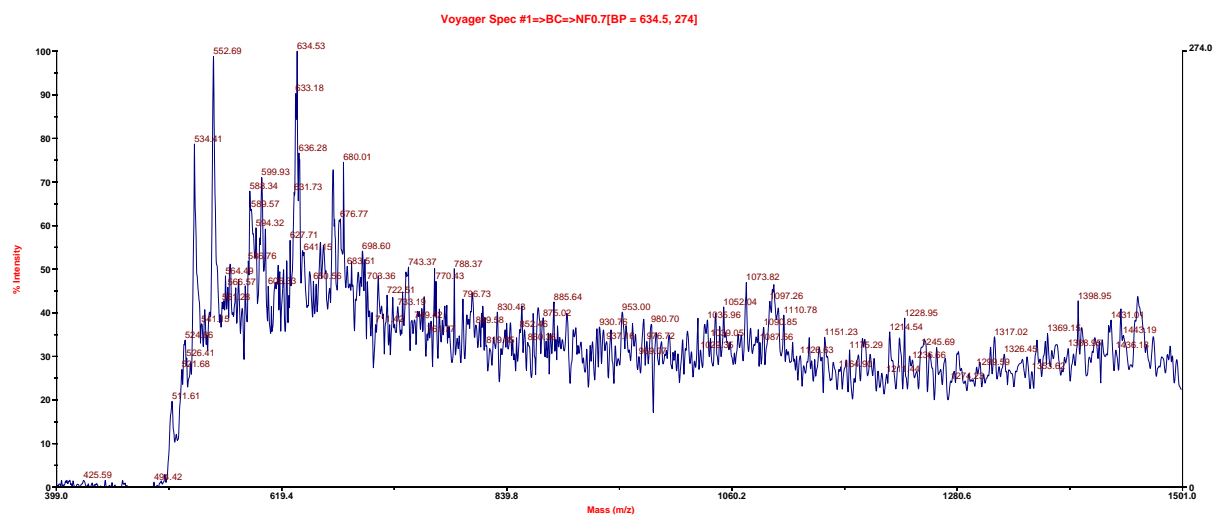


Figure A.3.17 Reaction 3 B2f_Decanol

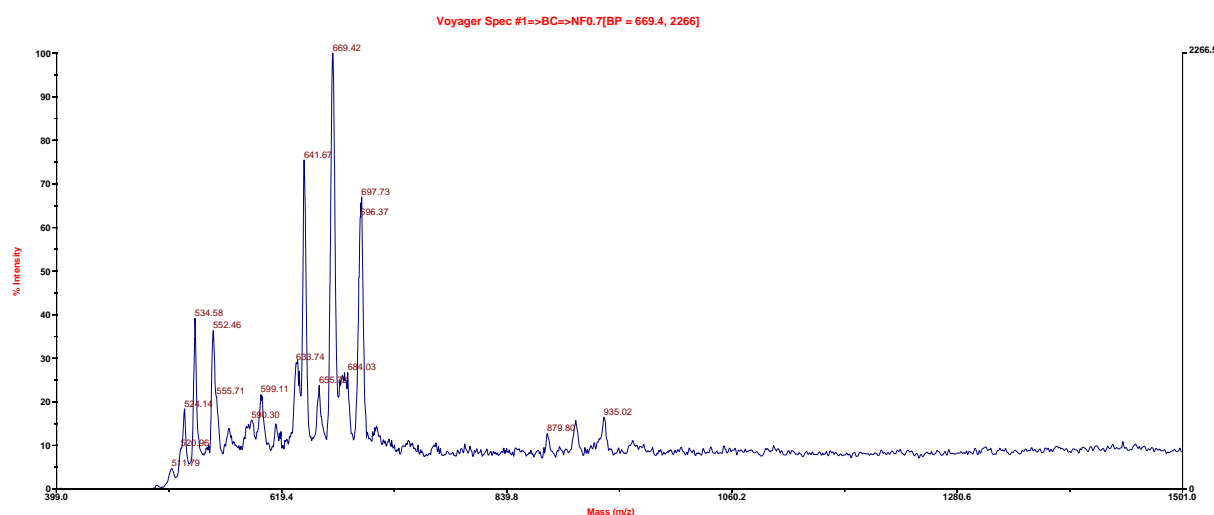


Figure A.3.18 Reaction 3 B2f_Terp

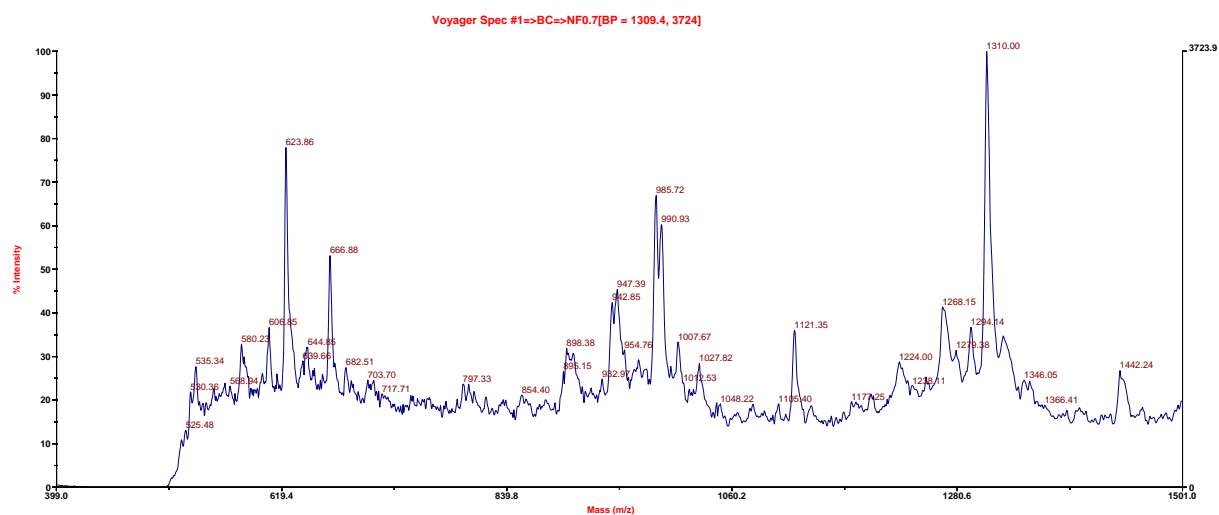


Figure A.3.19 Reaction 1 B2g_Cort

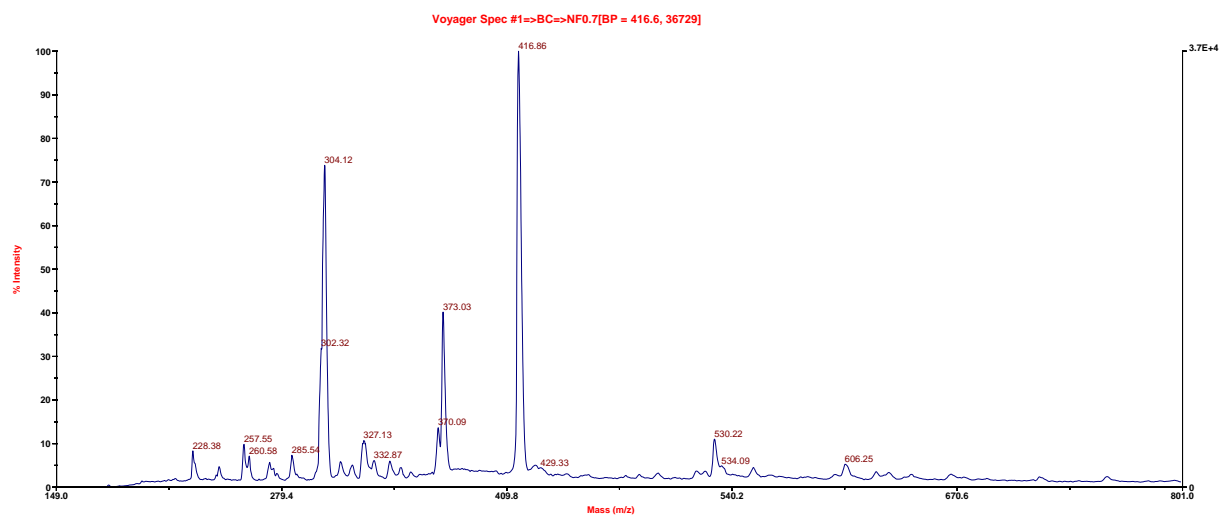


Figure A.3.20 Reaction 1 B2g_Decanol

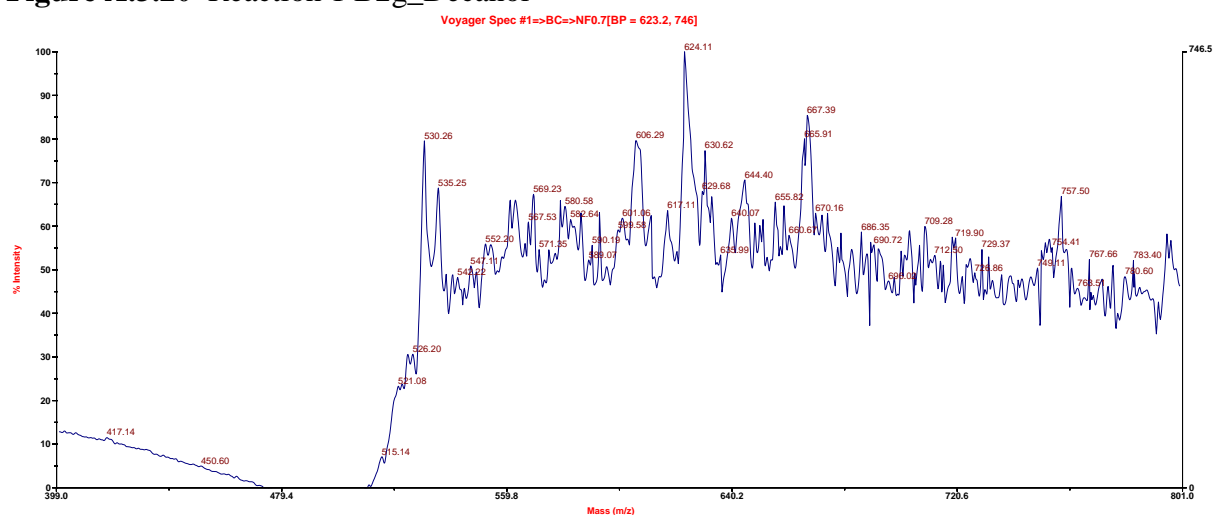


Figure A.3.21 Reaction 1 B2g_Terp

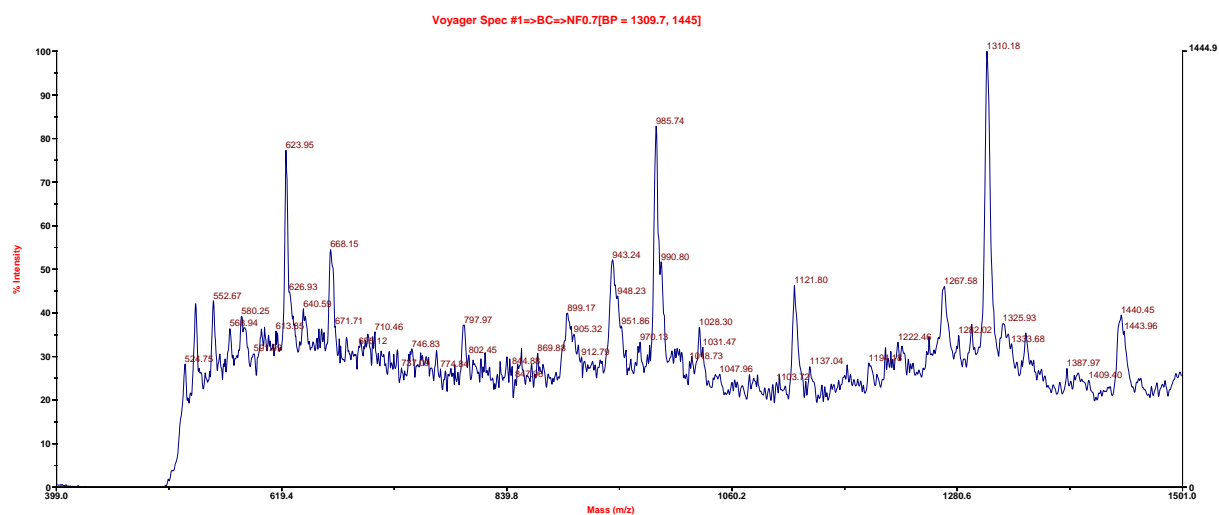


Figure A.3.22 Reaction 2 B2g_Cort

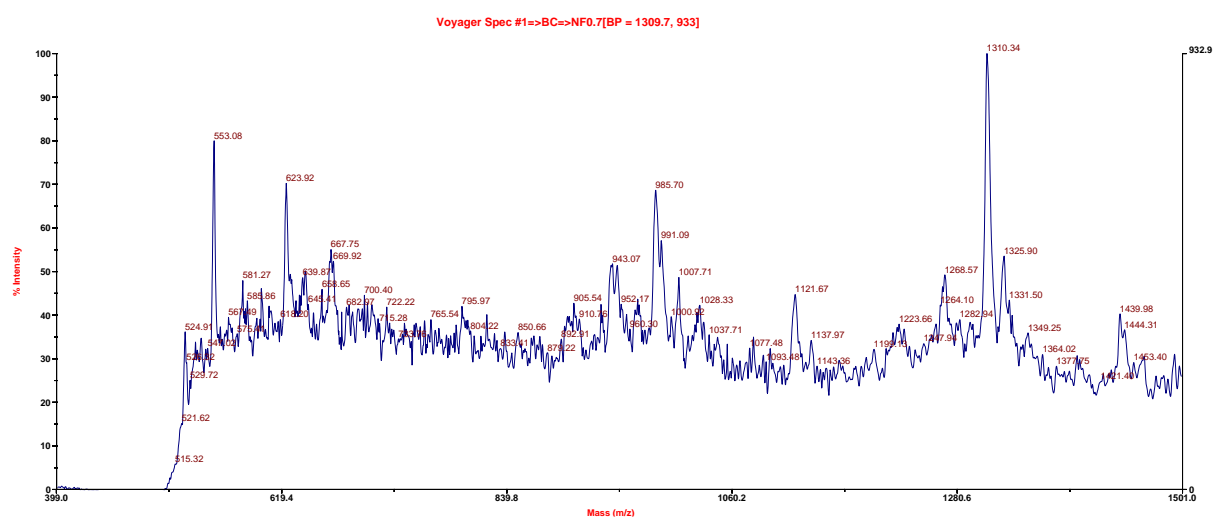


Figure A.3.23 Reaction 2 B2g_Decanol

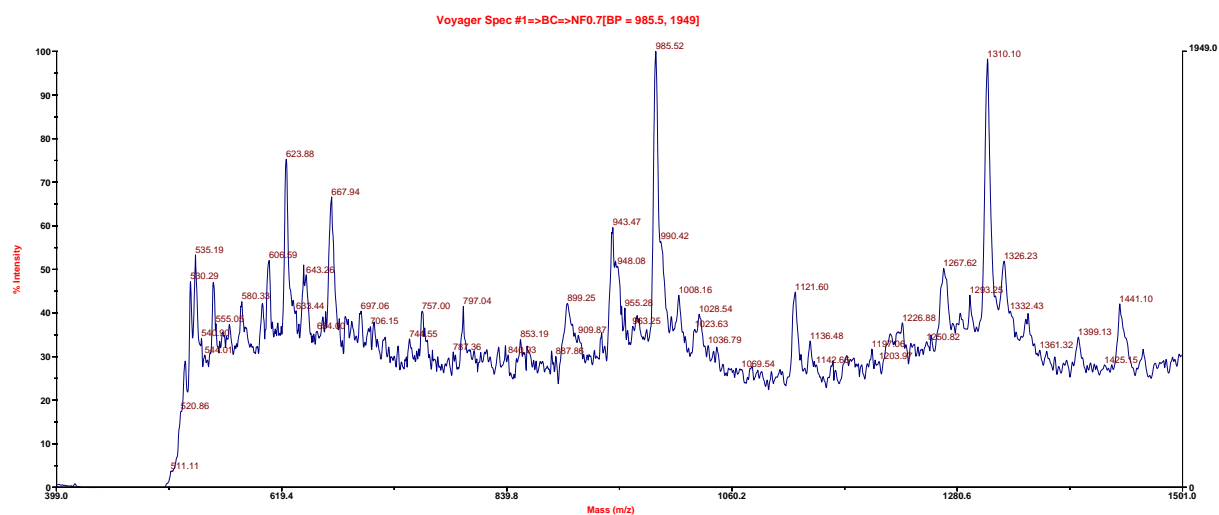


Figure A.3.24 Reaction 2 B2g_Terp

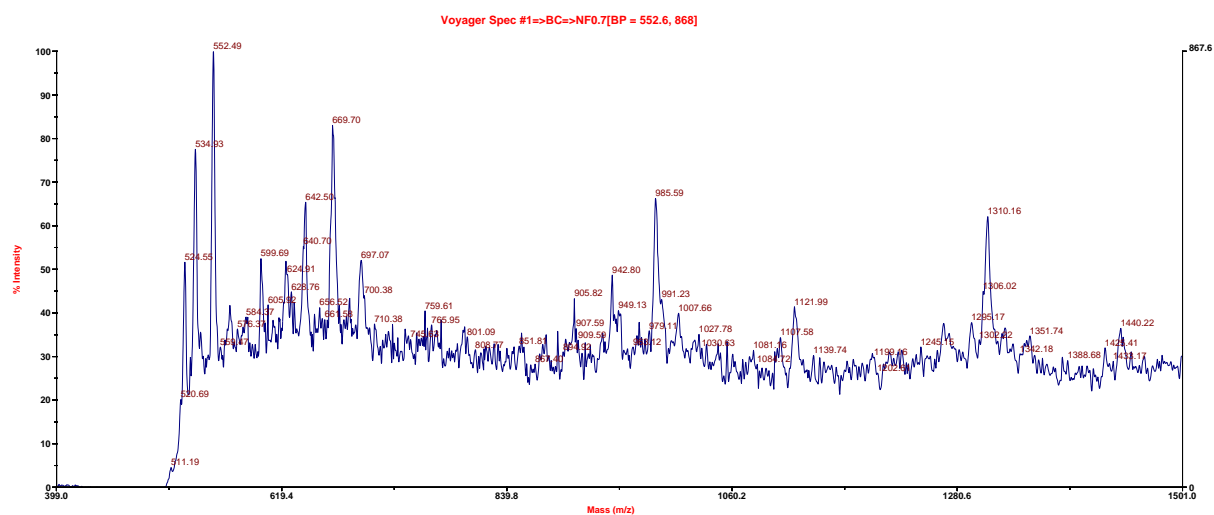


Figure A.3.25 Reaction 3 B2g_Cort

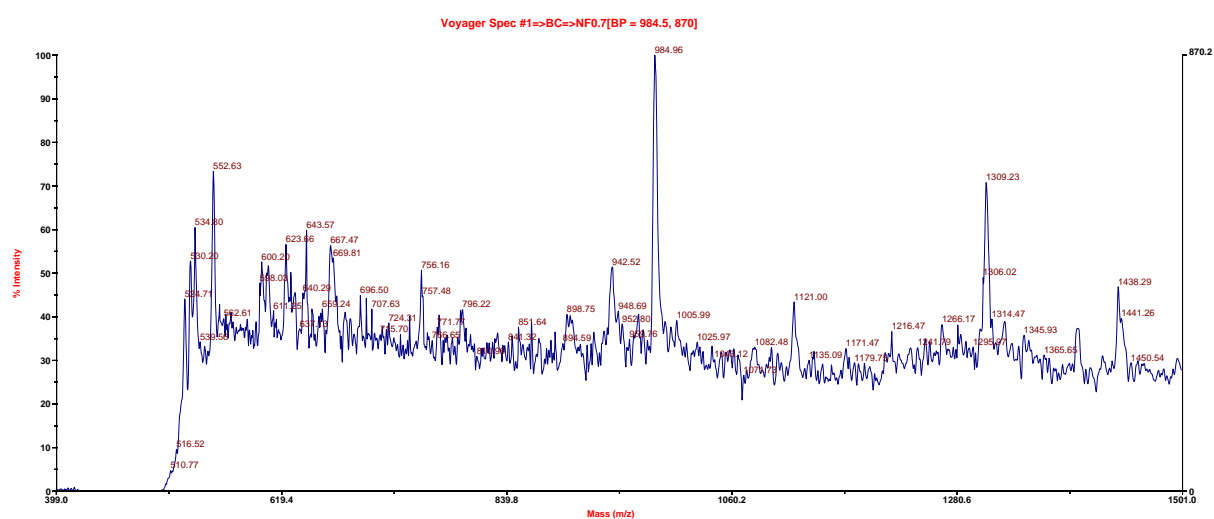


Figure A.3.26 Reaction 3 B2g_Decanol

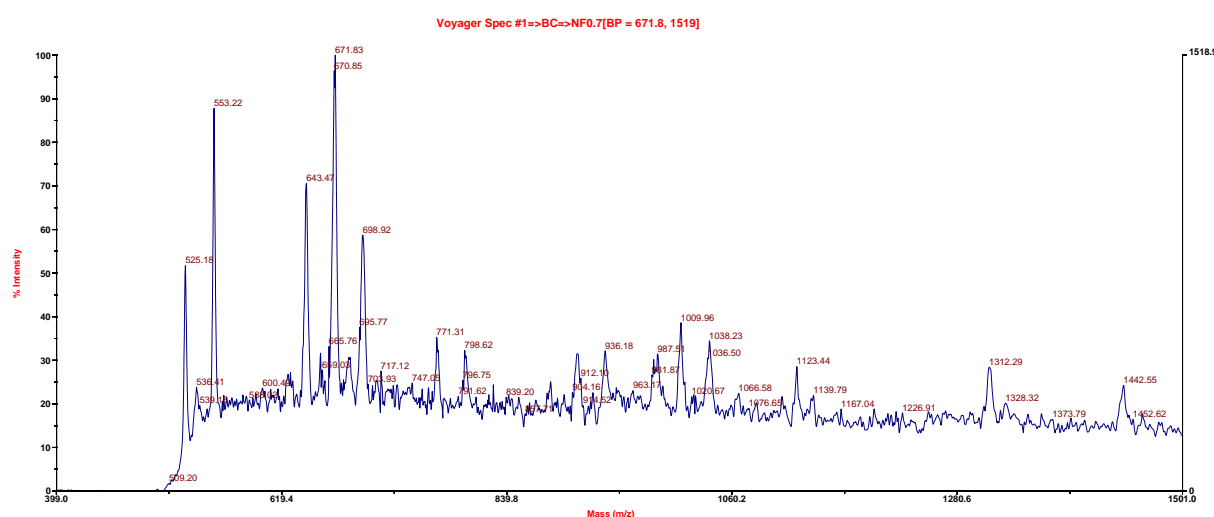


Figure A.3.27 Reaction 3 B2g_Terp

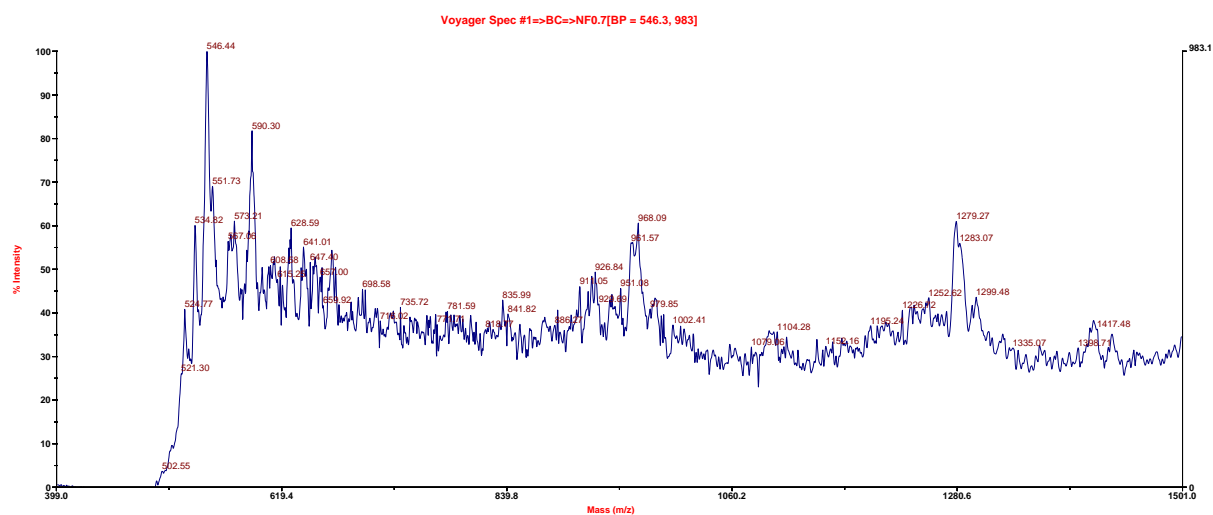


Figure A.3.28 Reaction 1 B2h_Cort

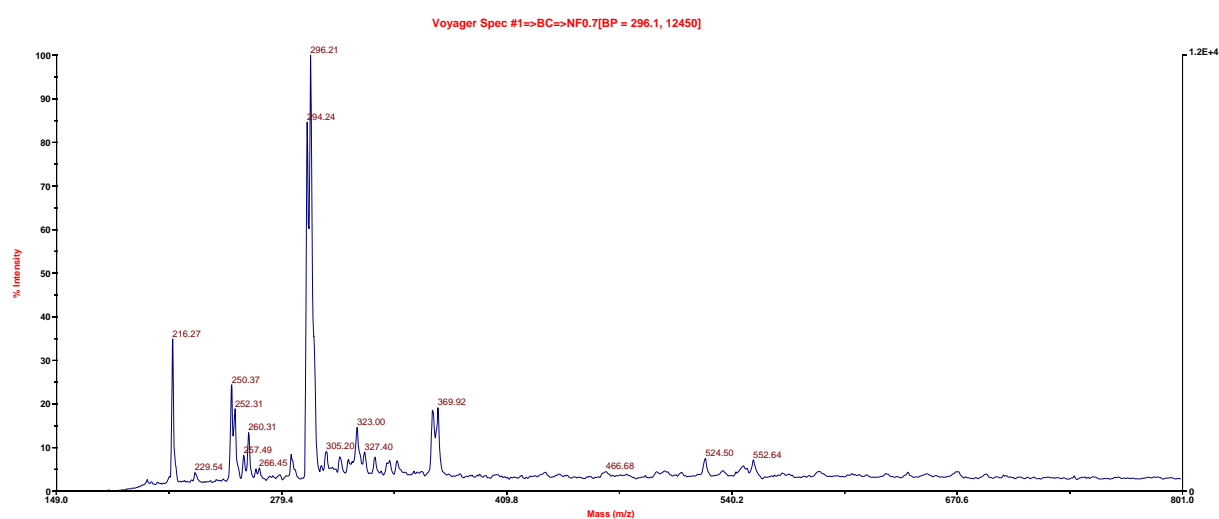


Figure A.3.29 Reaction 1 B2h_Decanol

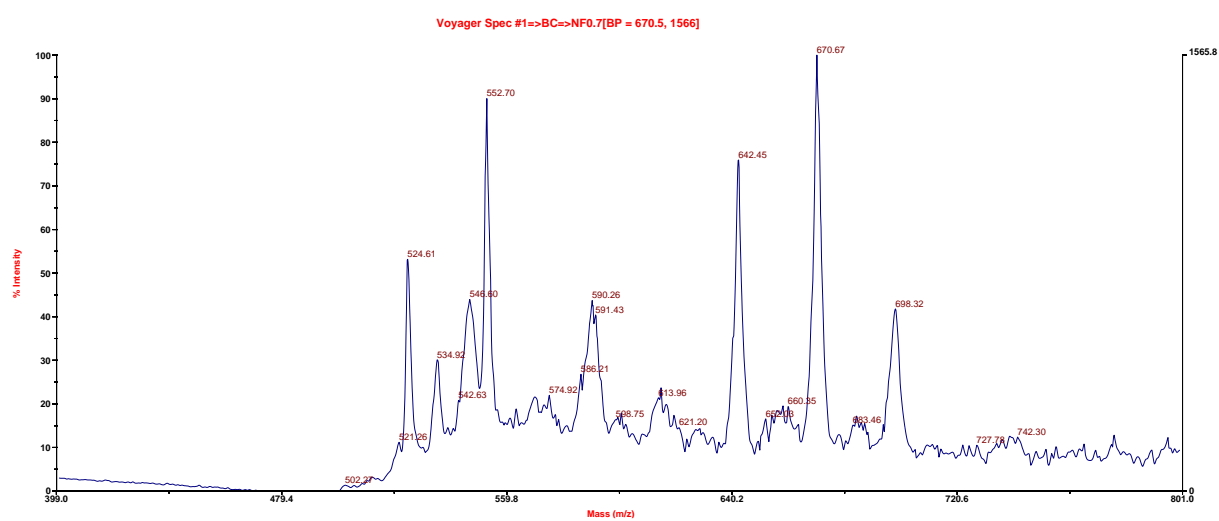


Figure A.3.30 Reaction 1 B2h_Terp

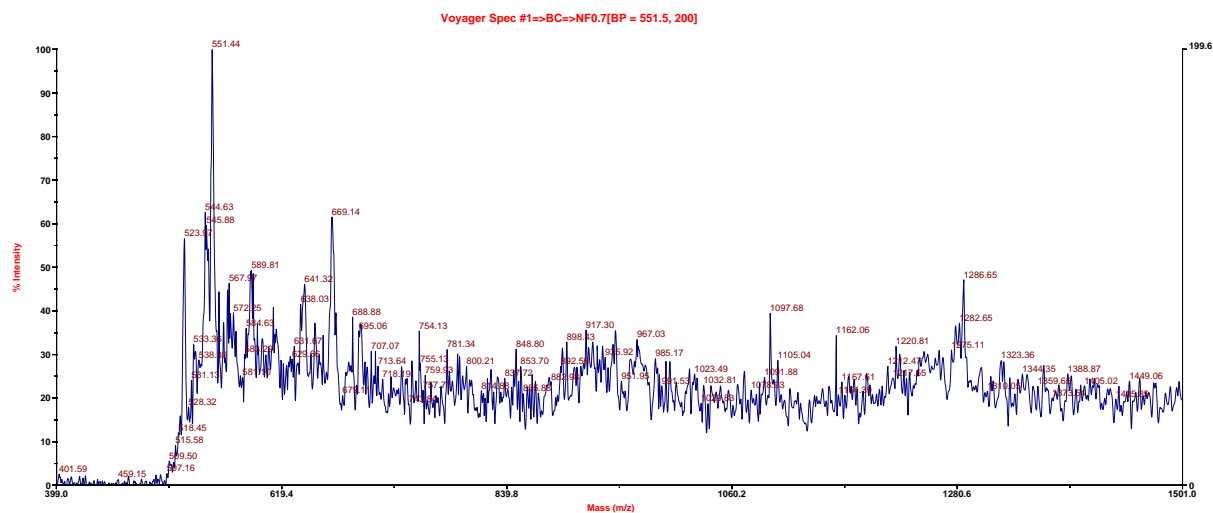


Figure A.3.31 Reaction 2 B2h_Cort

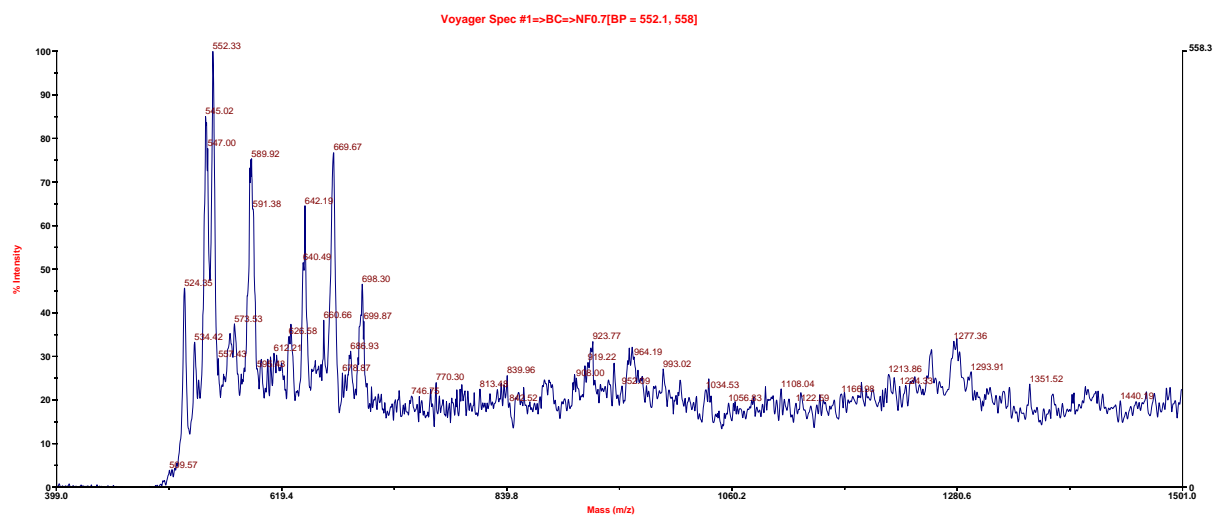


Figure A.3.32 Reaction 2 B2h_Decanol

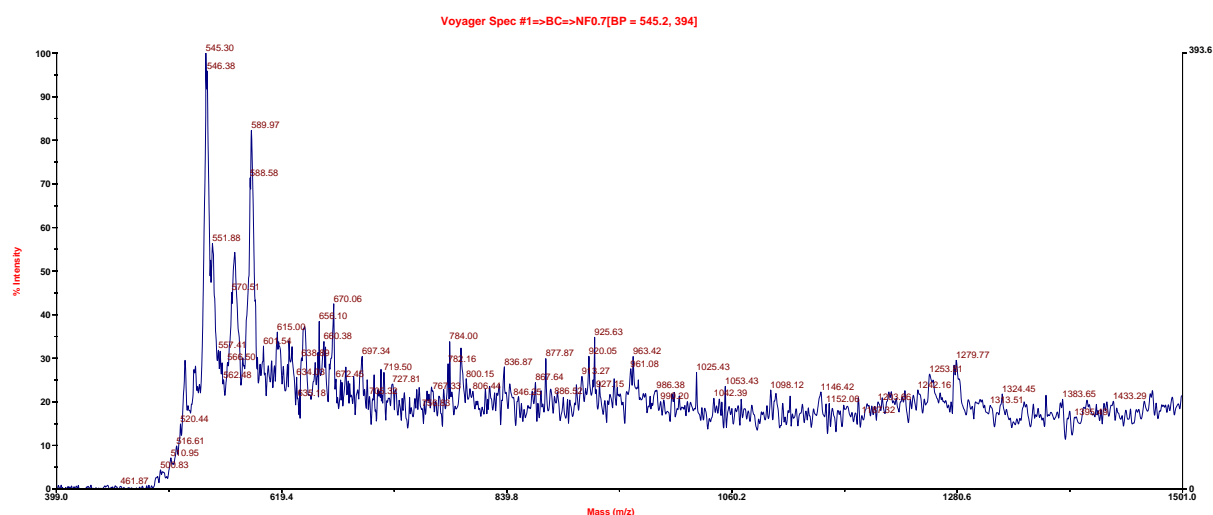


Figure A.3.33 Reaction 2 B2h_Terp

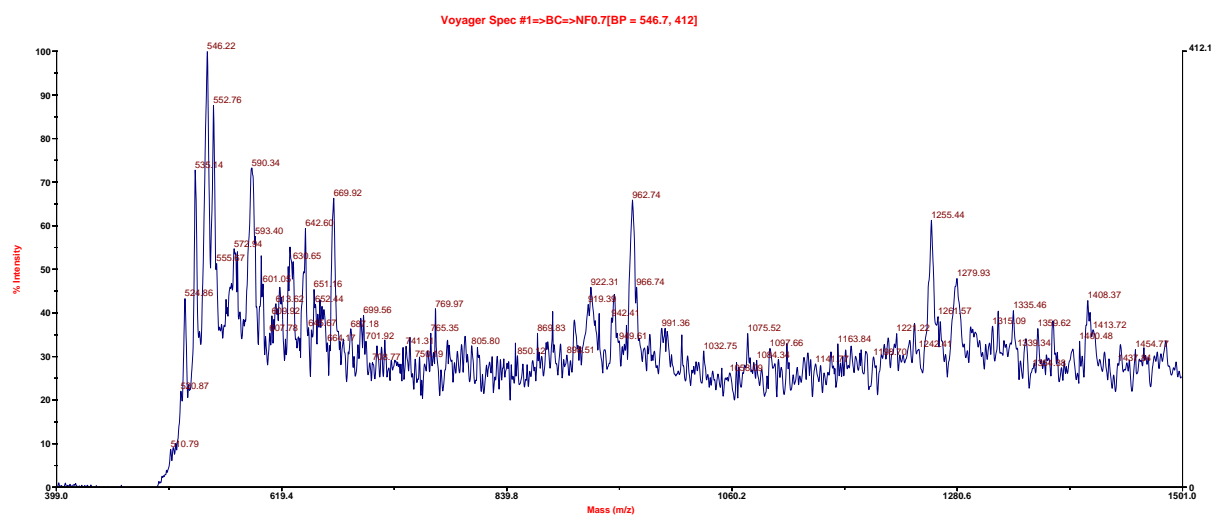


Figure A.3.34 Reaction 3 B2h_Cort

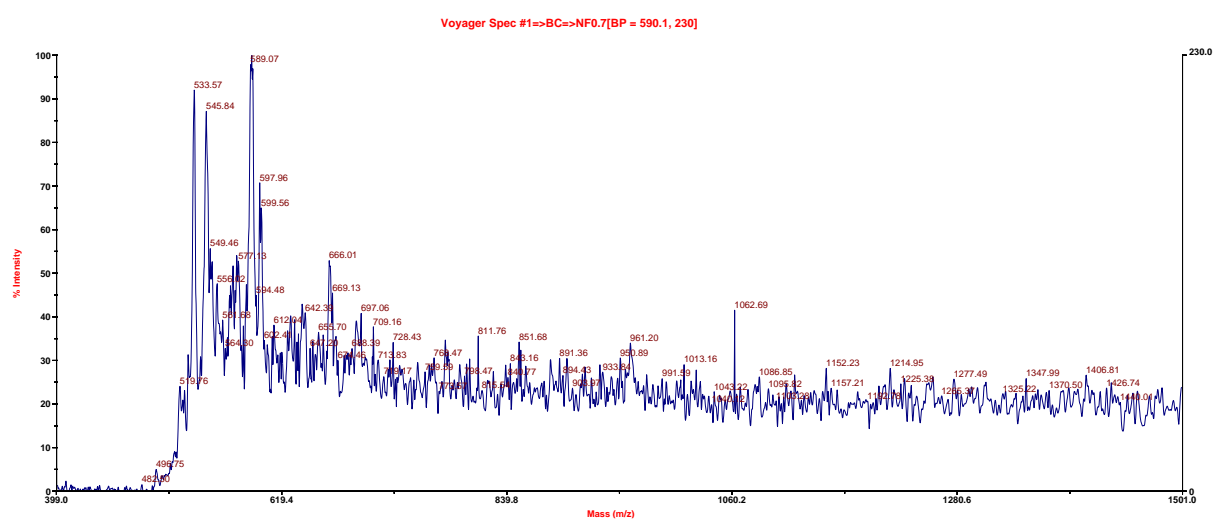


Figure A.3.35 Reaction 3 B2h_Decanol

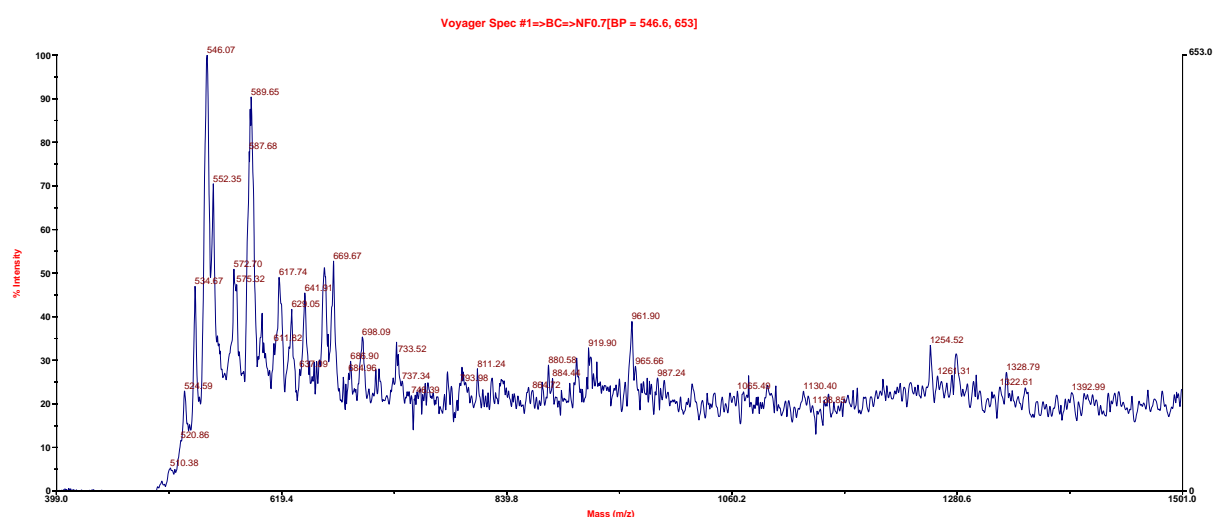


Figure A.3.36 Reaction 3 B2h_Terp

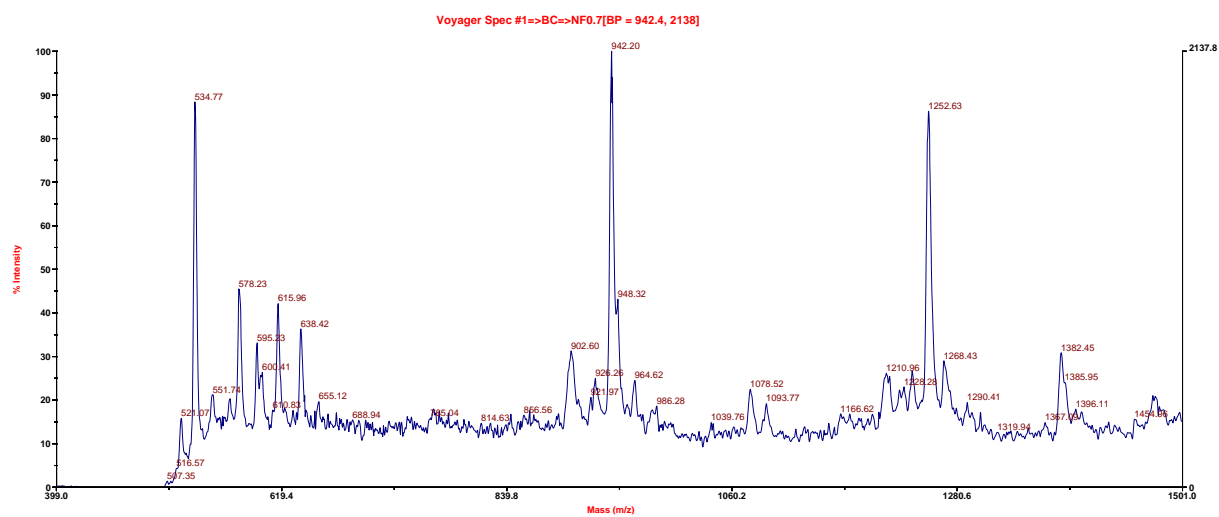


Figure A.3.37 Reaction 1 B2j_Cort

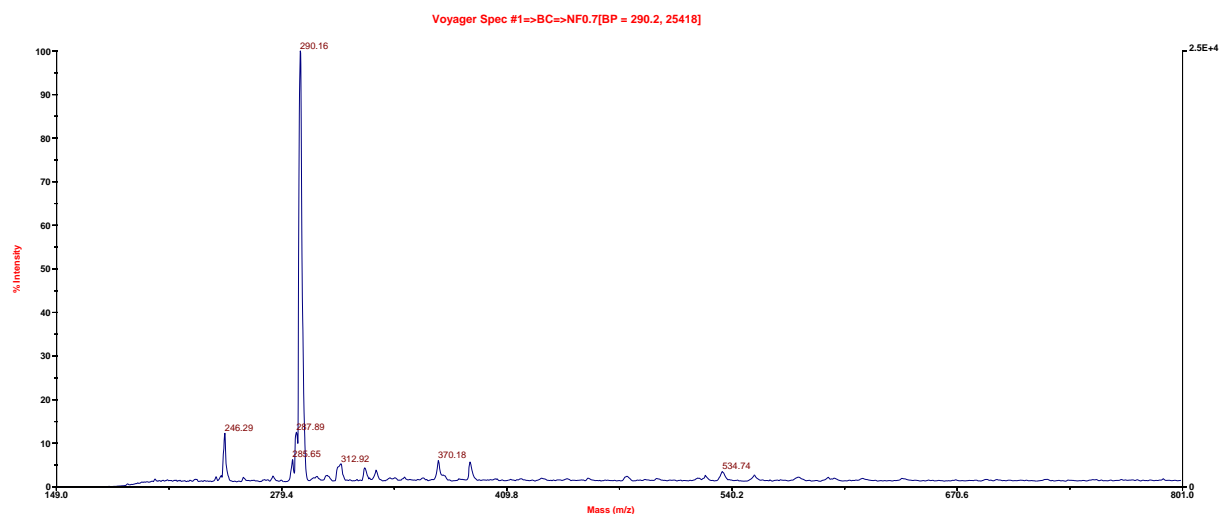


Figure A.3.38 Reaction 1 B2j_Decanol

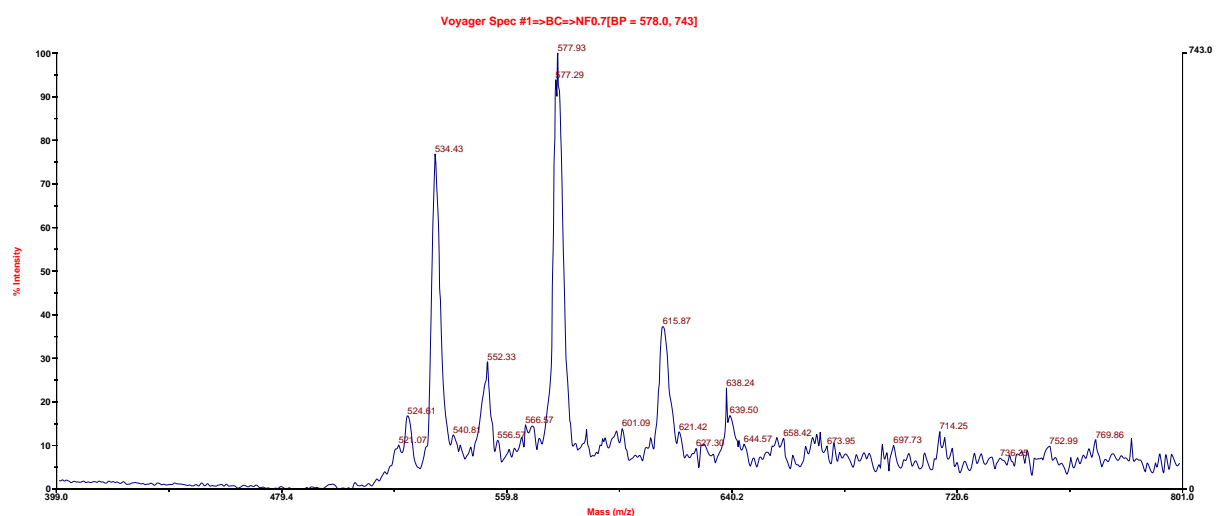


Figure A.3.39 Reaction 1 B2j_Terp

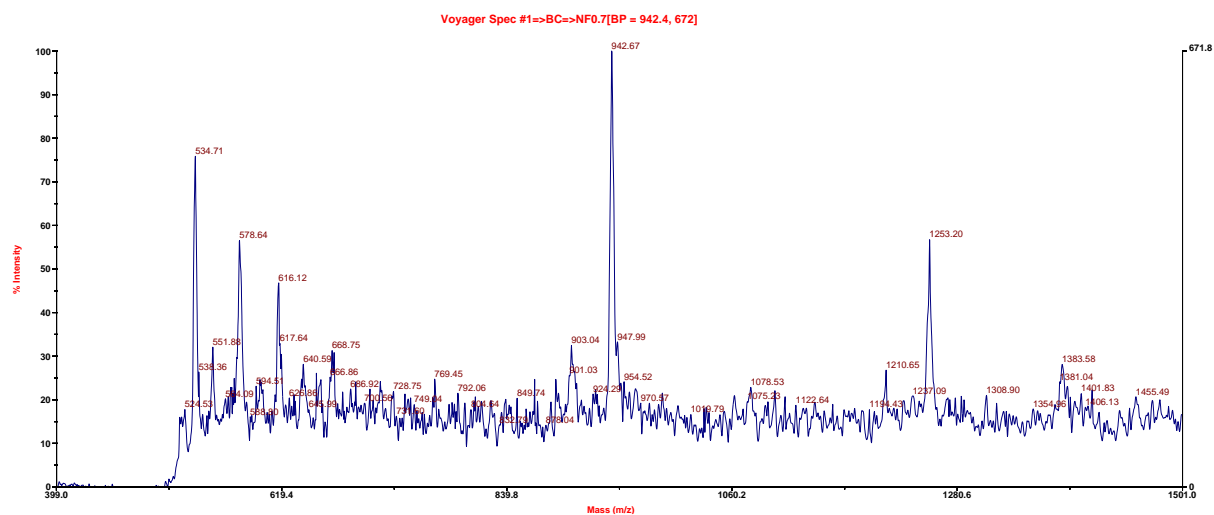


Figure A.3.40 Reaction 2 B2j_Cort

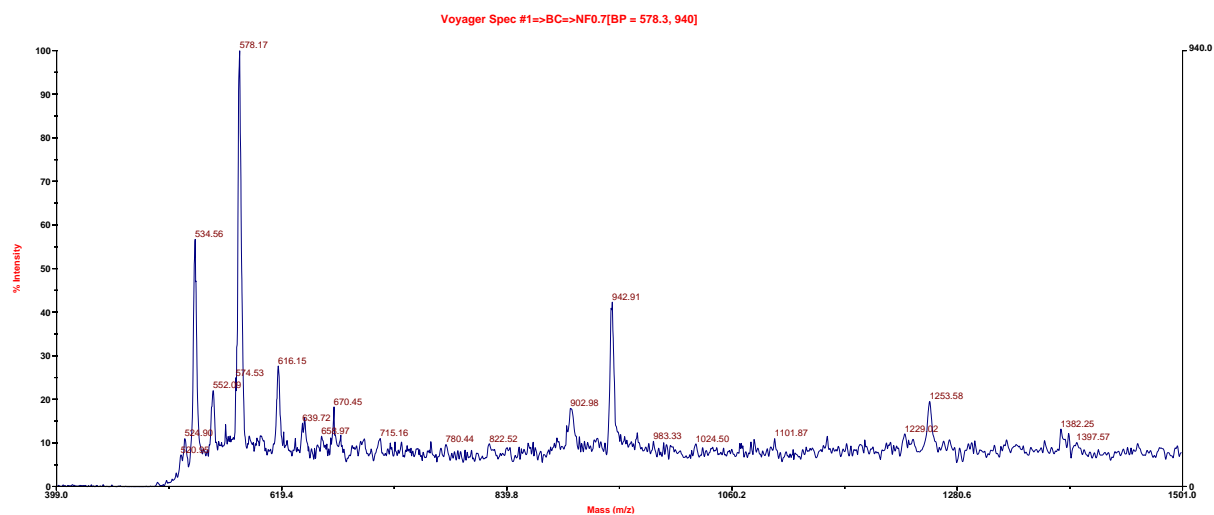


Figure A.3.41 Reaction 2 B2j_Decanol

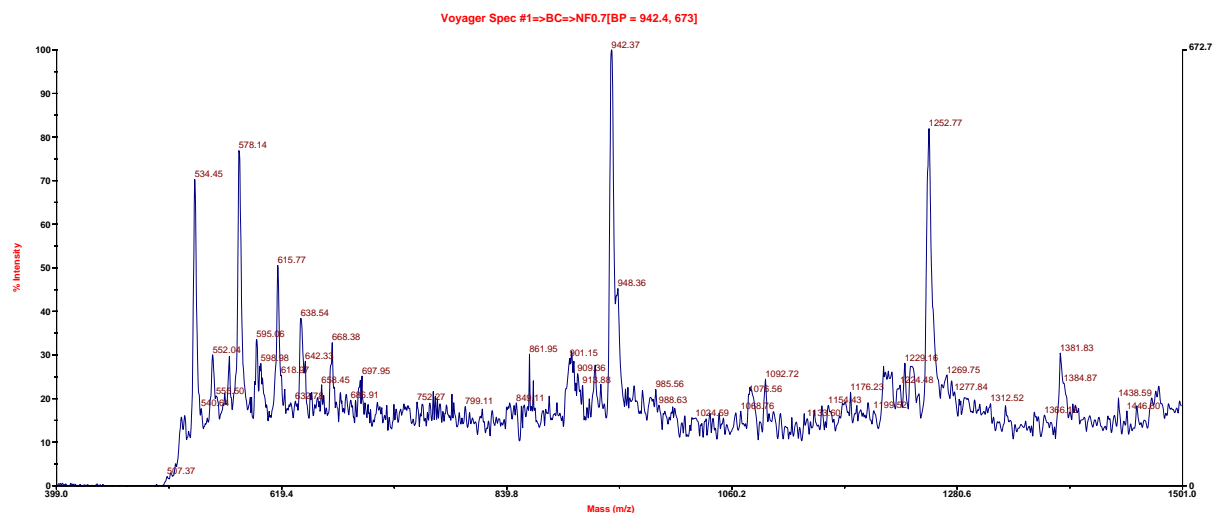


Figure A.3.42 Reaction 2 B2j_Terp

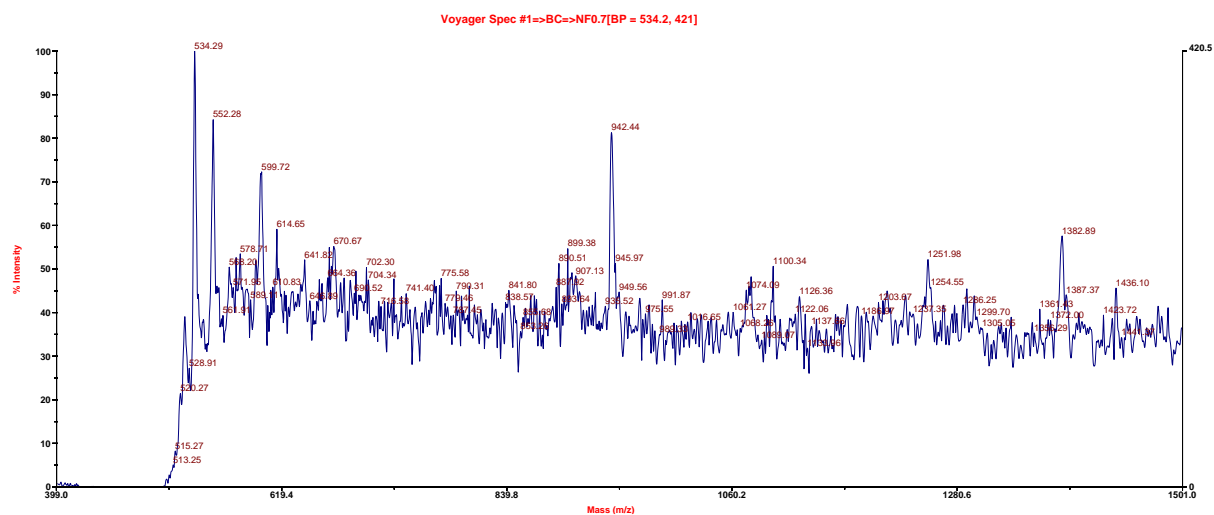


Figure A.3.43 Reaction 3 B2j_Cort

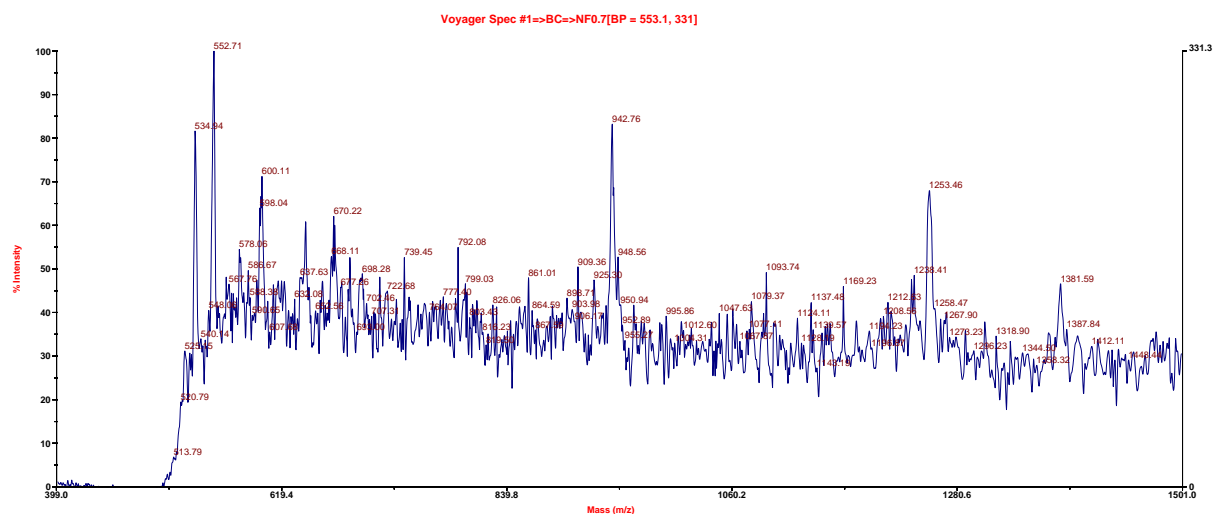


Figure A.3.44 Reaction 3 B2j_Decanol

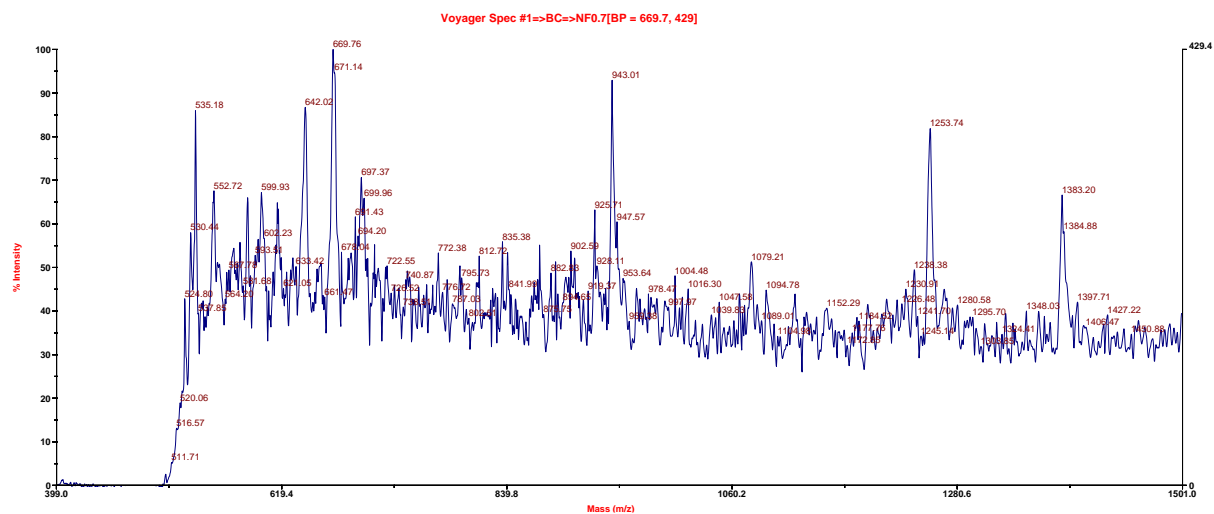
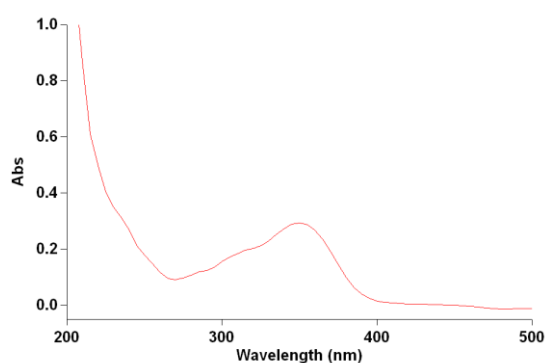


Figure A.3.45 Reaction 3 B2j_Terp

A.4 UV spectra



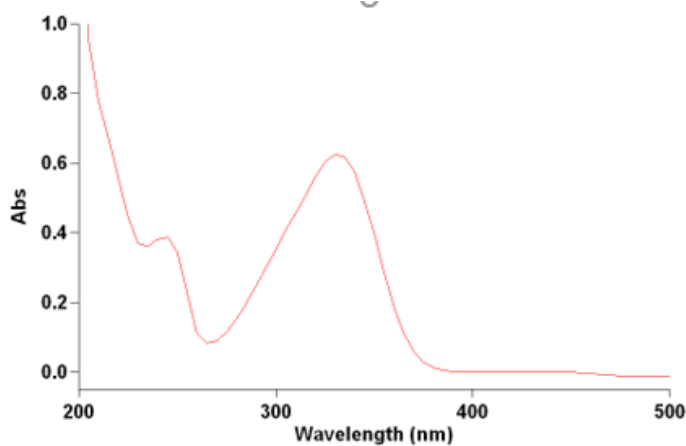
Sample Name: B2d_0.01mg_ml1

Collection Time 14/01/2019 17:22:56

Peak Table
 Peak Style Peaks
 Peak Threshold 0.0100
 Range 500.0nm to 200.0nm

Wavelength (nm)	Abs
350.1	0.294

Figure A.4.1 UV B2d



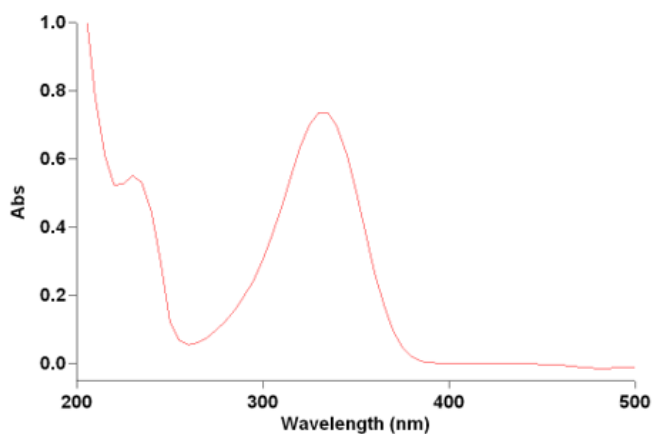
Sample Name: B2f_0.01mg_ml

Collection Time 14/01/2019 17:29:17

Peak Table
 Peak Style Peaks
 Peak Threshold 0.0100
 Range 500.0nm to 200.0nm

Wavelength (nm)	Abs
330.0	0.625
245.0	0.387

Figure A.4.2 UV B2f



Sample Name: B2j_0.01mg_ml

Collection Time 14/01/2019 17:39:34

Peak Table

Peak Style

Peak Threshold

Range

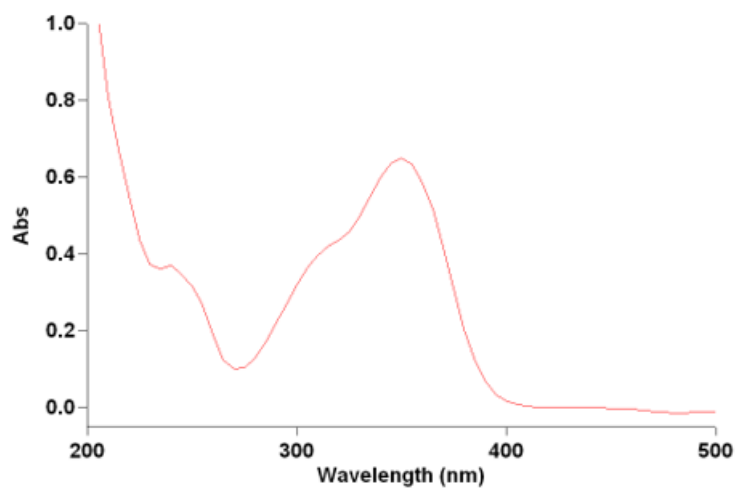
Peaks

0.0100

500.0nm to 200.0nm

Wavelength (nm)	Abs
330.0	0.737
230.0	0.553

Figure A.4.3 UV B2j



Sample Name: B2b_0.01mg_ml

Collection Time 14/01/2019 17:42:33

Peak Table

Peak Style

Peak Threshold

Range

Peaks

0.0100

500.0nm to 200.0nm

Wavelength (nm)	Abs
350.1	0.651

Figure A.4.4 UV B2b